# BEHAVIOUR OF BLIND BOLTED MOMENT CONNECTIONS FOR SQUARE HSS COLUMNS

By

SHEHAB ELDIN M. ABED EL LATIF MOURAD

A Thesis

Submitted to the School of Graduate Studies

in Partial Fullfilment of the Requirements

for the Degree

Doctor of Philosophy

McMaster University

December 1993

# BEHAVIOUR OF BLIND BOLTED MOMENT CONNECTIONS FOR SQUARE HSS COLUMNS

DOCTOR OF PHILOSOPHY (1993)
(Civil Engineering)

McMASTER UNIVERSITY
Hamilton, Ontario

TITLE: Behaviour of blind bolted moment connections for square HSS columns

AUTHOR: Shehab Eldin M. Abed El Latif Mourad, B.Sc. (Ain Shams University)
M.Sc. (Ain Shams University)

SUPERVISORS: Professor A. Ghobarah
Professor R.M Korol

NUMBER OF PAGES: xxvii, 240

To my dear wife ***Mona***

whose

Patience, Understanding and Assistance

are Deeply Appreciated

## ABSTRACT

Although hollow structural sections (HSS) are an efficient structural member and have attractive architectural appearance, their use as columns in low or medium-rise moment-resisting steel frames has been limited. Some of the difficulties are due to the lack of a simple and practical field-bolted moment connection between a W-shape beam and an HSS column.

The objectives of this research study are to develop a practical bolted moment connection between a W-shape beam and a square HSS column and to evaluate its behaviour experimentally under monotonic and cyclic loading. In addition, it is of interest to evaluate the effect of the developed connection response on the frame's overall behaviour, and provide guidelines and design rules for detailing the connection. In this research study, attention is focused on investigating the behaviour of bolted end-plate connections developed by blind fasteners. An experimental-analytical approach was used in this research program.

The experimental program which was carried out on full scale beam-to-column connections involved three phases. First, three monotonic tests were conducted to examine the behaviour of such a connection using blind fasteners and to compare their response with a similar connection using high strength A325 bolts. Second, four tests were conducted on connections utilizing larger HSS columns and with different stiffening

conditions to reveal different modes of failure. Third, two cyclic tests were performed to examine the effect of cyclic loading on such a connection.

Based on the observations and results of the experimental program, an analytical model to predict the behaviour of the connection was developed. The sensitivity of the model was checked by comparing its predictions with the experimental results. The model was then incorporated into "Drain-2DX" computer program to be used in analyzing moment resisting frames. Based on both experimental and analytical results, a design procedure for the connection was proposed.

The effect of connection flexibility on the response of a 4-storey steel moment frame was evaluated by comparing the response to that of a similar frame with rigid connections. The frames were analyzed statically under monotonically increasing loading and dynamically under two earthquake ground motions. It was concluded that, the flexibility of semi-rigid connections should be included in both static and dynamic analyses to determine a frame's structural response more realistically.

## ACKNOWLEDGEMENTS

I wish to express my sincere appreciation to my research supervisors, Dr. A. Ghobarah and Dr. R.M Korol for their guidance and encouragement throughout the course of this study. I am grateful to their dedication and the number of hours that they spent with me on this research.

I am indebted to my supervisor committee members, Dr. R. Sowerby and Dr. W. K. Tso for their valuable comments and suggestions on my research and also their time in reviewing this thesis.

I wish to express my sincere gratitude to Huck International Inc. and, in particular, to P. Lowe and S. Sadri for providing the blind fasteners, installation equipment and all information necessary to undertake this study.

Financial support from McMaster University is gratefully acknowledged. Also, the assistance offered by the Applied Dynamics Laboratory technicians in conducting the experimental work is greatly appreciated.

Last but not least, I must mention my deepest appreciation to my parents without their help, encouragement and patience this work would have been difficult to complete.

PAGINATION ERROR.

TEXT COMPLETE.

ERREUR DE PAGINATION.

LE TEXTE EST COMPLET.

NATIONAL LIBRARY OF CANADA.

CANADIAN THESES SERVICE.

BIBLIOTHEQUE NATIONALE DU CANADA.

SERVICE DES THESES CANADIENNES.

TABLE OF CONTENTS


| | | | PAGE |
|---|---|---|---|
| ABSTRACT | | | iii |
| ACKNOWLEDGEMENT | | | v |
| TABLE OF CONTENTS | | | vii |
| LIST OF FIGURES | | | xii |
| LIST OF TABLES | | | xx |
| LIST OF SYMBOLES | | | xxii |
| **CHAPTER 1** | **INTRODUCTION** | | 1 |
| | 1.1 | General | 1 |
| | 1.2 | Literature review | 1 |
| | 1.3 | Objectives and scope of work | 6 |
| | 1.4 | Organization of the thesis | 7 |
| **CHAPTER 2** | **BLIND FASTENING SYSTEM** | | 12 |
| | 2.1 | Introduction | 12 |
| | 2.2 | Types of blind fastening systems | 12 |
| | | 2.2.1 BOM fastening system | 12 |
| | | 2.2.2 HSBB fastening system | 13 |
| | 2.3 | Tensile tests | 14 |
| | 2.4 | Resistance factor of HSBB | 17 |
| | 2.5 | Summary | 18 |

Table of Contents (cont'd)


| | | | Page |
|---|---|---|---|
| CHAPTER 3 | EXPERIMENTAL PROGRAM ON EXTENDED END-PLATE CONNECTIONS | | 28 |
| | 3.1 | Introduction | 28 |
| | 3.2 | Experimental Program | 28 |
| | 3.3 | Specimens design and fabrication | 30 |
| | 3.4 | Test setup | 33 |
| | 3.5 | Instrumentation | 34 |
| | 3.6 | Loading sequence | 35 |
| | 3.7 | Experimental measurements | 36 |
| | 3.8 | Specimens' behaviour and modes of failure | 39 |
| | 3.9 | Analysis of experimental results | 45 |
| | 3.10 | Summary | 49 |
| CHAPTER 4 | CONNECTION RESPONSE | | 80 |
| | 4.1 | Introduction | 80 |
| | 4.2 | Modelling of the HSS column flange | 82 |
| | | 4.2.1 Modelling the column flange on the tension side of the connection | 85 |
| | | 4.2.2 Modelling the column flange on the compression side of the connection | 86 |
| | 4.3 | Comprehensive nonlinear model of the connection | 87 |
| | | 4.3.1 Evaluation of connection initial stiffness, $K_i$ | 88 |
| | | 4.3.2 Evaluation of connection plastic moment, $M_{pc}$ | 93 |

4.3.3 Evaluation of connection post-elastic stiffness, $K_p$ 98

4.3.4 Evaluation of parameter C 106

4.3.5 Evaluation of ultimate moment capacity, $M_u$ 106

4.3.6 Model verification 108

4.4 Simplified models 109

4.5 Computer modelling of a semi-rigid connection element 110

4.6 Summary 111

CHAPTER 5 PROPOSED DESIGN OF END-PLATE CONNECTIONS FOR RECTANGULAR HSS COLUMNS 131

5.1 Introduction 131

5.2 Connection geometry design 132

5.3 Connection strength design 133

5.3.1 Design of welds 135

5.3.2 Design of HSBB bolts 136

5.3.3 Design of end-plate 139

5.3.4 Design of HSS column flange 141

5.4 Summary 144

CHAPTER 6 STATIC AND DYNAMIC ANALYSIS OF A 4-STOREY BUILDING 151

6.1 Introduction 151

6.2 Design procedure 152

**Table of Contents (cont'd)** **Page**


6.2.1 Loads 153

6.2.2 Design of frame with rigid connections 156

6.2.3 Design of frame with semi-rigid connections 158

6.2.4 Design of end-plate connections 159

6.3 Cases studied 159

6.4 Computer modelling 162

6.5 Static analysis of the 4-storey frames 164

6.5.1 Effect of connection flexibility on the lateral deflections 164

6.5.2 Effect of connection flexibility on frame weight 165

6.5.3 Effect of connection flexibility on the internal forces in frame members 165

6.5.4 Effect of connection modelling on the top lateral deflection 167

6.5.5 Effect of connection flexibility on the overall strength of frames 168

6.6 Dynamic analysis of the 4-storey frames 169

6.6.1 Dynamic characteristics of frames Ffr and Ff1 169

6.6.2 Proposed artificial ground excitations 170

6.6.3 Generation of artificial earthquake records 171

6.6.4 Dynamic response to the high A/v ratio record 172

Table of Contents (cont'd) Page


6.6.5 Dynamic response to the low A/v ratio record 173

6.7 Summary 175

CHAPTER 7 CONCLUSIONS 205

7.1 Summary 205

7.2 Conclusions 206

7.3 Recommendations for future research 209

APPENDIX A DETERMINATION OF END-PLATE EFFECTIVE THICKNESS 211

APPENDIX B MODIFIED SLOPE DEFLECTION SOLUTION FOR THE END-PLATE MODEL 213

APPENDIX C DETERMINATION OF COLUMN FLANGE DEFLECTION AT BOLT LOCATIONS 217

APPENDIX D DETERMINATION OF THE AVERAGE COLUMN FLANGE DEFLECTION ON THE COMPRESSION SIDE 223

APPENDIX E YIELD LINE SOLUTION OF A STIFFENED HSS COLUMN FLANGE 228

APPENDIX F DEFLECTION DUE TO MEMBERANE ACTION 231

REFERENCES 235

## List of Figures


| Figure | | Page |
|---|---|---|
| 1.1 | Types of simple connections tested by White and Fang | 8 |
| 1.2 | Strap angle moment connections tested by Picard and Giroux | 8 |
| 1.3 | Types of moment connections tested by Dawe and Grondin | 9 |
| 1.4 | Flange diaphram moment connections tested by Kato et al. | 9 |
| 1.5 | Stiffening by tees on the beam flanges | 10 |
| 1.6 | Moment connectios developed by long bolts | 10 |
| 1.7 | A moment connection with nuts welded on the column flange | 11 |
| 1.8 | A typical extended end-plate connection for HSS column | 11 |
| 2.1 | BOM fastener before and after installation | 20 |
| 2.2 | Installation sequence for BOM fasteners | 21 |
| 2.3 | HSBB before and after installation | 22 |
| 2.4 | Installation sequence for HSBB fasteners | 23 |
| 2.5 | Installation equipment for HSSB fasteners | 24 |
| 2.6 | Details of testing device | 25 |
| 2.7 | Typical load-separation relationship for different types of bolts | 26 |
| 2.8 | Tensile test results of HSBB fasteners | 27 |
| 3.1 | A typical extended end-plate connection | 53 |
| 3.2 | Test specimen | 54 |
| 3.3 | Installation sequence of bolts across the end-plate | 54 |
| 3.4 | Details of tested connections | 55 |

List of Figures (cont'd)


| Figure | | Page |
|---|---|---|
| 3.5 | General arrangement of test setup | 56 |
| 3.6 | LVDTs arrangements | 57 |
| 3.7 | Typical loading sequence for specimens C1 and C2 | 58 |
| 3.8 | Connection deformations at the tension side of Specimen S3 | 59 |
| 3.9 | Connection deformations at the compression side of Specimen S3 | 59 |
| 3.10 | Determination of connection parameters experimentally | 60 |
| 3.11 | HSS side wall deflections of Specimen S5 | 60 |
| 3.12 | Beam moment versus plastic beam rotation relationship of specimen S7 | 61 |
| 3.13 | Connection moment-rotation relationship of specimen S1 | 61 |
| 3.14 | Specimen S1 after failure | 62 |
| 3.15 | Connection moment-rotation relationship of specimen S2 | 63 |
| 3.16 | Specimen S2 after failure | 63 |
| 3.17 | Connection moment-rotation relationship of specimen S3 | 64 |
| 3.18 | A typical print of the carbon sheet placed between the end-plate and column flange | 64 |
| 3.19 | Specimen S3 after failure | 65 |
| 3.20 | Connection moment-rotation relationship of specimen S4 | 66 |
| 3.21 | Specimen S4 after failure | 66 |
| 3.22 | Connection moment-rotation relationship of specimen S5 | 67 |

List of Figures (cont,d)


| Figure | | Page |
|---|---|---|
| 3.23 | Yield pattern of the HSS column flange at the tension side of the connection (specimen S5) | 67 |
| 3.24 | End-plate deformations of specimen S5 after test | 68 |
| 3.25 | Connection moment-rotation relationship of specimen S6 | 69 |
| 3.26 | Specimen S6 after failure | 69 |
| 3.27 | Connection moment-rotation relationship of specimen S7 | 70 |
| 3.28 | Specimen S7 after failure | 70 |
| 3.29 | Connection hysteretic curves of specimen C1 | 71 |
| 3.30 | Beam hysteretic curves of specimen C1 | 71 |
| 3.31 | Connection hysteretic curves of specimen C2 | 72 |
| 3.32 | Beam hysteretic curves of specimen C2 | 72 |
| 3.33 | Comparison of connection moment-rotation relationships of specimens S1, S2 and S3 | 73 |
| 3.34 | Comparison of connection moment-rotation relationships of specimens S4, S6 and C2 | 74 |
| 3.35 | Comparison of connection moment-rotation relationships of specimens S5, S7 and C1 | 75 |
| 3.36 | Comparison of connection deformations for specimens S5 and S7 | 76 |
| 3.37 | Comparison of HSS side walls deflections for specimens S5 and S7 | 76 |
| 3.38 | Cumulative energy dissipated by each component in specimen C1 | 77 |

**List of Figures (cont'd)**


| Figure | | Page |
|---|---|---|
| 3.39 | Cumulative energy dissipated by each component in specimen C2 | 78 |
| 3.40 | Variation of connection stiffness relative to initial stiffness | 79 |
| 4.1 | HSS column flange model | 113 |
| 4.2 | Idealization of HSS column flange at the tension side of the connection | 114 |
| 4.3 | Idealization of HSS column flange at the compression side of the connection | 115 |
| 4.4 | Typical moment-rotation curve shows the model parameters | 116 |
| 4.5 | Typical deformations of end-plate connection | 116 |
| 4.6 | End-plate idealization | 117 |
| 4.7 | Comparison between the predicted and the experimental connection initial stiffness | 118 |
| 4.8 | Different yield line mechanisms for end-plate | 118 |
| 4.9 | Yield line mechanisms for unstiffened HSS column flange | 119 |
| 4.10 | Yield line mechanism for column flange stiffened with a doubler plate | 120 |
| 4.11 | Loaded area and yield line mechanism of column flange (compression side) | 120 |
| 4.12 | Comparison between the predicted and the observed connection plastic moment | 121 |
| 4.13 | Equivelant beam model for HSS column flange | 121 |
| 4.14 | Deflection coefficients for simply supported column flange loaded with rectangular patch loads | 122 |

List of Figures (cont'd)


| Figure | | Page |
|---|---|---|
| 4.15 | Comparison between the predicted and the experimental connection post-elastic stiffness | 123 |
| 4.16 | Comparison between the predicted and the observed connection ultimate moment | 123 |
| 4.17(a) | Experimental vs. predicted moment rotation relationship for specimen S3 | 124 |
| 4.17(b) | Experimental vs. predicted moment rotation relationship for specimen S4 | 124 |
| 4.17(c) | Experimental vs. predicted moment rotation relationship for specimen S5 | 125 |
| 4.17(d) | Experimental vs. predicted moment rotation relationship for specimen S6 | 125 |
| 4.17(e) | Experimental vs. predicted moment rotation relationship for specimen S7 | 126 |
| 4.17(f) | Experimental vs. predicted moment rotation relationship for specimen C1 | 126 |
| 4.17(g) | Experimental vs. predicted moment rotation relationship for specimen C2 | 127 |
| 4.18 | The bi-linear model is superimposed on the moment-rotation relationship of specimen S3 | 128 |
| 4.19 | The tri-linear model is superimposed on the moment-rotation relationship of specimen S4 | 128 |
| 4.20 | Nodal degrees of fredom for the Idealized semi-rigid connection element | 129 |
| 4.21 | The bi-linear connection element components | 130 |
| 4.22 | Simulation of tri-linear model by using two bi-linear models | 130 |

List of Figures (cont'd)


| Figure | | Page |
|---|---|---|
| 5.1 | Geometery of an extended end-plate connection | 146 |
| 5.2 | Loads on the connection due to bending | 146 |
| 5.3 | Arrangement of welds | 147 |
| 5.4 | Bending and prying action of plate projection | 147 |
| 5.5 | Traditional prying force model | 148 |
| 5.6 | End-plate yield line mechanism | 148 |
| 5.7 | End-plate yielding with bolts failure | 149 |
| 5.8 | Yield line mechanisms for unstiffened HSS column flange | 149 |
| 5.9 | Yield line mechanism for HSS column flange stiffened with a doubler plate | 150 |
| 6.1 | Plan of a 4-storey steel building | 183 |
| 6.2 | Elevation of the moment resisting frame in E-W or N-S direction | 183 |
| 6.3 | Frames' lateral deflection and interstorey drift due to the specified wind loads | 184 |
| 6.4 | Frames' lateral deflection and interstorey drift due to the anticipated earthquake loads | 185 |
| 6.5 | Effect of connection flexibility on lateral deflections of frames | 186 |
| 6.6 | Effect of connection flexibility on its moments due to factored gravity loads only | 187 |
| 6.7 | Effect of connection flexibility on columns' normal forces due to factored gravity loads | 188 |
| 6.8 | Effect of connection flexibility on its moments due to 1.25D+Q | 189 |

List of Figures (cont'd)


| Figure | | Page |
|---|---|---|
| 6.9 | Effect of connection flexibility on columns' bending moments due to 1.25D+Q | 190 |
| 6.10 | Effect of connection modelling on the static roof deflection | 191 |
| 6.11 | Effect of connection flexibility on the frames' roof static deflection | 192 |
| 6.12 | Target and generated spectral acceleration for high A/v ratio record | 193 |
| 6.13 | Target and generated spectral acceleration for low A/v ratio record | 193 |
| 6.14 | Ground acceleration and velocity time histories for high A/v ratio record | 194 |
| 6.15 | Ground acceleration and velocity time histories for low A/v ratio record | 195 |
| 6.16 | Effect of connection flexibility on storey shear envelopes (high A/v ratio record) | 196 |
| 6.17 | Effect of connection flexibility on floor displacement envelopes (high A/v ratio record) | 196 |
| 6.18 | Effect of connection flexibility on roof displacement history (high A/v ratio record) | 197 |
| 6.19 | Effect of connection flexibility on floor displacements (low A/v ratio record) | 198 |
| 6.20 | Effect of connection flexibility on roof displacement history (low A/v ratio record) | 199 |
| 6.21 | Storey shear and interstorey drift envelopes (low A/v ratio record) | 200 |
| 6.22 | Effect of connection flexibility on bending moments and normal forces envelopes of exterior columns (low A/v ratio record) | 201 |

List of Figures (cont'd)


| Figure | | Page |
|---|---|---|
| 6.23 | Effect of connection flexibility on bending moments and normal forces envelopes of interior columns (low A/v ratio record) | 202 |
| 6.24 | Maximum plastic beam and column rotations for frame Ffr (Rigid frame) | 203 |
| 6.25 | Maximum plastic beam and column rotations for frame Ff1 (Flexible frame) | 204 |
| A.1 | Different portion areas of the end-plate on the compression side of the connection | 212 |
| B.1 | Positive sign convention for beam segment MN | 216 |
| B.2 | End-plate model | 216 |
| C.1 | Deflection coefficients for simply supported column flange loaded at bolt locations | 220 |
| C.2 | Reduction factors for column flange deflections at the tension side of the connection | 221 |
| C.3 | Deflection coefficients for column flange with fixed longitudinal edges loaded at bolt locations | 222 |
| E.1 | Yield line mechansim of a stiffened column flange | 230 |
| F.1 | Deflection due to membrane action in the end-plate | 233 |
| F.2 | Deflection due to membrane action in HSS column | 234 |

## List of Tables


| Table | | Page |
|---|---|---|
| 2.1 | Strength comparison for different types of fasteners | 19 |
| 3.1 | Experimental program on beam-to-column connections | 51 |
| 3.2 | Mechanical properties of tensile coupons | 52 |
| 3.3 | Connection parameters of tested specimens | 52 |
| 4.1 | Predicted connection parameters of tested specimens | 112 |
| 5.1 | Minimum tensile strength of HSBB bolts and the corresponding minimum HSS column flange thicknesses | 145 |
| 6.1 | Member sizes for frame Frr | 178 |
| 6.2 | Member sizes for frames Ff1, Ff2, and Ffr | 178 |
| 6.3 | End-plate design for frame Ff1 | 179 |
| 6.4 | Connection model parameters for frame Ff1 | 179 |
| 6.5 | End-plate design for frame Ff2 | 180 |
| 6.6 | Connection model parameters for frame Ff2 | 180 |
| 6.7 | Fixity factors of the connections | 181 |
| 6.8 | Weight comparison between Frr and Ff1 | 181 |
| 6.9 | Comparison of frames load factors | 181 |
| 6.10 | Maximum rotations at failure | 182 |
| 6.11 | Free vibration periods of frames Ffr and Ff1 | 182 |
| D.1 | $\alpha_c$ values for HSS 177.8 x 177.8 mm | 224 |
| D.2 | $\alpha_c$ values for HSS 203 x 203 mm | 225 |
| D.3 | $\alpha_c$ values for HSS 254 x 254 mm | 226 |

List of Tables (cont'd)


| Table | | Page |
|---|---|---|
| D.4 | $\alpha_e$ values for HSS 304 x 304 mm | 227 |

## LIST OF SYMBOLS

$A$ = Peak ground acceleration expressed in units of gravitational acceleration

$A_s$ = Effective shear area of end plate

$A_w$ = Area of fillet weld surrouding the beam flange

$A^*$ = Cross section area

$a$ = Vertical distance between the bolt centre and the end-plate edge

$B_{ep}$ = End-plate width

$B_f$ = Width of the simply supported plate

$b$ = Vertical distance between the bolt centre and the centre line of the beam flange fillet weld

$b_c$ = Centre line dimension of HSS column flange ($H_o$-$t_o$)

$b_{dp}$ = Doubler plate width

$b_f$ = Beam flange width

$C$ = Rate of decay parameter

$C_f$ = Factored axial load in the column

$C_r$ = Factored axial compression resistance of the column

$D$ = Dead loads

$D_{cf}$ = Column flange bending rigidity

$D_{sw}$ = Side wall bending rigidity

$d$ = Bolt hole diameter

$d_b$ = Beam depth

$E$ = Young's modulus

$F$ = Foundation factor

List of Symbols (cont,d)

$f$ = Fixity factor

$F_b$ = Bolt force

$F_f$ = Tensile beam flange force which cause failure of bolts and yielding in end-plate

$F_r$ = Tensile factored resistance of HSBB

$F_t$ = Concentrated force at the top of the building

$G$ = Steel shear modulus

$H_o$ = Outer dimension of HSS column

$h_i$ = The height of the ith storey

$I$ = Importance factor

$I_b$ = Beam moment of inertia

$I_{eb}$ = Equivalent beam moment of inertia

$I_{ep}$ = End-plate moment of inertia

$K_b$ = Equivalent rotational spring stiffness

$K_i$ = Connection initial stiffness

$K_p$ = Connection post-elastic stiffness

$K_{sw}$ = Rotational spring stiffness of HSS side walls

$K^*$ = Diameter of primary sleeve after installation

$L$ = Live loads

$L_b$ = Length of beam

$L_{ep}$ = Length of the modeled end-plate

$L_s$ = length of HSS side wall

**List of Symbols (cont,d)**

$L_w$ = Surrounding perimeter of beam flange welds

$M$ = Connection moment

$M_{fx}$ = Factored bending moment about the major axis

$M_p$ = Beam plastic moment

$M_{pc}$ = Connection plastic moment

$M_{pp}$ = End-plate plastic moment capacity at bolt line

$M_r$ = Factored moment resistance

$M_u$ = Connection ultimate moment capacity

$M^*$ = The lesser moment of $1.25M_{pc}$ or $M_u$

$m_p$ = Plastic moment per unit length of the column flange

$m_p^*$ = Plastic moment per unit length of the doubler plate

$N$ = Number of storeys

$P$ = Beam flange force

$P_f$ = Designed beam flange force

$P_{p(cfc)}$ = Yield load of the column flange at the compression side

$P_{p(cft)}$ = Yield load of the column flange at the tension side

$P_{p(cp)}$ = Yield load of the end-plate

$P_{r(cf)}$ = Resistance of the stiffened column flange

$Q$ = Earthquake loads

$R$ = Force modification factor

$R_m$ = Bolt mean strength

**List of Symbols (cont,d)**

$R^*$ = Deflection reduction factor

$r_w$ = raduis of bolt's washer

$S$ = seismic response factor

$T$ = Structure natural period

$T_{min}$ = Minimum tensile strength of HSBB

$t_{bf}$ = Beam flange thickness

$t_{bw}$ = Beam web thickness

$t_{cf}$ = Equivalent column flange thickness

$t_{dp}$ = Doubler plate thickness

$t_{ep}$ = End-plate thickness

$t_{ep(eff)}$ = Effective end-plate thickness

$t_o$ = HSS column flange thickness

$t_{sw}$ = Equivalent side wall thickness

$W$ = Building weight

$W_i$ = Weight of the ith floor

$w_b$ = Weld size based on base metal

$w_{bf}$ = Size of beam flange fillet weld

$w_{bw}$ = Size of beam web fillet weld

$w_w$ = Weld size based on weld metal

$V$ = Building base shear

$V_R$ = Coefficient of variation

List of Symbols (cont,d)

$v$ = Zonal velocity ratio or peak ground velocity expressed in units of m/sec

$X_B$ = Horizontal distance between bolts

$X_u$ = Ulimate strength of weld

$Y_B$ = Vertical distance between bolts

$Z_b$ = Beam plastic section modulus

$Z_c$ = Column plastic section modulus

$\alpha$ = Bolt over strength factor

$\alpha_c$ = Coefficient to determine the average column flange deflection at the compression side

$\beta$ = Ratio between the horizontal bolt distance and $(H_o-t_o)$

$\beta_o$ = Ratio between the horizontal bolt distance and $(H_o-2t_o)$

$\beta^*$ = Safity Index

$\gamma$ = Ratio of bolt hole diameter to $(H_o-t_o)$

$\gamma_F$ = Coefficient to determine the column flange deflection at bolt locations with fixed edges

$\Delta_{cfc}$ = Average column flange deflection at the compression side

$\Delta_{cft}$ = Column flange deflection at bolt locations

$\Delta_{ep}$ = End-plate deflection

$\Delta_T$ = Total connection deformation

$\eta$ = Ratio of vertical bolt spacing to $(H_o-t_o)$

$\eta_o$ = Ratio of vertical bolt spacing to $(H_o-2t_o)$

$\theta$ = Connection rotation

List of Symbols (cont,d)

$\theta_u$ = Connection rotation corresponding to the connection ultimate moment capacity

$\theta_y$ = Rotation at yield load

$\upsilon$ = Possion's ratio

$\sigma$ = Stress intensity due to the compression beam flange force

$\sigma_o$ = Sample standard deviation

$\sigma_y$ = Yield stress of base metal

$\sigma_{yc}$ = Column flange yield stress

$\sigma_{yd}$ = Doubler plate yield stress

$\sigma_{ye}$ = End-plate yield stress

$\rho_R$ = Ratio of mean strength to the nominal strength

$\phi$ = Resistance factor of base metal

$\phi_b$ = Resistance factor of bolts

$\phi_w$ = Resistance factor of weld metal

$\Psi$ = Prying factor

$[K_s]$ = Spring stiffness matrix

# CHAPTER 1

# INTRODUCTION

## 1.1 General

Hollow structural sections (HSS) have been widely used in many structural applications, especially as columns, because of their efficient structural performance and attractive architectural appearance. While W-shapes are efficient for use as beams, a problem arises when these different shapes have to be connected to produce a moment connection. Normally, the steel fabricating industry opts for the use of field bolted connections rather than field welded connections. However, due to the lack of access inside the hollow section column for bolting purposes, it has been difficult to develop a practical bolted moment connection between these two members. As such, field welded beam-to-HSS column connections have been the only viable method. Because of problems of ensuring a dry environment and the concern about the quality of field welds, the use of hollow section columns in low to medium-rise moment resisting steel frames has been limited.

## 1.2 Literature review

There have been several attempts to develop a connection between a W-shape beam and a hollow section column. White and Fang (1966) conducted the earliest experimental work which dealt with shear connections that involved a semi welded-bolted assembly using plates, tees and seat angles, as shown in Fig 1.1. Sherman and Ales

(1991) tested 12 shear tab connections using a flexible beam and a stiff beam combined with HSS columns having full width to thickness ratios from 8.0 to 48.0. It was demonstrated that the minimum thickness for the column flange should be related to the shear tab thickness in order to force yielding of the tab rather than allowing possible punching shear failure of the column flange.

Because of the difficulty of bolting into HSS columns to develop moment connections, most research has been limited to welded moment connections. For the case when the beams are in one plane only and they are of the same depth it is possible to use strap angles which connect the beams to the column faces parallel to the beam as shown in Fig 1.2. One leg of the straps is welded to the beam flanges and the other is welded to the column sides. Experimental programs (Picard and Giroux, 1976 and 1977) established satisfactory details to develop the plastic moment capacity of tested beams. The first series of specimens basically used HSS 203x203 mm with W 200x52 beams which provided matching column and beam flange widths. The second series of tests used HSS 305x305 mm with mostly W 310x67 beams to give beam flange widths which were 2/3 the width of the column. For the first series, the strap angles were able to carry both the moment and the shear loads from the beams, so that beam web connections were not necessary. However, the second series required shear connections for the full beam shear to avoid twisting the strap angles. One specimen from the first series had a beam connected to one side of the column only. This connection performed almost identically to the two beam connection. Another approach to develop a moment connection between a W-shape beam and an HSS column was adopted by reinforcing the HSS column flange

with a doubler plate. Dawe and Grondin (1990), carried out an experimental and analytical program to determine the behaviour of different beam connections with various amounts of reinforcing. The connections were developed by using tension and compression flange plates with web clip angles or tension flange plates and seat angles welded to a doubler plate to reinforce the column walls, as shown in Fig 1.3. Eight failure modes were identified for such connections and semi-empirical expressions were developed to predict failure modes and the corresponding moment capacities. It was indicated that the stiffness of the connection is enhanced when the doubler plate is nearly as wide as the flat portion of the column flange. Seat angles were found to be more effective than flange plates in distributing the bottom beam flange force into the HSS column. Meanwhile, Tabuchi et al. (1988) and Kato et al. (1981) used exterior diaphragms fitted and welded around the HSS column and the beam flanges, with vertical web plates located between the diaphragms, as shown in Fig 1.4. For such assemblage, beams are connected in field by simple shear connections at the expected contraflexure points. This arrangement can be adapted to locations with two, three or four beams framing at a column. Six specimens were tested when moment, shear and axial loads were combined. The investigation confirmed that the diaphragm width beyond the column needs only to be 0.12 times the column width, and the diaphragm width to thickness ratio should be more restricted than $480/\sqrt{\sigma_y}$. Ting et al. (1991) suggested to broaden the beam flanges with tee stiffeners to deliver beam flange forces directly into the column side walls, as shown in Fig 1.5. It was found that such arrangement can effectively increase both strength and stiffness of the connection. However, due to the complex design and

installation of the discussed connections, their use in practice has been rather limited.

Special techniques were used to develop bolted moment connections. Maquoi et al. (1984) developed a novel beam-to-column connection by welding threaded studs onto the wall of the hollow section column. The failure load of the connection under monotonic loading was found to be comparable to the theoretical load by considering all possible failure modes. However, such a technique requires protection of the threads during erection and hence may not be very practical. Kanatani et al. (1987) conducted an experimental study on concrete filled hollow section columns to W-shape beams employing long high strength bolts to be tighten from outside the opposite flange of the HSS column, as shown in Fig 1.6. Such technique was used to solve two problems. One problem is the susceptibility of tubular column walls to local failure and the other problem is the difficulty of fabricating moment connections in the field. Meanwhile, Kato (1989) investigated a new type of connection developed by welding special circular threaded nuts to the column's flange through conical holes, as shown in Fig 1.7. Unfortunately, the majority of these innovative connections involve complex arrangements, increased fabrication and significant added cost.

Recently, new types of blind fasteners were developed (Huck International Inc., 1990) for use in situations where the rear side of a connection is inaccessible, as the case in connecting to HSS columns. These fasteners have not yet been used in structural applications, however, they have been used in mechanical and aerospace applications. High strength blind fasteners seem to have a good potential in moment connections. In this research study, the feasibility of bolted moment connection between a W-shape beam

and a square HSS column using blind fasteners is investigated. The selected connection uses an extended end-plate welded to the beam, as shown in Fig 1.8. The method of connection assemblage is to shop weld the end-plate to the beam, and then to bolt the plate to the flange of the HSS column in the field. The proposed connection has the potential for good quality control and economy.

The use of extended end-plate (EEP) connection for HSS columns has not been investigated, however, the behaviour of extended end-plate connections for W-shape columns was extensively studied by several researchers (Zoetemeijer, 1974; Packer and Morris, 1977; Krishnamurthy, 1978; Mann and Morris, 1979 and Wittereen, 1982; Murray, 1988). The performance of the EEP connections with W-shape columns were investigated experimentally under monotonic loading. Improved performance was obtained when transverse stiffeners between the flanges of the W-shape column were introduced. From studying the tension region of the connection, it was found that the beam tension flange and the end-plate, can be represented by isolated T-stubs (Packer and Morris, 1979). The increase in bolt forces due to prying action was also investigated. Typical modes of failure were observed and yield-line method was used to predict the column flange and the end-plate flexural yield loads. Good agreement between the predictions of the yield line approach and the test results was achieved. A limit state design was proposed for extended end-plate connections having four bolts in the tension side. The research study was extended to investigate the behaviour of the EEP connections under severe cyclic loading conditions by Johnstone and Walpole (1982), Ballio et al. (1986) and Tsia and Popov (1990). Special attention was paid by Ghobarah

et al. (1990, 1992) and Korol et al. (1991) and Osman et al. (1991) to the behaviour of the individual components in the connection (end-plate, column flange, panel zone and bolts) when subjected to cyclic loading, in order to develop analytical models to simulate the connection behaviour.

## 1.3 Objectives and scope of work

The objectives of this research study are to:

1) Develop a practical connection between a W-shape beam and a square HSS column using blind fasteners with the following features; sufficient moment capacity, sufficient stiffness, ease of construction and practical. Evaluate the behaviour of such connection experimentally under both monotonic and cyclic loading.

2) Develop an analytical model to simulate the connection behaviour, and propose a design procedure for the developed connection, and evaluate the effect of such connection on the behaviour of moment resisting frames.

To conduct the proposed research program, both an experimental and analytical approaches were adopted. An experimental program was conducted to test a simple cantilever type beam-to-column connection under both monotonic and cyclic loading. The new type of blind fastener being proposed was employed in both types of loading. In order to investigate the performance of the blind fasteners, a similar test was performed by using A325 high strength bolts, to be used as a base line in comparison. The

experimental work also included studying the effect of stiffening the column flange by either doubler plates or by filling the hollow section column with concrete.

The theoretical part of the study included developing a simple model to determine the behaviour of the proposed connection in terms of the moment-rotation relationship as well as proposing a design criterion for the connection. The model was incorporated into the Drain-2DX computer program to study the effect of such semi-rigid connections on the behaviour of low-rise steel frames under both static and dynamic loading.

## 1.4 Organization of the thesis

A review and description of two blind fastening systems as well as tensile test results of blind fasteners are presented in Chapter 2. The experimental program on extended end-plate connections for square HSS columns is described in Chapter 3. In Chapter 4, a non-linear model which is capable of simulating the connection behaviour in terms of its moment-rotation relationship is developed and described. The model was simplified as either a bi-linear or a tri-linear, in order to be incorporated in a plane frame program. A proposed design criterion for such connection is presented in Chapter 5. In Chapter 6, the effect of such connection flexibility on a 4-storey steel moment resisting frame was investigated and compared with similar frames with rigid connections. The frames were analyzed statically under monotonically increasing loading and dynamically when the frames were subjected to two earthquake input ground motions. Finally, Chapter 7 presents a summary and the significant conclusions of this study as well as recommendations for future research.

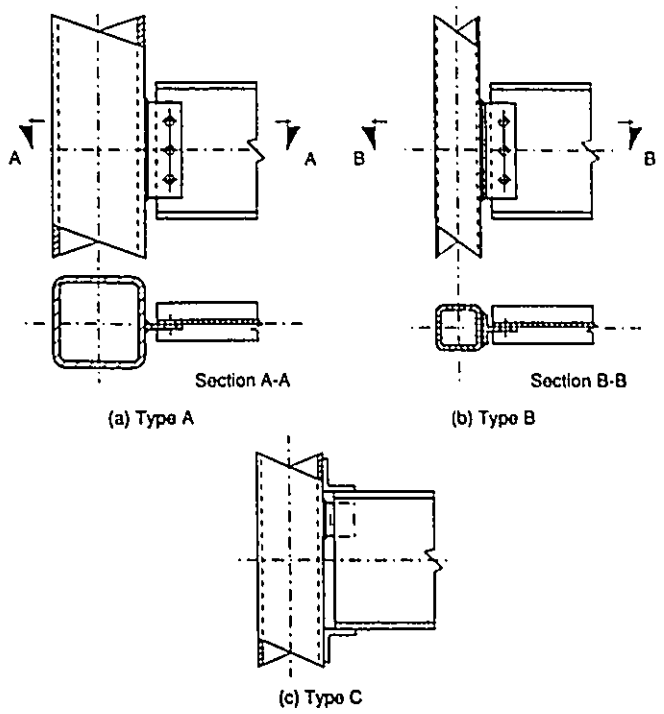


Fig 1.1 Types of simple connections tested by White and Fang (1966)

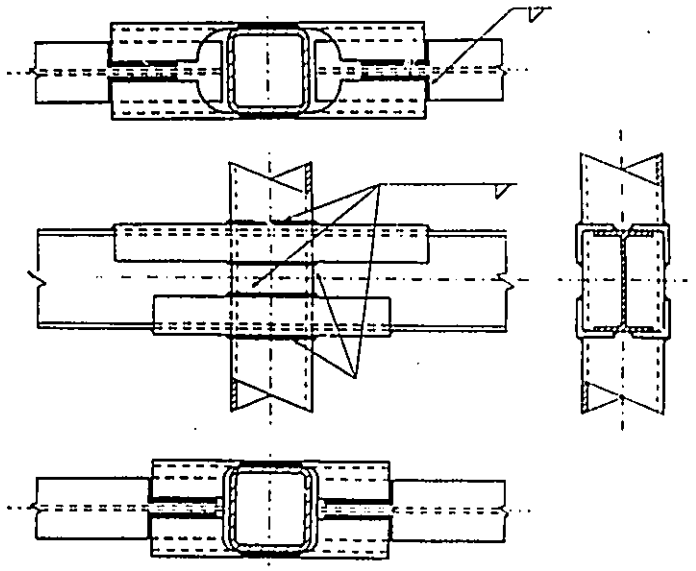

Fig 1.2 Strap angle moment connections tested by Picard and Giroux (1977)

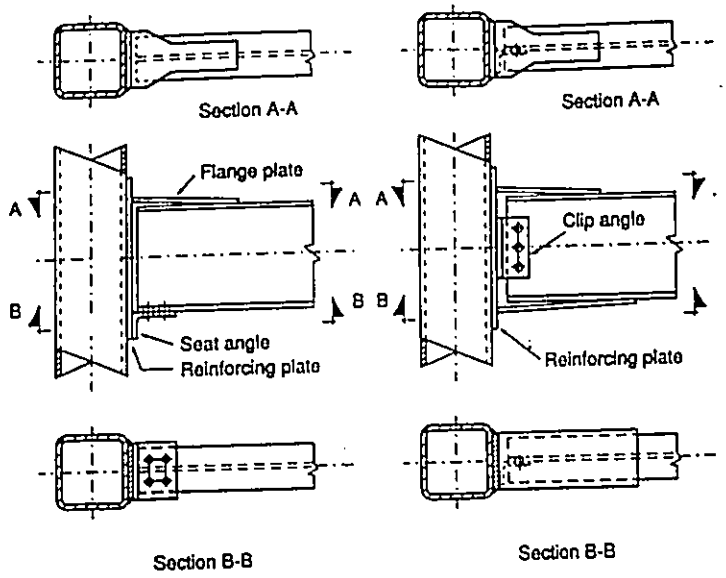


Fig 1.3 Types of moment connections tested by Dawe and Grondin (1990)

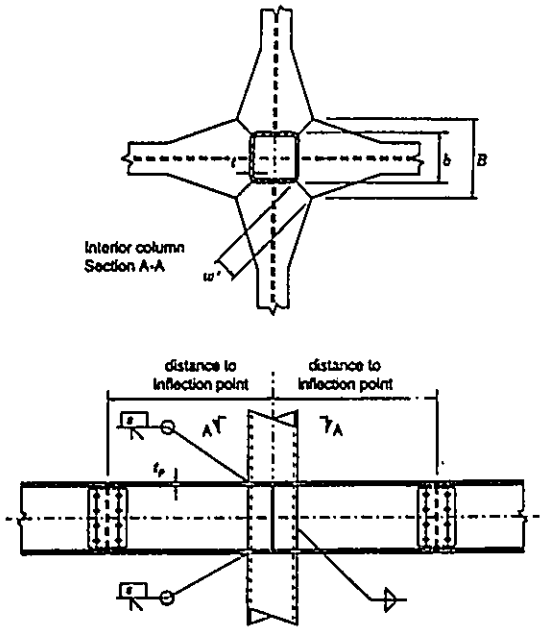


Fig 1.4 Flange diaphragm moment connections tested by Kato et al. (1981)

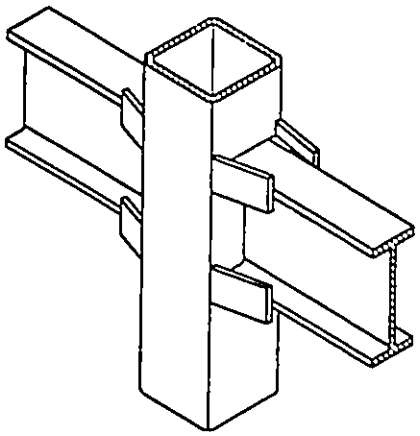

Fig 1.5 Stiffening by tees on the beam flanges
(after Ting et al. 1991)

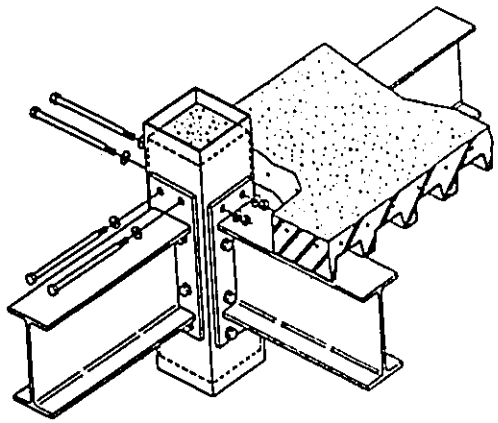

Fig 1.6 Moment connections developed by long bolts
(after Kanatani et al. 1987)

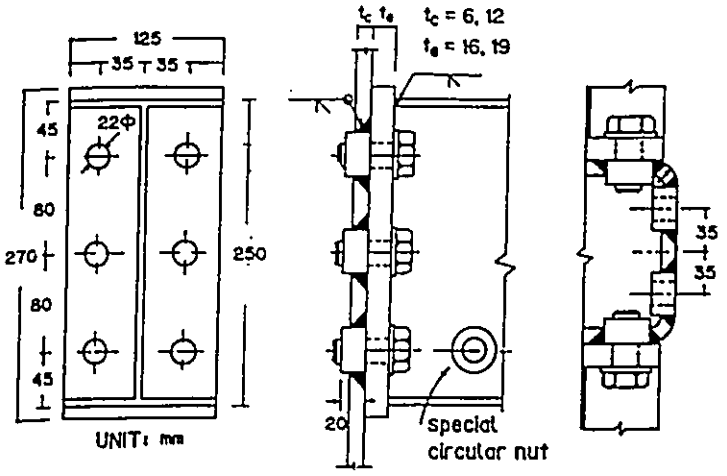


Fig 1.7 A moment connection with nuts welded on the column flange (after Kato 1989)

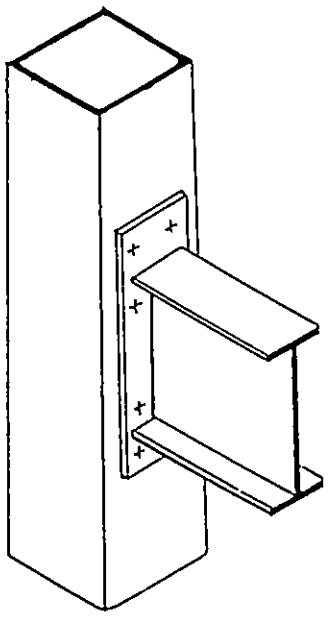

Fig 1.8 A typical extended end-plate connection for HSS column

# CHAPTER 2

# BLIND FASTENING SYSTEM

## 2.1 Introduction

In recent years, there has been a remarkable revolution in the development of new fastening systems (Huck International Inc., 1990) to be used in special industry applications such as aerospace and automotive industries. One of these fastening systems is known as a swage lock fastening system. By virtue of its design, it provides a consistent clamping force achieved through direct tension application. Swage lock fastening includes blind fasteners which are developed to be used in applications where access for installation is from one side of the connection only, such as in the case of connecting a beam's end-plate to a hollow section column. Blind fasteners can be installed by unskilled operators using electric-hydraulic equipment that is potentially portable on a job site. In this Chapter, two types of blind fasteners are introduced and their strengths are compared with similar sizes of A325 high strength bolts.

## 2.2 Types of blind fastening systems

### 2.2.1 BOM fastening system

One type of blind fastener that was investigated is known by the blind oversized mechanically locked (BOM) fastener. A schematic of BOM fastener before and after installation is shown in Fig 2.1. As can be noted that, the BOM fastener is a four piece mechanism. A set of diagrams of the BOM fastener installation sequence is shown in Fig

2.2. The installation tool grips the pintail, draws the fastener toward the exterior side of the connection, upsets the sleeve to form a head at the blind side of the connection, and then acts to swage the collar into the locking grooves on the exterior side of the connection. At this point, the pintail breaks off and is removed from the tool. The clamping forces in the BOM fasteners are developed during the installation process. The fasteners are available in different diameters ranging from 4.77 mm (3/16") to 19.08 mm (3/4") with a grip range up to 31.8 mm (1.25"). These fasteners have tensile strengths that are about 70% that of A325 bolts. However, their shear capacity is about twice that of A325 bolts of similar diameters when including the threads in the shear plane, as shown in Table 2.1. The high shear resistance of the BOM fastener is attributed to the higher heat treatment of its pin, thus allowing a higher level of hardness and strength than exhibited by the A325 bolts. Because of a BOM's high shear resistance, they are particularly suitable for shear connections.

### 2.2.2 HSBB fastening system

High strength blind bolt (HSBB) have been recently developed to meet the equivalent of ASTM specifications (1991) for A325 high strength bolts. HSBB fasteners have not been used in structural applications. A schematic representation of the HSBB before and after installation is shown in Fig 2.3. The HSBB fastener consists of six pieces. Its installation sequence is similar to that of the BOM fastener. However, the head on the blind side is formed by deforming the primary sleeve into a conical shape to be in full contact with the inner face of the connection, as shown in Fig 2.4. The tool

used in installation is potentially portable on a job site and is shown in Fig 2.5. The minimum tensile strength, clamping force and shear strength of HSBB fasteners (as provided by the manufacturer) are almost equal to those of similar sized A325 high strength bolts, as summarized in Table 2.1. Therefore, HSBB fasteners have the potential for use in tension applications and moment connections. It should be noted that, because of the presence of the sleeves in HSBB, the core bolt shank diameter is less than the nominal size of the equivalent size A325 bolt (20 mm HSBB has a core bolt shank diameter about 15 mm).

## 2.3 Tensile tests

To gain an appreciation for the difference in behaviour of the various fasteners under tensile loads, direct tensile tests were conducted on BOM and HSBB fasteners and compared to A325 bolts. Because of the limitations on available sizes of blind fasteners, only the one size of BOM fastener (3/4") and 20 mm HSBB were used in the tensile tests. Ten tensile tests were conducted on three installed 19 mm (3/4") BOM fastener, four installed 20 mm HSBB and three installed 19 mm (3/4") A325 bolts. The pre-tension forces in the A325 bolts were developed by the turn-of-nut method, while, the pre-tension forces in blind fasteners were developed during the installation process. A special testing device was constructed as shown in Fig 2.6, consisting of two 15 mm thick circular plates. Two Linear Variable Displacement Transducers (LVDTs) were mounted to measure the separation of the two plates. A washer was welded to an arm with the same thickness and placed between the two plates before installation to establish

the commencement of separation. The clamping force was determined when it was possible to move the washer between the two plates during the test. The testing device was attached to each of the circular plates by means of 6-12 mm bolts arranged around the plate. The testing device was attached to 25 mm high strength steel rod on each side and placed in a Tinius Machine for testing. Typical load-separation relationships for the three types of bolts are shown in Fig 2.7. The tensile tests on the A325 bolts were terminated at the point either when the shank failed or when the threads started to yield causing a drop in load carrying capacity of the bolt. The separation at failure, noted in Fig 2.7, was for an installed pre-tensioned A325 bolt, and hence it would be expected to be less than the elongation specified in the ASTM specifications (1991). The BOM bolts failed by shearing of the sleeve underneath and around the core bolt's blind head before the fracture of its pin, while the HSBB failed either by plastic deformation and bending of the primary sleeve or by stripping the swaged threads in the collar. In all cases, the HSBB and BOM bolts failed in a ductile manner. It should be noted that the large separation recorded for HSBB near its ultimate strength in Fig 2.7, is not only attributed to the elongation of the core bolt shank, but also due to the bending and compression deformation of the primary sleeve which became embedded in the 15 mm steel plate as well as the deformation of the swaged threads in the collar.

In order to examine the consistency of the HSBB tensile strength, the results of 20 tensile tests conducted by the manufacturer on 20 mm HSBB were obtained. There was a range of grip lengths ranging from 35 to 40 mm. These test results in addition to

the four described herein, were considered as a valid sample for a statistical analysis. The test results, the mean strength value and two standard deviations below and above the mean value are plotted in Fig 2.8. The following statistical quantities were calculated for that type of fastener;

Mean strength, $R_m$ = 198 kN

Sample standard deviation, $\sigma_o$ = 7.29 kN

Sample coefficient of variation, $V_R$ = 0.037

Mean strength to the nominal strength ratio, $\rho_R$ = 1.03

It can be noted that the test results are consistent and closely distributed around the mean value which is 3% higher than the nominal strength. Therefore, an over strength factor $\alpha$, can be defined as the ratio of the maximum tensile strength to the nominal tensile strength of the HSBB. The maximum tensile strength of HSBB is considered to be 2 $\sigma_o$ above the mean value. The over strength factor $\alpha$ can be used to determine the maximum tensile strength of HSBB based on its nominal strength and it was found to be equal to 1.11. For this sample, it was found that six fasteners had tensile strength less than the minimum tensile strength specified by the manufacturer (192 kN), however, the lowest strength was only 2.5% less than the minimum specified tensile strength.

## 2.4 Resistance factor of HSBB

The resistance factor $\phi$, is introduced in both Limit State Design (CSA- S16.1-M89) and Load Resistance Factor Design (AISC) to account for the variation of the element strength from the nominal value, and is expressed as given by Fisher et al. (1978) as follows;

$$\phi = \rho_R \; e^{(-0.55\,\beta^* V_R)} \qquad (2.1)$$

where, $\beta^*$ is a safety index and is equal to 4.5 for connectors (fasteners and welds) as suggested by Fisher et al. (1978) to have higher degree of reliability than the members they join. $\rho_R$ is the ratio of the mean strength to the nominal strength, while $V_R$ is the strength coefficient of variation.

By substituting the values of $\rho_R$ and $V_R$ into Eq 2.1, the resistance factor of HSBB bolts $\phi_b$, was found to be equal to 0.94. For comparison, the resistance factor for A325 bolts in tension, as given by Fisher et al. (1978), was equal to 0.97. It is concluded that, the resistance factor of HSBB is almost equal to that of A325 bolts.

However, the Load Resistance Factored Design (AISC) reduced the resistance factor of bolts to 0.75, while the Limit State Design Code of steel buildings (CSA-S16.1-M89) reduced the resistance factor of bolts to 0.67, to insure that bolts will not fail before the member. Until a more comprehensive study of the tensile strength of HSBB

is conducted on a larger scale, it is suggested that the resistance factor of HSBB $\phi_b$, be taken conservatively equal to 0.67 as given by CSA S16.1-M89. Therefore, the factored resistance of HSBB "$T_r$", is given by;

$$T_r = \phi_b T_{min} \tag{2.2}$$

where, $\phi_b = 0.67$ and $T_{min}$ is the minimum specified tensile strength of HSBB as provided by the manufacturer and given in Table 2.1.

## 2.5 Summary

The blind fastening system which includes BOM and HSBB fasteners was reviewed. It was shown that, HSBB fasteners have a comparable strength to that of a high strength A325 bolts. This indicates that the HSBB fasteners have a good potential to be used in structural connections especially those involving tension applications such as moment connections of steel beams to rectangular or square hollow section columns.

Table 2.1 Strength comparison for different types of fasteners

| Fastener type | Bolt size | Minimum tensile strength (kN) | Minimum clamping force (kN) | Minimum shear strength (kN) |
|---|---|---|---|---|
| **A325** | 16 mm | 125 | 88 | 100[1] - 70[2] |
| | 20 mm | 196 | 137 | 157[1] - 109[2] |
| | 22 mm | 237 | 166 | 190[1] - 133[2] |
| | 24 mm | 281 | 197 | 225[1] - 158[2] |
| | 28 mm (1-1/8") | 349 | 244 | 279[1] - 195[2] |
| **BOM** | 16 mm (5/8") | 91 | N/A | 142 |
| | 19 mm (3/4") | 130 | 30[3] | 200 |
| **HSBB** | 16 mm | 124 | 83 | 65 |
| | 20 mm | 192 | 130 | 91 |
| | 22 mm | 237 | 162 | 118 |
| | 24 mm | 276 | 188 | N/A |
| | 28 mm | 376 | 256 | N/A |

(1) Threads are excluded from the shear plane
(2) Threads are included in the shear plane
(3) Based on test results described herein

N.B: All above strength values for BOM and HSBB fasteners are provided by the manufacturer

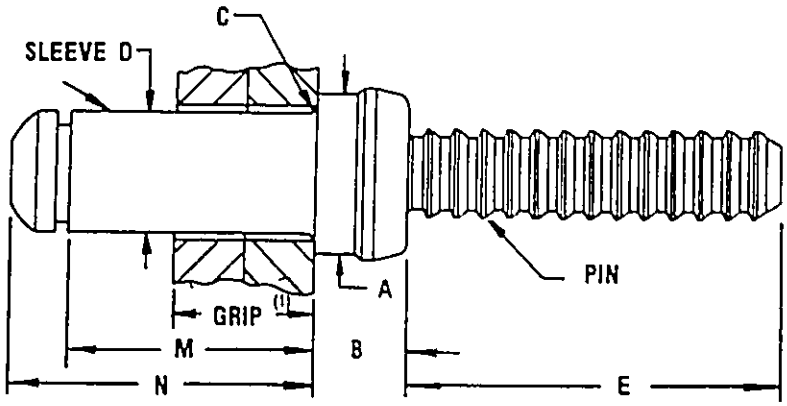


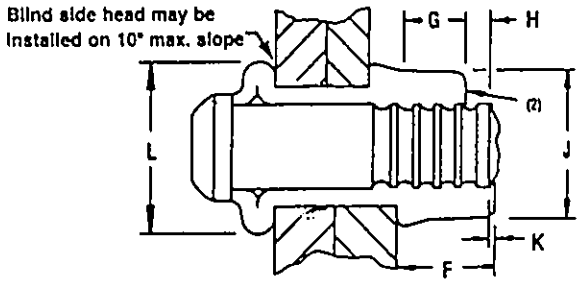


Installed Fastener

*(1) Grip is actual thickness of material to be fastened*

*(2) Huck Symbol*

( courtesy of Huck International Inc.)

Fig 2.1 BOM fastener before and after installation

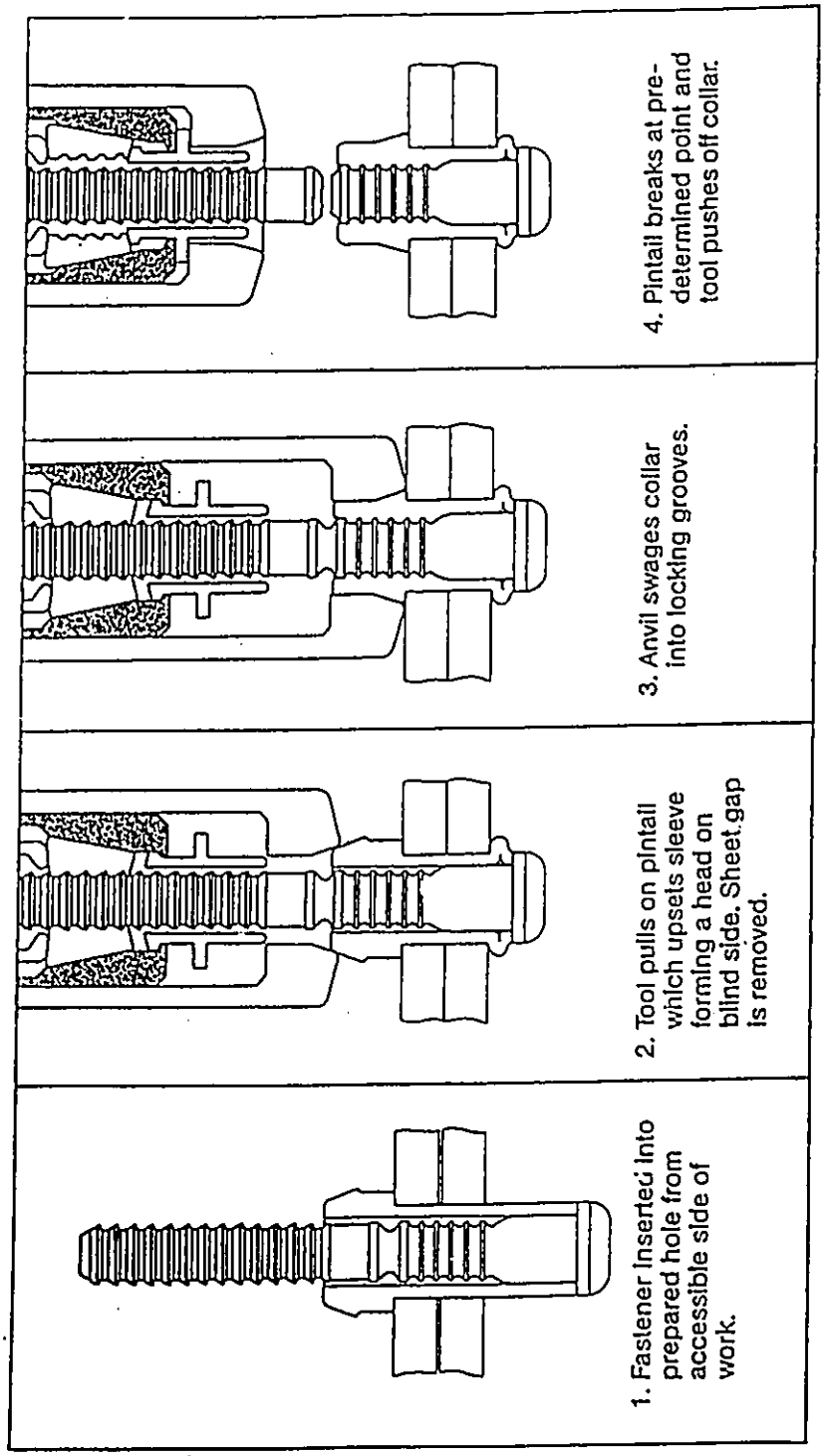


( courtesy of Huck International Inc.)

Fig 2.2 Installation sequence for BOM fasteners

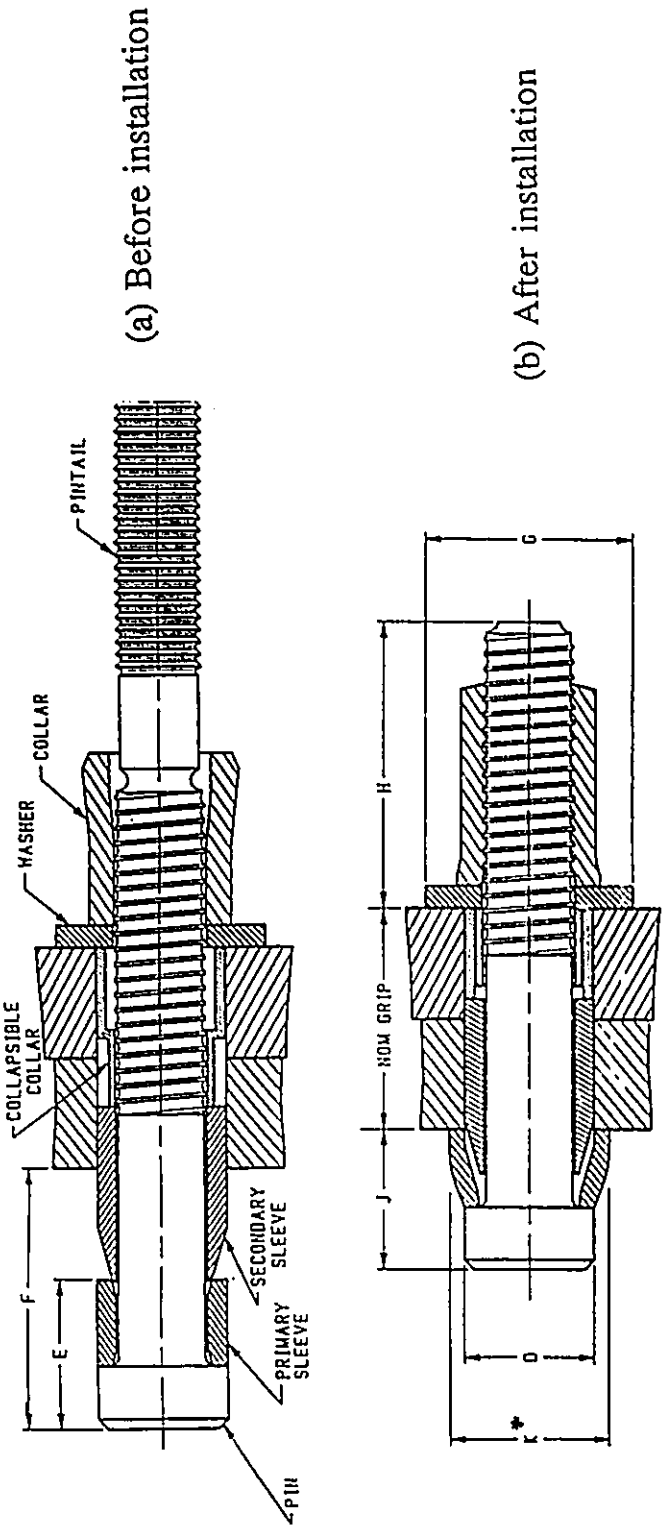


( courtesy of Huck International Inc.)

Fig 2.3 HSBB before and after installation

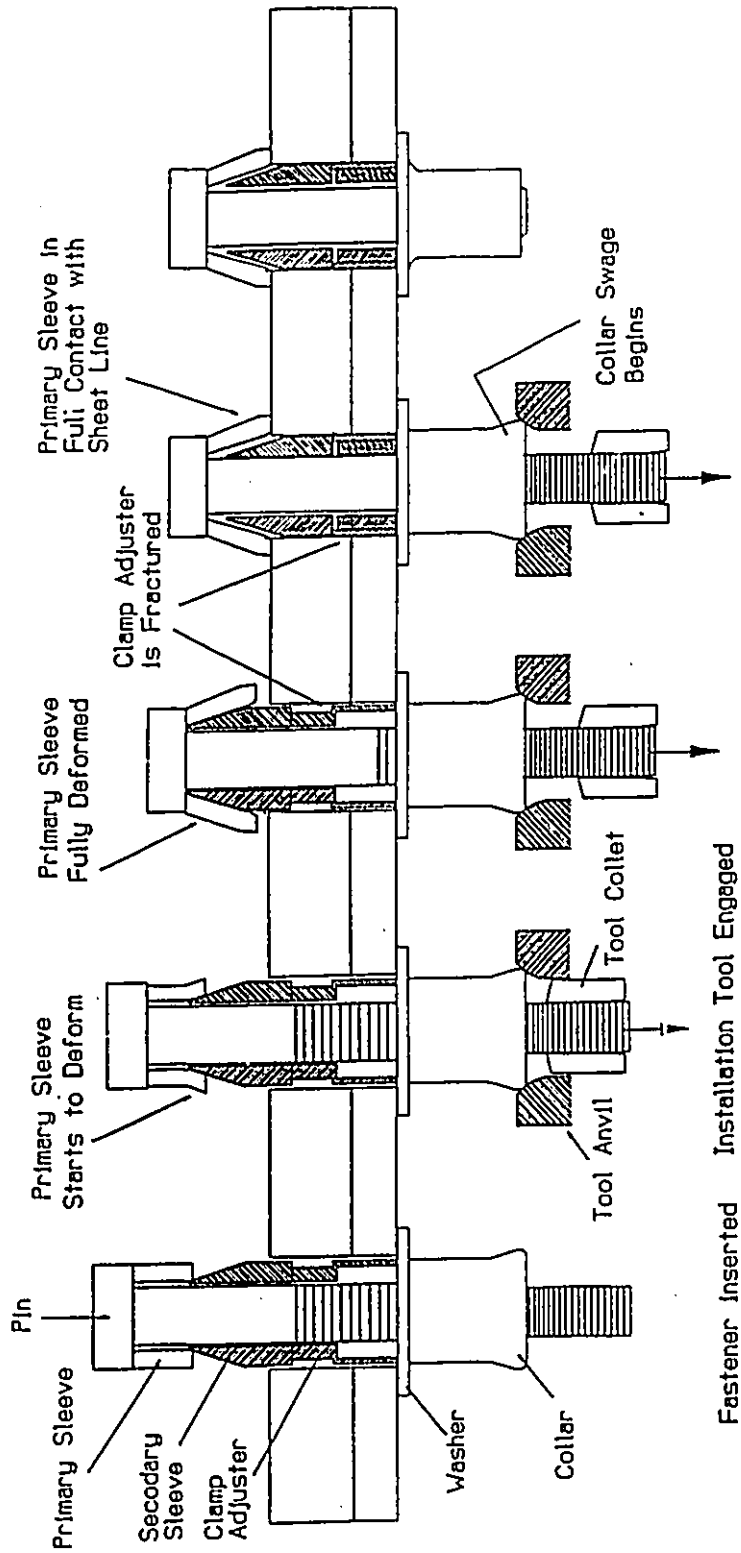


( courtesy of Huck International Inc.)

Fig 2.4 Installation sequence for HSBB fasteners

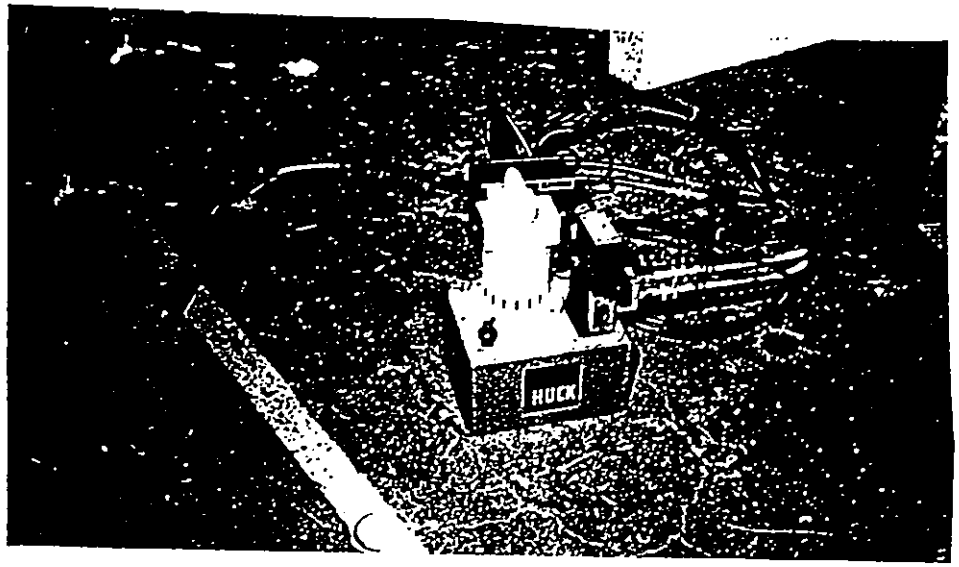


Fig 2.5 Installation equipment for HSSB fasteners

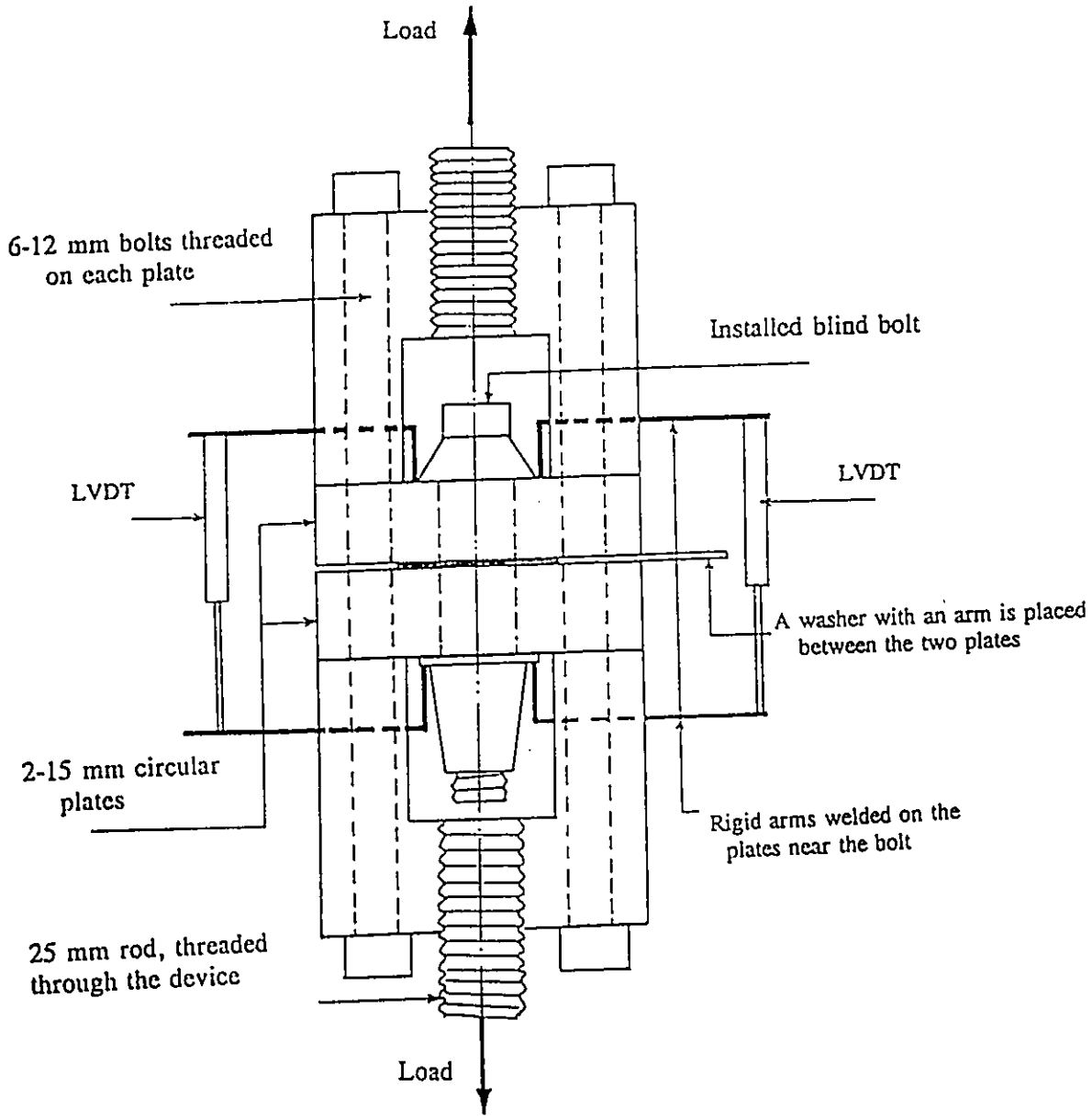


Fig 2.6 Details of testing device

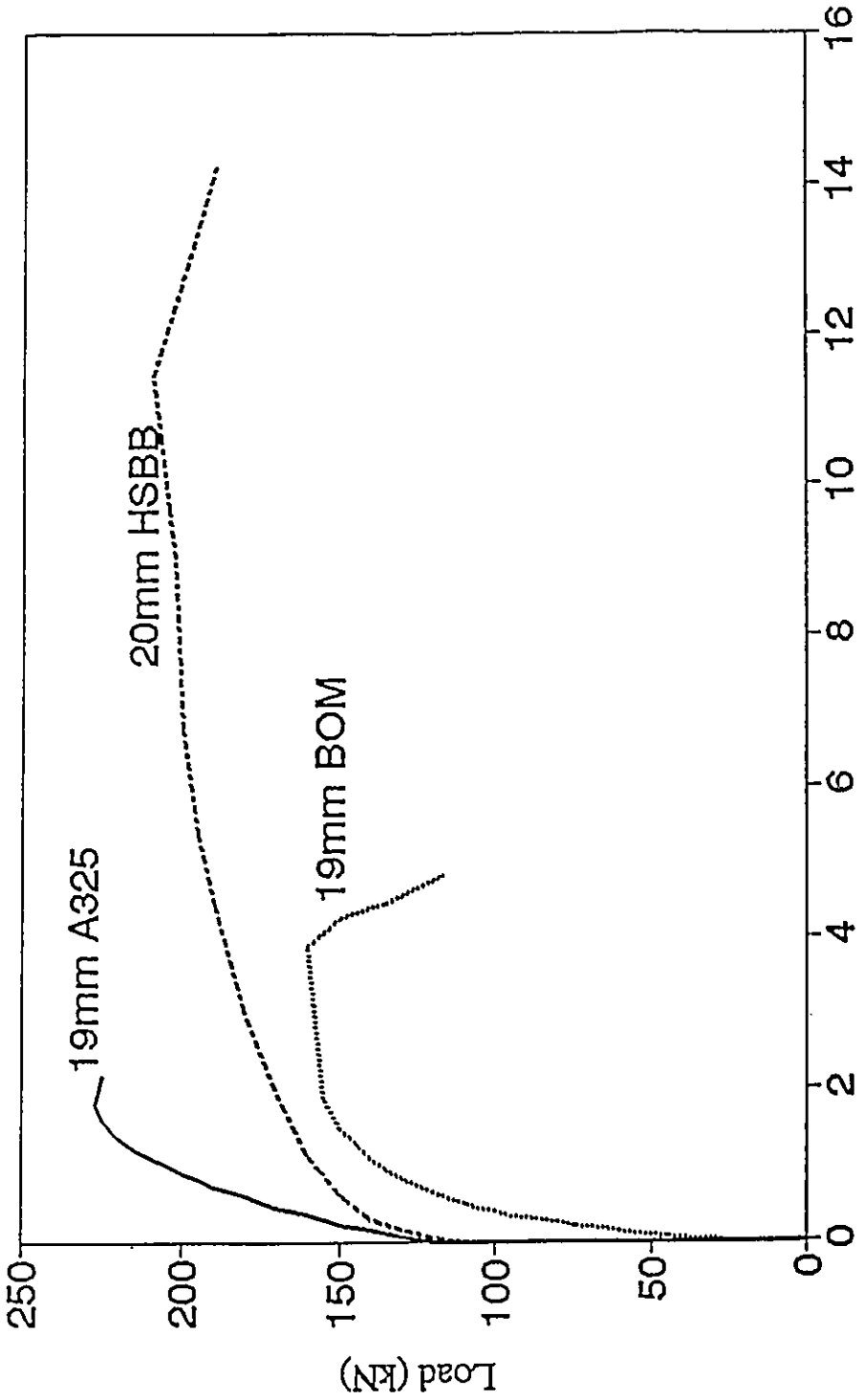


Fig 2.7 Typical load-separation relationship for different types of bolts

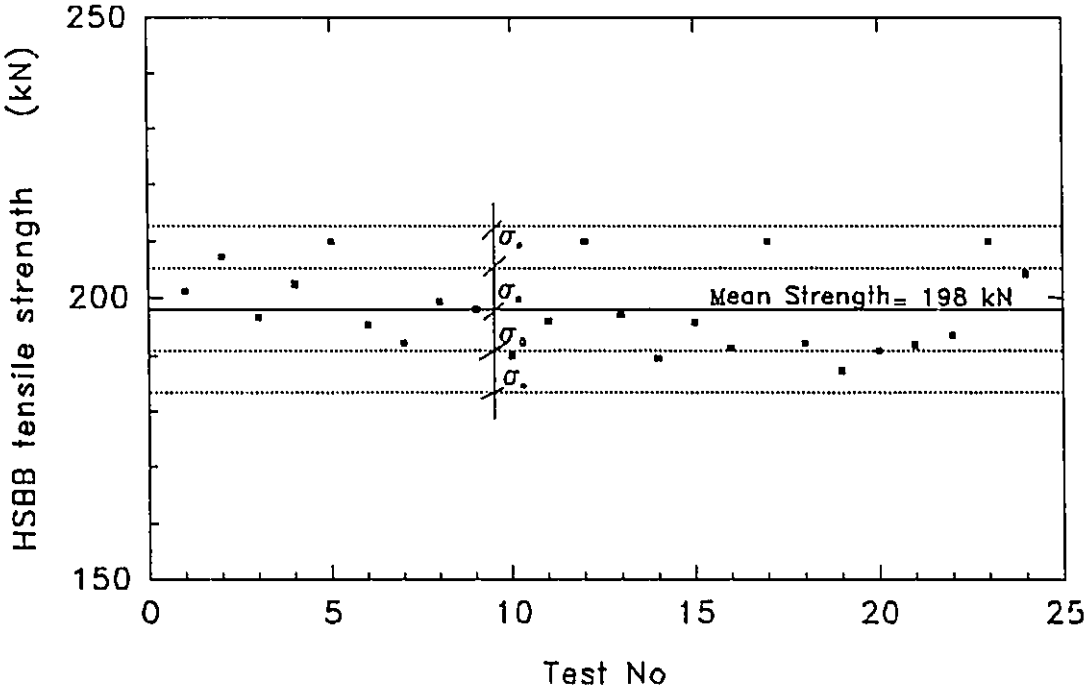


Fig 2.8 Tensile test results of HSBB fasteners

# CHAPTER 3

# EXPERIMENTAL PROGRAM ON EXTENDED END-PLATE CONNECTIONS

## 3.1 Introduction

In this chapter, the potential for using the blind fasteners in an extended end-plate connection for square hollow structural section "HSS" columns is investigated. The proposed connection, shown in Fig 3.1, is assembled by welding an extended end-plate to the W-shape beam in the shop, and then bolting the plate to the flange of an HSS column in the field. Such a connection permits shop welding of the end-plate and on-site bolting, hallmarks for good quality control and economy. An experimental program on such connections was conducted. The objective of the tests was to compare the connections' performance using blind fasteners with a similar one using ordinary high strength A325 bolts. In addition, it was interesting to compare different connections' behaviour in terms of their moment-rotation relationships, moment capacities and different modes of failure. The effect of cyclic loading on such connections was also included in the experimental program.

## 3.2 Experimental program

In the design of the testing program, the beams' section, W 360X33, was unchanged in all specimens. The experimental program consisted of 9 specimens tested in 3 phases, as summarized in Table 3.1.

Phase 1.

In the first phase, the behaviour of the connection under monotonic loading was determined when using the new type of blind fasteners (BOM & HSBB) as well as A325 high strength bolts. Three identical beam-to-column connections (S1, S2 & S3) were fabricated, the only difference being the type of bolts used. In test specimen S1, 3/4" diameter A325 bolts were used, while 3/4" BOM fasteners were used for S2 and 20 mm HSBB were used for S3.

Phase 2.

In this phase, large column sizes with thinner wall thicknesses and different end-plate dimensions were employed in the beam-to-column connections to evaluate different possible modes of failure. Also, the effect of stiffening the column flange either by welding a 6 mm doubler plate or filling the HSS with concrete was included in this phase. Phase 2 consisted of 4 specimens (S4, S5, S6 & S7) tested under monotonic loading. Specimen S6 was identical to S4 except that a 6mm doubler plate was welded onto the column flange of specimen S6. Specimens S5 and S7 were identical except that the column stub of specimen S7 was filled with concrete.

Phase 3.

In phase 3, specimens C1 & C2 were tested under increasingly cyclic loading. These two specimens were considered as pilot tests to determine the effect of cyclic loading on connection behaviour. Specimen C1 was the same as S5 except that a 6mm

doubler plate was welded onto the column flange of specimen C1 as shown in Table 3.1. Specimen C2 duplicated S6 but with bolts closer to the beam's flange to reduce end plate bending and prying action.

### 3.3 Specimens design and fabrication

A simple cantilever type beam-to-column specimen was selected to represent a subassemblage of a moment resisting frame as shown in Fig.3.2. The material used for all nine specimens including beams, end plates and doubler plates was in accordance with specification CSA G40.21-M92-300W, which is applicable to steel having a minimum yield strength of 300 MPa and certain other characteristics (e.g. weldable). The hollow section stub columns conformed to CSA G40.21-M92 class H with a minimum yield strength of 350 MPa. Standard tensile tests (ASTM No. A370-92), were conducted on coupons from HSS columns, beams, end-plates and doubler plates to assess the members' actual mechanical properties. The average tensile test results of two coupons from each element are listed in Table 3.2. Such values are beleived to be applicable to a typical connection, provided that it is tested under a slow rate of loading.

The beam section was selected to be a plastic design section, a W360x33, class 1, with its nominal plastic moment being 162 kN.m. The thicknesses of end plates and column flanges were designed in accordance with the beam's flange forces resulting from the beam's nominal plastic moment. The yield line mechanism developed by Packer and Morris (1977) was used as a guideline in determining the end-plate thickness, while an assumed yield line mechanism was used to evaluate the column flange thickness. In this regard, each one of the group of four bolts on one side of the connection was assumed

to resist the beam's tension flange force (associated with the nominal beam plastic moment). To focus on the behaviour of the connection itself (column flange, end plate and the fasteners) while achieving ultimate capacity, it was deemed preferable to eliminate plastic deformation from taking place in the beams during the early stages of loading. To insure that the beam behaves in a linear elastic manner to near the end of each test, its top and bottom flanges were stiffened by 6 mm thick cover plates near the connection, as shown in Fig.3.2. The stiffened beam was welded to the end plate by 12 mm and 6 mm fillet welds for the stiffened flange and web respectively. All welds were made using compatible electrodes, with the welding being in accordance with CSA-W59. The welds were visually inspected and repaired if any defects were discovered. The nominal plastic moment of the stiffened beam was 225 kN.m based on the nominal yield stress 300 MPa, while its actual plastic moment was 233 kN.m.

For specimens S6, C1 and C2, a doubler plate (1000x220x6 mm) was welded onto the column flange around its perimeter using 6 mm filet welds and 6 plug welds each of 12 mm diameter along a vertical line located between the bolts. Bolt holes were drilled 2 mm larger than the nominal bolt diameter. It should be noted that due to the absence of the internal washer between the bolt's head and the column flange, the tolerance in the hole's diameter in the column flange for blind fasteners is more restricted than that for ordinary bolts to permit proper upsetting of the sleeve on the blind side of the connection. Consequently, the hole diameter in the HSS column for 20 mm HSBB should be about 22 mm, given that the diameter of the bolt head is 21.5 mm. In the case of S1, the pre-tensioned force in A325 bolts was achieved by the turn-of-the-nut method.

It should be noted that the full pre-tensioning force in HSBB bolts is developed at the moment of installation. The sequence of installing the blind bolts was done in a diagonal manner across the end-plate as illustrated in Fig 3.3, to minimize any relaxation in the pre-tensioning force of the bolts resulting from end-plate deformations.

The connection configurations for the nine tested specimens are shown in Fig 3.4 and are described as follows;

**a) Specimens S1, S2 and S3**

In order to compare the performance of the BOM and HSBB blind bolts with A325 bolts, the first three specimen S1, S2 and S3 were designed to be identical. The only difference was in the type of bolt used in the connection. In test specimen S1, 3/4" diameter A325 bolts were used, while 3/4" BOM bolts were used for S2 and 20 mm HSBB were used for S3. The stiffened beam was welded to a 19 mm thick end-plate (520x170 mm) and bolted to the 203x203x12.7 mm column stub. The connection configuration for the specimens is shown in Fig 3.4.a.

**b) Specimens S4 and S6**

Specimen S4 was constructed by welding a 19mm thick end-plate (550x230 mm) to the stiffened beam and employing eight 20mm HSBB to connect it to an HSS 254x254x9.53mm column stub. Specimen S6 was identical to S4, however, the column flange of specimen S6 was stiffened by welding a 6mm doubler plate (1000x220 mm) onto its column flange. Further details are shown in Fig 3.4.b.

**c) Specimens S5, S7 and C1**

Specimen S5 was constructed by welding a 22 mm thick end-plate (550x230 mm) to the stiffened beam. Due to the limited number of HSBB available at the time of testing, only four 20 mm HSBB were used on the tension side of the connection and four 3/4" A325 bolts were used on the compression side to connect the end-plate to the 254x254x11.13 mm column stub. The response of the connection was not expected to be different from one employing eight HSBB fasteners. Specimen S7 was identical to S5 except that the column stub of specimen S7 was stiffened by filling it with concrete with a nominal strength of 25 MPa, after installing the high strength blind bolts. Specimen C1 was a duplicate of specimen S5, except that the column flange of specimen C1 was stiffened by welding a 6mm doubler plate (550x230 mm) onto its column flange. Details are given in Fig.3.4.c.

**d) Specimen C2**

Specimen C2 was identical to specimen S6, however, the HSBB were installed closer to the beam's flange with larger end-plate edge distance, to reduce end plate bending and prying action in the bolts. Details of specimen C2 are shown in Fig.3.4.d.

## 3.4 Test setup

A reaction frame was fabricated especially for use in the tests. To prevent overall rotation of the column, the column stub was rigidly clamped to the fixture frame by sixteen 25 mm diameter grade A490 bolts. The frame was prestressed to the 600 mm

thick floor slab of the laboratory by four threaded 50 mm diameter rods. A hydraulic actuator was used to apply the load to the beam tip in a vertical direction. The actuator was fixed to the floor by a pair of stiff angles prestressed to the floor slab by two 38 mm rods. The general arrangement of the set-up is shown in Fig.3.5. A clevis welded to a 50 mm diameter high grade steel rod was bolted to the end of the beam by a 50 mm diameter pin, the other end of which was connected to the actuator. Two angles were installed near the end of the beam to provide lateral support to prevent lateral buckling.

## 3.5 Instrumentation

To monitor the actuator load, a special built-up load cell was used. The cell consisted of eight strain gages attached to the actuator rod (four transversely and four longitudinally). The load cell was calibrated after each test on a uniaxial Tinius machine. A cable type linear voltage displacement transducer (LVDT) was used to measure the beam-tip displacement. Sixteen LVDTs were used to measure the connection deformation at different locations as illustrated in Fig 3.6. Four LVDTs were used to measure the total connection deformation and hence its rotation, L1 and L2 measured the total connection deformation at the compression of the connection, while L3 and L4 measured the total connection deformation at the tension side. Another four LVDTs were located on the centre of HSS side walls to measure the out-of-plane deformation; L5 and L6 mounted at the compression side of the connection, while L7 and L8 were mounted at the tension side. Eight LVDTs were positioned inside the HSS column stub to measure the out-of-plane deformation of the column flange of which three (L9, L10 and L11)

were at the level of the beam's compression flange with four (L12, L13, L14 and L15) located on the bolt heads on the tension side of the connection. The eighth LVDT (L16) was mounted at the centre of the beam's tension flange, as shown in Fig 3.6. Strain gages were used to monitor the stresses in the beam flanges and to determine initial yielding of the beam. All data from the strain gages and transducers were scanned by a multi-channel Autodata 9 scanner system. The readings were recorded using a micro-computer system and were also punched onto a paper tape device to provide backup. White wash was painted on the sides of the HSS column stub, the inside face of the column flange, and, as well as the beam near the connections to reveal where large inelastic deformations would take place. A carbon-paper sheet was placed between the end plate and the column flange before bolt installation to reveal the relative intensity and the distribution of the prying action between the two faces.

### 3.6 Loading sequence

Specimens S1 to S7 were loaded monotonically until the connection reached its ultimate capacity. To simulate the effect of seismic loads, the test specimens C1 and C2 were subjected to a quasi-static cyclic loading. Although in practice the severe lateral loads are of a dynamic nature, the rate of strain developed in the structural system is not sufficiently high to introduce significant variations in the so-called "Static Characteristics" of the steel material (Almuti and Hanson, 1973).

Since the specimens were expected to be loaded past the elastic range, the loading sequence was controlled by the beam-tip displacement in terms of the beam's yield

displacement rather than the beam-tip load. The beam-tip yield displacement is defined as the beam-tip displacement corresponding to the expected beam-tip load which would cause initial yielding in the unstiffened beam. Firstly, the specimens were subjected to four load cycles of half the expected yield load value. The behaviour of the connection and the beam were therefore expected to be elastic. This pre-test technique was employed to ensure proper connection setup, welding, bolting and to check the data recording devices for proper functioning. The load was increased until it reached the expected yield load value. Two cycles of reversed loads of this magnitude were then slowly applied. For subsequent loading cycles, the beam-tip displacement was incrementally increased by half yield displacement up to ductility of four (Displacement ductility is defined as the ratio of the beam-tip displacement to the beam-tip displacement at first yield). If no failure was detected, two additional cycles, one at five and another at six displacement ductility, were applied. Subsequently, the test was terminated since at this level a high ductility was achieved. A typical loading sequence for the test is shown in Fig 3.7. During both monotonic and cyclic loading, the load was temporarily stopped at each 5 mm displacement increment to allow for scanning the strain gages and transducers by the data acquisition system.

## 3.7 Experimental measurements

The data recorded during each test can be grouped into the following categories; 1- beam-tip load versus beam-tip deformation relationship. This provides the basic data for determining the overall behaviour of the specimen.

2- beam flange force versus the total connection deformation at the tension side (average reading of LVDTs L3 and L4). The average deformation of HSS column flange at bolt locations (L12, L13, L14, L15) as well as at the centre of the bolt group (L16) were recorded for each test and compared with the total connection deformation at the tension side. A typical test behaviour of specimen S3 is shown in Fig 3.8. The deformation of the HSS column flange at the centre of the bolts was slightly greater than the average deformation at bolt locations. The total connection deformation on the tension side was larger than the average deformation of the column flange at bolt locations, because of the inclusion of both end-plate and bolt deformations.

3- beam flange force versus the total connection deformation at the compression side (average reading of L1 and L2). The average deformation of the column flange across the compression beam flange level was computed (average reading of L9, L10 and L11) and compared with the total connection deformation at that level. A typical test behaviour of specimen S3 is shown in Fig 3.9. The total connection deformation at the compression side mainly results from the average column flange deformation across the beam flange.

4- beam moment versus the connection rotation relationship. Such a curve represents the gross connection behaviour, i.e the connection rotation due to end-plate, column flange and bolts deformations. The connection moment-rotation relationship can be characterized by four parameters, as illustrated in Fig 3.10. The connection initial stiffness "$K_i$" (initial slope of the moment-rotation curve), the connection post-elastic

stiffness "$K_p$", connection plastic moment "$M_{pc}$" and the connection's ultimate moment "$M_u$". The post-elastic stiffness "$K_p$" was taken as the slope of the tangent on the moment-rotation curve at a rotation equal to 0.5 $\theta_u$ ($\theta_u$ is the connection rotation at its ultimate moment $M_u$), the intersection point of that tangent with the initial stiffness line defines $M_{pc}$. The above parameters were obtained for each test and listed in Table 3.3.

5- beam flange force versus the HSS side wall deformations at the both tension zone (average reading of LVDTs L7 and L8) and the compression zone (average reading of LVDTs L5 and L6). A typical test behaviour of specimen S5 is shown in Fig 3.11. On the tension side of the connection, the HSS side walls deform inwards, while on the compression side of the connection, the HSS side walls deform outwards. Hence, it can be concluded that the corners of the hollow section column experience some rotation due to the column flange loading.

It was also possible to isolate the behaviour of other components, such as the inelastic deformation of the beam. That was done by multiplying the recorded connection rotation by the cantilever length and subtracting this from the overall beam-tip displacement. The resulting deformation is due to elastic and inelastic beam rotations. Using elastic structural theory, the inelastic deformation of the beam can be separated. The beam moment - plastic rotation relationship for specimen S7 which exceeded the plastic moment capacity of the stiffened beam, is shown in Fig 3.12.

### 3.8 Specimens' behaviour and modes of failure

The behaviour of each specimen as well as it's modes of failure is described as follows:

**Specimen S1**

The moment-rotation relationship of this connection is shown in Fig. 3.13. The specimen experienced a ductile behaviour until it reached an ultimate moment capacity of 215 kN.m. At the later stages of the test, a cleavage crack was initiated at the toe of the weld between the end plate and the beam's tension flange and propagated through the end plate thickness. This fracture, in the heat affected zone of the end plate, caused a sudden drop in load-carrying capacity. Significant bending took place in the end plate at the tension side of the connection, resulting in remarkable bending of the exterior A325 bolts causing yielding of the threads. The column flange of the HSS 203x203x12.7mm appeared to have remained rigid, because it did not experience significant visual deformation while local buckling of the stiffened beam's compression flange was observed near the end of the test. Specimen S1 after test is shown in Fig 3.14.

**Specimen S2**

The moment-rotation relationship of this connection is shown in Fig. 3.15. The maximum moment capacity of the connection was measured at 166 kN.m. The two drops observed in the curve resulted from failure of BOM bolts, which was caused by shearing of the primary sleeve underneath and around the bolt's blind head. Such a failure was

not unexpected since the tensile strength of BOM bolts is less than that of A325 bolts by about 30%. Also, significant inelastic deformation was observed in the end-plate by the end of the test, as shown in Fig. 3.16.

**Specimen S3**

The ultimate moment capacity of this connection was 200 kN.m with the moment-rotation relationship shown in Fig. 3.17. At a latter stage of loading, significant bending took place in the exterior HSBB of the tension side of the connection, causing partial failure of their primary sleeves. This seemed to have been caused as a result of the bending stiffness of HSBB bolts being less than that of equivalent A325 bolts. It should be noted that the diameters of the core bolt shank of the 20 mm HSBB are only 15 mm as opposed to 19 mm for the A325 bolts. The column flange thickness of 12.7 mm seems to have been just adequate to hold the bolt's force without shearing the column flange underneath the primary sleeve. Only the column flange underneath the primary sleeve of one of the interior HSBB was partially sheared. From examining the carbon print sheet shown in Fig. 3.18, most prying action took place at the lower edge of the end-plate on the tension side of the connection. The compression beam flange force was distributed over a larger area on the HSS column flange. Although there was no direct measurement of the bolt forces during the test to measure the prying forces, the prying force factor just prior to failure was estimated to be about 30%. At ultimate load, the connection suffered a brittle failure in the heat affected zone of the beam's flange near the end plate. Extensive inelastic deformation had taken place at the corners of the HSS column near

the HSBB bolts as was indicated by the flaking of white wash in those regions, as shown in Fig. 3.19.

**Specimen S4**

For this specimen, the measured moment-rotation relationship is shown in Fig. 3.20. The maximum moment capacity was recorded as 193 kN.m. Significant yielding was observed in the end-plate and the column flange as well as the column sides near the HSBB on the tension side of the connection. Test results showed that yielding of the connection was governed by the yielding of the column flange rather than the end-plate. Just before the connection reached its ultimate capacity, it was observed that the column flange underneath the primary sleeve of the interior HSBB started to shear off. The failure mode was complete shearing of the column flange thickness underneath and around the primary sleeves of the interior bolts and partial shearing of the column flange underneath the primary sleeve of the exterior bolts, as shown in Fig. 3.21. On the basis of this test, it can be concluded that column flange thickness of 9.53 mm is inadequate to attain the maximum strength of the 20 mm HSBB bolts.

**Specimen S5**

The maximum moment capacity sustained by specimen S5 was 250 kN.m, as noted from Fig. 3.22. At failure, significant yielding was observed in the column flange on the tension side of the connection. Significant yielding was observed to have taken place at the corners of the HSS column near the bolts. Fig. 3.23, shows the yield pattern

of the inner face of the column flange on the tension side of the connection after the test, as indicated by flaking of the white wash. The test results show that yielding of the connection was governed by the yielding of the column flange rather than of the end-plate. This was due to the larger thickness of the end plate and greater edge distance of the exterior bolts of specimen S5 as compared to specimen S4, resulting in less end-plate bending and reduced bending of the exterior bolts and their prying action. In addition, the prying factor just prior to failure was estimated to be about 10%. However, the end plate on the compression side of the connection experienced significant plastic bending across the column flange at the later stages of loading. The deformation of the end plate after the test on both compression and tension sides of the connection is shown in Fig. 3.24. The failure mode was by complete shearing of the column flange thickness underneath and around the primary sleeves of the HSBB bolts, similar to that of S4. Again, the column flange thickness of 11.13 mm was not adequate to resist the maximum strength of the 20 mm HSBB.

**Specimen S6**

The moment-rotation relationship of specimen S6 is shown in Fig 3.25. The maximum moment capacity was recorded at 235 kN.m, when the collar of one of the HSBB stripped from the swaged threads, thus causing a sudden drop in the moment capacity. Significant yielding was observed in the end-plate at the end of the test, as shown in Fig.3.26. No shearing of the column flange thickness under neath the primary sleeves of HSBBs was observed. Welding a 6 mm doubler plate onto the 9.53 mm thick

column flange seems to have been adequate to avoid column flange shear failure and to resist the maximum strength of the 20 mm HSBB.

**Specimen S7**

Fig 3.27 shows the moment-rotation relationship for Specimen S7. The maximum moment capacity was recorded at 240 kN.m with a mode of failure similar to that for specimen S5, since the same nominal column flange thickness was used. However, filling the HSS stub column with concrete resulted in a significant reduction in connection deformations on both the tension and compression sides as well as the column side walls. Significant yielding of the column flange was observed, while none was observed at the corners on the tension side of the connection, as shown in Fig. 3.28.

**Specimen C1**

Moment-rotation hysteretic curves of this connection are shown in Fig 3.29. The connection behaviour was consistently stable up to a moment of 238 kN.m attained during the eleventh cycle. The test was terminated when a brittle failure occurred in the heat affected zone of the beam flange, after completing eight inelastic cycles and reaching a displacement ductility of 4. As was expected, the beam behaviour during the test was mainly elastic as indicated from the beam moment-rotation hysteretic curves shown in Fig 3.30. From an examination of Figs 3.29 and 3.30, it can be concluded that most of the energy was dissipated in the connection components (column flange, end-plate and bolts). Yielding of the specimen was observed at a moment equal to 180 kN.m and was

initiated in the column flange. The connection behaved mainly elastic in the range of ±139 kN.m, which is about 0.77 the observed plastic moment of the connection. Connection stiffness degradation was obvious through the progression of the subsequent cycles. This degradation was attributed to the yielding of the column flange and bolt deformations. Although there was no bolt force measurements during the test, at the end of testing the HSBB collars were partially stripped indicating that the bolts almost reached their ultimate strength. The bolts were also found to be loose, indicating that they lost their pre-tensioning forces during the loading cycles. Ghobarah et al. (1990) recorded degradation in pre-tension forces due to cyclic loading when A490 high strength bolts were used in extended end-plate connections for W-shape columns. A similar behaviour would be expected for HSBB bolts, also, under cyclic loading. This severe deterioration was attributed to the inelastic strains developed in the primary sleeves and the threaded region of the HSBB bolts as well as local yielding of HSS column flange beneath the HSBB primary sleeve at that high level of bolt loading and prying action. Examination of the column flange around the bolt holes after the test, indicated that substantial bearing strains were developed on the column flange beneath the HSBB primary sleeve.

**Specimen C2**

The resulting hysteretic curves of the connection and the beam are shown in Fig 3.31 and 3.32 respectively. A behaviour similar to that of specimen C1 was observed. However, the test was terminated when a weld fracture occurred between the doubler

plate and the HSS column flange near the bolts after achieving ten inelastic cycles.

### 3.9 Analysis of experimental results

The experimental program was developed so that it would be possible to compare the behaviour of similar specimens in groups as follows:

**Specimens S1, S2 and S3**

These specimens differed only in the type of fasteners used. Comparing the moment-rotation relationships of specimens S1, S2 and S3, as shown in Fig 3.33, indicates that the behaviour of the connection using HSBB appears to be similar to that of connection S1 employing A325 bolts, with its initial stiffness slightly higher and its ultimate moment capacity slightly less. The slightly higher initial stiffness of connection S3, may be attributed to the high and consistent clamping force of the HSBB. On the other hand, specimen S2 showed rather poor performance due to the BOM bolt's premature failure. However, its behaviour was similar to that of S1 and S3 up to a rotation equal to about 0.005 radians. This result was not unexpected since the nominal tensile strength of BOM bolt is less than that of A325 by about 30%.

**Specimens S4, S6 and C2**

The equivalent monotonic moment-rotation relationship for specimen C2 can be obtained from the hysteretic curves by using the shifting rule suggested by Kato et al. (1981). The resulting predicted monotonic moment-rotation relationship of specimen C2

and the measured relationships for specimens S4 and S6, are shown in Fig 3.34. It can be concluded that, the 6 mm doubler plate welded onto the column stub of specimen S6 caused a slight increase (10%) in the connection's initial stiffness and a significant reduction in the connection rotation especially at high loads as compared to specimen S4 due to the reduced column flange deformations. The observed plastic moment and the ultimate moment capacity of specimen S6 increased by 14% and 22%, respectively, as compared to specimen S4. These increases are attributed to the stiffening of the HSS column flange by the 6 mm doubler plate and eliminating the HSS column flange shear failure beneath the primary sleeves of the bolts. Installing the HSBB closer to the beam flange of specimen C2, resulted in an increase in its initial stiffness by about 18% and a slight increase in its ultimate moment as compared to that of specimen S6. These increases are attributed to the reductions in end-plate deformation as well as to reduced prying action on the bolts.

**Specimen S5, S7 and C1**

Specimens S7 and C1 were identical to specimen S5 except that specimen S7 was filled with concrete, while the column flange of specimen C1 was stiffened with a welded 6 mm doubler plate. The moment-rotation relationships of specimens S5, S7 and C1 are plotted in Fig 3.35. It can be noted that, filling the column stub of specimen S7 with concrete resulted in a surprising increase in the connection's initial stiffness, (about 3 times that without concrete "specimen S5") and a significant decrease in its maximum rotation. The increase in the connection's initial stiffness is attributed to the significant

reduction in the connection deformations at both tension and compression sides when compared to specimen S5, as shown in Fig 3.36. The reduction of the connection deformation on the compression side resulted from the presence of concrete, while the reduction at the tension side was due to the prevention of the HSS side walls from deflecting inwards due to the concrete. The deflections of the column sides at both compression and tension sides of specimen S7 were very small as compared to that of specimen S5 without concrete, as shown in Fig 3.37. Therefore, it can be concluded that the corners of the column stub are essentially restrained from rotation and hence may be considered to act as fixed supports for the column flange when filled with concrete. Again the effect of the doubler plate on the connection behaviour can be observed by comparing the moment-rotation relationships of specimens S5 and C1. The doubler plate resulted in a slight increase in the connection's initial stiffness while a significant reduction in the connection rotation especially at high loads due to the reduced column flange deformations and the elimination of the column flange shear failure.

**Specimen C1 and C2**

In seismic design, the ability of the members in a structural frame to dissipate earthquake input energy is important. As such, sufficient energy dissipation without a substantial loss of strength and stiffness is required for beam-column subassemblages. Moment hinging in the beams allows a dissipation of large amounts of an earthquake's input energy. Connections are generally not the ductile elements and hence cannot be relied upon for dissipating energy. However, studying their inelastic behaviour is

necessary to ensure that the beams will yield first. In this study, it was decided that the beams should behave mainly elastically with minimal participation in energy dissipation, in order to examine the effect of cyclic loading on a connection's behaviour.

For the tested specimens C1 and C2 and their individual components, the energy dissipated in each cycle can be assessed by calculating the area within the moment-rotation loop for that cycle. Popov et al. (1973) suggested that the energy dissipation associated with inelastic load excursions (half cycle) is a more meaningful measure. The cumulative energy dissipated by specimens C1 and C2 are plotted against the number of inelastic excursions as shown in Figs 3.38 and 3.39, respectively. It will be noted that, 93% and 98.5% of the total energy dissipated in specimens C1 and C2, respectively, was dissipated through the connection components. The energy dissipated in connection C1 was almost equally shared between the HSS column flange on one side and the end-plate and bolts on the other side. Meanwhile 40% of the energy dissipated in connection C2 was by the column flange.

As a general observation, connections C1 and C2 experienced degradation in their stiffness with load cycling. The variation of the connection stiffness relative to its initial stiffness with the number of inelastic excursions for connections C1 and C2 is shown in Fig. 3.40. Connection degradation was possibly due to both loss of HSBB pre-tensioning forces with loading cycles and the permanent deformation of the column flanges or the end-plate. Since connection stiffness degradation could have a deleterious effect on the drift of a moment resisting frame, it has to be minimized in order to achieve satisfactory performance of such a frame. It was observed from Fig 3.29 and 3.31 that

the connections behaved mainly elastically up to 0.77 times its plastic moment which was attained after four inelastic excursions. Therefore, if this value is selected to be higher than the beam plastic moment, this would allow the connection to behave almost elastically without any significant stiffness degradation until the beam reaches its plastic moment capacity and experience large plastic deformations. In such a case, it is suggested that the connection be designed so that its plastic moment be equal to 1.3 times the beam plastic moment to minimize the connection's stiffness degradation.

## 3.10 Summary

Based on the observations of the tests conducted in this study and results obtained, some remarks can be made:

1- With the use of HSBB, a bolted end-plate connection between W-shape beams and HSS columns is a plausible option.

2- The behaviour of the proposed bolted moment connection using HSBB is judged to be similar to that using A325 bolts. It appears that HSBB have a promising potential in structural connection applications.

3- It was confirmed that BOM bolts do not achieve the equivalent strength of A325 bolts.

4- Stiffening the HSS column flange with a welded doubler plate is needed since a washer cannot be installed under the bolt's head inside the HSS column. Welding a doubler plate on the column flange in an extended end-plate connection slightly increases its initial stiffness, and significantly reduces the connection rotation at high loads. In

addition, it increases the plastic capacity of the column flange and prevents the occurrence of column flange shear failure beneath the head of the HSBB fasteners.

5- Filling the HSS column with concrete appears to significantly increase the initial stiffness of the connection, thus reducing excessive rotations at such joints in building frames.

6- Using thicker end-plates with HSBB bolts installed closer to the beam flange, reduces the bolts' bending and prying action, which results in improved performance of such a connection.

7- Connections which are expected to experience cyclic loading, should be designed so that their plastic moments equal to 1.3 times the attached beam plastic moment. In such a case, energy is dissipated in a beam's plastic hinges while the connection would behave essentially elastically.

**Table 3.1 Experimental program on beam-to-column connections**

| | Specimen No. | HSS column section (mm) | End-plate dimension (mm) | Number and type of bolts | Remarks |
|---|---|---|---|---|---|
| **Phase (1) Monotonic loading** | S1 | 203x203x12.7 | 520x170x19 | 8 - 3/4" A325 | Unstiffened HSS column flange |
| | S2 | | | 8 - 3/4" BOM | |
| | S3 | | | 8 - 20mm HSBB | |
| **Phase (2) Monotonic loading** | S4 | 254x254x9.53 | 550x230x19 | 8 - 20mm HSBB | Unstiffened column flange |
| | S5 | 254x254x11.13 | 550x230x22 | 4 - 3/4" A325<br>4 - 20mm HSBB | Unstiffened column flange |
| | S6 | 254x254x9.53 | 550x230x19 | 8 - 20mm HSBB | HSS column flange stiffened with 6 mm doubler plate |
| | S7 | 254x254x11.13 | 550x230x19 | 8 - 20mm HSBB | HSS concrete filled |
| **Phase (3) Cyclic loading** | C1 | 254x254x11.13 | 550x230x22 | 8 - 20mm HSBB | HSS column flange stiffened with 6mm doubler plate |
| | C2 | 254x254x9.53 | 550x230x19 | 8 - 20mm HSBB installed closer to beam flange | |

Table 3.2 Mechanical properties of tensile coupons

| Coupon location | Yield stress (MPa) | Tensile stress (MPa) |
|---|---|---|
| HSS 203x203x12.7 | 390 | 506 |
| HSS 254x254x9.53 | 460 | 500 |
| HSS 254x254x11.13 | 444 | 520 |
| End-plate | 320 | 483 |
| Doubler plate | 320 | 497 |
| Beam flange | 310 | 500 |
| Beam web | 315 | 480 |

Table 3.3 Connection parameters of tested specimens

| Specimen No. | Initial stiffness $K_i$ (kN.m/rad) | post-elastic stiffness $K_p$ (kN.m/rad) | Connection plastic moment $M_{pc}$ (kN.m) | Connection ultimate moment $M_u$ (kN.m) |
|---|---|---|---|---|
| S1 | 37000 | 1800 | 150 | 215 |
| S2 | 45000 | 3740 | 115 | 166 |
| S3 | 45470 | 2400 | 130 | 200 |
| S4 | 14500 | 1000 | 136 | 193 |
| S5 | 20370 | 1320 | 161 | 250 |
| S6 | 16000 | 1130 | 160 | 235 |
| S7 | 66750 | 3500 | 163 | 240 |
| C1 | 24000 | 2000 | 180 | 238 |
| C2 | 18820 | 1400 | 169 | 246 |

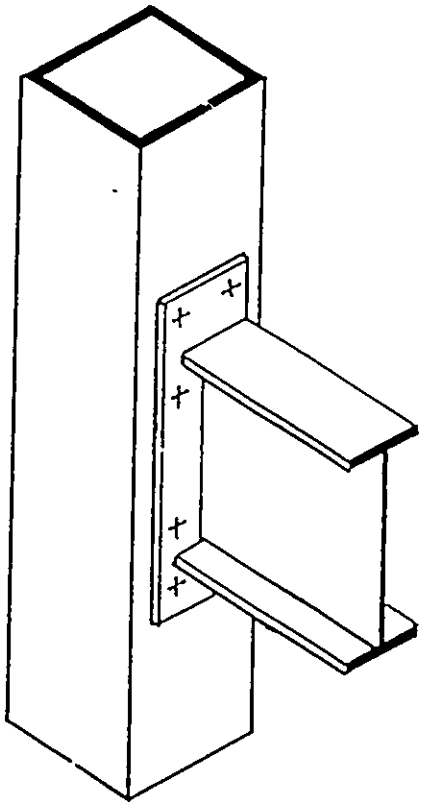

Fig 3.1 A typical extended end-plate connection

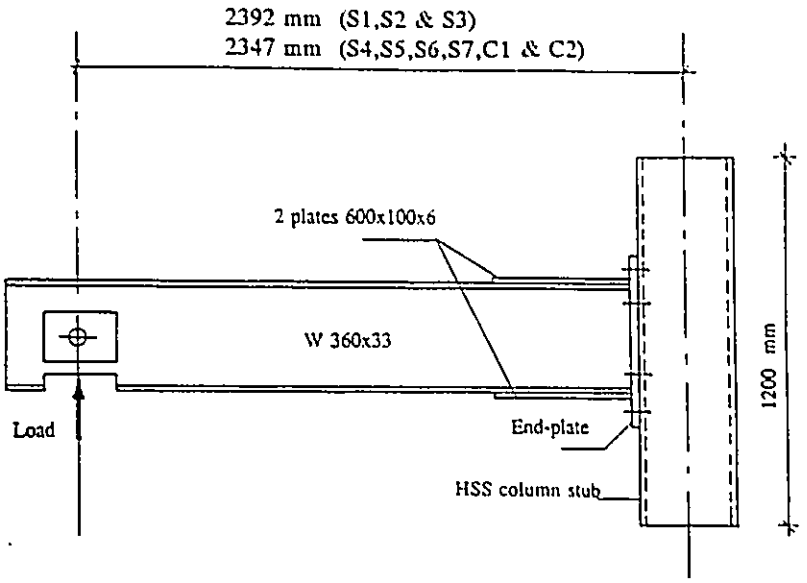


Fig 3.2 Test specimen

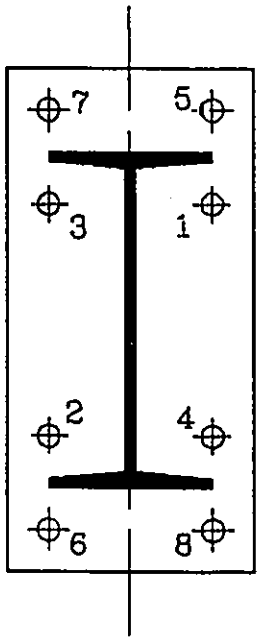


Fig 3.3 Installation sequence of bolts across the end-plate

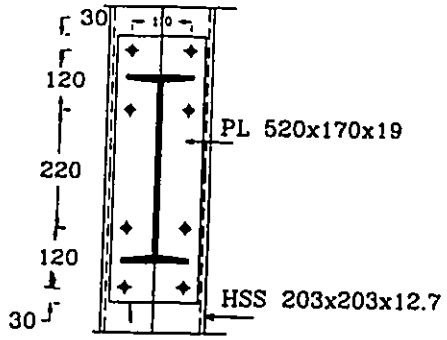


(a) Specimens S1,S2 & S3

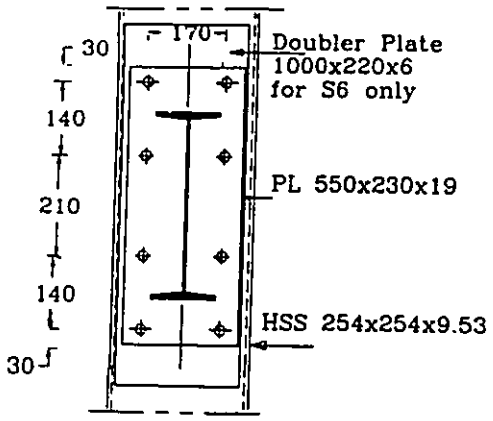


(b) Specimens S4 & S6

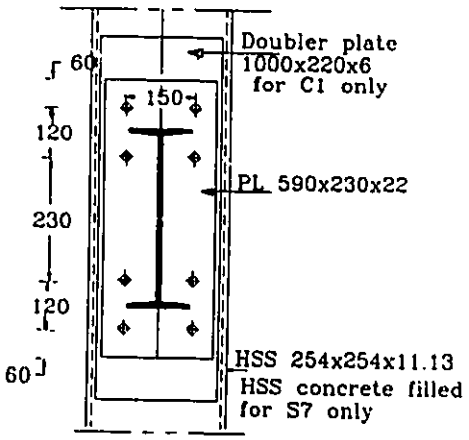


(c) Specimens S5,S7,&C1

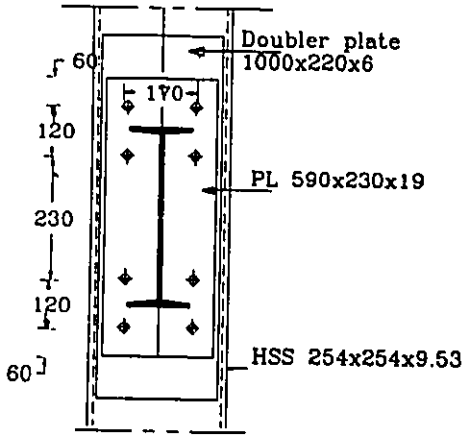


(d) Specimen C2

**(all dimensions in mm)**

Fig 3.4 Details of tested connections

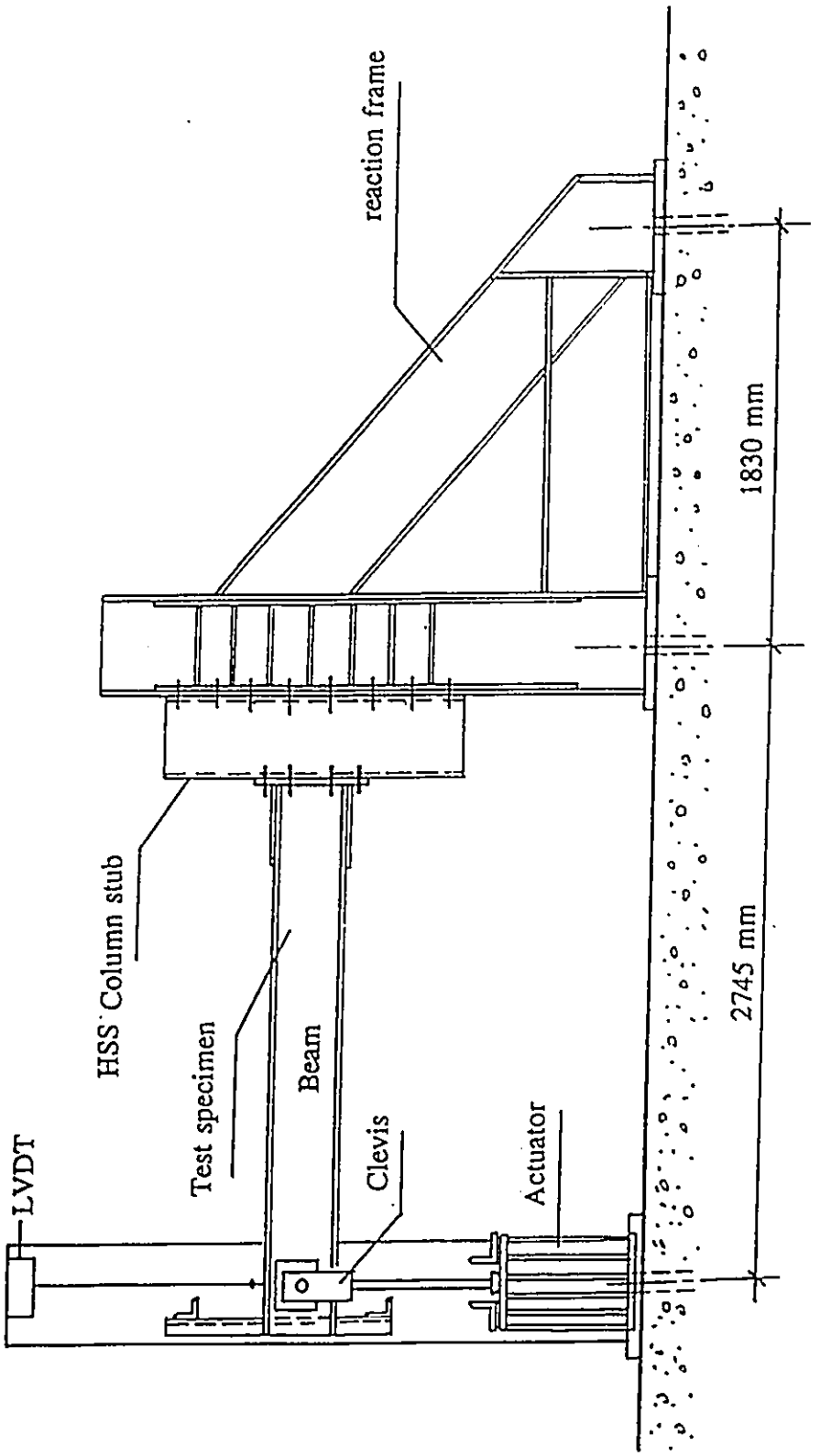


Fig 3.5 General arrangement of test setup

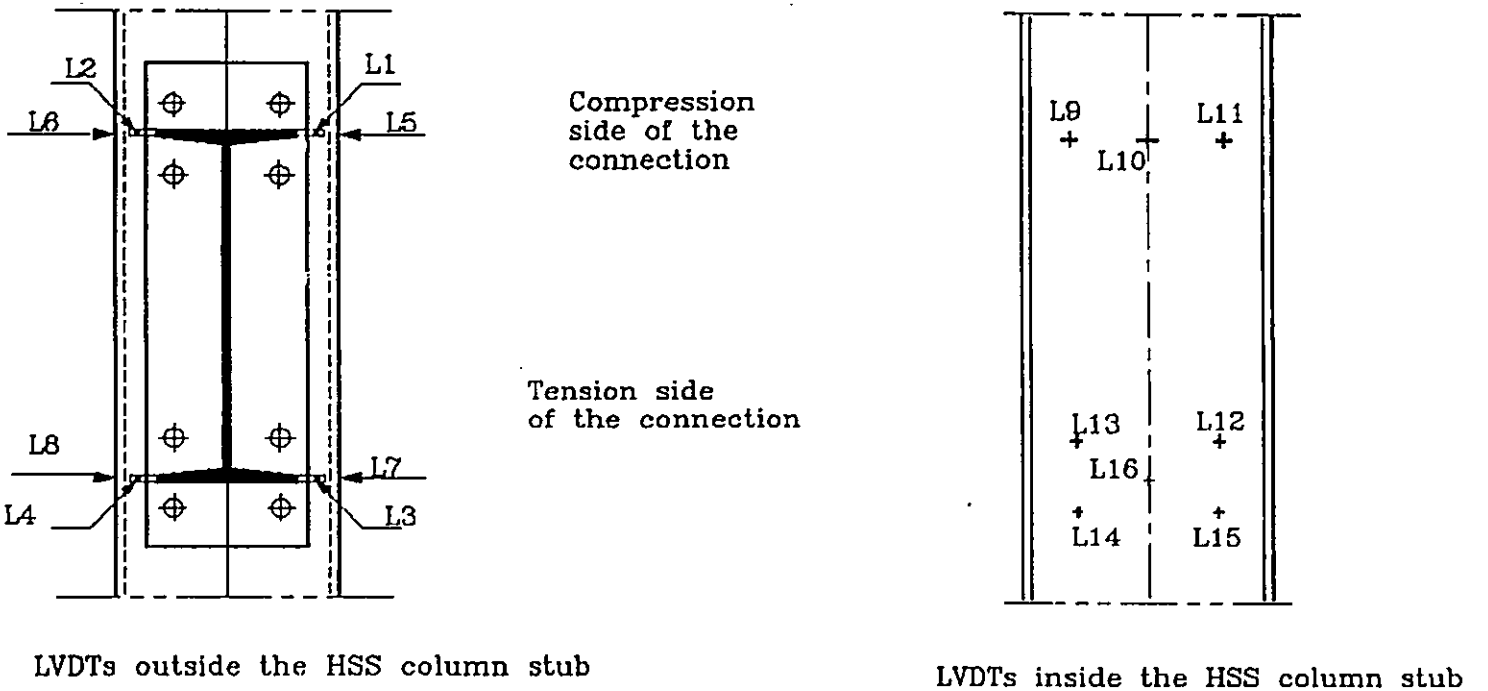


Fig 3.6 LVDTs arrangements

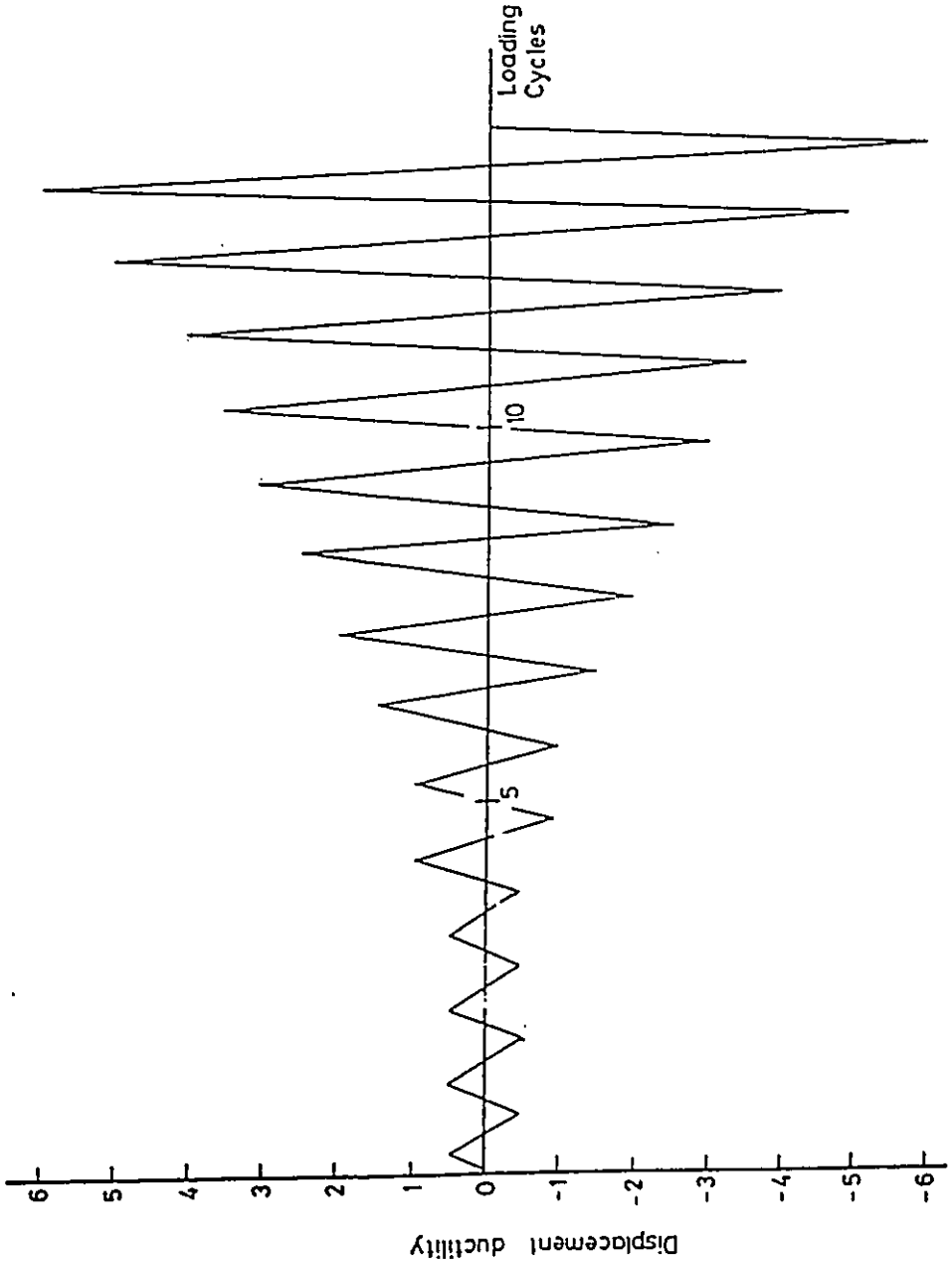


Fig 3.7 Typical loading sequence for specimens C1 and C2

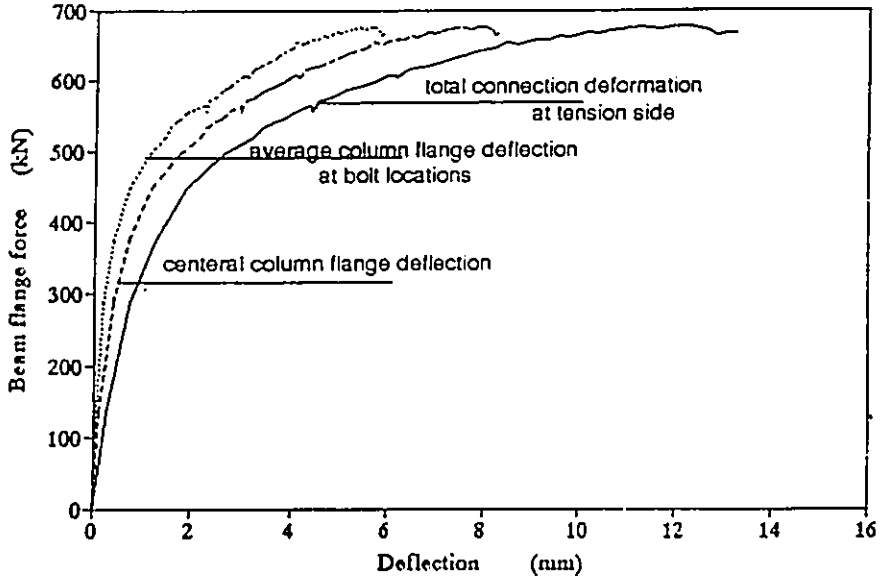


Fig 3.8 Connection deformations at the tension side of specimen S3

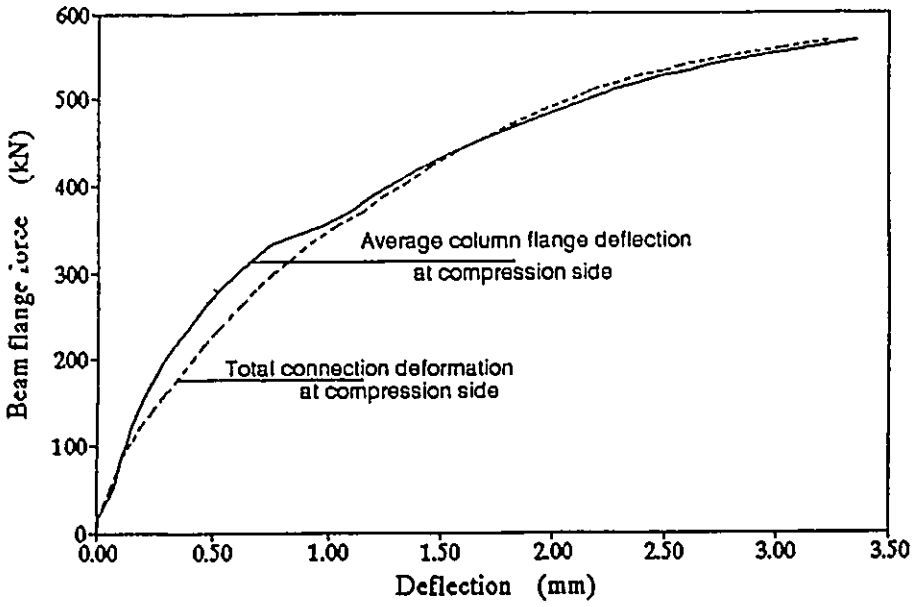


Fig 3.9 Connection deformations at the compression side of specimen S3

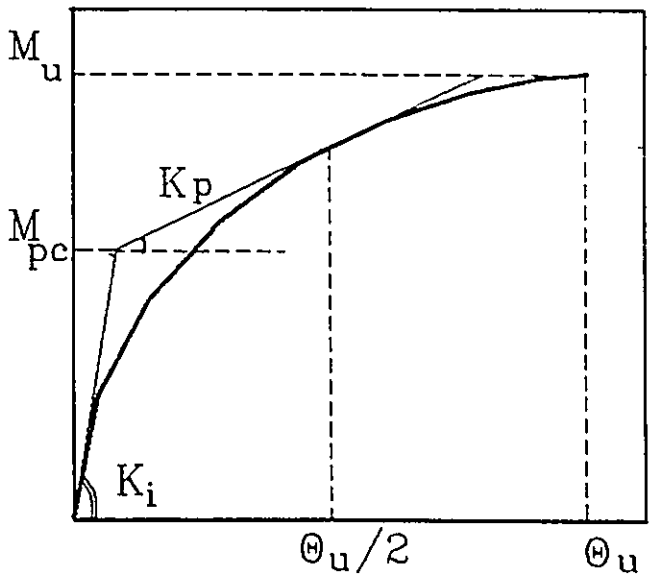


Fig 3.10 Determination of connection parameters experimentally

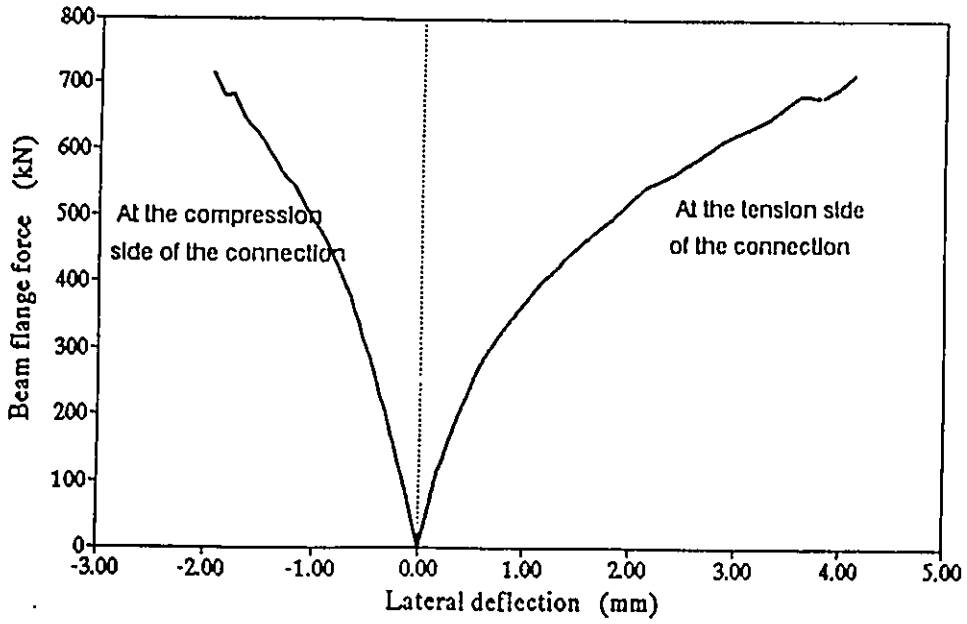


Fig 3.11 HSS side wall deflections of specimen S5

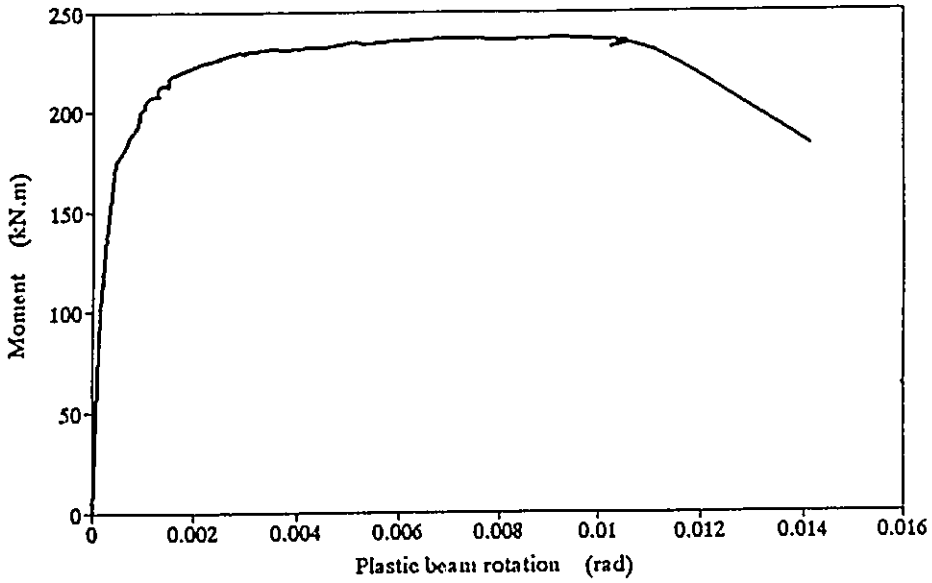


Fig 3.12 Beam moment versus plastic beam rotation relationship of specimen S7

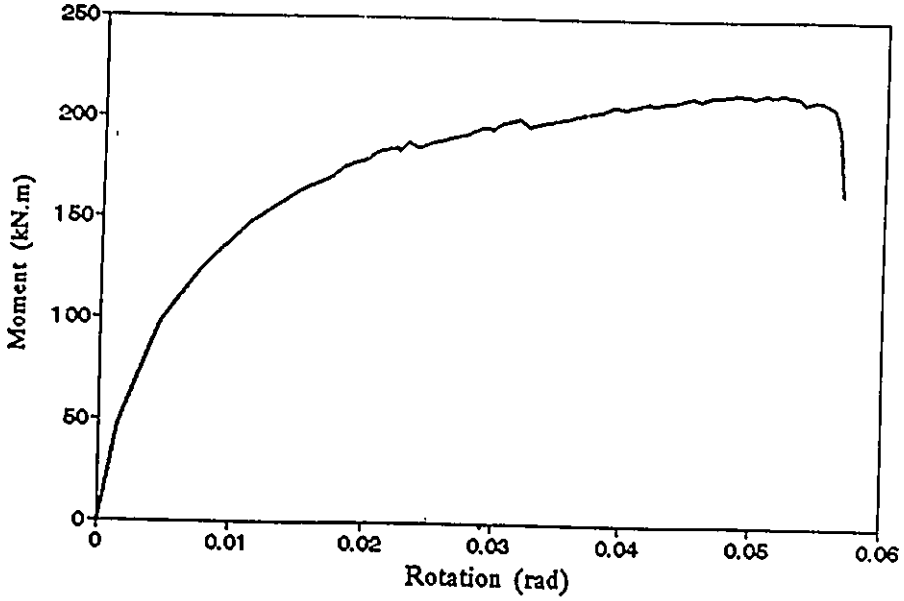


Fig 3.13 Connection moment-rotation relationship of specimen S1

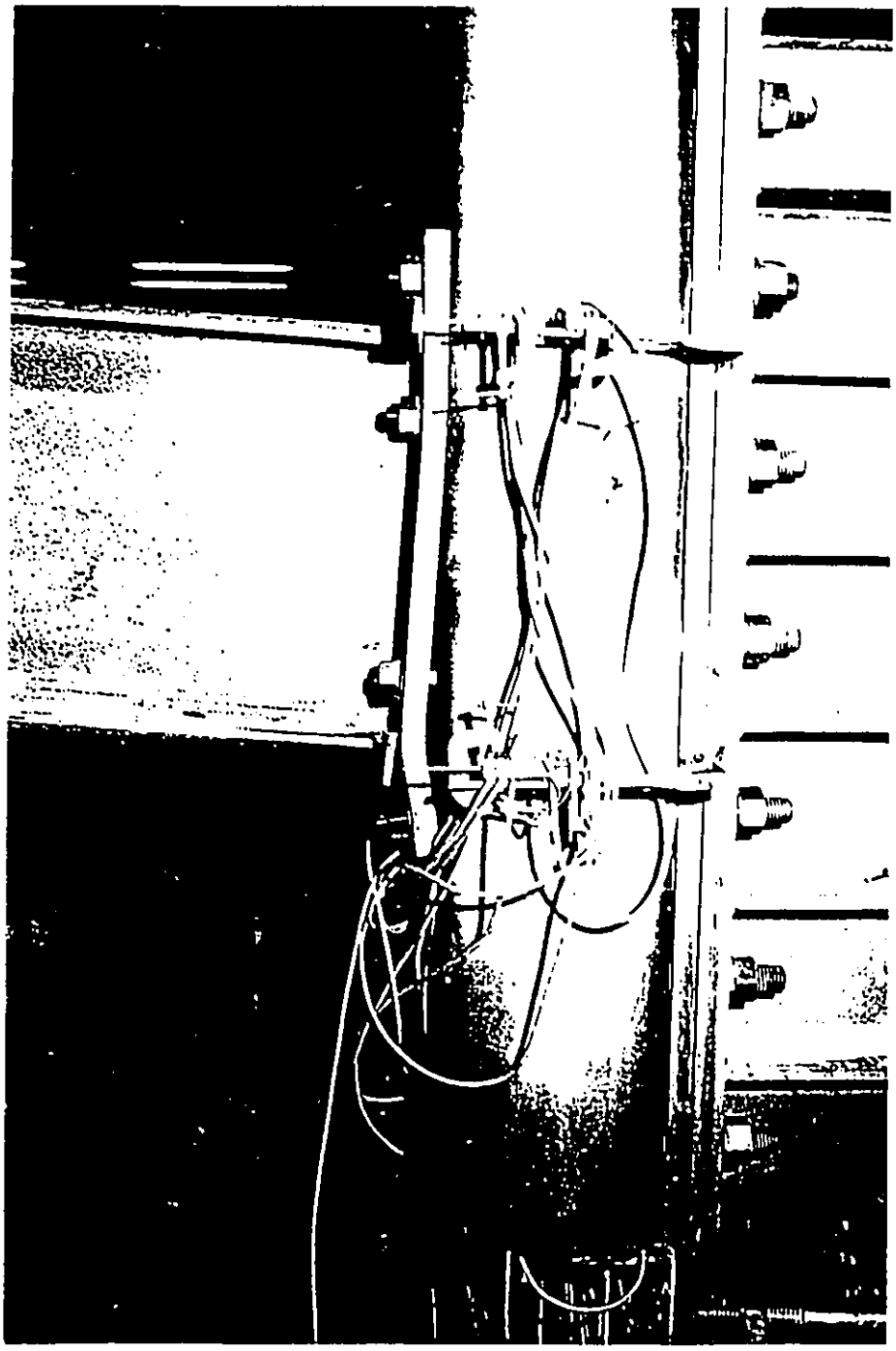

Fig 3.14 Specimen S1 after failure

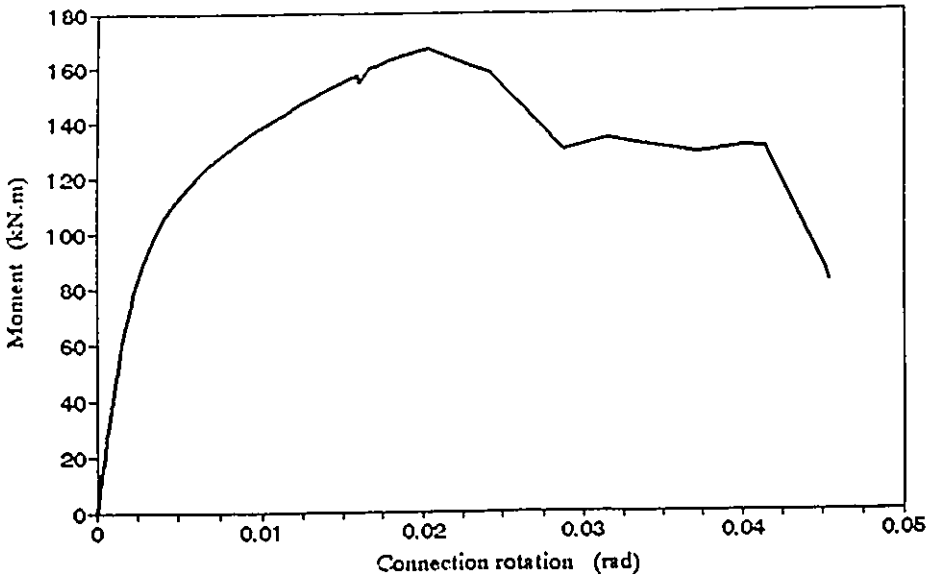


Fig 3.15 Connection moment-rotation relationship of specimen S2

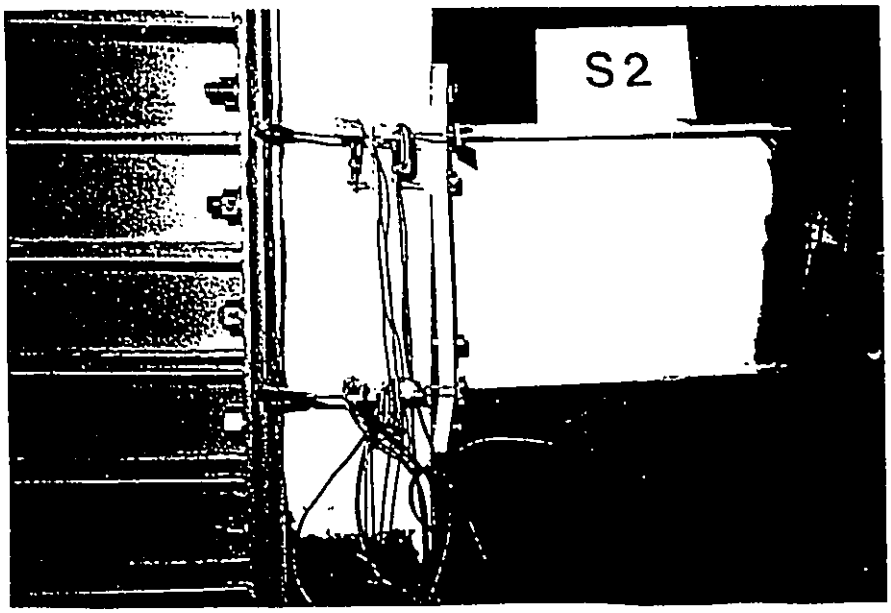


Fig 3.16 Specimen S2 after failure

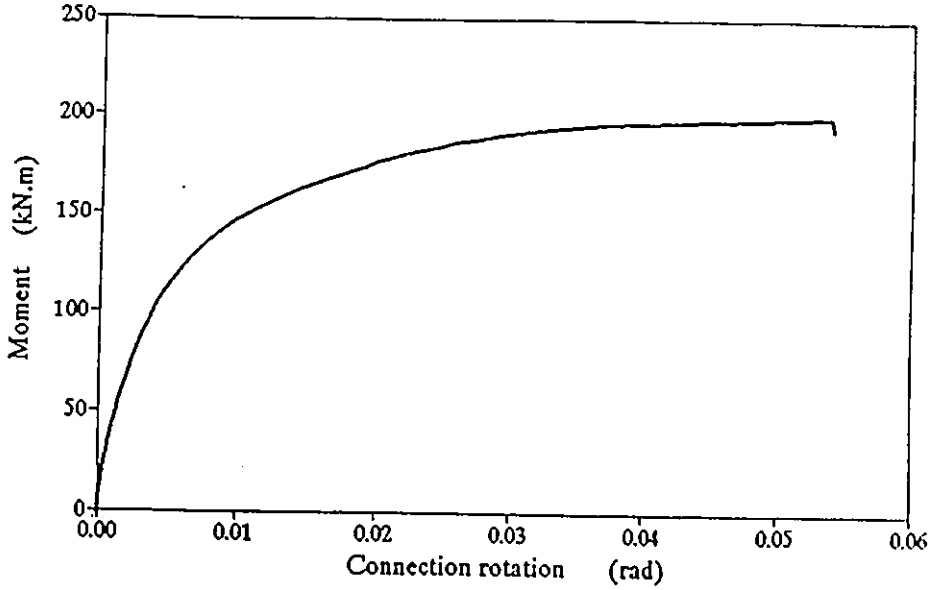


Fig 3.17 Connection moment-rotation relationship of specimen S3

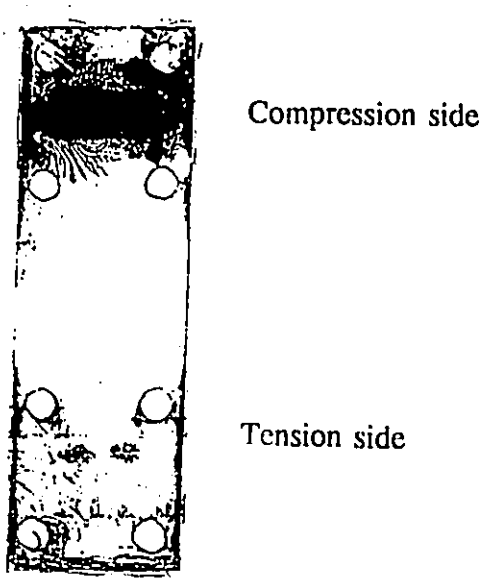


Fig 3.18 A typical print of the carbon sheet placed between the end-plate and column flange

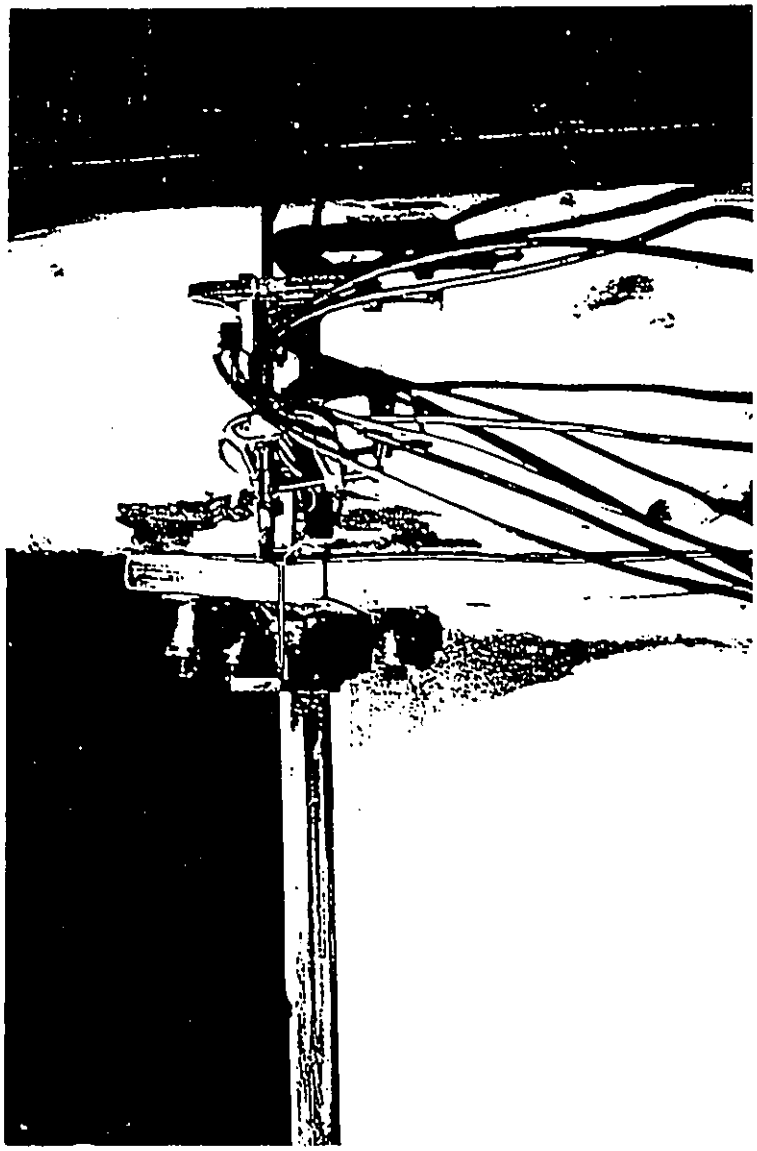

Fig 3.19 Specimen S3 after failure

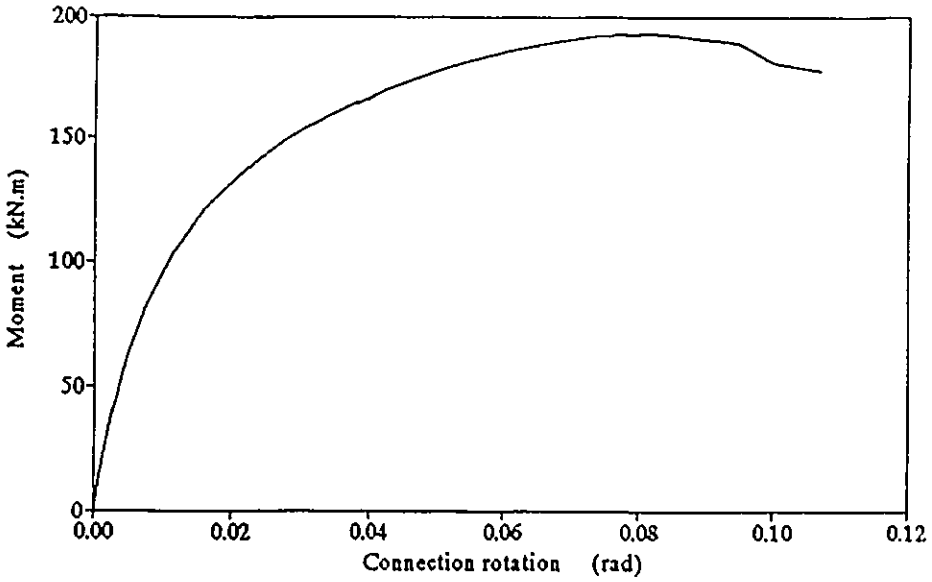


Fig 3.20 Connection moment-rotation relationship of specimen S4

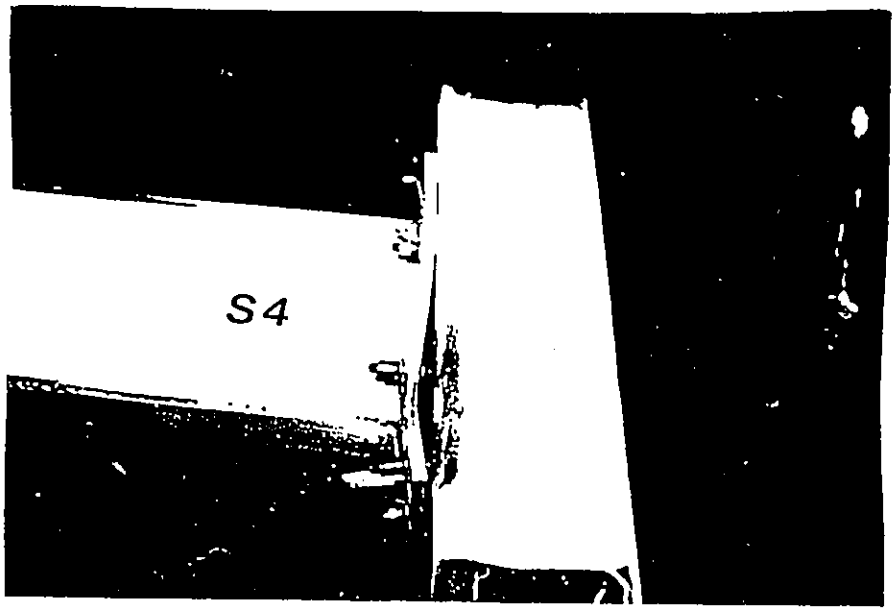


Fig 3.21 Specimen S4 after failure

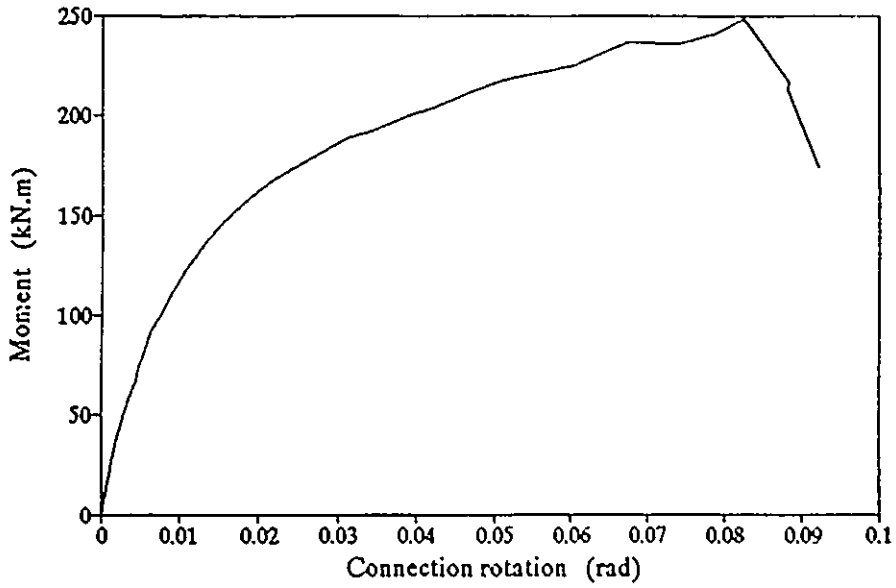


Fig 3.22 Connection moment-rotation relationship of specimen S5

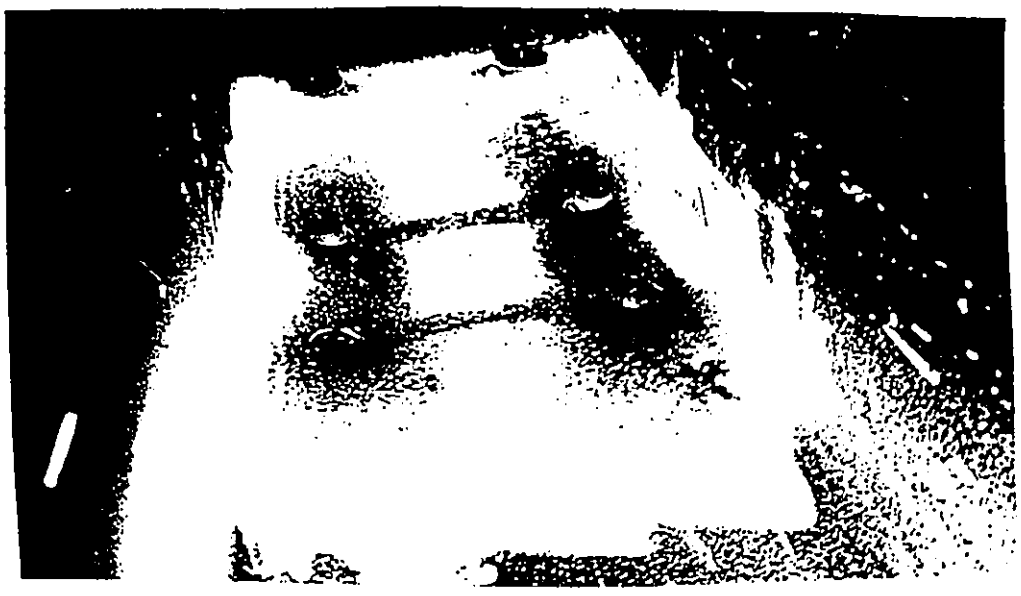

Fig 3.23 Yield pattern of the HSS column flange
at the tension side of the connection (specimen S5)

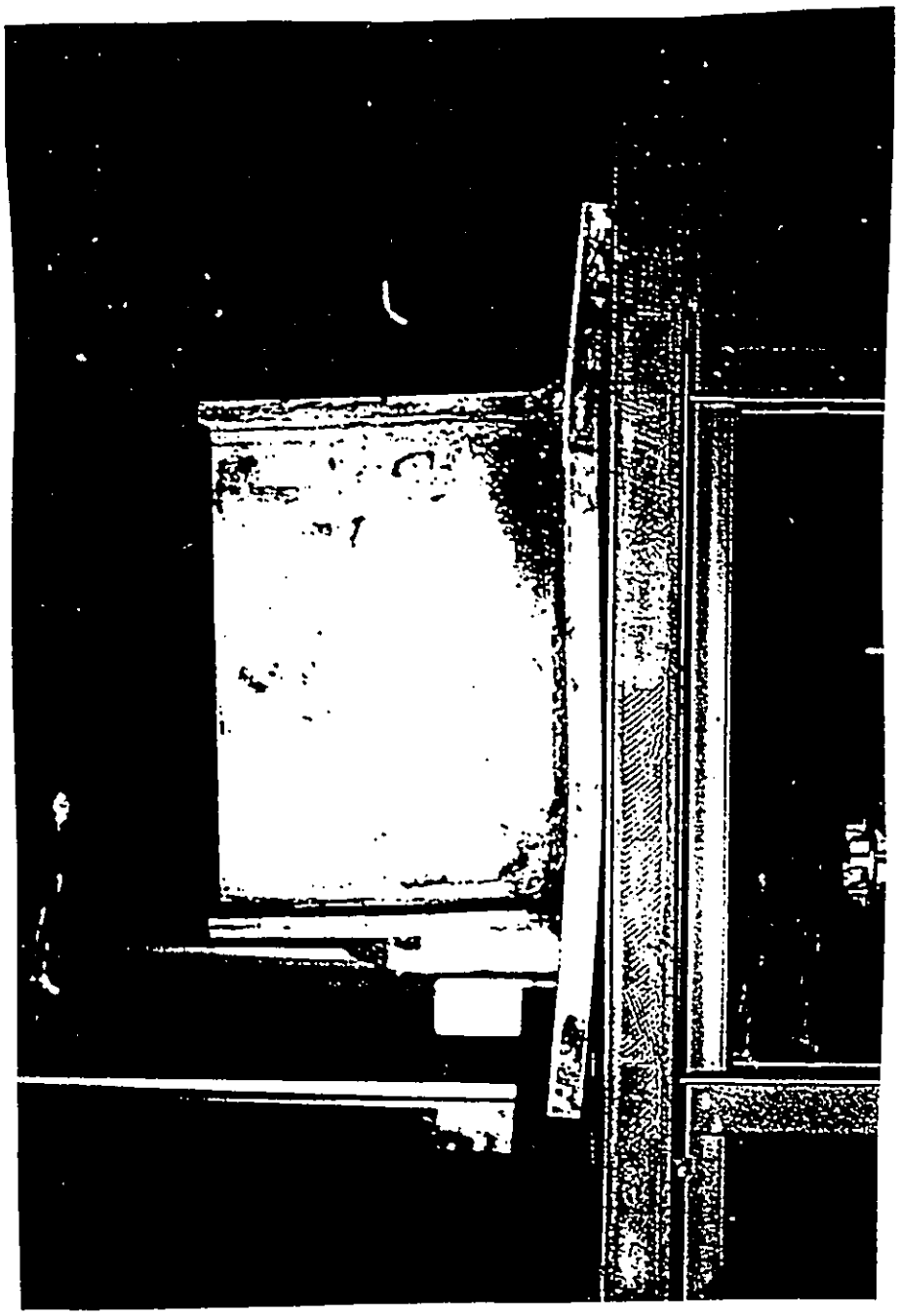

Fig 3.24 End-plate deformations of specimen S5 after test

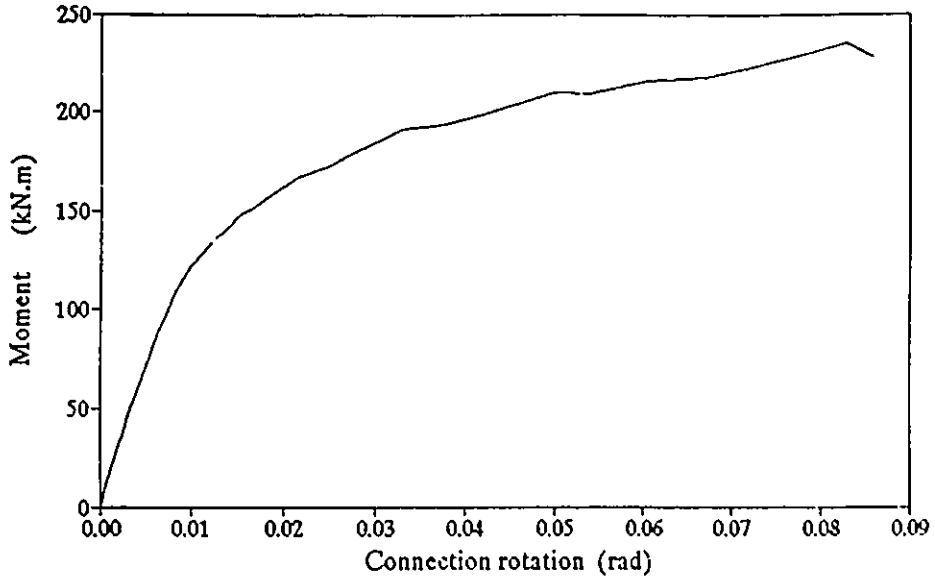


Fig 3.25 Connection moment-rotation relationship of specimen S6

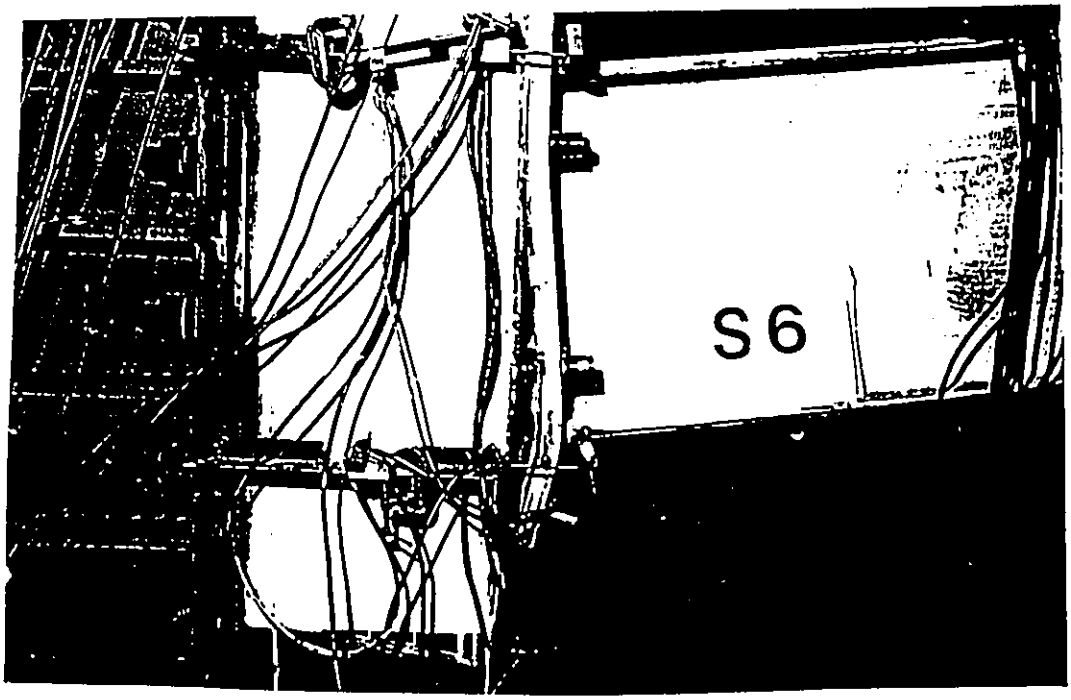


Fig 3.26 Specimen S6 after failure

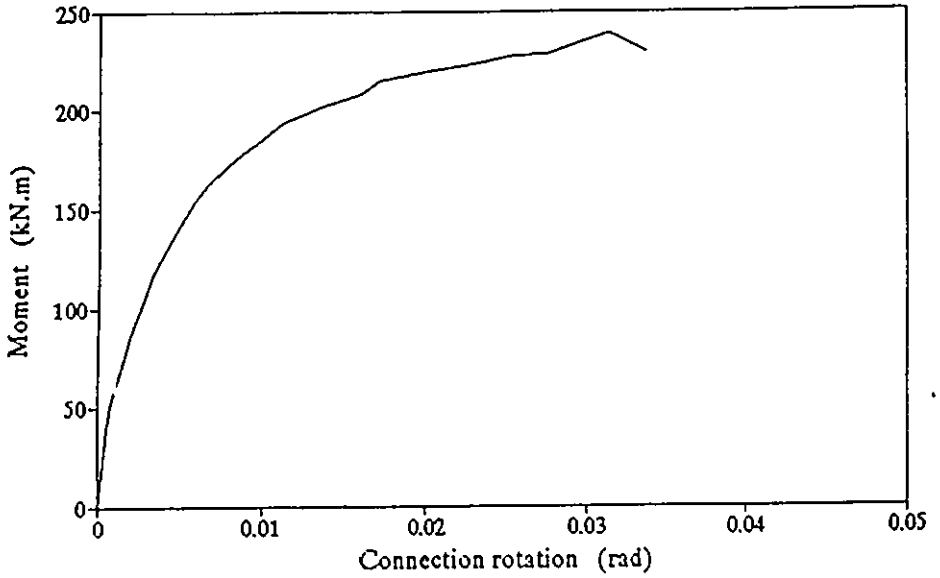


Fig 3.27 Connection moment-rotation relationship of specimen S7

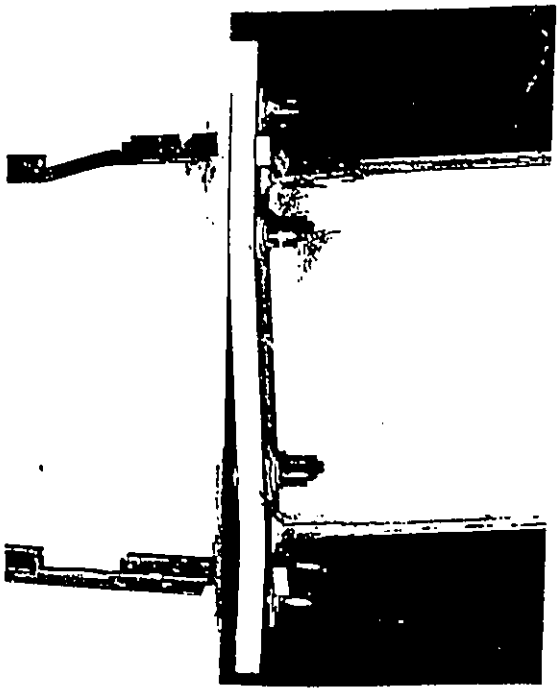

Fig 3.28 Specimen S7 after failure

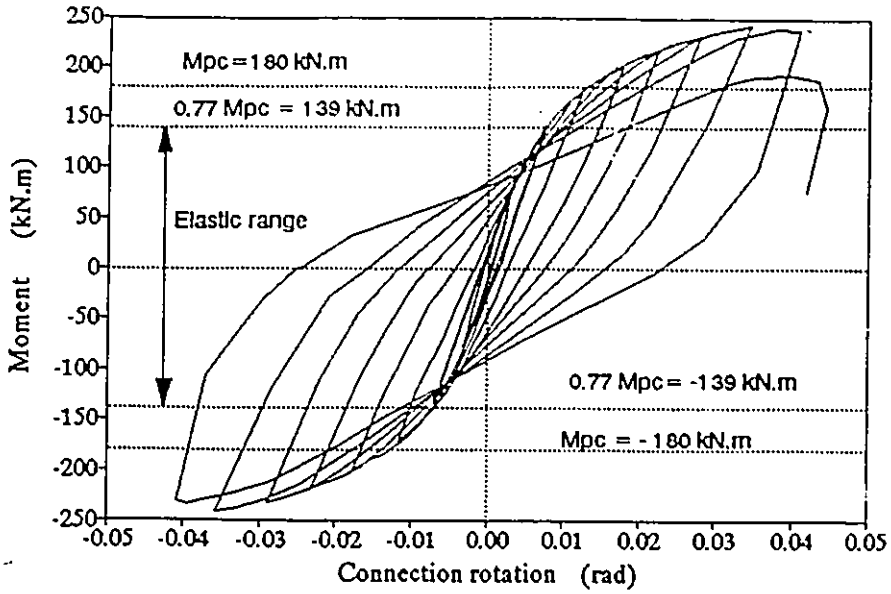


Fig 3.29 Connection hysteretic curves of specimen C1

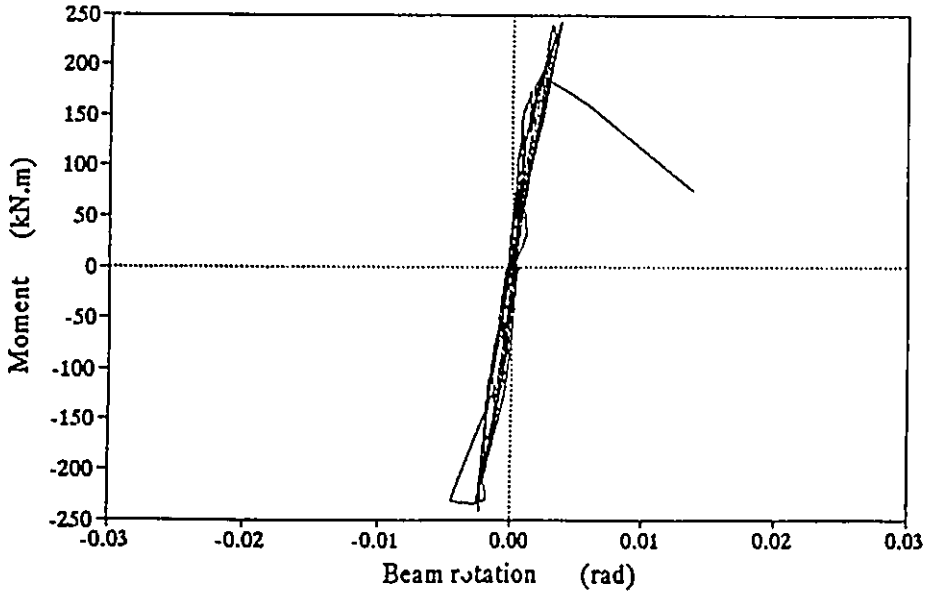


Fig 3.30 Beam hysteretic curves of specimen C1

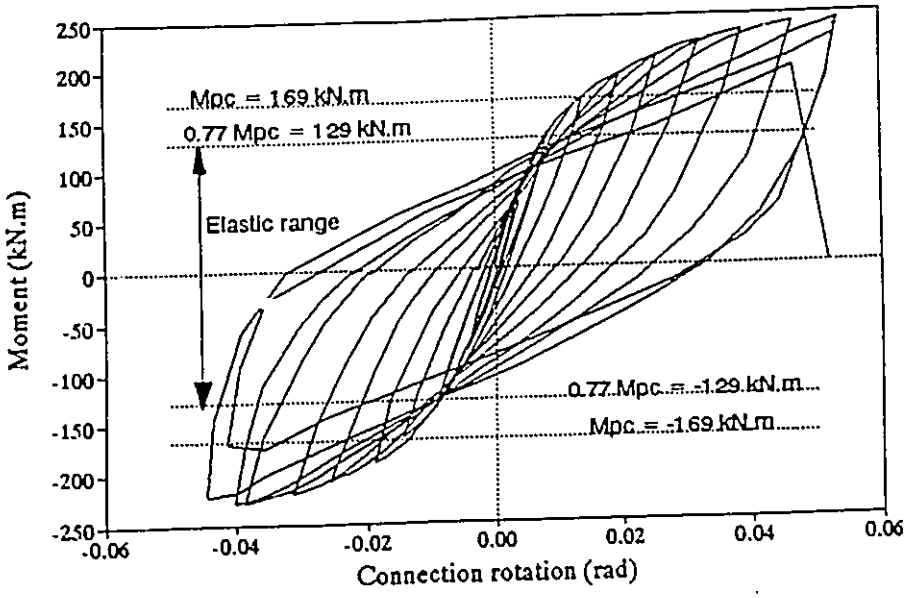


Fig 3.31 Connection hysteretic curves of specimen C2

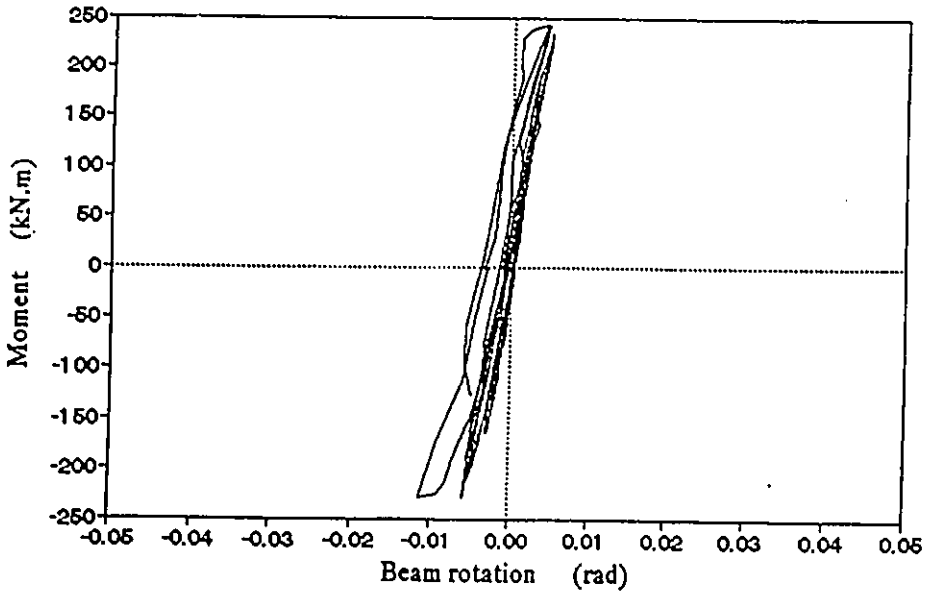


Fig 3.32 Beam hysteretic curves of specimen C2

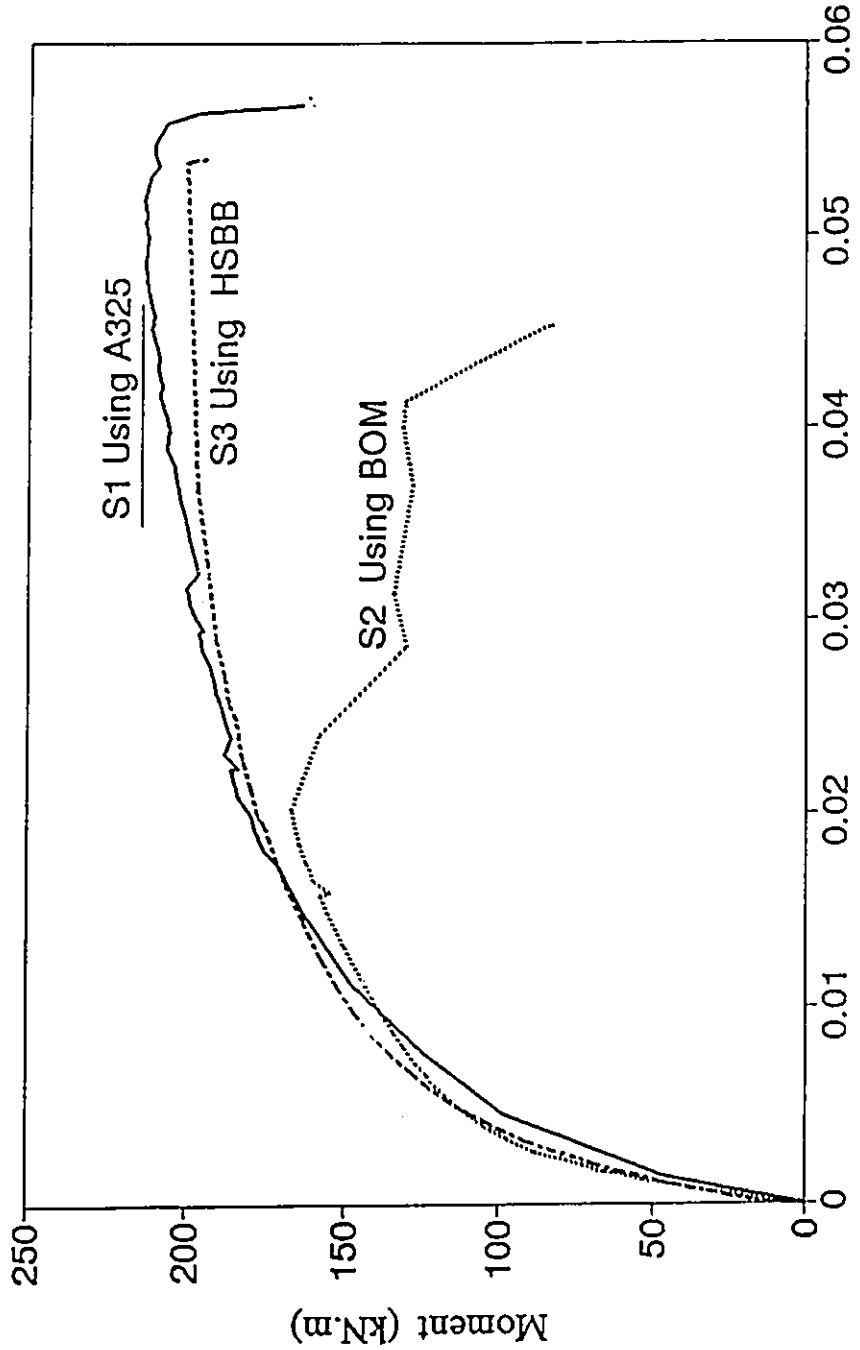


Fig 3.33 Comparison of connection moment-rotation relationships of specimens S1, S2 and S3

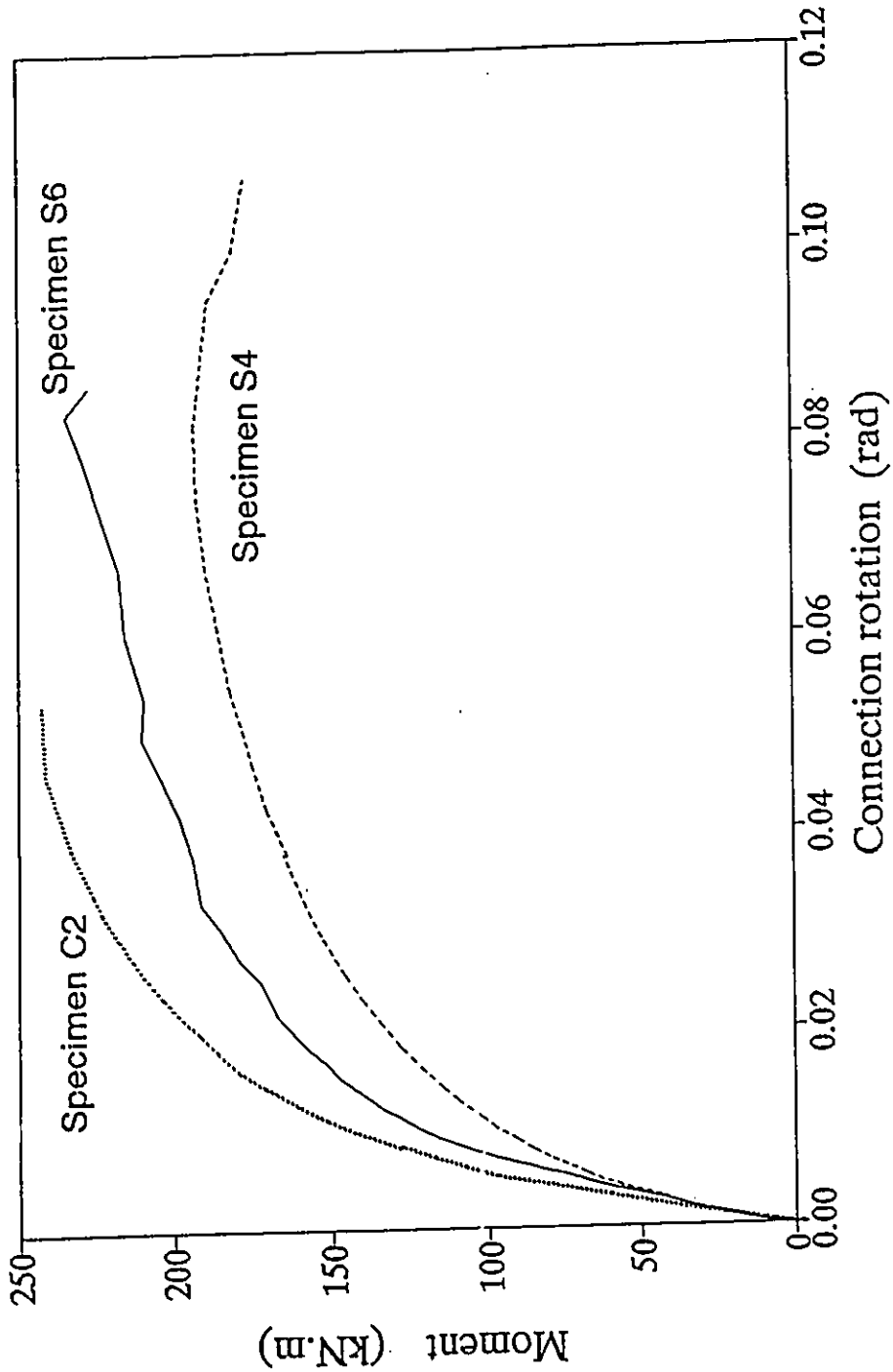


Fig 3.34 Comparison of connection moment-rotation relationships of specimens S4, S6 and C2

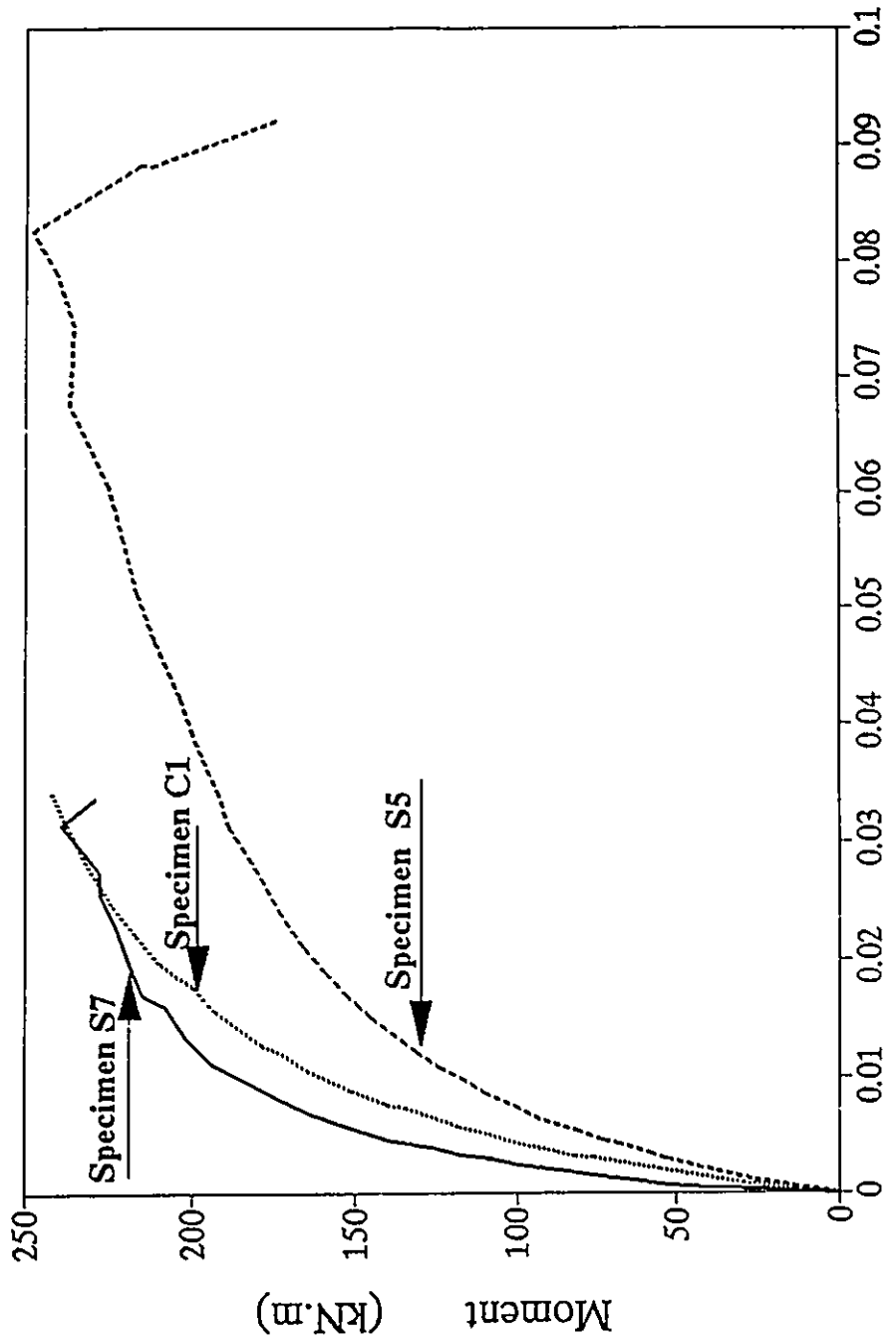


Fig 3.35 Comparison of connection moment-rotation relationships of specimens S5, S7 and C1

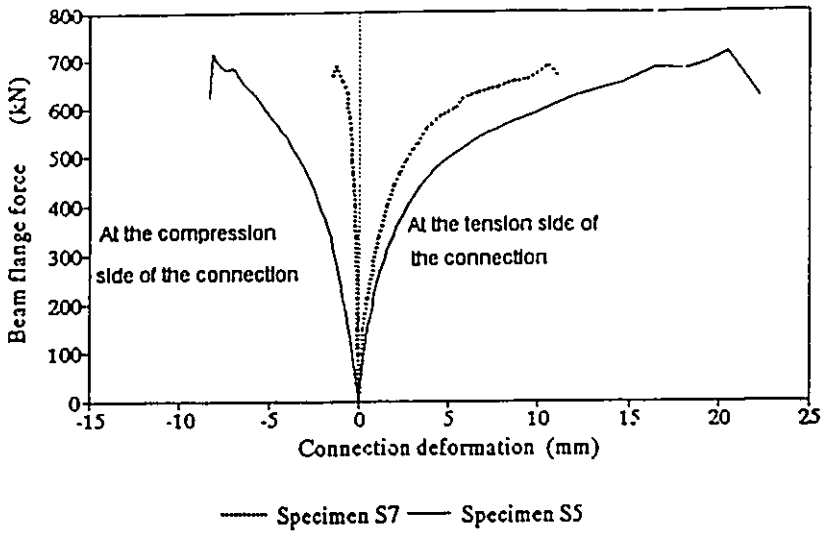


Fig 3.36 Comparison of connection deformations for specimens S5 and S7

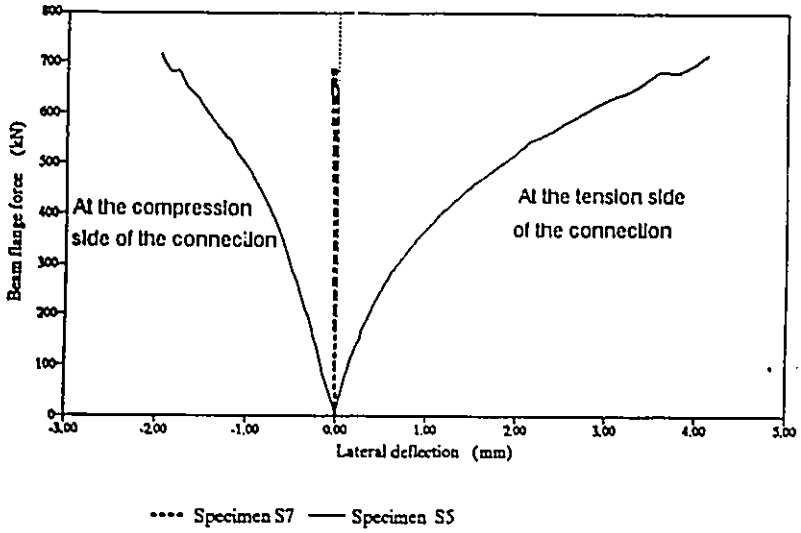


Fig 3.37 Comparison of HSS side walls deflections for specimens S5 and S7

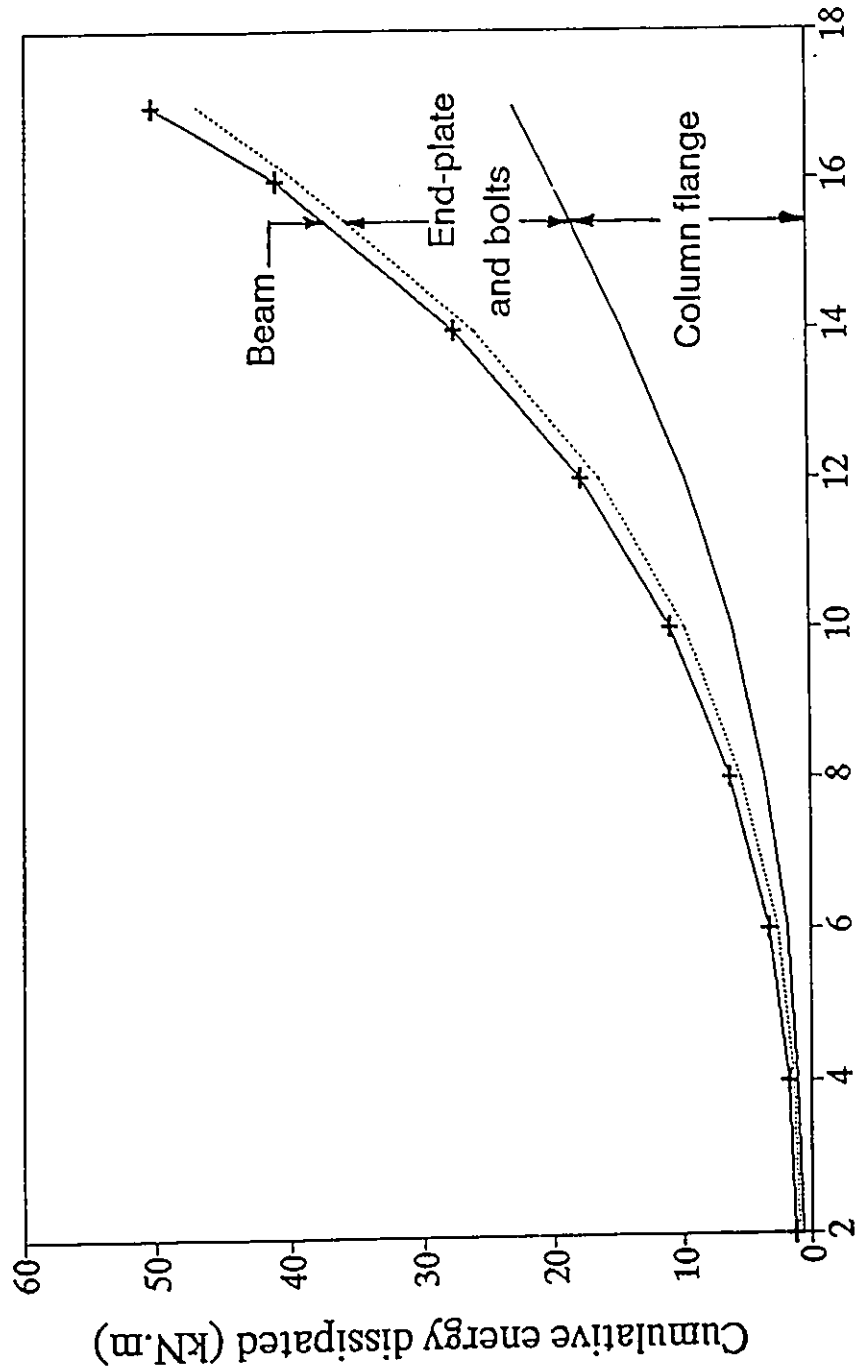


Fig 3.38 Cumulative energy dissipated by each component in specimen C1

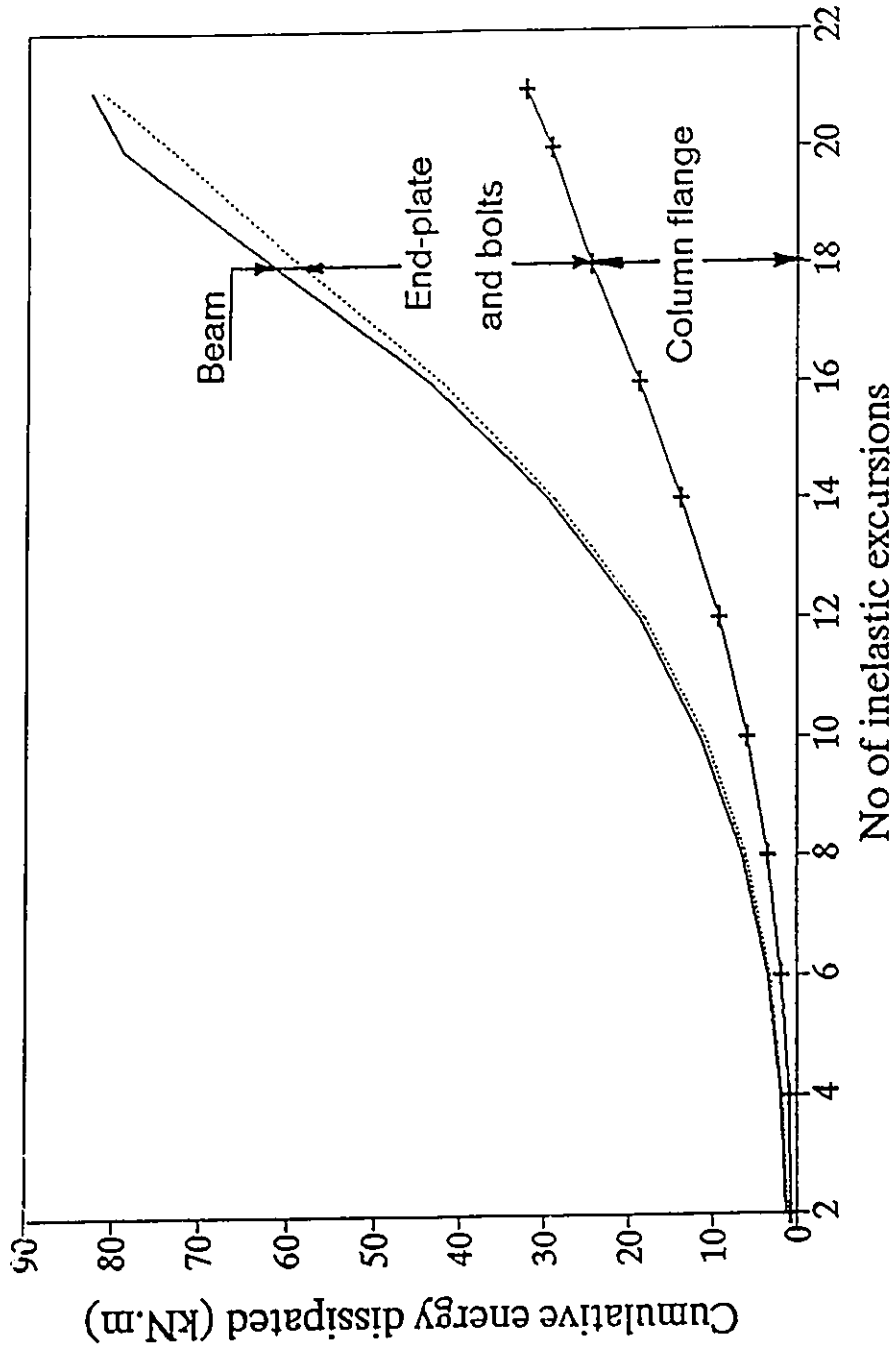


Fig 3.39 Cumulative energy dissipated by each component in specimen C2

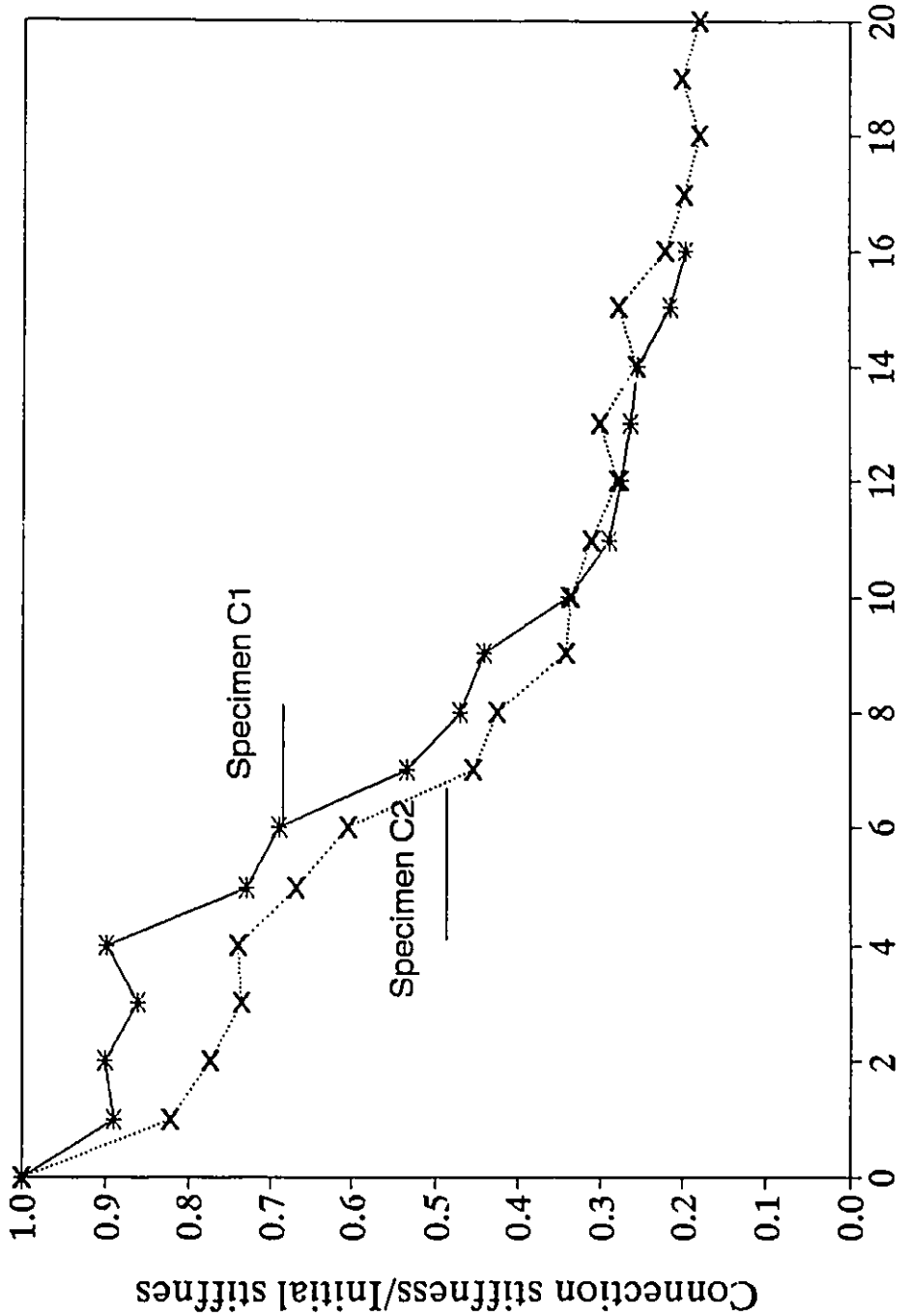


Fig 3.40 Variation of connection stiffness relative to initial stiffness

# CHAPTER 4

# CONNECTION RESPONSE

## 4.1 Introduction

In the experimental program on extended end-plate connection for square HSS columns, the connections showed a degree of flexibility especially in the post-elastic range. As such, the actual response of frames utilizing this type of connection should be assessed by incorporating the connection flexibility in the analysis. This requires the development of a constitutive moment-rotation relationship capable of representing such connection response.

In the past, several researchers attempted to simulate connection behaviour under general loading conditions. Different models have been used which include purely empirical curve fitting of test data (Frye and Morris, 1976; Ang and Morris, 1984), analogy and semi-empirical techniques (Mzzalani, 1987), and comprehensive theoretical models. Some of these models are sophisticated and fairly accurate in predicting connection response; others are simple with only a limited ability to approximate the key features of the connection response.

The degree of model sophistication and its capability of accurately predicting the connection behaviour depends mainly on the purpose for which it is to be used. For example, if the overall response of a moment resisting frame is to be determined, simple models that are capable of handling only the key aspects of the connection response may be adequate. Nethercot and Zandonini (1989) suggested that, in such cases, the adequacy

of the predicted model should be judged not merely on the basis of the level of accuracy achieved in approximating the actual moment-rotation curve, but rather on the effect of this approximation on the overall frame performance. On the other hand, if the influence of the end-restraint on strength or stability of the column is to be investigated, Jones et al. (1982) have suggested that an accurate prediction of the connection response is necessary.

In this chapter three models have been developed to predict the moment-rotation relationship of an extended end-plate connection for square HSS columns. The first model is analytically sophisticated and is capable of accurately predicting the connection's non-linear response under monotonic loading. The model uses parameters that are determined based on both geometrical and mechanical properties of the connection without the need for physical tests. In order to simplify the use of the model, graphs and tables for various parameters have been prepared. The second and the third models are simplified versions that represent the response as either bi-linear or tri-linear. These simplifications were developed to study the effect of a connection's flexibility on frame response. A connection element based on the latter two models has been incorporated in a computer program for evaluating the behaviour of the frame.

In an extended end-plate connection for hollow section columns, the main components that contribute to the connection rotation are;

1- End-plate deformation on the tension side of the connection $\Delta_{ep}$,

2- Column flange deformation at bolt locations on the tension side of the connection $\Delta_{cft}$,

3- Column flange deformation on the compression side of the connection $\Delta_{cfc}$.

The contribution of the bolt elongation in evaluating the connection rotation is assumed to be negligible, since the bolts are pre-tensioned to about 70% of their tensile strength.

Since the flange of the hollow section column contributes to the connection rotation, it needs to be modelled properly to take into account the effect of restraints at the corners. Modelling the behaviour of the column flange will be discussed in the next section before describing the more sophisticated connection model.

## 4.2 Modelling of the HSS column flange

To evaluate the initial stiffness of the connection, elastic deflections of the column flange on both the tension and compression sides should be determined. Several researchers have modelled the flange for different types of joints employing rectangular hollow sections (RHS) as single chord T-joints under axial load and applied moment. In these models the flat part of the RHS flange is separated from the rest of the section. The effect of the rest of the section on the flat part of the column flange may be modelled by introducing both translational and rotational springs along the longitudinal edges of the flat plate portion of the member. Mansour and Korol (1977) solved the plate numerically in the elastic range by considering the springs to be uncoupled. Their results compared well with available experimental results when the vertical spring constant approaches infinity while the rotational spring constant $>0$. Shehata (1983) and El-Hifnawy (1980) considered the springs to be coupled in solving the flat part of the hollow section.

Elasto-plastic finite element formulation utilizing rectangular plate bending elements and boundary spring elements was proposed to model the flange plate. These models were used to determine the initial stiffness as well as the ultimate strength of truss T-joints and to compare the predictions with experimental results availale in the literature.

Modelling the elastic behaviour involved several assumptions:

1- The deflection of the column flange due to either tension loading on one side of the beam or compression loading on the other side, are assumed uncoupled. This assumption may not be quite applicable for end-plate cases of low length/width ratio, however such an assumption is needed to simplify the determination of the connection initial stiffness. The stiffness determined using the uncoupling assumption is slightly lower than the case of coupling the beam flange forces.

2- The inplane deformation of the side walls of the column is negligible, and, as such, the side walls can be assumed to act as rigid supports for the column flange.

3- The side walls of the column will provide rotational restraints to the longitudinal edges of the column flange.

According to the above assumptions, the column flange can be modeled as a thin plate with width equal to $H_o - 2t_o$, where $H_o$ and $t_o$ are the outer dimension and thickness of the square column respectively. The plate is assumed to be long enough to be considered as an infinitely long plate. A plate length several times the width exhibits behaviour much like an infinite long plate (approximation of storey height). In this study it was found that a length 4 times the width approaches this response. The longitudinal edges of the flange plate are assumed to be simply supported in the normal direction to the column flange with both rotational and horizontal translational coupled springs along

its longitudinal edges (Fig 4.1). The transverse edges are assumed to be simply supported.

The coefficients of the spring stiffness matrix per unit length were determined by considering the stiffness matrix of a unit width of the side of the column (AB) with a length equal to $H_o$- $t_o$, as shown in Fig 4.1. Based on tests of an earlier study, Korol et al. (1977) suggested that the lower third of the height of the side walls of the HSS section remained relatively undeformed, when subjected to loading on the column flange only. As such, a fixed support was assumed at the far end "A". To account for plate action, the member flexural rigidity "EI" per unit width was replaced by the plate bending rigidity "D", while, the spring stiffness matrix $[K_s]$ relates the force vector with the deformation vector at point "B" as follows;

$$\begin{bmatrix} F_B \\ M_B \end{bmatrix} = [K_s] \begin{bmatrix} u_B \\ \theta_B \end{bmatrix} \tag{4.1}$$

where,

$$[K_s] = \begin{bmatrix} \frac{12D_{sw}}{L_s^3} & \frac{-6D_{sw}}{L_s^2} \\ \frac{-6D_{sw}}{L_s^2} & \frac{4D_{sw}}{L_s} \end{bmatrix}$$

with,

$D_{sw}$ : side wall bending rigidity = $E\, t_{sw}^{\,3} / 12(1-\nu^2)$
$E$ : modulus of elasticity
$t_{sw}$ : side wall thickness; for unstiffened side wall= $t_o$
$\nu$ : Poisson's ratio
$L_s$ : side wall length = $H_o$- $t_o$

The column flange was analyzed using a finite element program utilizing rectangular plate bending elements with inplane degree of freedoms (5 degrees of freedom at each node - $w$, $w_x$, $w_y$, $u$ *and* $v$). The program was modified to account for the additional spring boundary elements along the longitudinal edges of the column flange. A complete formulation of the finite element solution as well as the incorporation of the spring boundary elements in the analysis were reported by Shehata (1983) and El-Hifnawy (1980).

### 4.2.1 Modelling the column flange on the tension side of the connection.

The column flange on the tension side of the connection was modeled as a long plate. The thickness of the unstiffened column flange $t_{cf}$ is equal to $t_o$ (thickness of HSS). In the case of a stiffened column flange with a doubler plate of thickness $t_{dp}$, the equivalent thickness of the column flange is taken as if the two plates (column flange and the doubler plate) are sliding on each other. This assumption is made because there is unlikely to be full shear interaction between the two plates due to perimeter welds only, and lack of flatness after welding. This behaviour was observed from the tested connections. As such, a conservative assumption made for the equivalent column flange thickness is thus:

$$t_{cf} = t_o \qquad \textit{for an unstiffened column flange} \tag{4.2}$$

$$t_{cf} = \sqrt[3]{t_o^3 + t_{dp}^3} \qquad \textit{for a stiffened column flange}$$

In the case of a concrete filled HSS column such as specimen S7, the side walls are prevented from deflecting inwards. The longitudinal edges of the column flange on the tension side were therefore assumed to be totally fixed against rotation.

The tension beam flange force "P" is assumed to be transmitted to the column flange by 4 equal forces each P/4 at the bolt locations, as shown in Fig 4.2 (a). If double symmetry is assumed on the idealized column flange, only one quarter of the plate needs to be analyzed. As described earlier, a finite element program was used taking into account the appropriate boundary spring elements with the specified boundary conditions, as shown in Fig 4.2 (b). From the analysis, the column flange deflection at a bolt location $\Delta_{cft}$ was obtained in terms of the beam flange force P.

### 4.2.2 Modelling the column flange on the compression side of the connection.

The column flange on the compression side was modeled as a long plate, with its deflection depending not only on the thickness of the column flange, but also on the size of the end-plate. The end-plate width was taken equal to the idealized column flange width "$H_o$-2$t_o$"; meanwhile, the modeled length of the end-plate "$L_{tp}$" was taken to be equal to twice the projection of the end-plate from the centre of the beam compression flange. The portion of the end-plate around the external washer of the HSBBs was considered to be in full contact with the column flange due to the bolt's pre-tension force, while the rest of the end-plate was assumed to freely slide on the column flange surface. To determine the deflection of the column flange on the compression side $\Delta_{cfc}$, an effective end-plate thickness $t_{tp}$(eff) was obtained on the basis of allocating

proportionate areas with corresponding equivalent thicknesses as illustrated in Appendix A. The beam compression flange force "P" is assumed to be uniformly distributed over the area of the beam flange and the surrounding welds, with a stress intensity $\sigma$, given by;

$$\sigma = \frac{P}{(t_{bf}+2w_{bf})\ (b_f+2w_{bf})} \tag{4.3}$$

where

$b_f$ : beam flange width
$t_{bf}$ : beam flange thickness
$w_{bf}$ : size of beam flange fillet weld

The column flange on the compression side was analyzed with the spring boundaries and the effective end-plate thickness under the loading given by Eq 4.3, as shown in Fig 4.3 (a). Since double symmetry about the centre lines of the beam flange and column was assumed, only one quarter of the plate needed to be analyzed by the finite element program with the appropriate specified boundary conditions, as shown in Fig. 4.3 (b). From the analysis, the average column flange deflection $\Delta_{cfc}$ across the beam width was then obtained as a linear function of the beam flange force P.

## 4.3 Comprehensive nonlinear model of the connection.

A four parameter exponential model (Yee and Melcher, 1986) was used to predict the overall non-linear connection response, typified by the curve shown in Fig 4.4. Osman et al. (1990) used such a model to represent the moment-rotation relationship of an extended end-plate connection to W-shape column, where it was shown to be capable

of predicting the response of a single beam to column connection with good accuracy. The equation is given by;

$$M = M_{pc} \left[1 - e^{-(K_i - K_p + C\,\theta)\frac{\theta}{M_{pc}}}\right] + K_p\theta \qquad (4.4)$$

where

$K_i$ = initial elastic stiffness,
$K_p$ = post elastic stiffness,
$M_{pc}$ = plastic moment capacity of the connection,
C = rate of decay parameter, and,
$\theta$ = connection rotation in radians.

This equation has the following characteristics; $dM/d\theta = K_i$ at $\theta=0$ (the slope of the curve at the origin is equal to the initial elastic stiffness of the connection); $dM/d\theta = K_p$ as $\theta$ tends to $\infty$ (as the rotation becomes large, the slope of the curve approaches the post elastic stiffness); and $M=0$ at $\theta=0$. However, the use of this expression requires the determination of connection parameters $K_i$, $K_p$, C and $M_{pc}$. Rather than determining these parameters experimentally, an approach which would be both costly and impractical, this study has employed an analytical technique which is explained in the following sub-sections:

### 4.3.1 Evaluation of connection initial stiffness ($K_i$)

For evaluating the initial stiffness, the following assumptions are made;

1- The material is linear elastic,

2- The deformations are small and mainly due to bending, and,

3- In-plane deformations are insignificant and negligible.

On the basis of these assumptions, the connection's initial stiffness is given by:

$$K_i = \frac{M}{\theta} \tag{4.5}$$

Referring to Fig 4.5, the connection rotation "$\theta$" can be related to the connection deformations as:

$$\theta = \frac{\Delta_T}{(d_b - t_{bf})} \tag{4.6}$$

where;

$\Delta_T$ = total connection deformation,
$d_b$ = beam depth, and
$t_{bf}$ = beam flange thickness

The connection moment "M" can be replaced by two equal and opposite forces acting through the beam flange as

$$M = P\ (d_b - t_{bf}) \tag{4.7}$$

Substituting Eqs. 4.6, 4.7 into Eq 4.5, the initial stiffness can be related to both the beam flange force "P" and the total connection deformation "$\Delta_T$"

$$K_i = \frac{P\ (d_b - t_{bf})^2}{\Delta_T} \tag{4.8}$$

Eq. 4.8 suggests that once $\Delta_T$ is calculated in terms of the beam flange force "P" the connection initial stiffness "$K_i$" can be determined. The total deformation can be calculated by superimposing the deformation of individual components. Thus

$$\Delta_T = \Delta_{ep} + \Delta_{cft} + \Delta_{cfc} \tag{4.9}$$

These elastic deformations can be determined in terms of the beam flange force "P" as described below.

**a) End-plate deformation, $\Delta_{ep}$**

The end-plate can be idealized by using a T-stub model (Osman et al., 1990) and is shown by the shaded area in Fig 4.6. The analysis is based on the modified slope deflection equation (Azizinamini et al., 1987) to account for shear deformation effects especially for thick end-plates. The following assumptions were made to be consistent with the deformation model in Fig 4.6 (b).

1- The bolts are fully pre-tensioned (i.e with infinite stiffness).

2- The end-plate allows deformation only between the bolts and the tensile beam flange.

3- Stiffening from the beam's web is neglected.

4- Prying action is concentrated at the tips of the end-plate.

According to the above assumptions, the end-plate deflection was derived (Osman et al., 1990) as illustrated in Appendix B for the case of $b_1=b_2=b$, and given by;

$$\Delta_{ep} = \frac{P}{R_{ep}} \tag{4.10}$$

where,

$$R_{ep} = \frac{12EI_{ep}}{b^3\,(1+r_2)}\left[\,2 - \frac{6}{b(1+r_2)}\,\frac{1}{\dfrac{12}{a(4+r_1)}+\dfrac{4+r_2}{b(1+r_2)}}\,\right] \qquad (4.11)$$

Here,

$r_i$ = $12EI_{ep}/L_i^2GA_s$, ($r_1$ is associated with the length a, $r_2$ is associated with b)
$L_i$ = length of the segments such as (a) or (b)
a = edge distance of exterior bolts
b = distance from one bolt line to the centre of beam flange weld
$I_{ep}$ = moment of inertia of the end-plate = $B_{ep}\,(t_{ep})^3/12$
G = shear modulus
$A_s$ = effective shear area of end-plate = 2/3 ($B_{ep}$ $t_{ep}$)
$B_{ep}$ = end-plate width
$t_{ep}$ = end-plate thickness

**b) Deflection of column flange at bolt locations on tension side, $\Delta_{cft}$**

**i) Hollow steel box column**

The column flange deflection at bolt location can be determined from the finite element analysis described earlier in Section 4.2.1. Two graphs were obtained from the finite element analysis for the direct determination of the deflection at bolt locations $\Delta_{cft}$ as given and explained in Appendix C. The first graph, Fig C.1, was obtained to evaluate the column flange deflection $\Delta_{cfts}$ assuming its longitudinal edges were simply supported in terms of coefficient $\gamma_s$. The second graph, Fig C.2, was obtained to evaluate the reduction factor "R*" in deflection due to the rotational restraints at the longitudinal

edges. To evaluate the column flange deflection at bolt locations $\Delta_{cft}$, the following approach is proposed

1- Determine the deflection of the column flange at bolt location assuming the longitudinal edges are simply supported "$\Delta_{cfts}$" using Fig C.1

2- Determine the reduction factor "R*" for the deflection "$\Delta_{cfts}$" due to the restraining effect of the rotational springs along the longitudinal edges of the column flange from Fig C.2.

The deflection of the column flange at a bolt location on the tension side, can be obtained as:

$$\Delta_{cft} = R^* \Delta_{cfts} \tag{4.12}$$

**ii) Concrete filled HSS column**

For the case when the column is filled with concrete, the assumption is made that the longitudinal edges of the flange plate are fixed. Therefore, a similar graph was obtained for the case of a long plate with fixed longitudinal edges to evaluate the deflection of the column flange at bolt location $\Delta_{cft(concrete)}$ in terms of coefficient $\gamma_f$ as shown in Fig C.3. The deflection $\Delta_{cft(concrete)}$ is given by:

$$\Delta_{cft(concrete)} = \frac{\gamma_f \; P \; (H_o - 2t_o)^2}{D_{cf}} \tag{4.13}$$

c) **Average column flange deflection across the beam flange, $\Delta_{cfc}$**

The average deflection of the column flange on the compression side can be calculated from the formula

$$\Delta_{cfc} = \alpha_c \, 10^{-3} \, P \tag{4.14}$$

where, "P" is the beam flange force and "$\alpha_c$" is a coefficient determined analytically from the finite element analysis described earlier and listed in Tables D.1 to D.4 given in Appendix D for different column and end-plate sizes.

In the case of an HSS concrete filled column, the deflection of the column flange on the compression side can be assumed to be negligible when compared to that at the tension side, as was illustrated by the test results of specimen S7 (Fig 3.36).

The initial stiffnesses of the tested connections (S3 to C2) were evaluated using the proposed analytical approach, as listed in Table 4.1, and were compared with the test results as shown in Fig 4.7. Good agreement exists between the model and test results with the maximum absolute difference not exceeding 10%.

### 4.3.2 Evaluation of connection plastic moment, $M_{pc}$

The plastic moment capacity of the connection $M_{pc}$ is defined as the maximum moment that can be transmitted by the connection prior to the first yielding of its

components. It represents the smallest moment that will cause yielding to either the end-plate or the column flange.

**a) Yield load of end-plate, $P_{p(ep)}$**

Fig 4.8 shows two different yield line mechanisms by which the end-plate may fail. These mechanisms are kinematically feasible and represent very closely the observed yield lines in experiments. Mechanism (1), (Packer and Morris, 1979) was based on the behaviour of T-stubs, while Mechanism (2), (Surtess and Mann, 1970, and Whittaker and Walpole, 1982) was based on the behaviour of extended end-plates. For the tested connections, it was found that the end-plate can be represented better by isolated T-stubs, as was established by Packer and Morris (1979) and Osman et al. (1990). Because the bending stiffness of HSBBs is much less than that of the ordinary high strength bolts (smaller shanke diameter), the internal work done by HSBBs due to bending does not compensate for the reduction of the internal work done due to the existence of the holes in the plate. Conservatively, the end-plate yield load was modified to take into account the reduction in its strength due to the existence of the holes, as follows:

For mechanism 1

$$P_{p(ep)} = \frac{\sigma_{ye}\, t_{ep}^{\,2}\, (B_{ep}-d)}{b} \qquad (4.15)$$

For mechanism 2

$$P_{p(ep)} = t_{ep}^{2}\ \sigma_{ye}\ [\frac{2\ (B_{ep}-d)}{(Y_B-t_{bf}-2w_{bf})} + \frac{2\ (p-d/2)}{(X_B-t_{bw}-2w_{bw})}] \qquad (4.16)$$

where;

$\sigma_{ye}$ = yield stress of end-plate
d = diameter of bolt's hole
b = distance from one bolt line to the centre of the beam flange fillet weld
p = 0.6 ($d_b$-$t_{bf}$)
$t_{bw}$ = beam web thickness
$w_{bw}$ = size of beam web fillet weld

Later, Walpole (1985) recommended that mechanism (1) be used when the beam is fillet welded to the end-plate, while mechansim (2) be used when the beam is butt weld to the end-plate.

**b) Yield load of column flange on tension side, $P_{p(cft)}$.**

Two mechanisms were developed for the unstiffened column flange on the tension side of the connection, as shown in Fig 4.9 (a) & (b). The first is a quadrilateral mechanism, while the second is conical. The corresponding yield loads are given in the form:

For mechanism 1

$$P_{p(cft)} = \frac{2\ \sigma_{yc}\ t_o^{2}}{(1-\beta)}[\ (\eta-\gamma) + 2\ \sqrt{(1-\gamma)(1-\beta)}\ ] \qquad (4.17)$$

For mechanism 2

$$P_{p(cft)} = \sigma_{yc}\, t_o^2 \left[\pi \left(1-\frac{\gamma}{2\,(1-\beta)}\right) + 2\,\frac{(\beta+\eta-\gamma)}{(1-\beta)}\right] \qquad (4.18)$$

where;

$$\beta=\frac{X_B}{(H_o-t_o)} \qquad \eta=\frac{Y_B}{(H_o-t_o)} \qquad \gamma=\frac{d}{(H_o-t_o)}$$

$\sigma_{yc}$ = yield stress of HSS column flange,
$X_B$ = horizontal distance between bolts and
$Y_B$ = vertical distance between bolts

From a theoretical point of view, mechanism 1 usually governs the column flange yield load for $\beta$ values $\geq$ 0.65.

In the case of a stiffened column flange with a doubler plate, the yield line mechanism developed by Korol et al. (1982) for a stiffened column flange is modified (Appendix E) to take into account the variation in the yield strength in both the column flange "$\sigma_{yc}$" and the doubler plate "$\sigma_{yd}$" as well as the reduction in strength due to the holes. The yield load is given by mechanism 3 as illustrated in Fig 4.10 as follows;

$$P_{p(cft)} = m_p \left[\frac{4(b_c-d)}{u}+8\frac{(Y_B+2u-d)}{(b_c-X_B)}\right] + m_p^*\left[\frac{4(b_{dp}-d)}{u}+\frac{4}{(b_c-X_B)}\left\{Y_B+2u\left(\frac{b_{dp}-X_B}{b_c-X_B}\right)-2d\right\}\right] \qquad (4.19)$$

where;

$m_p$ = plastic moment per unit length of column flange = $\sigma_{yc}\, t_o^2/4$
$m_p^*$ = plastic moment per unit length of doubler plate = $\sigma_{yd}\, t_{dp}^2/4$
g = $m_p^*/mp$
$b_{dp}$ = width of doubler plate
$b_c$ = $H_o$ - $t_o$
u = dimension shown in Fig 4.10

For a minimum value of $P_{p(cfl)}$, u is given by;

$$u = \sqrt{\frac{(b_c - X_B)^2 \ [(b_c - d) + g(b_{dp} - d)]}{4(b_c - X_B) + 2g(b_{dp} - X_B)}} \qquad (4.20)$$

It should be noted that Eq 4.19 degenerates to Eq 4.17 when $t_{dp}=0$.

**c) Yield load of column flange on compression side, $P_{p(cfc)}$.**

The load on the column flange due to the beam compression flange force was assumed to be uniformly distributed over a rectangular area, as shown in Fig 4.11. This assumption is in agreement with the observed prints of the carbon paper used in tests. The yield load of the column flange at the compression side $P_{p(cfc)}$ will be as given by Eq 4.17 (mechanism 1) in the case of an unstiffened column flange, or as given by Eq 4.19 (mechanism 3) in the case of a stiffened column flange with the following substitutions; $X_B=X^*_B$, $Y_B=Y^*_B$ and $d=0$.

where, $X^*_B = b_f+2w_{bf}+2t_{ep}+t_{cf} \leq B_{ep}$

$Y^*_B = t_{bf}+2w_{bf}+2t_{ep}+t_{cf}$

For the tested connections, it was found that the column flange yield load was governed by that obtained from the tension side rather than the compression side.

Once the different values of "$P_p$" are calculated, the least value is selected. This value will correspond to the load required to yield the weakest element in the connection. This value is used to calculate the plastic moment capacity of the connection by the formula:

$$M_{pc} = P_p (d_b - t_{bf}) \quad (4.21)$$

The yield load corresponding to each component of the tested connections (S3 to C2) was evaluated using the above equations. The lowest value was selected to compute the connection plastic moment as listed in Table 4.1, and was compared with test results as shown in Fig 4.12. The component which governed the connection plastic moment was in accordance with that obtained from the experimental results. Good agreement is evident with a maximum absolute difference not exceeding 10%.

### 4.3.3 Evaluation of post-elastic stiffness $K_p$.

In the experimental phase of this study, tests conducted on full scale specimens showed that such a connection exhibits a post-elastic stiffness $K_p$ (strain-hardening) especially when the column flange is stiffened with a doubler plate. The post-elastic stiffness was observed to be between 5% - 10 % of the initial stiffness. Although this range is higher than expected for strain-hardening ranges, it appears that changes in geometry of the column flange and end-plate during loading account for part of the stiffening effect. It was also observed that the strain-hardening branch in the moment-rotation curves of the tested connections, is almost linear in the range of 1.2 - 1.3 $M_{pc}$ (Plastic moment of the connection), provided that it reaches its ultimate capacity "$M_u$". The evaluation of the ultimate moment capacity of the connection "$M_u$", is presented in Section 4.3.5. The post-elastic stiffness "$K_p$" of the connection was evaluated at an intermidiate moment level equal to 1.25 $M_{pc}$, except where the connection reached its

ultimate moment capacity "$M_u$". The post-elastic stiffness "$K_p$" may therefore be defined as:

$$K_p = \frac{(M^* - M_{pc})\ (d_b - t_{bf})}{(\Delta_T)^*} \qquad (4.22)$$

where;

$M^*$ = the lesser moment of 1.25 $M_{pc}$ or $M_u$

$(\Delta_T)^*$ = the total deformation experienced by the connection at a moment equal to M* and given by:

$$(\Delta_T)^* = (\Delta_{ep})^* + (\Delta_{cft})^* + (\Delta_{cfc})^* \qquad (4.23)$$

where $(\Delta_{ep})^*$, $(\Delta_{cft})^*$ and $(\Delta_{cfc})^*$ are the total deflections of the end-plate, column flange on the tension side and compression side respectively at a moment equal to M*.

In evaluating the total deflection of each component $(\Delta)^*$, it was assumed that once each component formed a mechanism and reached its own yield load with a deflection equal to $(\Delta)_y$, the behaviour of the material would be rigid-plastic behaviour, (i.e. the material being free to rotate about all yield lines without strain-hardening). If any component had to resist loads above its own yield load, it would be by membrane action due to a change in geometry with the resulting deflection equal to $(\Delta)_m$.

Therefore,

$$(\Delta)^* = (\Delta)_y + (\Delta)_m \qquad (4.24)$$

For each component (end-plate, column flange tension or at compression side), deflection at its own yield load $(\Delta)_y$ was assumed to be the sum of two parts. The first part "$(\Delta)_1$" is the elastic deflection due to bending until first yield lines are formed. The

second part "$(\Delta)_2$" results from the rest of the yield load acting on that component assuming hinges where the first yield lines are formed. Thus:

$$(\Delta)_y = (\Delta)_1 + (\Delta)_2 \tag{4.25}$$

The deflections $(\Delta)_y$ and $(\Delta)_m$ for each component can be determined separately as described below.

**a) Total deflection of the end-plate, $(\Delta_{ep})^*$**

The total end-plate deflection for this component $(\Delta_{ep})^*$ at a moment equal to M* is given as follows:

$$(\Delta_{ep})^* = (\Delta_{ep})_y + (\Delta_{ep})_m \tag{4.26}$$

and,

$$(\Delta_{ep})_y = (\Delta_{ep})_1 + (\Delta_{ep})_2 \tag{4.27}$$

where $(\Delta_{ep})_1$ is the end-plate deflection when the first yield lines are formed at the beam flange junction for a beam flange force equal to $(P_{ep})_1$. The beam flange force $(P_{ep})_1$, can be obtained by equating the moment developed in the end-plate at the beam flange junction to the plastic moment capacity of the end-plate, given by:

$$(P_{ep})_1 = \left[\frac{b^2\,(1+r_2)\,R_{ep}}{6\,E\,I_{ep}}\right] \frac{B_{ep}\,\sigma_{ye}\,t_{ep}^{\,2}}{4} \tag{4.28}$$

Therefore, from Eq. 4.10

$$(\Delta_{ep})_1 = \frac{(P_{ep})_1}{R_{ep}} = \frac{b^2(1+r_2)\ B_{ep}\ \sigma_{ye}\ t_{ep}^2}{24\ E\ I_{ep}} \tag{4.29}$$

The rest of the end-plate load $(P_{ep})_2$ is assumed to act on the idealized end-plate model with hinges at the beam flange junction. Taking shear deformation into account, the resulting end-plate deflection $(\Delta_{ep})_2$ is given by:

$$(\Delta_{ep})_2 = (P_{ep})_2\ \left[\frac{b^2\ (b+a)}{6\ E\ I_{ep}} + \frac{b\ (1+b/a)}{2\ G\ A_s}\right] \tag{4.30}$$

where, $(P_{ep})_2$ is the lesser load of $[P_{p(ep)}-(P_{ep})_1]$ or $[\{M^*/(d_b-t_{bf})\}-(P_{ep})_1]$. Membrane action will take place in the end-plate only if it has to resist loads higher than its yield load $P_{p(ep)}$, or when

$$\Delta P^*_{(ep)} = \left(\frac{M^*}{d_b-t_{bf}} - P_{p(ep)}\right) > 0 \tag{4.31}$$

The end-plate deflection due to membrane action $(\Delta_{ep})_m$ which results from $\Delta P^*_{(ep)}$ is obtained as explained in Appendix F and given by:

$$(\Delta_{ep})_m = \frac{b\ \sin\ (\Delta\theta)}{\cos\ (\theta_y+\Delta\theta)} \tag{4.32}$$

where, $\theta_y = (\Delta_{cp})_y/b$, and $\Delta\theta$ is determined as illustrated in Appendix F.

**b) Total deflection of the column flange on the tension side, $(\Delta_{cft})^*$**

The total deflection of the column flange on the tension side of the connection, $(\Delta_{cft})^*$, at moment equal to M* is given by:

$$(\Delta_{cft})^* = (\Delta_{cft})_y + (\Delta_{cft})_m \tag{4.33}$$

where,

$$(\Delta_{cft})_y = (\Delta_{cft})_1 + (\Delta_{cft})_2 \tag{4.34}$$

$(\Delta_{cft})_1$ is the column flange deflection at bolt locations at a beam flange force equal to $(P_{cft})_1$. The beam flange force $(P_{cft})_1$ is the load which develops the longitudinal yield lines at the column flange edges in mechanisms (1), (2) or (3) shown in Figs 4.9 and 4.10. Subsequently, the column flange is assumed to deflect as a long simply supported plate until it reaches its full yield load $P_{p(cft)}$, to produce an additional deflection equal to $(\Delta_{cft})_2$. The beam flange force $(P_{cft})_1$ can be obtained by equating the moment developed along the longitudinal edges of the column flange to its plastic moment capacity. Moments developed in the longitudinal edges of the column flange can be obtained by modelling the column flange as a simply supported beam with an equivalent rotational spring at each support, to take into account the effect of the rest of the column section, as shown in Fig 4.13. The width of the equivalent beam "$b_{av}$" is taken to be equal to "$Y_B+u$", while its span "$b_e$" is taken to be equal to "$H_o-t_o$". The equivalent rotational spring stiffness "$K_b$" is given by;

$$K_b = K_{sw} (Y_B+2u) \tag{4.35}$$

where, "$K_{sw}$" and "u" were previously defined in Eqs C.3 and 4.20 respectively. The beam flange force $(P_{cf})_1$ is given by;

$$(P_{cft})_1 = \sigma_{yc} t_o^2 b_{av} \frac{b_c \left(\frac{2 E I_{eb}}{b_c}+K_b\right)}{2 b_x (b_c-b_x) K_b} \tag{4.36}$$

where;

$b_c = H_o-t_o$
$b_x = (b_c-X_B)/2$
$b_{av} = Y_B + u$
$I_{eb}$ = moment of inertia of the equivalent beam = $b_{av} t_{cf}^3/12$

The column flange deflection $(\Delta_{cft})_1$ with the beam flange force equal to $(P_{cft})_1$ can be evaluated elastically as described earlier in Appendix C in terms of " $\gamma_s$" and "R*" as follows:

$$(\Delta_{cft})_1 = R^* \frac{\gamma_s (P_{cft})_1 (H_o-2t_o)^2}{D_{cf}} \tag{4.37}$$

The column flange deflection $(\Delta_{cft})_2$ due to the rest of the beam flange force $(P_{cft})_2$ is obtained by assuming the longitudinal edges as simply supported, and is given by:

$$(\Delta_{cft})_2 = \frac{\gamma_s (P_{cft})_2 (H_o-2t_o)^2}{D_{cf}} \tag{4.38}$$

where, $(P_{cft})_2$ is the lesser of $\{P_{p(cft)}-(P_{cft})_1\}$ or $\{M^*/(d_b-t_{bf})-(P_{cft})_1\}$. The membrane action will only take place if

$$\Delta P^*_{(cft)} = [\frac{M^*}{d_b-t_{bf}} - P_{p(cft)}] > 0 \qquad (4.39)$$

It is assumed that $\Delta P^*_{(cft)}$ is mainly transmitted to the longitudinal edges across the width of the column flange. The column flange deflection due to membrane action $(\Delta_{cft})_m$ resulting from $\Delta P^*_{(cft)}$ is obtained as explained in Appendix F, and is given by:

$$(\Delta_{cft})_m = \frac{(b_c-X_B)\ \sin\Delta\theta}{2\ \cos\ (\theta_y+\Delta\theta)} \qquad (4.40)$$

where, $\theta_y = 2\ (\Delta_{cft})_y/(b_c-X_B)$ and $\Delta\theta$ is determined as illustrated in Appendix F.

### iii) Total deflection of the column flange on the compression side, $(\Delta_{cfc})^*$

The same procedure described for the total deflection of the column flange on the tension side is adopted herein. However, the column flange on the compression side of the connection is assumed to behave elastically until it reaches a beam flange force $(P_{cfc})_1$ given by:

$$(P_{cfc})_1 = \sigma_{yc}\ t_o^2\ b_{av}^* \frac{b_c\ (\frac{2\ E\ I_{eb}^*}{b_c}+K_b^*)}{2\ K_b^*\ (b_x^{*2}+b_x^*\ X_B^*+\frac{X_B^{*2}}{6})} \qquad (4.41)$$

where,

$K^*_b = K_{rw}\,(Y^*_B+2u)$

$X^*_B = b_f+2w_{bf}+2t_{cp}+t_{cf}$

$Y^*_B = t_{bf}+2w_{bf}+2t_{cp}+t_{cf}$

$b^*_x = (b_c-X^*_B)/2$

$b^*_{av} = Y^*_B + u$

$I^*_{cb}$ = the moment of inertia of the equivalent beam = $b^*_{av}\,[t_{cf}+t_{cp}(eff)]^3/12$

The average elastic deflection $(\Delta_{cfc})_1$, due to $(P_{cfc})_1$ can be computed from Tables D.1 to D.4 (Appendix D). The rest of the column flange load $(P_{cfc})_2$ ( the lesser of $[P_{p(cfc)}-(P_{cfc})_1]$ or $[\{M^*/(d_b-t_{bf})\}-(P_{cfc})_1]$ would act on the column flange assuming that its longitudinal edges are simply supported. From the finite element analysis, the coefficient $\gamma_c$ was determined to evaluate the average deflection across the beam flange of a long simply supported plate with different patch loading areas ($X^*_B$ $Y^*_B$), the results are plotted in Fig 4.14. Therefore, the resulting average deflection $(\Delta_{cfc})_2$ can be obtained as follows:

$$(\Delta_{cfc})_2 = \frac{\gamma_c\,(P_{cfc})_2\,(H_o-2t_o)^4}{X_B^*\,Y_B^*\,D_{cf}} \qquad (4.42)$$

The membrane action will take place in the column flange on the compression side of the connection if:

$$\Delta P^*_{(cfc)} = \left(\frac{M^*}{d_b-t_{bf}} - P_{p(cfc)}\right) > 0 \qquad (4.43)$$

The associated column flange deflection $(\Delta_{cfc})_m$ can be obtained as described earlier for $(\Delta_{cft})_m$.

Once the total deflection of each component is obtained, the post-elastic stiffness $K_p$ can be calculated from Eq 4.22. The post-elastic stiffnesses of the tested connections (S3 to C2) were evaluated using the proposed approach, as listed in Table 4.1, and were compared with the test results, as shown in Fig 4.15. It can been seen that good agreement exists between the model and the test results. The computed post-elastic stiffnesses of the tested connections were found to be in the range of 5% - 10% of the initial connection stiffness.

### 4.3.4 Evaluation of parameter, C

There is no established analytical procedure to determine the value of the rate of decay parameter "C", which only governs the shape of the transition curve between the two lines $K_i$ and $K_p$. As the value of parameter "C" approaches infinity, the moment-rotation curve approaches a bi-linear model. The parameter can be determined from tests results, as recommended by Yee and Melcher (1986). Through the experimental program on end-plate connections for unstiffened HSS columns, a value of "C" equal to zero was found to be appropriate. Meanwhile, for a stiffened HSS column either with a doubler plate or concrete filled, a value of "C" equal to $1x10^5$ kN.m/rad$^2$ was found to be appropriate for such connections.

### 4.3.5 Determination of ultimate moment capacity, $M_u$

The ultimate moment capacity of the connection "$M_u$" is considered to be the minimum moment which either causes welds fracture or bolts failure, as follows:

1- Weld fracture

According to CSA-S16.1-M89, the moment which causes either fracture of the fillet welds between the beam flange and the end-plate or failure of the base metal, is the lesser of

*For weld metal* $$M_u = \left( 0.67 \frac{A_w}{\sqrt{2}} X_u \right) \left( d_b - t_{bf} \right) \qquad (4.44)$$

*For base metal* $$M_u = \left( 0.67 A_w \sigma_y \right) \left( d_b - t_{bf} \right) \qquad (4.45)$$

where;

$A_w$ : Area of fillet welds surrounding the beam flange
$X_u$ : ultimate strength of weld as rated by electrode classification number
$\sigma_y$ : minimum yield stress of base metal

The above equations are based on the assumption that stress distribution in the weld metal and the heat affected zone of the base material would be uniform at failure.

2- High strength blind bolts failure

The moment which would cause the failure of the four bolts on the tension side of the connection, is given as:

$$M_u = \frac{(4\ T_{min})}{\Psi} \left( d_b - t_{bf} \right) \qquad (4.46)$$

where,

$T_{min}$ : minimum specified tensile strength of a HSBB bolt
$\Psi$ : prying factor to account for the exceedence in bolt's force due to prying action, it can range from 1.2 to 1.4 and is given by Eq 5.5 in chapter 5.

The ultimate moments of the tested connections (S3 to C2) were computed as listed in Table 4.1, and were compared with test results, as shown in Fig 4.16. It was found that the computed ultimate moments of the tested connections were governed by the failure of HSBBs in all cases. It can be observed that the predicted values are lower than the observed values by a maximum of 20%, except that of specimen S3 where a brittle failure occured in the heat affected zone of the beam flange due to excessive heating during welding.

### 4.3.6 Model verification.

The accuracy of the proposed model was verified by comparing its predictions with those obtained from experimental tests. Comparison between the predicted and the experimental moment-rotation curves of the tested specimens are shown in Fig 4.17 (a) through (g). As indicated from the figures, the model accurately predicts the moment-rotation relationships. Close agreement between the experimental and the predicted curves is evident. The predicted ultimate moment capacity of each connection is indicated on the curves to represent an upper bound of the moment-rotation relationship.

## 4.4 Simplified models

To incorporate the non-linear model presented in section 4.3 into a computer program for the purpose of predicting the effect of the connection flexibility on the response of a frame, the comprehensive nonlinear model was simplified and approximated to either a bi-linear or a tri-linear model. The bi-linear model of specimen S3 and the tri-linear model of specimen S4 are superimposed on their corresponding nonlinear moment-rotation relationships, as shown in Figs 4.18 and 4.19 respectively. The bi-linear model requires only four parameters to describe M-$\theta$ curve. These parameters are: (1) the connection initial stiffness $K_i$, which can be determined as described in section 4.3.1; (2) the plastic moment capacity of the connection $M_{pc}$, which can be calculated according to section 4.3.2; (3) the connection post-elastic stiffness $K_p$, as determined in section 4.3.3; and (4) the ultimate moment capacity of the connection $M_u$, as determined in section 4.3.5. The bi-linear model is obtained by plotting the initial stiffness line $K_i$ from the origin, and constructing the post-elastic stiffness line from $M_{pc}$ on the y axis. Therefore, the bi-linear model is represented by the initial stiffness line until it intersects the post-elastic line, then it follows the post-elastic stiffness line to $M_u$, as indicated in Fig 4.18.

The tri-linear model simulates the behaviour of the connection more realistically, especially for those connections which are classified as semi-rigid. The tri-linear model can be obtained from the bi-linear model by constructing a tangent at $M_{pc}$ on the comprehensive nonlinear M-$\theta$ curve, as shown in Fig 4.19. The slope of that tangent "$K_t$" is given by:

$$K_t = \frac{dM}{d\theta} = (K_i - K_p + 2C\,\theta_{pc})\; e^{-(K_i - K_p + C\,\theta_{pc})\frac{\theta_{pc}}{M_{pc}}} + K_p \qquad (4.47)$$

where; $\theta_{pc}$ is obtained from Eq 4.4 by setting $M = M_{pc}$

The intersection points "$M_1$" and "$M_2$" of that tangent with both the initial stiffness line $K_i$ and the post-elastic stiffness line $K_p$ can be determined, to develop the tri-linear model of the connection, as shown in Fig 4.19. The $K_p$ stiffness line is terminated when $M_u$ is reached.

## 4.5 Computer modelling of a semi-rigid connection element

If only flexural deformation of the connection is considered, a one degree of freedom connection element can be introduced at the beam-column intersection to model the M-$\theta$ relationship as shown in Fig 4.20. The connection element is placed between two nodes and is only influenced by the relative rotation between the nodes. The deformation of the element represents the angle change between the connected beams and columns due to connection rotation. In this element, translational displacements of the nodes at both ends of the element are constrained to be identical. In addition, they are assigned similar coordinates to satisfy equilibrium.

For a bi-linear representation of a connection, the element consists of an elastic and elastic-plastic components in parallel as shown in Fig 4.21. A plastic hinge is introduced into the elasto-plastic component once the connection yield moment is reached.

The tri-linear behaviour of a connection can be simulated by using two bi-linear elements in parallel. In this case, an elastic-perfectly plastic behaviour with initial stiffness of ($K_i$-$K_t$), yield moment equal to "$\theta_y$ ($K_i$-$K_t$)" and zero strain hardening is assigned for the first element. An elastic-strain hardening response with initial elastic stiffness equal to "$K_t$", post-elastic stiffness equal to "$K_p$" and yield moment equal to "$\theta_t$ $K_t$" is assigned to the second element, as shown in Fig 4.22.

## 4.6 Summary

A comprehensive nonlinear model that is capable of predicting the moment-rotation relationship for extended end-plate connections for HSS column is proposed. The model predicts the connection behaviour solely on the basis of its geometrical and mechanical properties without requiring physical tests on actual connections. The comparison between the experimental and analytical results of the model shows that the initial and post-elastic stiffnesses as well as the plastic and ultimate moment capacities correlate well. The model predicts with sufficient accuracy the connection rotation at all load levels. The non-linear model was approximated to either a bi-linear or a tri-linear model to be incorporated into a plane-frame computer program to assess the influence of connection flexibility on the response of a frame.

Table 4.1 Predicted connection parameters of tested specimens

| Specimen No. | Initial stiffness $K_i$ (kN.m/rad) | Post-elastic stiffness $K_p$ (kN.m/rad) | Connection plastic moment $M_{pc}$ (kN.m) | Connection ultimate moment $M_u$ (kN.m) |
|---|---|---|---|---|
| S3 | 40260 | 2100 | 133 | 215 |
| S4 | 15400 | 300 | 146 | 190 |
| S5 | 20960 | 1400 | 155 | 213 |
| S6 | 17050 | 900 | 151 | 192 |
| S7 | 67400 | 3200 | 155 | 213 |
| C1 | 23680 | 2430 | 187 | 220 |
| C2 | 19100 | 1000 | 161 | 228 |

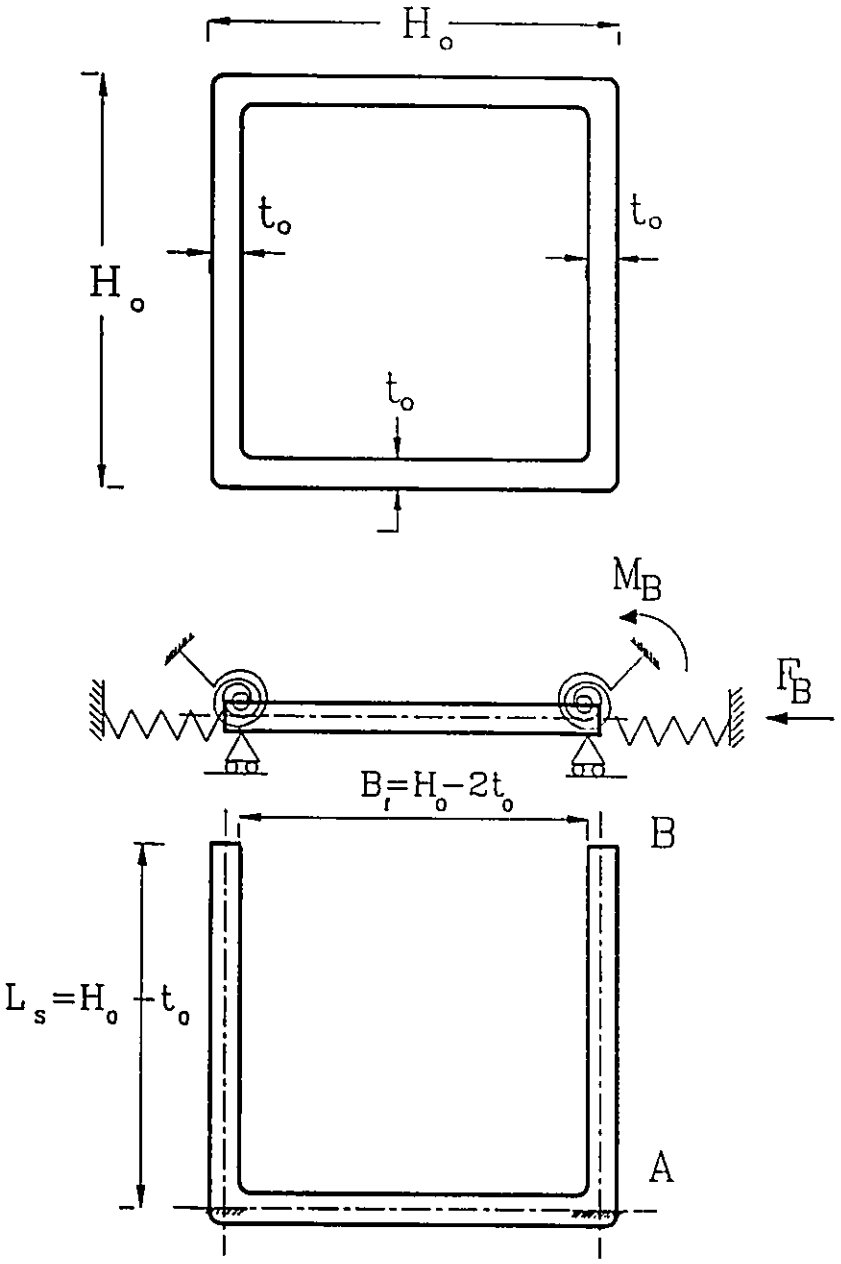


Fig 4.1 HSS column flange model

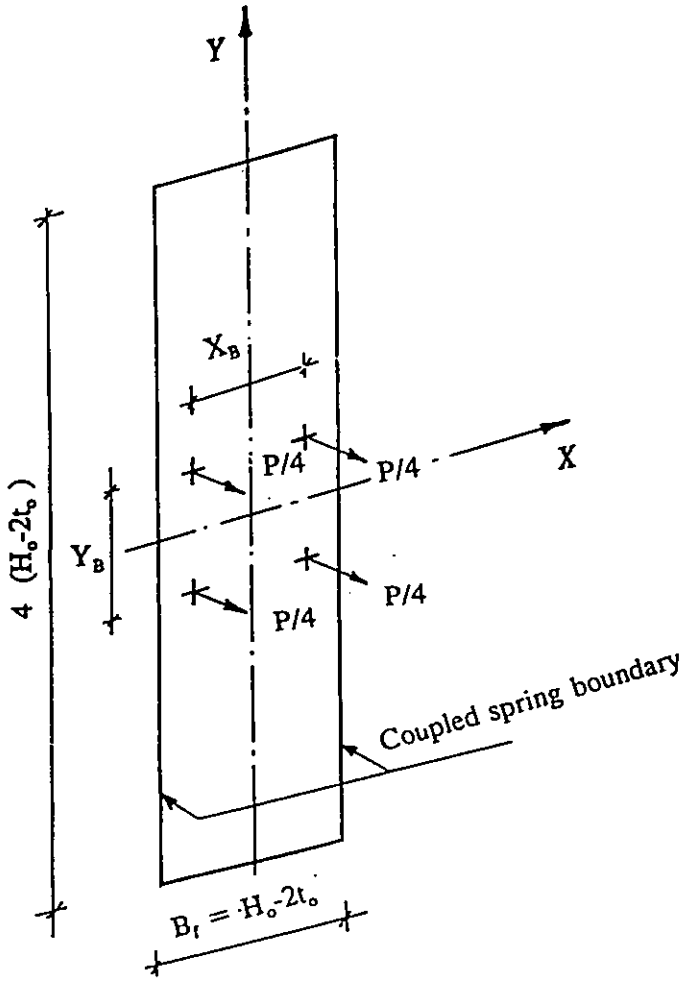


a) Loads on column flange

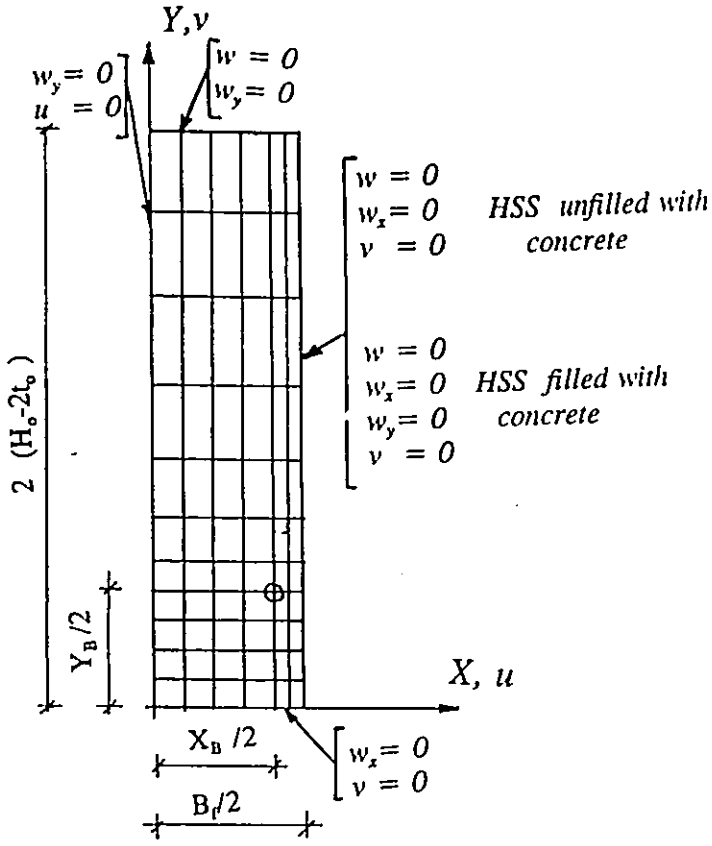


b) Finite element grid and boundary conditions of one quarter

Fig 4.2 Idealization of HSS column flange at the tension side of the connection

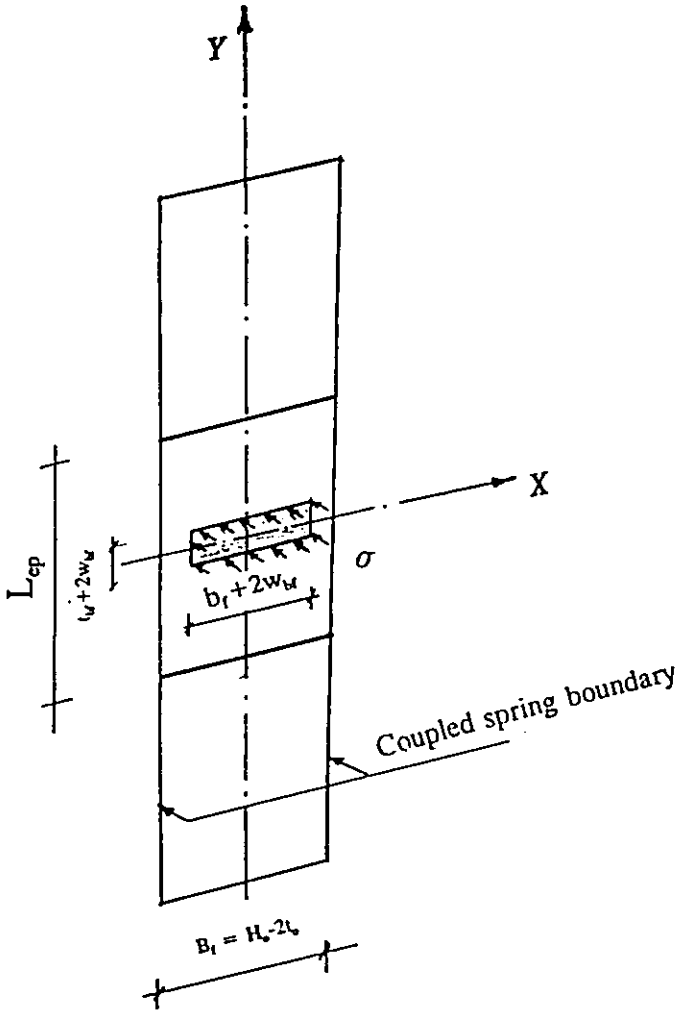


a) Loads on column flange

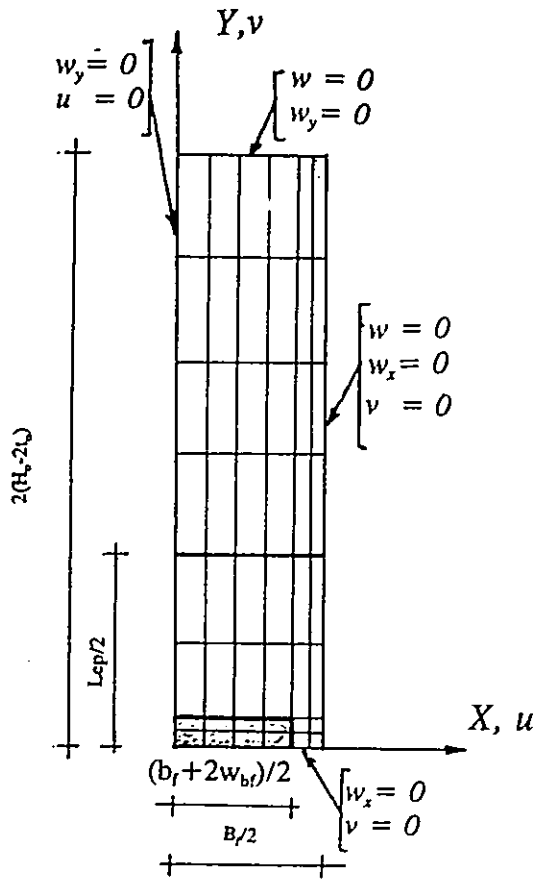


b) Finite element grid and boundary conditions of one quarter

Fig 4.3 Idealization of HSS column flange at the compression side of the connection

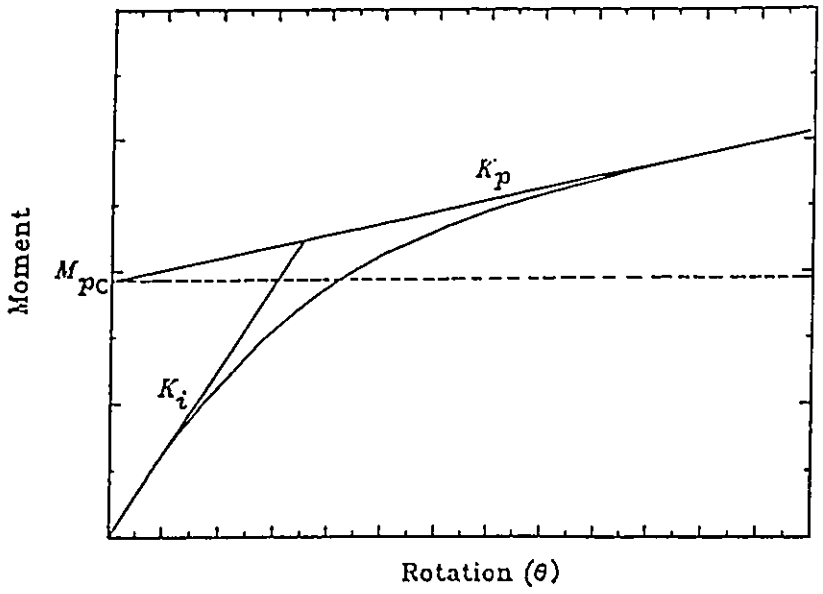


Fig 4.4 Typical moment-rotation curve shows
the model parameters (after Yee and Melcher 1986)

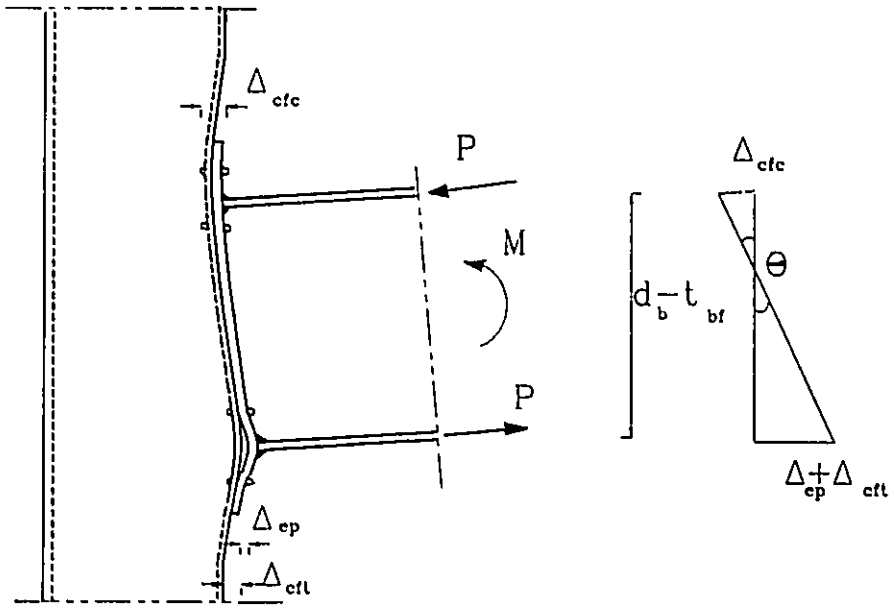


Fig 4.5 Typical deformations of end-plate connection

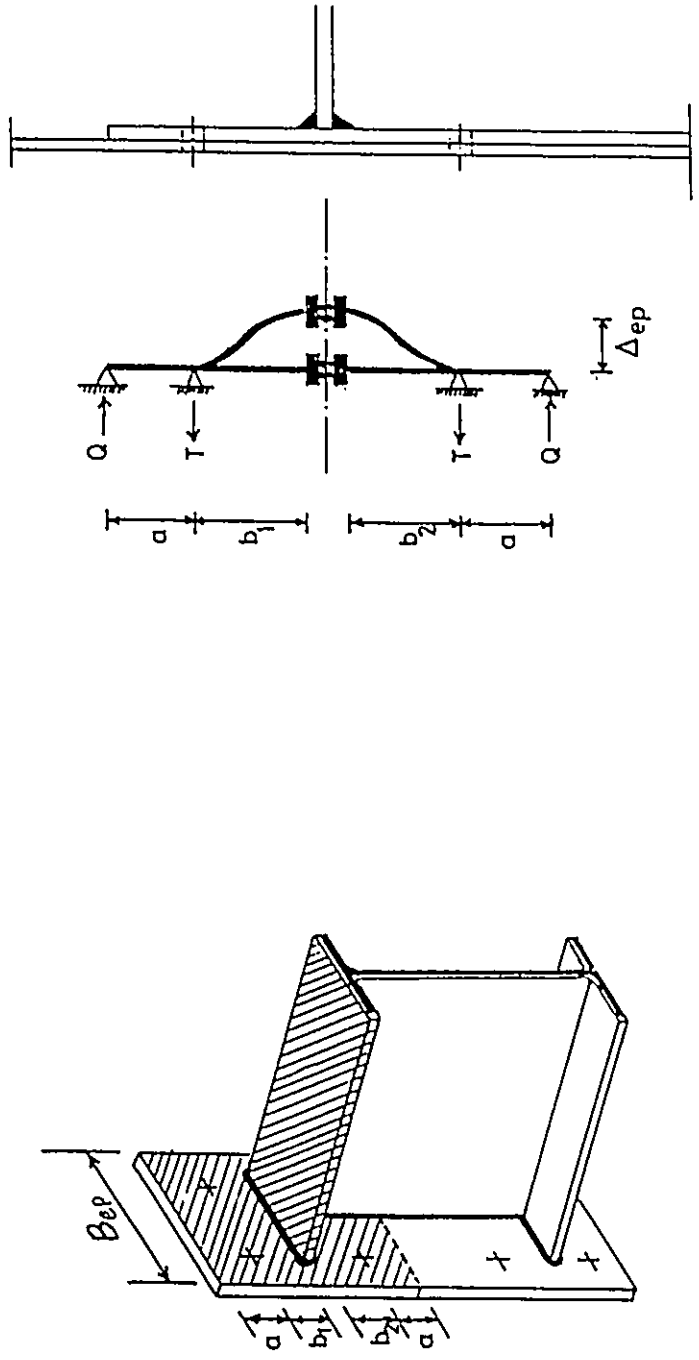


b) End-plate model

a) T-stub model

Fig 4.6 End-plate idealization (after Osman et al 1990)

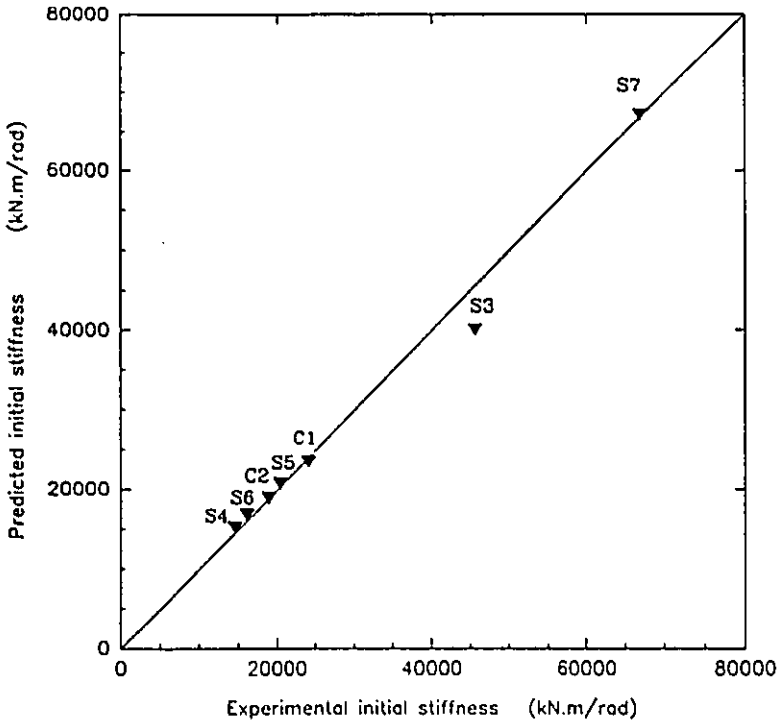


Fig 4.7 Comparison between the predicted and the experimental connection initial stiffness

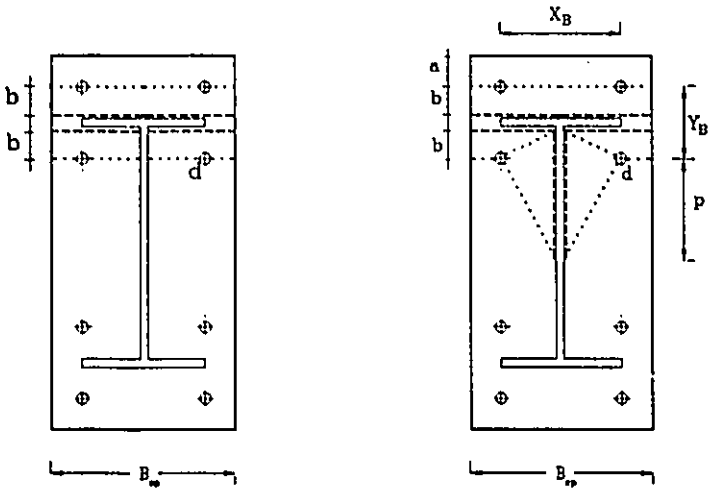


Mechanism 1 Mechanism 2

Fig 4.8 Different yield line mechanisms for end-plate

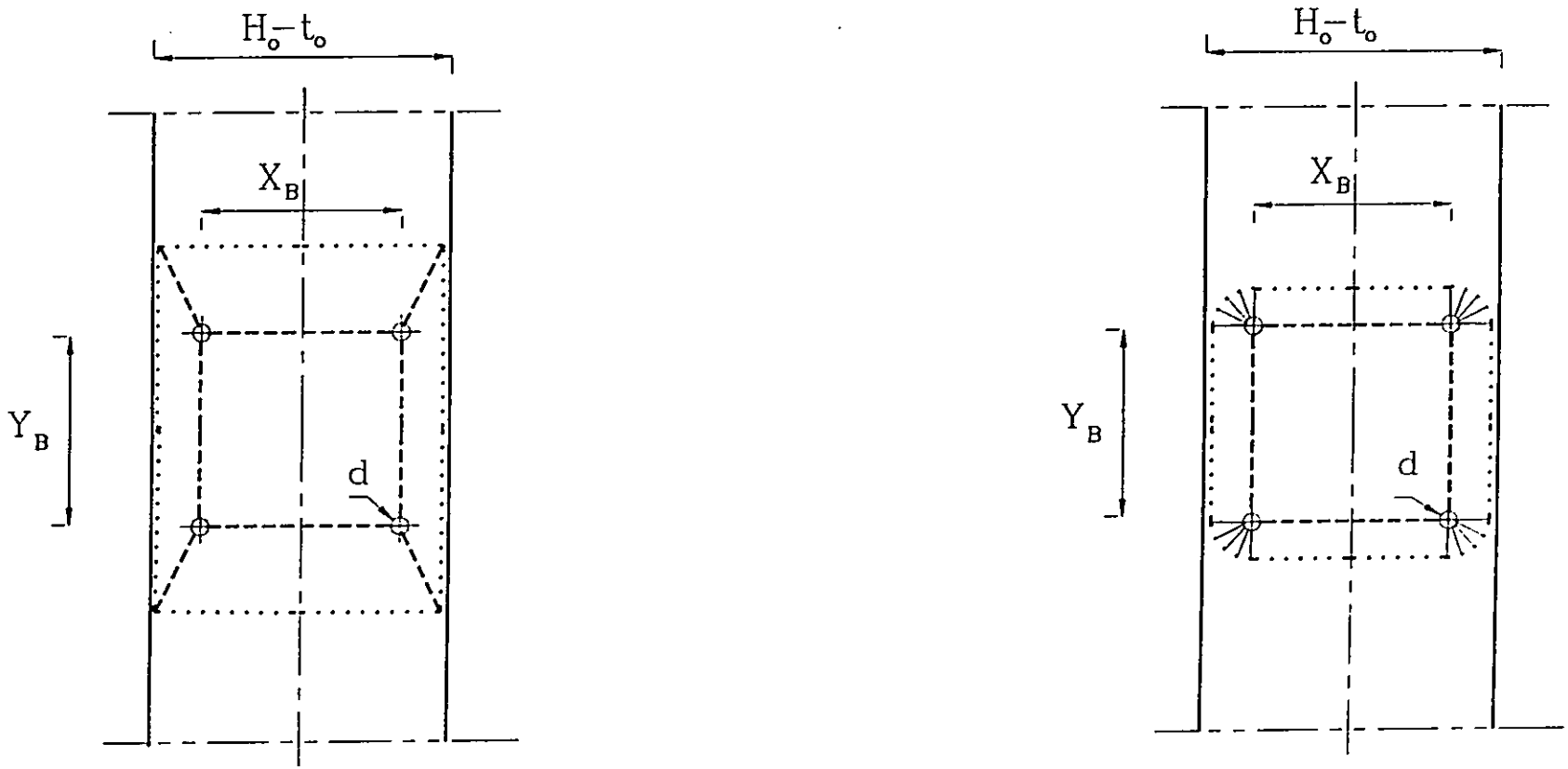


(a) Mechanism 1

(b) Mechanism 2

Fig 4.9 Yield line mechanisms for unstiffened column flange

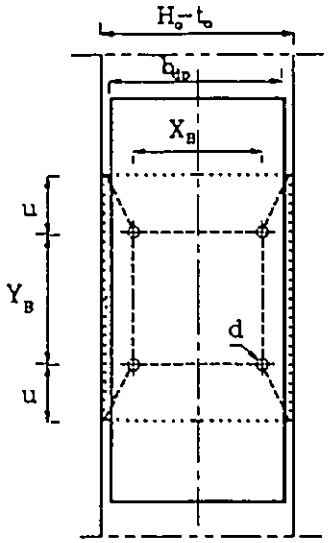


Mechanism 3

Fig 4.10 Yield line mechanism for column flange stiffened with a doubler plate

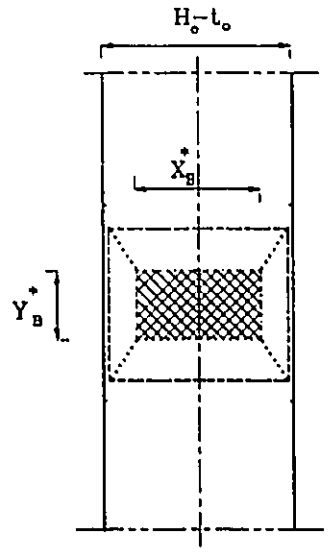


Fig 4.11 Loaded area and yield line mechanism of column flange (compression side)

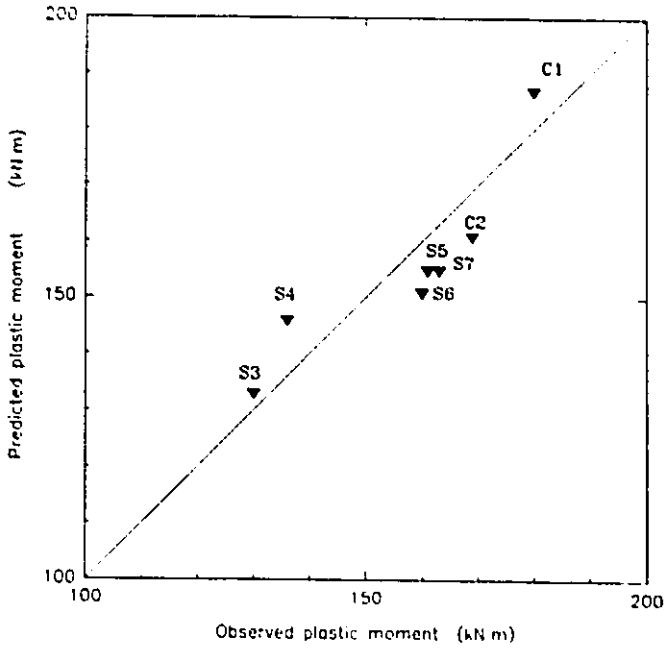


Fig 4.12 Comparison between the predicted and the observed connection plastic moment

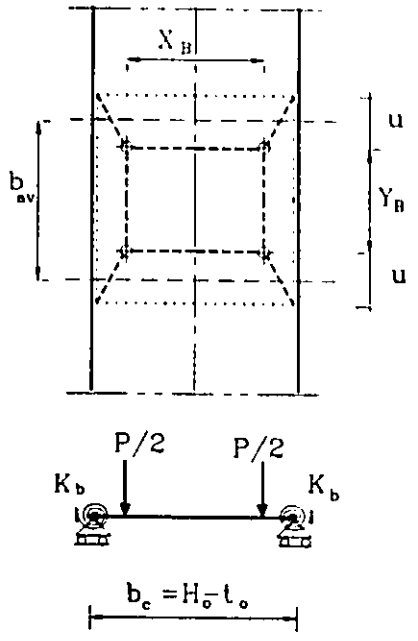


Fig 4.13 Equivalent beam model for HSS column flange

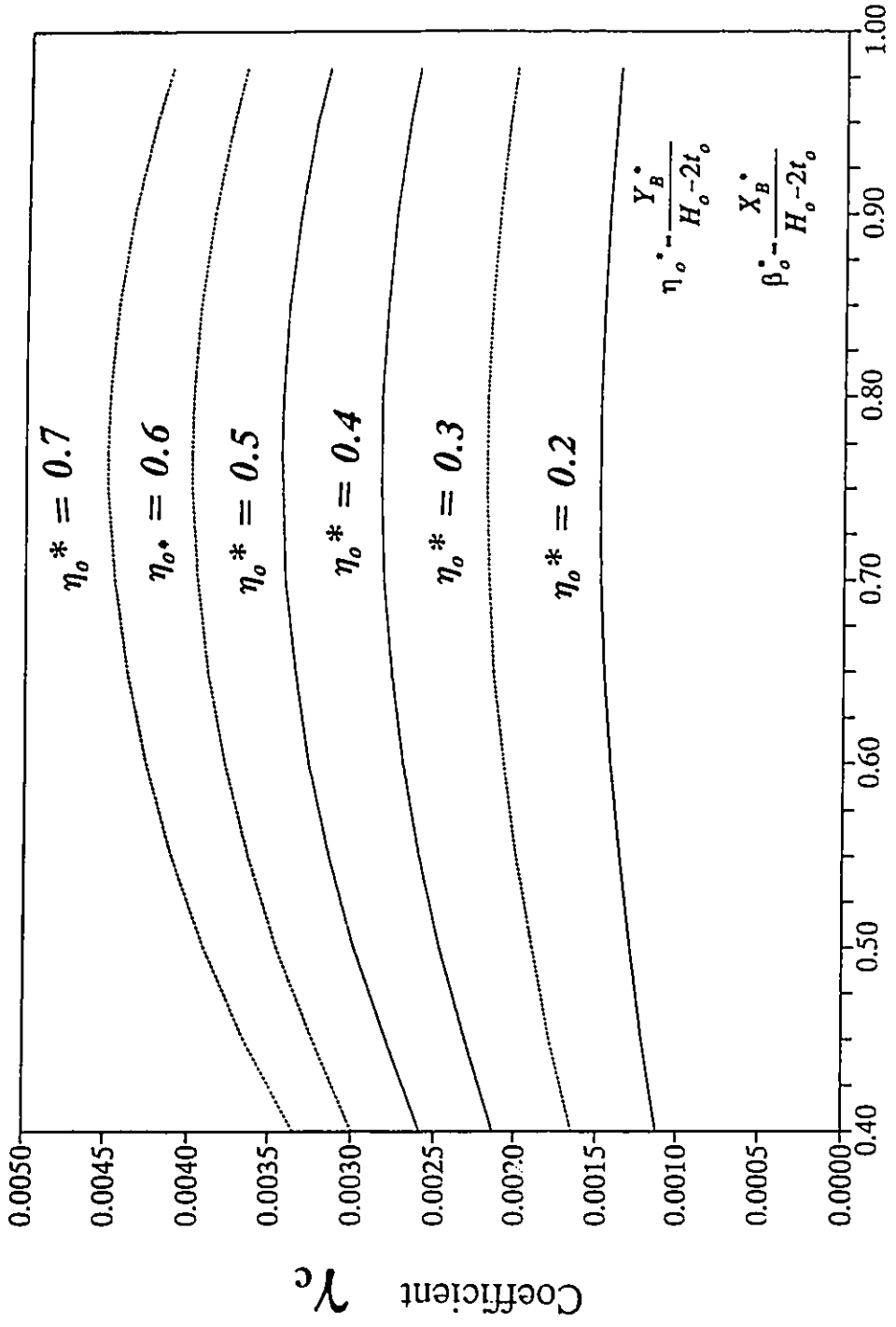


Fig 4.14 Deflection coefficients for simply supported column flange loaded with rectangular patch loads

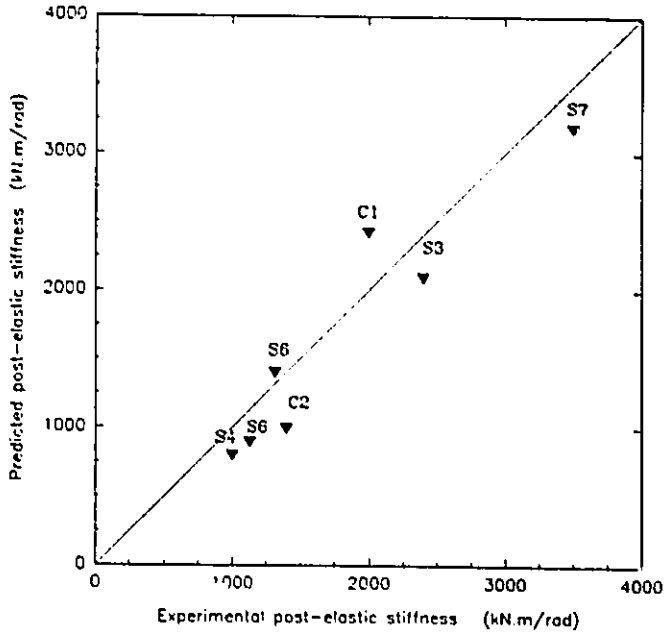


Fig 4.15 Comparison between the predicted and the experimental connection post-elastic stiffness

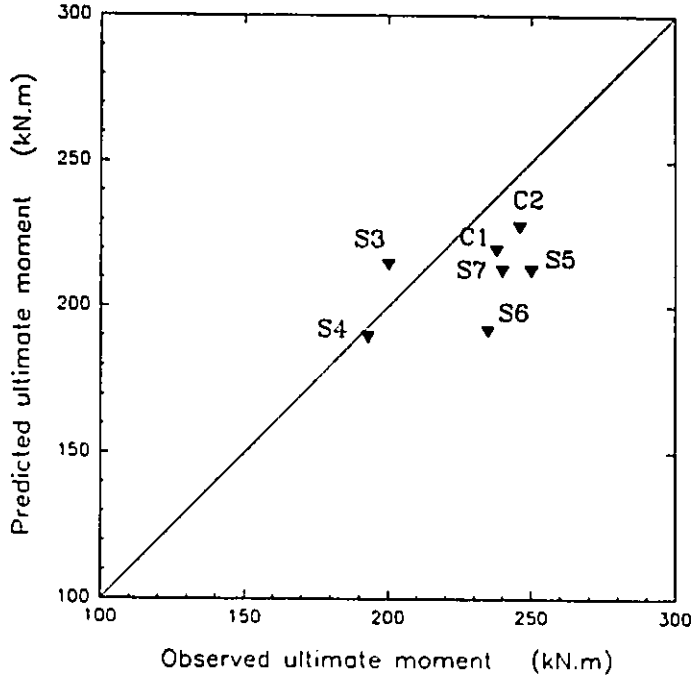


Fig 4.16 Comparison between the predicted and the observed connection ultimate moment

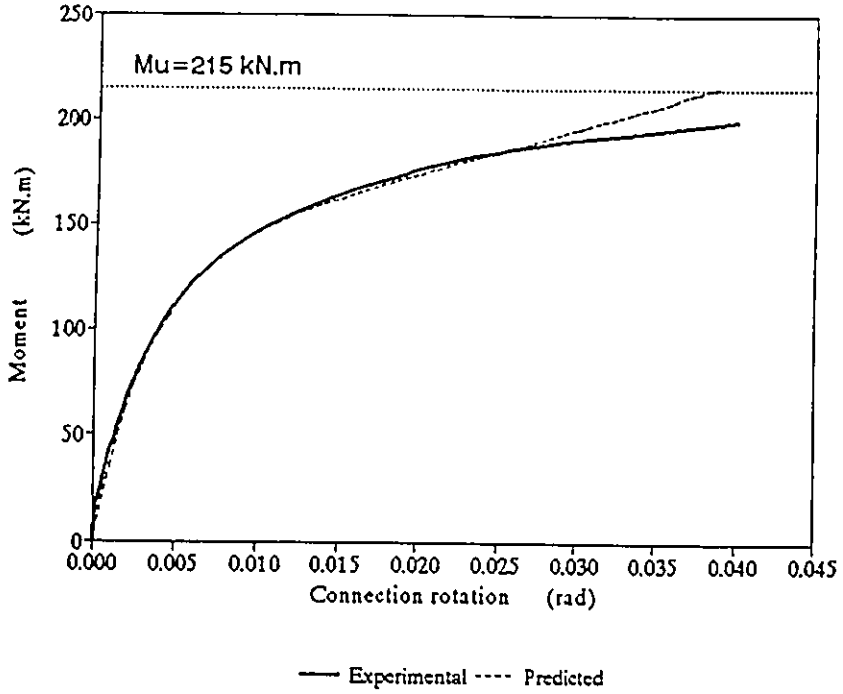


Fig 4.17 (a) Experimental vs. predicted moment-rotation relationship for specimen S3

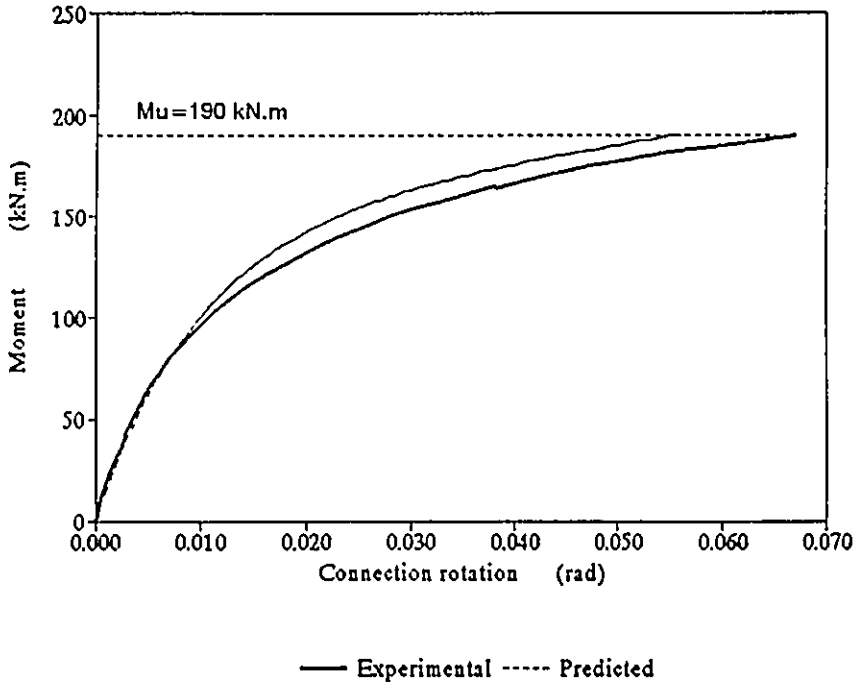


Fig 4.17 (b) Experimental vs. predicted moment-rotation relationship for specimen S4

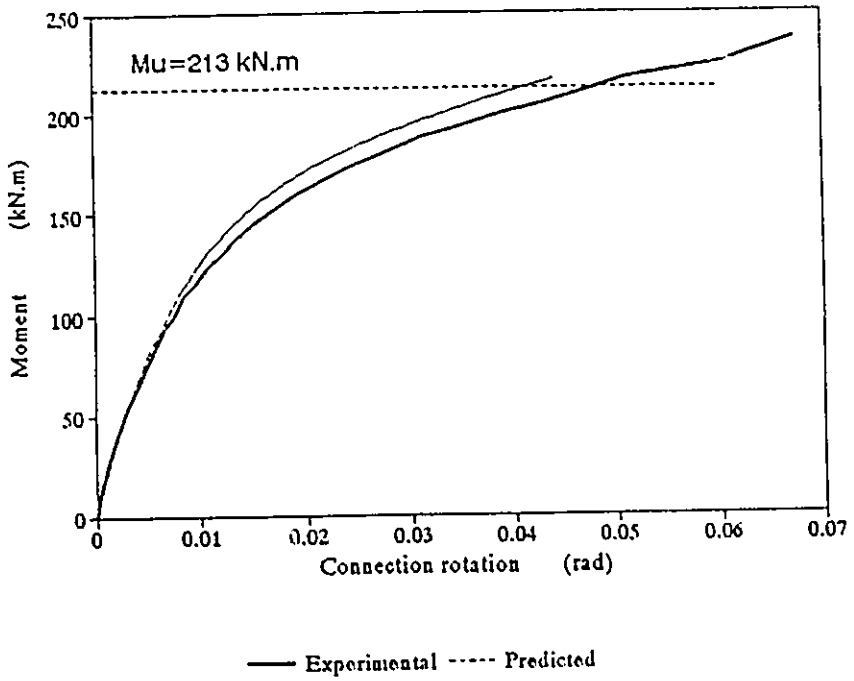


Fig 4.17 (c) Experimental vs. predicted moment-rotation relationship for specimen S5

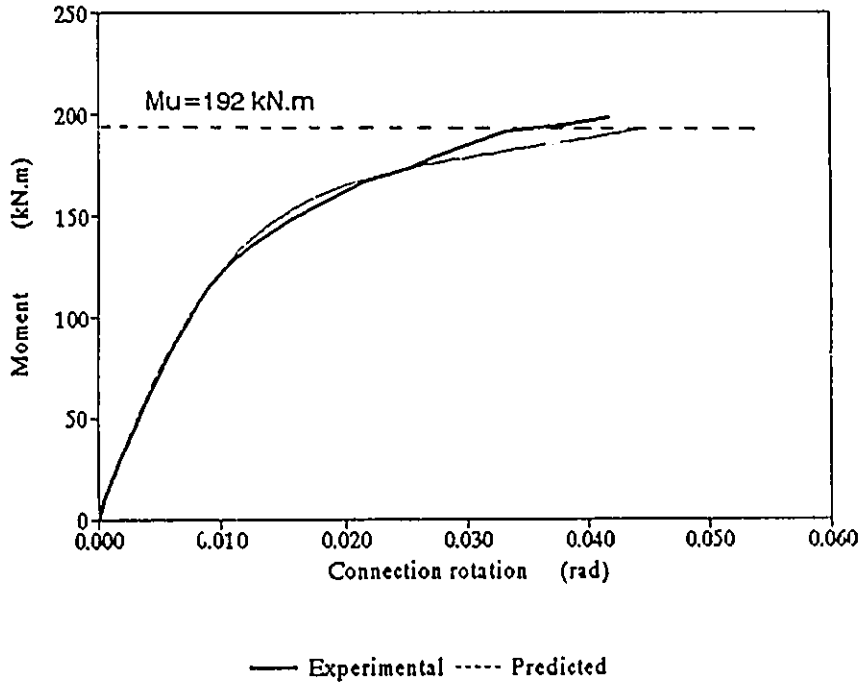


Fig 4.17 (d) Experimental vs. predicted moment-rotation relationship for specimen S6

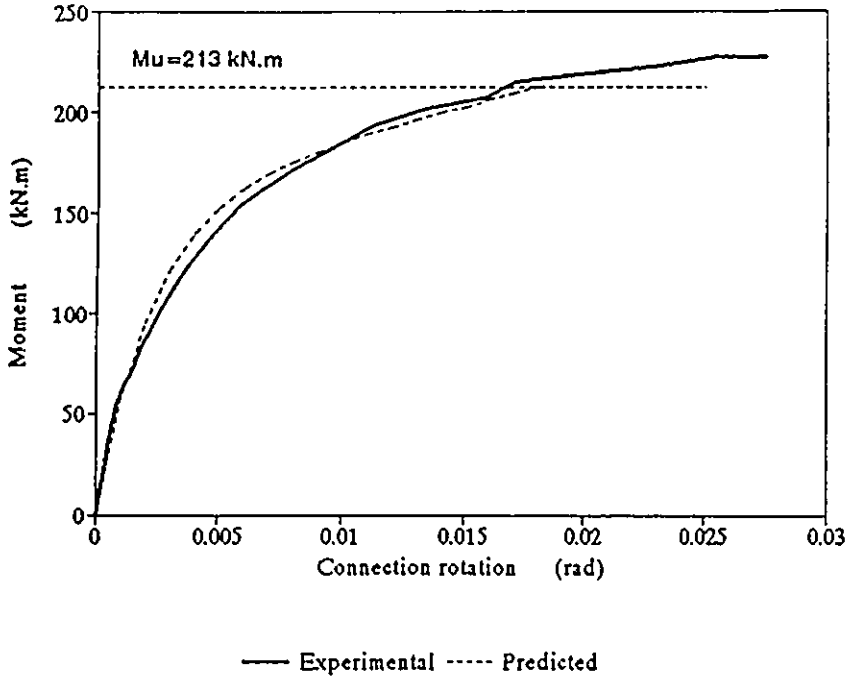


Fig 4.17 (e) Experimental vs. predicted moment-rotation relationship for specimen S7

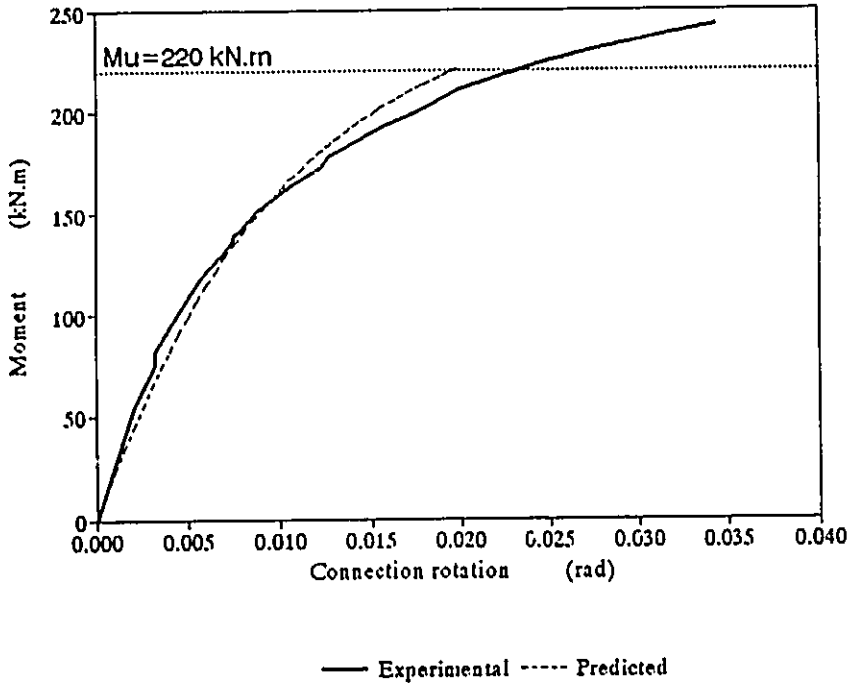


Fig 4.17 (f) Experimental vs. predicted moment-rotation relationship for specimen C1

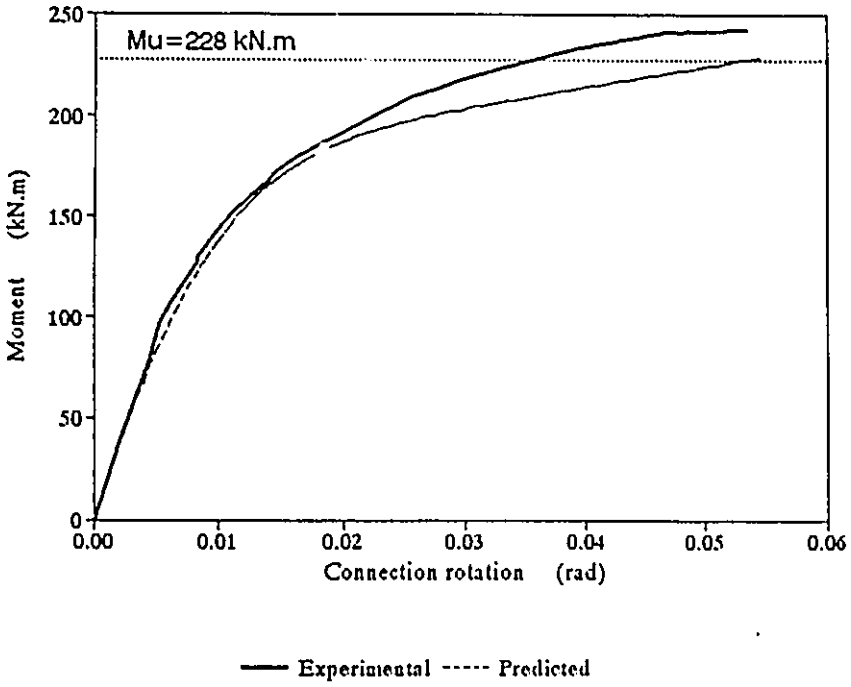


Fig 4.17 (g) Experimental vs. predicted moment-rotation relationship for specimen C2

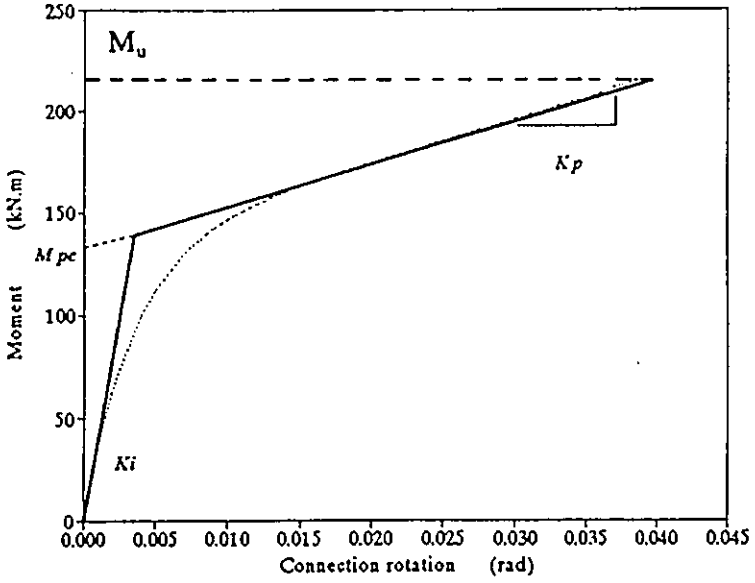


Fig 4.18 The bi-linear model is superimposed on the moment-rotation relationship of specimen S3

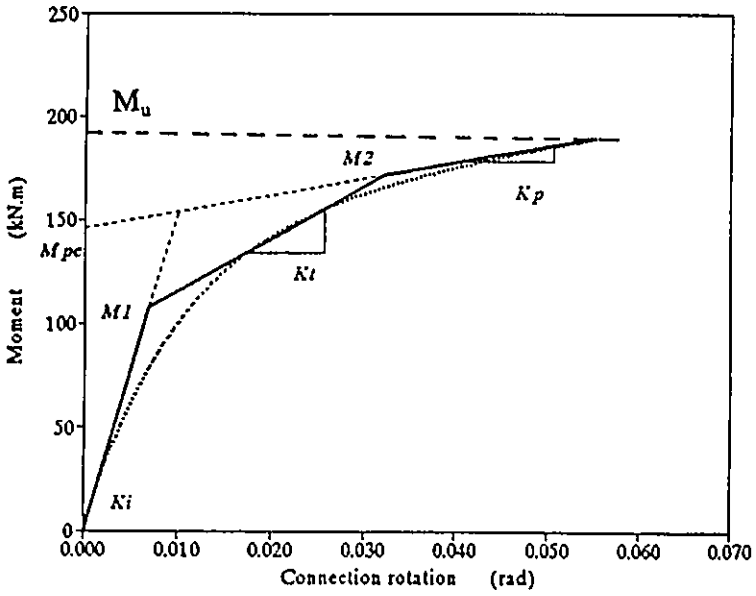


Fig 4.19 The tri-linear model is superimposed on the moment-rotation relationship of specimen S4

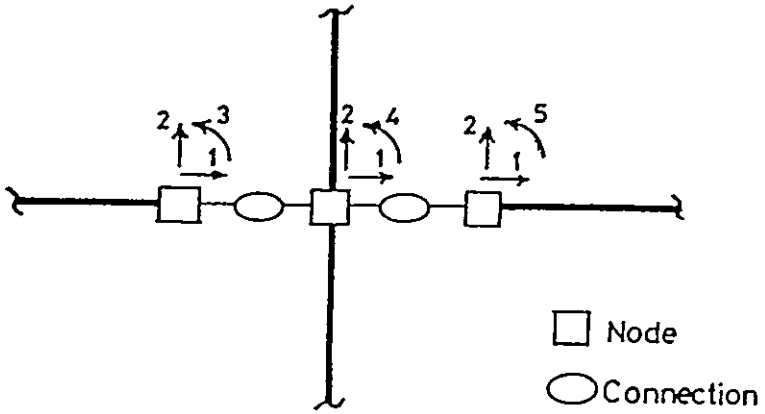


Internal joint

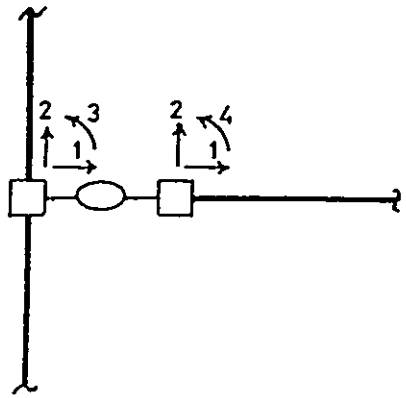


Exterior joint

1. Horizontal displacement 2. Vertical displacement 3, 4 and 5 rotations

Fig 4.20 Nodal degrees of freedom for the idealized semi-rigid connection element

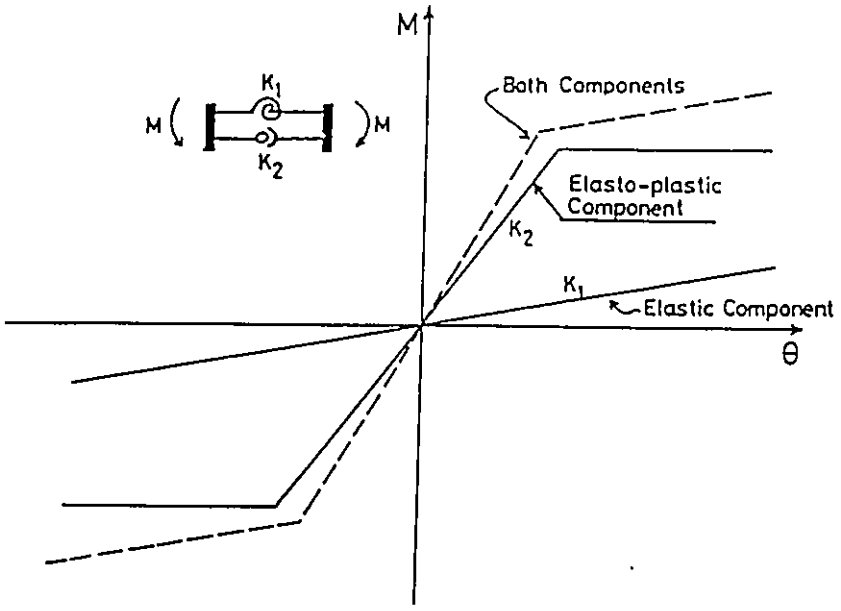


Fig 4.21 The bi-linear connection element components

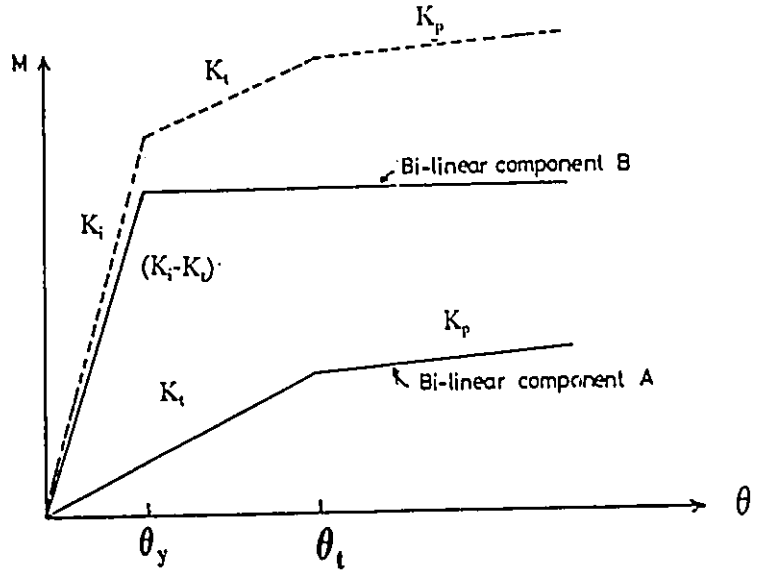


Fig 4.22 Simulation of tri-linear model by using two bi-linear models

# CHAPTER 5

# PROPOSED DESIGN OF END-PLATE CONNECTIONS FOR RECTANGULAR HSS COLUMNS

## 5.1 Introduction

Steel structures are allowed to reach certain limit states according to different design approaches, as Limit States Design CSA-S16.1-M89 adopted by the Canadian standards or the Load and Resistance Factored Design "LRFD", 1986, approach adopted by the American standards. These approaches are based on many scientific studies. No attempt has been made to provide an exhaustive listing of research work, but the reader may wish survey references listed in the Canadian Institute of Steel Construction "CISC" or LRFD handbook.

According to the requirements fashioned by those approaches, moment connections need to be designed so as to attain a certain moment capacity without significant plastic deformation or brittle failure. That moment capacity is known as the plastic moment of the connection, after which the connection experiences strain hardening to reach its ultimate capacity. Usually the connection plastic moment will exceed that of the attached beam's plastic moment in a moment-resisting frame.

In this chapter, a quantitative procedure for detailing and designing extended end-plate connections for rectangular HSS columns using High Strength Blind Bolts "HSBB" is proposed. The design procedure is consistent with the design philosophy given in the

limit state codes mentioned earlier. The proposed design is based on the results obtained from the experimental program and the analytical modelling. The criteria for the end-plate connection design are;

1- The connection deformation should be limited to avoid excessive structural drift.

2- Failure of welds and bolts before either the end-plate, column flange or the beam reach its plastic capacity and experience strain hardening, should be avoided.

3- The HSS column flange thickness should be adequate to hold the maximum tensile force of the (HSBB) bolts without shear failure.

4- No significant inelastic action should take place in the end-plate to avoid brittle failure in the heat affected zone.

5- Connection stiffness degradation resulting from application of cyclic loading should be minimized to avoid deleterious effects on the drift of moment resisting frames.

## 5.2 Connection geometry design

Both connection strength and stiffness are a function of its geometry. Referring to the schematic drawing of the connection shown in Fig 5.1, the following considerations will improve the end-plate connection strength and stiffness.

1- Since the in-plane stiffness of HSS column side walls is greater than the out-plane stiffness of its flanges, it is important to transfer the forces near the column side walls rather than the centre of the HSS column flange to prevent excessive rotation. The end-plate width "$B_{ep}$" should be as wide as possible so that it can be supported by the sides of the HSS column at the compression side of the connection. Therefore, it is

recommended that "$B_{cp}$" be selected such that it is larger than the flat width of the HSS column "$H_o$-$3t_o$" and less than $H_o$, where $H_o$ and $t_o$ are the outer dimension and the thickness of the HSS column respectively.

2- The blind bolts are recommended to be placed as close as possible to the side walls of the HSS column in order to minimize the column flange deformation on the tension side of the connection. Consequently, the maximum horizontal distance "$X_{ll}$" between the bolts would be equal to "$B_{cp}$-3d", where "d" is the bolt nominal diameter as shown in Fig 5.1.

3- To minimize end-plate deformation and prying forces, the bolts should be located as close as possible to the beam flange with approximately equal distance above and below the beam flange, Fig 5.1. The minimum distance "b" between the centre line of the blind bolts and the centre line of the beam flange fillet weld would normally be equal to 2.5 times the bolt's nominal diameter for installation requirements

4- In order to minimize the prying action on the exterior bolts in the end-plate connection, the minimum edge distance "a" between the exterior bolts and the end-plate edge ought to be larger than "b" (i.e, $b/a \leq 1$) as suggested by Mann and Morris (1979).

## 5.3 Connection strength design

The end-plate connection should be designed so that its plastic moment "$M_{pc}$" is at least equal to the design moment "$M_{design}$". For moment resisting frames in which wind loads govern the design rather than earthquake, connections can be designed so that its

plastic moment "$M_{pc}$" is just equal to the plastic moment of the attached beam "$M_p$". However, for frames which are designed to sustain severe earthquake load, it is preferable to design the connections to behave mainly elastically during such an event, thus minimizing the degradation in its stiffness due to inelastic deformations. Therefore, for this case, it is proposed that connections be designed so that their plastic moment values "$M_{pc}$" equal to 1.3 times the plastic moment of the attached beam "$M_p$". In such case, the connection is believed to behave mainly elastically up to the beam plastic moment "$M_p$", which corresponds to about 0.77 $M_{pc}$ as was illustrated in the testing of specimens C1 and C2 in Chapter 3.

Therefore, the design moment of the connection "$M_{design}$" is taken as follows; $M_{design} = M_p$, when lateral loads are governed by wind loads, where $M_p$ is the plastic moment of the attached beam, and $M_{design} = 1.3\ M_p$, when lateral loads are governed by earthquake loads.

It is an accepted assumption that the beam moment can be replaced by a couple whose forces "$P_f$" act at the beam flange level, as shown in Fig 5.2.

$$P_f = \frac{M_{design}}{d_b - t_{bf}} \tag{5.1}$$

where, $d_b$ and $t_{bf}$ are the beam depth and beam flange thickness, respectively.

Each component of the connection; welds, bolts, end-plate and HSS column flange should be able to transmit the beam flange forces without brittle failure or significant plastic deformation. The design and detail of each of these components is discussed in the following sections.

### 5.3.1 Design of welds

The welds that connect the end-plate to the beam are crucial, because weld fractures may occur suddenly with few warning signs. Beam flange fillet welds should be used rather than full penetration welds since the cost of edge preparation is eliminated and the risks associated with lamellar tearing are reduced. It is advantageous to have beam flange fillet welds completely surrounding the beam's flange, and continued at least 50 mm along both sides of the web, as recommended by Morris (1964) and illustrated in Fig 5.3. Such precautions reduce the stress concentration in welds. CSA-S16.1-M89 explicitly recognizes that the shear resistance of a weld must be evaluated on the basis of both the resistance of the weld itself and of the base metal adjacent to the weld. According to CSA-S16.1-M89, the minimum size for the beam flange fillet weld will be the greater of $w_b$ or $w_w$ as follows;

For weld metal

$$w_w = \frac{P_f \sqrt{2}}{0.67 \phi_w L_w X_u} \qquad (5.2)$$

For base metal

$$w_b = \frac{P_f}{0.67\ \phi\ L_w\ \sigma_y} \tag{5.3}$$

where;

$P_f$ : designed beam flange force
$X_u$ : weld ultimate tensile strength as rated by electrode classification number
$\sigma_y$ : minimum yield strength of base metal
$L_w$ : surrounding perimeter of beam flange and equal to $2(b_f+t_{bf})-t_{bw}$
$b_f$ : beam flange width
$t_{bw}$ : beam web thickness
$\phi_w$ : resistance factor of weld metal and equal to 0.67 (CSA-S16.1-M89)
$\phi$ : resistance factor of base metal and equal to 0.90 (CSA-S16.1-M89)

The numerical modifier (0.67) which appears in above equations, is specified by CSA-S16.1-M89 and relates the shear strengths of weld and base metal to their specified tensile strengths. Usually the size of fillet weld "$w_w$" based on weld metal governs the weld design, and is almost equal to that obtained from the LRFD (1986) specifications although it uses different factors. LRFD uses a higher factor for weld resistance (0.75) and a lower weld shear strength (0.6 $X_u$).

Similarly, the minimum size of web fillet weld needed to resist the designed factored shear force of the beam "$V_b$", can be obtained by using Eqs 5.2 and 5.3 with the substitutions of "$V_b$" and "$2(d_b-2t_{df})$" instead of "$P_f$" and "$L_w$", respectively.

### 5.3.2 Design of HSBB bolts

When the four bolts on the tension side of an end-plate moment connection are located at approximately equal distance above and below the beam flange, the force applied to each bolt by the beam flange force "$P_f$" can be considered equally distributed

to become "$P_f/4$" per bolt. However, clause 23.1.4 of S16.1-M89 requires that for bolts loaded in direct tension, the effect of prying action must also be taken into account in designing such bolts. Due to the applied load "$P_f$", the end plate bends about the bolt line and the prying force "Q" develops together with the bending moment in the plate, as illustrated in Fig 5.4. The bolt force "$F_b$" includes contributions from the applied load and prying forces. The maximum prying force is a function of the end-plate plastic bending moment capacity "$M_{pp}$" and the location of the bolt. Based on analytical and experimental work on ordinary high strength bolts, several researchers have suggested using a percent increase in bolt forces for design. Grundy et al (1980) suggested a 20% increase in the bolt force due to prying forces, while Packer and Morris (1977) recommended a 33% increase. On the other hand, many models have been developed to predict the magnitude of prying forces in bolted connections. These include the works of Fisher and Struik (1974), Agerskov (1977) and Kennedy et al (1981). Until future studies of prying action in High Strength Blind Bolt (HSBB) connections prove otherwise, it is assumed that the prying forces in HSBB connections are similar to those when using ordinary high strength bolts. The traditional prying force model developed by Kennedy et al (1981) was adopted to account for prying forces in the HSBB end-plate connections. It was assumed that the maximum prying force exists when the end-plate has formed a plastic hinge along the bolt line, and that the force "Q" acts at the end-plate edge, as shown in Fig 5.5 . It was also assumed that prying forces will only increase the forces in the two exterior bolts. Therefore, the maximum force in each of the exterior bolts "$(F_b)_{max}$" taking into account prying action, can be written in the form:

$$(F_b)_{max} = \frac{P_f}{4} + \frac{M_{pp}}{2a} \qquad (5.4)$$

where $M_{pp}$ is the end-plate plastic moment capacity at the bolt line, given by;

$$M_{pp} = \frac{(B_{ep} - 2d)\ t^2_{ep}\ \sigma_{ye}}{4}$$

where,

d : bolt's hole diameter
$t_{ep}$ : end-plate thickness
$\sigma_{ye}$ : end-plate yield strength

The ratio of the total bolt forces including prying forces to the applied beam flange force "$P_f$", is known as the prying factor "$\psi$", and is given by;

$$\psi = \frac{\Sigma F_b}{P_f} = 1 + \frac{M_{pp}}{a\ P_f} \qquad (5.5)$$

The factored resistance of HSBB "$F_r$" is taken to be

$$F_r = \phi_b\ T_{min} \qquad (5.6)$$

where $\phi_b$ is the resistance factor for HSBBs and is taken to be 0.67 as given by CSA-S16.1-M89 and discussed in Chapter 2, to insure that the bolts will not fail before the member. "$T_{min}$" is the minimum tensile strength of HSBB as provided by the manufacturer and given in Table 5.1. The size of HSBB should be selected so that;

$$F_r \geq (F_b)_{max} \qquad (5.7)$$

For connections which are designed to have a plastic moment equal to 1.3 times the plastic moment of the attached beam, the maximum prying forces will not be achieved because the beam will reach its full plastic moment "$M_p$" before the end-plate reaches its plastic capacity at $1.3M_p$. Concerning the shear acting on the connection it is usually small and would be expected to be carried by the blind bolts on the compression side.

### 5.3.3 Design of end-plate

The end-plate is designed so that it is fully yielded before the failure of HSBB, when subjected to a beam flange force "$P_f$" given by Eq 5.1. The yield line mechanism developed by Packer and Morris (1977), was used with a slight modification to design the end-plate, as shown in Fig 5.6. The end-plate was assumed to behave as a T-stub, and yield lines were assumed to form along both bolt lines and at the beam flange junctions. Such a design has been proven to sustain the beam plastic moment with limited plastic deformation (Packer and Morris, 1977). In the case of ordinary high strength bolts, it has been suggested that the work done in causing them to deform can compensate for the loss of plate strength due to the holes. However, due to the fact that the bending stiffness of (HSBB) bolts is less than that of ordinary bolts because of the reduced shank diameters, it will be assumed that the internal work done by the (HSBB) bolts in bending can not compensate for the reduction of the internal work in the plate due to the existence of the holes. Therefore, a reduction in end-plate strength resulting from the existence of bolt holes will be assumed. The end-plate thickness $t_{ep}$ is therefore

given by;

$$t_{ep} = \sqrt{\frac{P_f \; b}{\phi \; \sigma_{ye} \; (B_{ep}-d)}} \qquad (5.8)$$

where, b is the distance from the centre line of the bolts to the centre line of the beam flange fillet weld, $\phi$ is the resistance factor and equal to 0.9.

After designing the end-plate thickness, the maximum force developed in the exterior bolts has to be checked when prying forces are included using Eq 5.4 to Eq 5.7. Since the end-plate was designed to be fully yielded, a determination is needed that such a mechanism will occur before the HSBB bolts themselves fail. This can be done by evaluating the beam flange force "$F_f$" which causes the mechanism shown in Fig 5.7. Here, yield lines are assumed to form along the beam flange junctions while the bolts reached the ultimate state. The tensile flange force "$F_f$" is therefore given by

$$F_f = \frac{t^2_{ep} \; \sigma_{ye} \; B_{ep} + 8 \; T_{min} \; a}{2(a+b)} \qquad (5.9)$$

where "$T_{min}$" is the minimum tensile strength of HSBB as listed in Table 5.1.

If $F_f < P_f$ (the designed beam flange force), then, larger bolts have to be selected. It should be noted that, the end-plate thickness resulting from Eq 5.8 is slightly greater than that from LRFD specifications (1986). For HSBB, a thicker end-plate is preferable to reduce the bending of the bolts due to the end-plate deformation.

### 5.3.4 Design of HSS column flange

As was reported in the results of the testing program, the column flange thickness of Specimens S4, S5 and S7 governed the failure mode of the connection. In these tests, the HSS flange thickness was not adequate to resist the maximum strength of the 20mm HSBB. Since the column flange was sheared underneath and around the primary sleeve of the HSBB bolts acting in tension, a relationship can be developed to link the minimum column flange thickness of the hollow section column with the maximum strength of HSBB. The minimum thickness of the column flange required to resist the maximum strength of HSBB can be found by requiring the material shear resistance around the primary sleeve of the fastener to withstand the maximum strength of the bolt. This relationship can be expressed in the form

$$\pi \; K^{*} \; t_{min} \; \frac{\sigma_{yc}}{\sqrt{3}} \geq \alpha \; T_{min} \qquad (5.10)$$

where:

$T_{min}$ : is the minimum specified tensile strength of HSBB as noted by the manufacturer,
$\alpha$ : is an over strength factor for HSBB, determined from tests and equal to 1.11 (Chapter 2)
$K^{*}$ : is the diameter of the primary sleeve after installation as given in Table 5.1 and
$\sigma_{yc}$ : is the minimum yield strength of the hollow section column

Rearranging Eq.5.10, the minimum thickness of the column flange can be obtained as:

$$t_{min} \geq \alpha \; \frac{T_{min}}{\pi \; K^{*} \; \frac{\sigma_{yc}}{\sqrt{3}}} \qquad (5.11)$$

From Eq.5.11, the minimum thicknesses of the column flange required for different sizes of HSBB are given in Table 5.1. Should the column flange have a smaller thickness, a doubler plate can be welded around its perimeter onto the hollow section column to achieve the required minimum thickness. The length of the doubler plate is suggested to be 1.5 times the end-plate length, with its width slightly less than the flat part of HSS column flange to allow for proper welding.

Another detail that needs to be considered is the adequacy of the column flange. Tests on the end-plate connection to HSS columns showed significant inelastic deformation in the column flange which caused an increase in connection rotation. Therefore, it is important to check for column flange strength especially in the tension region. Based on the experimental observations and the analytical results, two idealized yield mechanisms are suggested to evaluate the unstiffened column flange thickness, as shown in Fig 5.8 (a) and (b). The first is a quadrilateral mechanism, while the second is a conical mechanism. The corresponding column flange thicknesses are given as follows;

For mechanism 1

$$t_o = \sqrt{\frac{P_f \quad (1-\beta)}{2\ \phi\ \sigma_{yc}\ [\ (\eta-\gamma) + 2\ \sqrt{(1-\gamma)(1-\beta)}\ ]}} \qquad (5.12)$$

For mechanism 2

$$t_o = \sqrt{\frac{P_f}{\phi\ \sigma_{yc}\ [\pi\ (1-\frac{\gamma}{2\ (1-\beta)}) + 2\ \frac{(\beta+\eta-\gamma)}{(1-\beta)}\ ]}} \qquad (5.13)$$

where;

$$\beta = \frac{X_B}{(H_o - t_o)} \qquad \eta = \frac{Y_B}{(H_o - t_o)} \qquad \gamma = \frac{d}{(H_o - t_o)}$$

It was observed that mechanism 1 governs the design of the column flange when $\beta \geq 0.65$. If the required column flange thickness is greater than the available thicknesses of HSS columns, therefore, a doubler plate needs to be welded onto the HSS column flange to resist such a design beam flange force "$P_f$".

In the case of a stiffened column flange with a doubler plate, the yield line mechanism developed by Korol et al (1982) is modified to take into account the variation in the yield strength in both the column flange, "$\sigma_{yc}$", and the doubler plate, "$\sigma_{yd}$", as well as to account for the reduction in strength due to the holes. The minimum required thickness for the doubler plate "$t_{db}$" can be determined by equating the resistance of the stiffened column flange "$P_{r(cf)}$" to the design beam flange force "$P_f$". The stiffened column flange resistance "$P_{r(cf)}$" is given by mechanism 3, Fig 5.9 in the following form;

$$P_{r(cf)} = \phi\ m_p\ \left[\frac{4(b_c-d)}{u}+\frac{8(Y_B+2u-d)}{(b_c-X_B)}\right]+\phi\ m_p^*\ \left[\frac{4(b_{dp}-d)}{u}+\frac{4}{(b_c-X_B)}\ (Y_B+2u\ (\frac{b_{dp}-X_B}{b_c-X_B})-\ 2d\right]$$

(5.14)

where, "u" is defined in Fig 5.9 and given by:

$$u = \sqrt{\frac{(b_c-X_B)^2\ \{\ (b_c-d)+g(b_{dp}-d)\ \}}{4(b_c-X_B)\ +\ 2g\ (b_{dp}-X_B)}} \qquad (5.15)$$

Here:

$m_p$ : plastic moment per unit length of column flange = $\sigma_{yc}\ t_o^2/4$
$m_p^*$ : plastic moment per unit length of doubler plate = $\sigma_{yd}\ t_{dp}^2/4$
$t_{dp}$ : doubler plate thickness
$g$ : $m_p^*/m_p$
$b_{dp}$ : width of doubler plate
$b_c$ : $H_o - t_o$
$\phi$ : resistance factor equal to 0.9

## 5.4 Summary

A quantitative procedure for the design of extended end-plate connections for HSS columns using High Strength Blind Bolts "HSBB", is proposed. It is believed that a connection designed according to this procedure will perform satisfactorily without displaying undesirable modes of failure when employed in steel moment resisting frames. The connection design is based on the results obtained from the experimental program and the analytical modelling and consistent with the limit states design philosophy.

Table 5.1 Minimum tensile strength of HSBB bolts and the corresponding minimum HSS column flange thicknesses

| Size of HSBB (mm) | Diameter of primary sleeve after installation+ K* (mm) | Minimum specified tensile strength+ $T_{min}$ (kN) | Minimum column flange thickness $t_{min}$ (mm) |
|---|---|---|---|
| 16 | 21.5 | 124 | 10.4 |
| 20 | 26 | 192 | 13.4 |
| 22 | 29 | 237 | 14.8 |
| 24 | 32 | 276 | 15.6 |
| 28 | 37.5 | 377 | 18.2 |

+ Values provided by Huck International Inc.

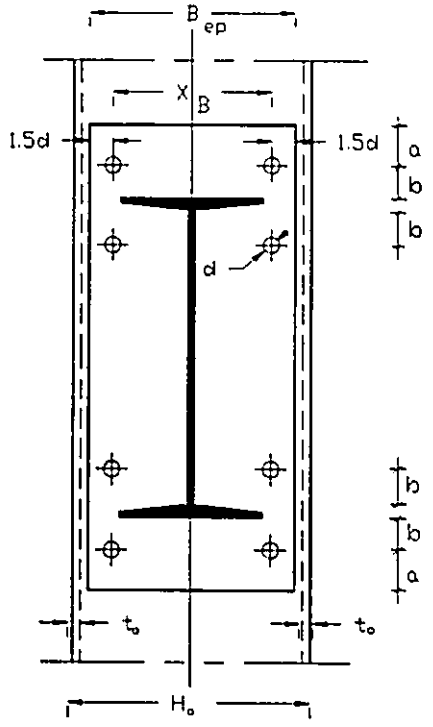


Fig 5.1 Geometry of an extended end-plate connection

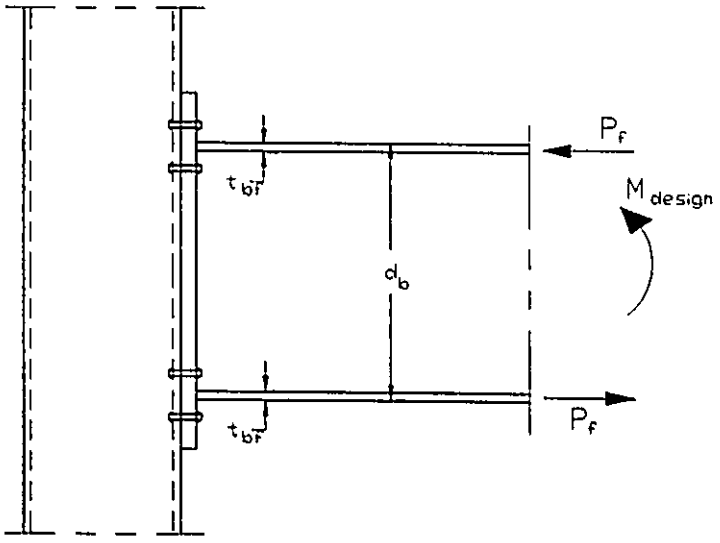


Fig 5.2 Loads on the connection due to bending

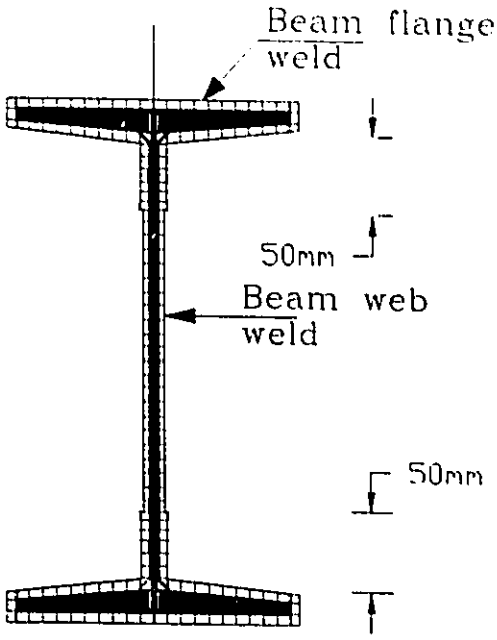


Fig 5.3 Arrangement of welds

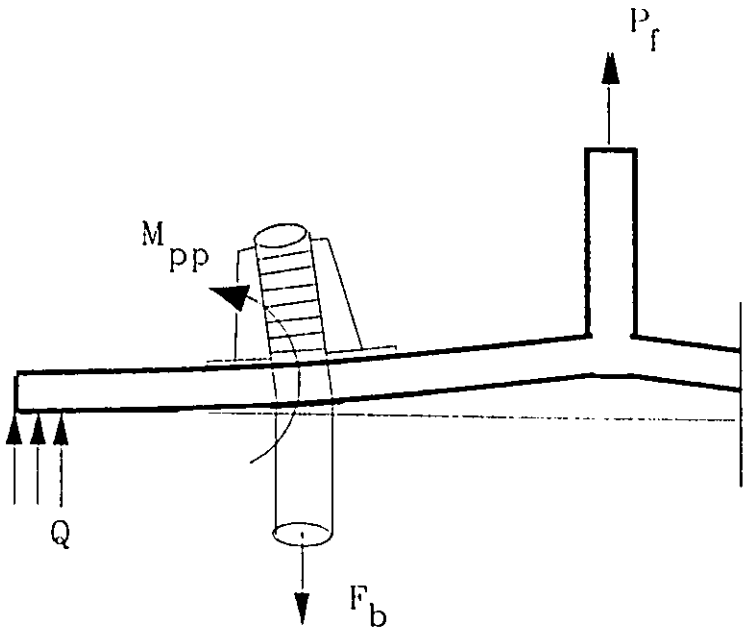


Fig 5.4 Bending and prying action of plate projection

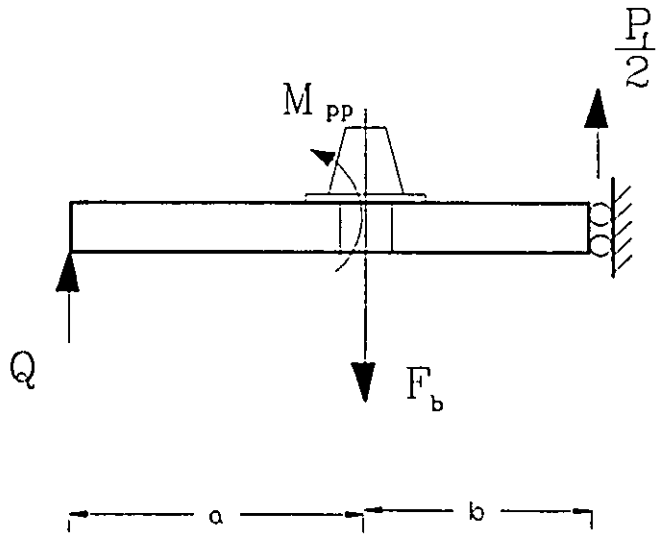


Fig 5.5 Traditional prying force model

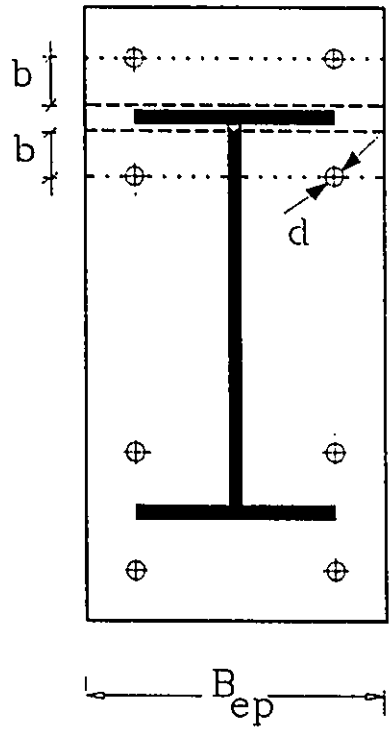


Fig 5.6 End-plate yield line mechanism

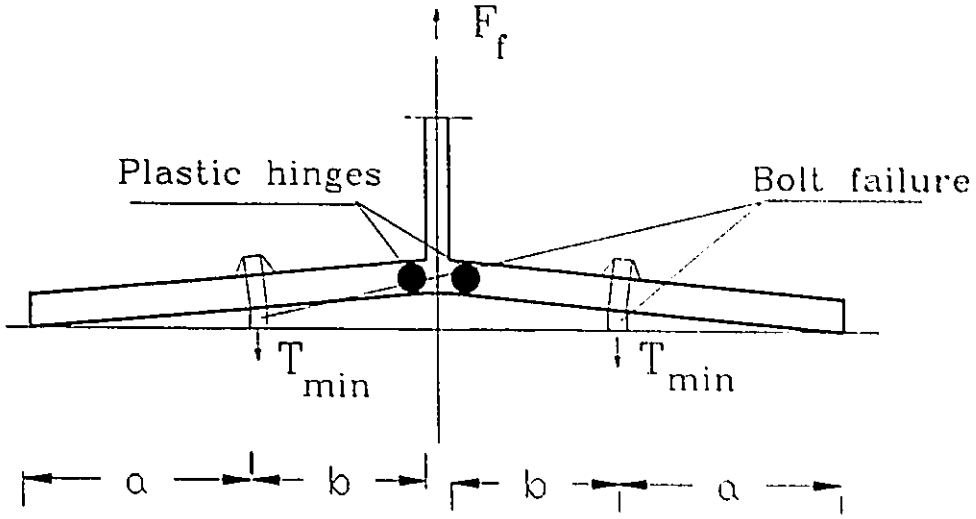


Fig 5.7 End-plate yielding with bolts failure

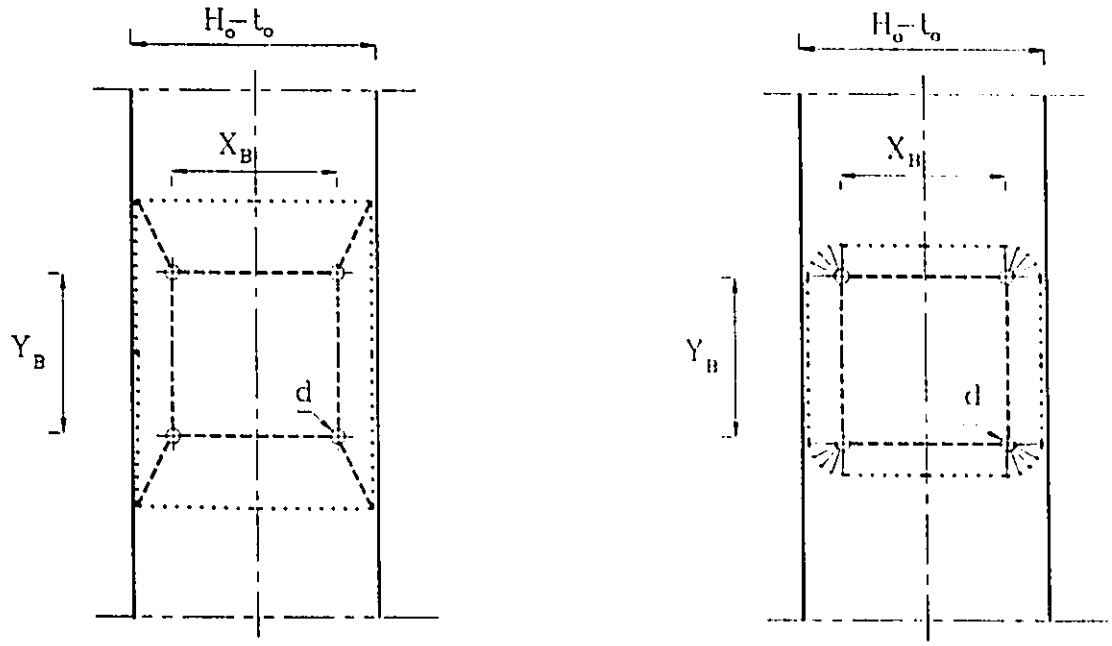


(a) Mechanism 1

(b) Mechanism 2

Fig 5.8 Yield line mechanisms for unstiffened HSS column flange

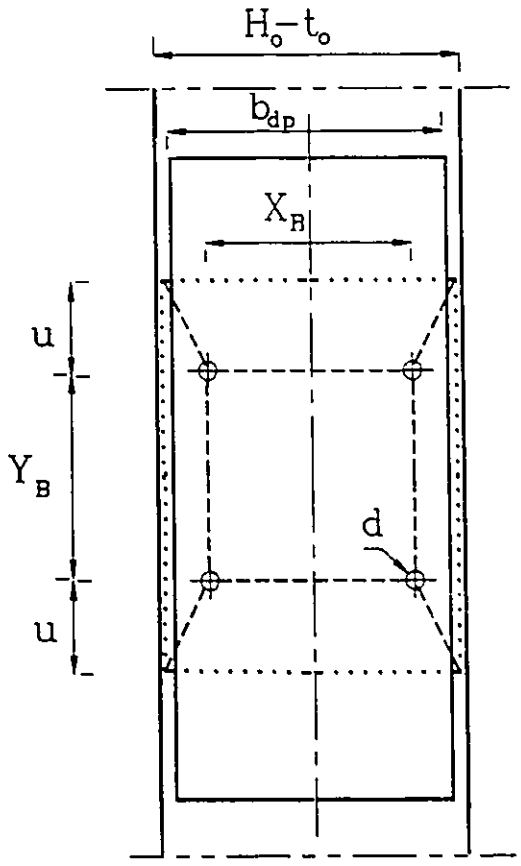


Fig 5.9 Yield line mechanism for HSS column flange stiffened with a doubler plate

# CHAPTER 6

# STATIC AND DYNAMIC ANALYSIS OF A 4-STOREY BUILDING

## 6.1 Introduction

The design and detailing of beam-to-column connections can significantly affect their behaviour and modes of failure. Also, the flexibility and the non-linear behaviour of the connection may significantly affect the static and dynamic characteristics of the Moment Resisting Frames (MRFs) and contribute to the frame interstorey drift, when utilizing such semi-rigid connections. Either employing A325 high strength bolts or HSBB in extended end-plate connections between rectangular HSS columns and W-shape beams, is believed to have insignificant effect on either the connection or the frame behaviour, provided that the bolts are designed as described earlier and remain rigid.

To investigate the effect of the connection on the performance of the MRF, the following questions were posed:

- How will the connection that meets the proposed design criterion affect frame response under both static and dynamic loading?
- How will the flexibility of such connection affect the overall strength of the MRF as well as the distribution of the internal forces in the frame's elements?
- What is the effect of different designs and models of such a connection type on frame behaviour?

To address these issues, the connection model (described in Chapter 4) was incorporated into computer program Drain-2DX (Prakash and Powell, 1992). This program was used to investigate the effect of connection flexibility on the response of a 4-storey steel frame when subjected to both static and dynamic loading. Non-linear inelastic frame analyses were performed on frames employing extended end-plate connections between W-shape beams and HSS columns. The results were then compared with similar frames with fully rigid connections. In detailing such connections, the proposed criterion for designing the connection as presented in chapter 5 was employed.

## 6.2 Design Procedure

For the purpose of this analytical study, a 4-storey, four-bay by four-bay square steel office building located in Montreal, Quebec was selected. The total height of the building is 14.50 m and the plan area is 576 $m^2$, as shown in Fig 6.1 and Fig 6.2. The lateral load resisting system consists of a perimeter moment resisting frame in both the E-W and N-S directions. The gravity load is supported by interior leaning HSS columns in conjunction with the perimeter framing system. As a result, each frame in the E-W direction would be expected to resist 50% of the total lateral load, but carry only about 12.5% of the total gravity loads. This simple framing system is common and is widely used in office buildings in North America. The benefit in using HSS columns in moment resisting frames is to avoid having to brace the columns in the direction causing weak axis bending i.e. connecting to the web of W-shape columns.

The storey height for the building was selected to be 3.5 m for typical floors and

4.0 m for the ground floor. The nominal yield stress of the hollow structural steel columns was 350 MPa and conformed to CSA G40.21-M92 class H, while the nominal yield stress of the structural steel used in the beams and plates was 300 MPa and conformed to CSA G40.21-M300W 1992. The building was designed in accordance with CAN3-S16.1-M89 (1989) and the National Building Code of Canada (NBCC), 1990.

### 6.2.1 Loads

**a) Gravity loads and floor system:**

The structure was designed to sustain two types of gravity load- dead and live. A typical floor construction was considered to consist of a composite beam and girder floor system. Except for the roof, all other floors consisted of 75 mm metal deck with 65 mm concrete cover. The concrete was taken as normal density of 2300 kg/m$^3$ and 20 MPa compressive strength. The roof was assumed to be 38 mm steel roof deck . In addition to the floor dead weight, loads due to fire protection, mechanical services and ceiling fixtures were included also. The exterior windows wall system was assumed to weigh 1.65 kPa over the exterior surface of the building for the office floors. A live load of 2.4 kPa and a partition load of 1.0 kPa was applied to all office floors. The roof was subjected to vertical loads due to self weight, snow and rain. A uniformly distributed snow load was estimated to be 1.92 kPa which corresponds to 80% of the ground snow load in Montreal, with a probability of exceedence of one in 30 years on average. In addition, a 0.4 kPa load as the rain component was also included. The mechanical room which includes all mechanical services from heating, ventilation, and plumbing was

assumed to be located on the ground floor.

**b) Lateral loads**

The building was designed to sustain two types of lateral loads, wind and earthquake. In the design, the equivalent static lateral forces recommended by the NBCC (1990) were used. The reference velocity pressure "q" of the wind for designing the members was taken to be 0.37 kPa which is "$q_{1/30}$" for the Montreal area. Variation of the wind load with building height was also considered. The factored base shear due to wind load on each frame in the E-W direction was calculated to be 165 kN. The base shear formula for seismic loading is given by NBCC (1990) as follows;

$$V = \frac{V_e}{R}.U \tag{6.1}$$

where, "$V_e$ "is the elastic base shear; "R" is the force modification factor which depends on the type of structural system used and is equal to 4 in the case of a ductile moment resisting frame; "U" is a factor representing a level of protection based on experience, which has a value equal to 0.6 for all structural systems; and

$$V_e = v.S.I.F.W \tag{6.2}$$

where, "v" is defined as the zonal velocity ratio which corresponds to 10% probability of exeedance in 50 years, and is equal to 0.1 for Montreal region. "S" represents the seismic response factor which depends on the region and the fundamental period of the structure "T". The fundamental period of the structure "T" is equal to 0.1 N for unbraced steel frames (N is the total number of storeys), as given in item 4.1.9.1.(7)-a

of the NBCC (1990). However, for most frame structures as well as the studied 4-storey steel frames described herein, the periods calculated using established methods of mechanics exceeded the above value by a considerable margin, leading to a reduced value of base shear. Usually in calculating the periods of a framed structure, the stiffening effects resulting from the exterior and interior walls of the building are not taken into account because of the complexity involved in including them in the analysis. Such effects will reduce the calculated periods significantly. However their weight have been included in ascertaining the floor masses of the structure with the result that the period will slightly increase. The NBCC (1990) restricts the value of "T" to a maximum of 1.2 times the above specified value, as mentioned in item 4.1.9.1.(7)-c . Therefore, according to this standard, the estimated period of the 4-storey steel frame is equale to 0.48 seconds. Meanwhile, "F" is the foundation factor, and was taken equal to 1.3 which corresponds to a coarse-grained soil. "I" is the importance factor and assumed to be equal to 1.0. While "W" is the total dead load of the structure which includes the dead loads of all floors, roof, walls and 25% of the roof snow loads.

Based on these inputs, the base shear acting in the E-W direction was found to be 227 kN. The shear is distributed to each floor using the following equation given in the NBCC (1990);

$$F_i = (V-F_t)\left(\frac{W_i\, h_i}{\sum W_i\, h_i}\right) \qquad (6.3)$$

where;

V : Base shear as given by Eq 6.1
$F_t$ : Concentrated force at the top of the building and equal to "0.07 T V" and considered zero if $T < 0.75$ s.
$W_i$ : The portion of W that is located at the ith floor.
$h_i$ : The height of the ith floor.

For this building, the storey shear forces due to earthquake loads were higher than that due to wind loads. As such, earthquake governed the strength design of the building.

### 6.2.2 Design of frame with rigid connections

Frames subjected to gravity and wind loads must be designed to provide the necessary strength requirements and must satisfy drift limitations under various load combinations. However, frames designed to sustain earthquake loading should also be designed and detailed to provide adequate ductility, i.e. to be able to experience large inelastic deformations in the case of a major seismic event. In this section, the steps for designing the 4-storey frame will be explained in detail.

**a) Design for strength**

The " portal frame method " was used to obtain the preliminary moments and axial forces in the beams and columns due to both gravity and lateral loads. The moments and axial forces were then factored and combined for a preliminary selection of the beams and columns. It was found that the combination (1.25D+Q), where "Q" represents the earthquake load, governs the design of all the columns and the beams. An elastic first order analysis of the frame was performed using the Drain-2DX (Prakash and

Powel, 1992) computer program. In this analysis, the member designs were checked for the following load combinations;

1) 1.25D + Q

2) 1.25D + 0.7(1.5L+Q)

3) 1.25D + 1.5L

The analysis was refined until final member sizes were selected. In these analyses, the structural stiffness was formulated based on center line dimensions and infinitely rigid connections.

**b) Drift limitations**

Interstorey drift is one of the significant parameters in assessing the performance of a structure under wind and earthquake loads. The control of drift is to ensure satisfactory occupancy requirements under wind loads and to minimize nonstructural damage during earthquakes. The NBCC (1990) recommends that interstorey drifts resulting from the anticipated deflections due earthquake loads should not exceed 0.02 $h_i$, where "$h_i$" is the height of the ith floor. Also, the NBCC recommends that the interstorey drift should not exceed $h_i/500$ when the building is subjected to specified wind loads. The reference velocity pressure "q" used for the deflection calculation due to wind loads is based on the "$q_{1/10}$" value which represents 10% probability of being exceeded in any one year. The building was checked for the previous drift limitations and the design was refined until it met the code requirements. Analysis showed that the structural design was controlled by drift limitations rather than strength requirements.

### 6.2.3 Design of frame with semi-rigid connections

The design procedure of a frame with semi-rigid connections differs from that of a frame with rigid connections, in that the former is an iterative procedure, whereas the latter leads to a direct solution. The iterative procedure results from the fact that the stiffness of the designed semi-rigid connection will affect the internal force distribution in the frame elements (beams and columns) and the interstorey drift, and subsequently influence the member sizes. Therefore, both the strength and stiffness of the semi-rigid connections will affect the frame design. In general the strength of the connection should be at least equal to the nominal plastic moment of the connected beam, to avoid any early failure of the connection at the ultimate stage of loading. Also, member design depends on the relative stiffness of the semi-rigid connection to the attached member, which is known as the fixity factor. Monfortan and Wu, (1963) defined the fixity factor "f" in the form:

$$f = \frac{1}{1+\frac{3\,E\,I_b}{K_i\,L_b}} \tag{6.4}$$

where, "E" is modulus of elasticity, "$K_i$" is the initial stiffness of the semi-rigid connection, "$L_b$" and "$I_b$" are the length and cross-section moment of inertia of the attached beam, respectively. For a pinned connection the value of the fixity factor is zero (f=0), while for a fully rigid connection it is unity (f=1). It follows that a semi-rigid connection will have a fixity factor between zero and unity ($0<f<1$).

### 6.2.4 Design of end-plate connections

The connections and the frame designs should be carried out in parallel since the connection design affects the frame design. The end-plate connections for joining W-shape beams to the HSS columns were designed according to the method proposed in Chapter 5, after which the parameters that describe the moment-rotation relationship of each connection were calculated, as described in Chapter 4.

## 6.3 Cases studied

In order to study the effect of the connection flexibility on the response of the 4-storey steel frame in the E-W direction, four cases of different designs were selected:

**1) Frame Frr**

This frame was designed to have infinitely rigid connections. In practice, this represents the case when fully welded connections are used with external diaghrams welded around the HSS column and the connecting beams (Kato, 1981). The final member sizes of this case are shown in Table 6.1.

**2) Frame Ff1**

This frame was designed to have end-plate connections with plastic moment capacity "$M_{pc}$" higher than that of the nominal plastic moment of the connected beam "$M_p$". This frame represents the case of frames designed to sustain earthquake loading. The plastic moment capacity of the connections "$M_{pc}$" was taken to be equal to 1.3 $M_p$, to ensure that the connection would behave mainly elastically up to the plastic moment

of the beam ($M_p$), as described in the tri-linear model of Chapter 4. Inelastic action in the connection which could cause significant degradation in stiffness is therefore avoided. Frame Ff1 does not only satisfy the strength and drift requirements specified by the code, but also satisfies the ductility requirements allowing large inelastic deformations in the beams in the case of a major seismic event. Local stability of the members was assured by selecting class 1 sections and providing adequate lateral bracing.

In the seismic design of steel frames, it is often prudent to design the girders to be weaker than the columns. As such, inelastic action is expected to take place in the beams which are capable of developing large inelastic rotations without strength deterioration. In the absence of an approach to satisfy such a requirement in CAN3-S16.1-M89 (1989), the frame design was checked using the equation recommended by the Uniform Building Code, UBC (1989).

$$\frac{\sum Z_c(\sigma_y-\sigma_a)}{\sum Z_b\ \sigma_y} > 1.0 \qquad (6.5)$$

Where;

$Z_c$ : Column plastic section modulus.
$Z_b$ : Beam plastic section modulus.
$\sigma_y$ : Yield stress
$\sigma_a$ : Axial stress in columns.

The final member sizes for the 4-storey frame Ff1 are listed in Table 6.2. The dimensions of the connections and its parameters for both the bi-linear and tri-linear models are given in Table 6.3 and Table 6.4, respectively.

**3) Frame Ff2**

This frame was designed to have end-plate connections with a plastic moment capacity "$M_{pc}$" equal to the nominal plastic moment of the connected beam "$M_p$". Such a frame would represent the case when wind loads govern the design for strength rather than earthquake loading. For this case, it was decided to use the same member sizes of frame Ff1, as listed in Table 6.2, to provide a comparison and to evaluate the effect of connection strength on the frame behaviour. The dimensions of the connections and its parameters for both bi-linear and tri-linear models are given in Tables 6.5 and 6.6, respectively.

The fixity factors for the connections used in frames Ff1 and Ff2 were calculated from Eq. 6.4 and are given in Table 6.7. The connections as designed were found to have relatively high fixity factors especially the exterior ones, indicating that they are closer to fully rigid connections rather than to the pinned case.

**4) Frame Ffr**

This frame was selected to have rigid connections, however, members sizes were taken to be the same as those of frames Ff1 and Ff2. This frame was taken as the base-line to be compared with frames Ff1 and Ff2 to determine the effect of connection flexibility and strength on the behaviour of the frame.

The four selected frame designs were checked for lateral deflection and interstorey drift when subjected to the code specified wind loads; the results are shown in Fig 6.3. Also, the anticipated deflections and interstorey drift resulting from earthquake loads

were obtained and checked against the code limits, as shown in Fig 6.4.

## 6.4 Computer modelling

In modelling the frame, two dimensional beam-column elements (Prakash and Powel, 1992) were used to represent the beams and columns. Plastic hinges in the beams were assumed to take place only at concentrated points at the element ends. The beams' shear deformations were neglected and the yield interaction limits were assumed to be affected by bending moment only. The effect of axial forces in the beams was neglected. Since the beams were selected to be class 1 sections, the beam resistance ($M_r$) was assumed to be limited to its factored plastic moment ( $\phi$ Z $\sigma_y$). The performance factor "$\phi$" is equal to 0.9 as given by CAN3-S16.1-M89, "Z" is the plastic modulus of the beam section and $\sigma_y$ is the yield stress. In the case of the HSS columns where the axial forces are high, beam-column elements possessing flexural and axial stiffness were used. Member stability considerations were excluded while yielding was assumed to take place only in concentrated hinges at the elements ends. Yield interaction relationships for the beams and columns were assumed to govern the strength, and are given by Eqs 6.6 and 6.7 respectively (CAN3-S16.1-M89, 1989)

$$\frac{M_{fx}}{M_r} \leq 1.0 \qquad (6.6)$$

and

$$\frac{C_f}{C_r} + \frac{M_{fx}}{M_r} \leq 1.0 \qquad (6.7)$$

Here $C_f$ and $M_{fx}$ are the axial load and bending moment about the major axis due to factored gravity and lateral loads, while $C_r$ is the factored axial compression resistance "$\phi$ A $\sigma_y$".

The connection between the beam and the column was modelled using both bi-linear and tri-linear springs. The spring parameters were calculated as described in Chapter 4. For the beam and beam-column elements, a strain hardening modulus of 0.03E was used, where "E" is the modulus of elasticity for steel and taken to be 200,000 MPa.

A damping proportional to both the mass and the initial stiffness was used. A damping ratio of 3% of critical was employed to the first two modes. The damping coefficients were determined as explained by Clough and Penzien, 1975. It is believed that the error in estimating the amount of damping is within an acceptable range of accuracy implicit in the analysis.

For both static and dynamic analyses, the frames were subjected to gravity loads that included specified dead and live loads. Gravity loads applied to the beams were modelled by specifying fixed end forces at the beam ends. Masses of the tributary floor areas, wall units, partitions and glazing were all assumed to be lumped to the column-beam joints and were associated with the horizontal displacement of the floors only. The mass included 25% of the design snow load.

## 6.5 Static analysis of the 4-storey frames

To determine the effect of the semi-rigid connection design on the behaviour of the frame, static analyses were carried out for the four studied cases, and the results are compared.

### 6.5.1 Effect of connection flexibility on the lateral deflections.

To examine the effect of the connection flexibility on the static lateral deflections of the 4-storey frame, frames Ffl and Ffr were subjected to the code specified lateral earthquake loads. The resulting lateral deflections are shown in Fig 6.5. Frame Ffl with extended end-plate connections exhibited larger drifts than the rigidly connected frame Ffr. The contribution of the connections' flexibility to the increase of the roof lateral deflection was about 35%. Thus, it can be concluded that employing extended end-plate connections to HSS columns, designed and detailed in accordance with the design criteria proposed in this study tends to increase the frame lateral deflection by about one third. Although, the frame is only 4 storeys high, it was decided to investigate the extent to which the effect of P- $\Delta$ would increase the lateral deflections of the flexible frame more than it did for the rigid frame. The deflections taking into account P-$\Delta$ effect were determined and plotted in Fig 6.5. It can be observed that P-$\Delta$ effects tend to increase the roof lateral deflection of the flexible frame Ffl and the rigidly connected frame Ffr by 13% and 10% respectively. Therefore, there is no significant increase in the roof's lateral deflection of Ffl as compared to the rigidly connected frame Ffr when P- $\Delta$ effects are included.

### 6.5.2 Effect of connection flexibility on frame weight

The structural design of the moment resisting frame with rigid connections, Frr, was controlled by drift limitations rather than strength requirements. Introducing semi-rigid connections in the frame will result in increasing the member sizes (beams and columns) to satisfy the drift requirements of the code. This increase in frame weight is determined by comparing the steel weight of frame Frr and frame Ff1, as given in Table 6.8. For this case, the increase in the total weight of the frame due to introducing semi-rigid connections is 13.4%. However, if gravity loads alone were to control the design of low-rise steel frames, member weights of semi-rigidly connected frames would be expected to be less than that of the fully rigidly connected frame as suggested by Xu et al (1993).

### 6.5.3 Effect of connection flexibility on the internal forces in frame members

Connection flexibility is expected to affect the distribution and the magnitude of internal forces in the frame members and joints. The internal forces in frames Ffr, Ff1 and Ff2 were compared when subjected to two cases of loading.

**a) Case 1: Factored gravity loads only (1.25D + 1.5L)**

In general, introducing semi-rigid connections in a frame will result in a reduction in the moments at the connections. The bending moments at the exterior and interior connections for the 3 frames along different storey levels when subjected to factored gravity loads (1.25D + 1.5 L) are plotted in Fig 6.6. It can be observed that there is no significant reduction in bending moments at the exterior connections, while there is a

remarkable reduction in the moments of interior connections. At the first storey, a moment reduction of 25% and 30% for frames Ff1 and Ff2 respectively was observed in the interior connections. However, the reduction in moment at the fourth storey dropped to 15% and 18% for frames Ff1 and Ff2 respectively. This behaviour is attributed to the fact that a flexible connection attracts less moment. Because the exterior connections have relatively higher stiffness than that of the interior ones (about 1.7 - 2.0 times), the exterior connections attract higher moments than do the interior ones.

Insignificant changes were observed in the bending moments of both exterior and interior columns due to connection flexibility. The normal forces due to gravity loads decreased in the interior columns by only 2.5% and 3.8% for frames Ff1 and Ff2, respectively as shown in Fig 6.7. However, the normal forces in the exterior columns increased by only 4.7% and 6.5% for frame Ff1 and Ff2, respectively.

**b) Case 2: Factored dead loads and lateral loads (1.25D + Q)**

When the frames were subjected to the factored dead loads and specified earthquake loading (1.25D + Q), similar behaviour to the case of gravity loads only was observed in the moments of the exterior and interior connections, as shown in Fig 6.8. However, the moments in the exterior connections for the flexible frames Ff1 and Ff2 exceeded that of the rigid frame Ffr above the first storey. The distribution of the bending moments of the exterior and interior columns for the three frames along the height are plotted in Fig 6.9. No significant variation in bending moments was observed. However, an increase of 10% and 13% in the base moments were observed in the columns of frame Ff1 and Ff2, respectively, due to the connection's flexibility.

### 6.5.4 Effect of connection modelling on the top lateral deflection

Each of the frames Ff1 and Ff2 was subjected to the specified dead and live gravity loads as well as the specified lateral earthquake loads. The frames were analyzed under increasing lateral static loads as factored from the design earthquake base shear. To determine the effect of connection modelling on the top lateral deflection, each frame was analyzed using bi-linear and tri-linear models for the moment-rotation behaviour of the connections. As noted from Tables 6.4 and 6.6, the connections of frame Ff1 behave elastically up to about $1.3M_p$ ($M_p$ is the beam's nominal plastic moment) in the bi-linear model and up to about $M_p$ in the tri-linear model. Meanwhile, in frame Ff2, the connections behave elastically up to about $M_p$ in the bi-linear model and up to about $0.76M_p$ in the tri-linear model. Top lateral deflections of frame Ff1 and Ff2 resulting from the static analysis for both bi-linear and tri-linear models, are plotted in Fig 6.10.

For frame Ff1, because the connections in both models behaved elastically up to $M_p$, there was no significant difference in the lateral deflections at the top when either model was used. Because of the connection design, the behaviour of frame Ff1 was governed by yielding of the beams rather than the connections. On the other hand, the connections of frame Ff2 in both models behaved elastically up to about $0.76M_p$, at which point the connections with tri-linear models started to yield. This point corresponds to a load factor equal to 2.0, as shown in Fig 6.10. Although the difference in using the bi-linear or tri-linear models were insignificant up to failure of frame Ff1 and up to a load factor 2.0 for frame Ff2, the tri-linear model was adopted in this investigation because it provides a more realistic representation of the connection behaviour for both

frames.

### 6.5.5 Effect of connection flexibility on the overall strength of frames

Each of the four frames was subjected to the specified dead and live loads and an increasing lateral static load as represented by a factor times the design earthquake base shear. The lateral loads were increased until a failure mechanism was formed to determine the over strength factors of the frames. The static analysis results of the top lateral deflection of each frame are plotted in Fig 6.11. As indicated on the plot are, the design base shear, the anticipated over strength factor interpreted from the NBCC (1990) (1/U =1.66), the over strength factors at maximum allowed top deflection, and that at failure for each frame. The four frames behaved elastically until it reached the anticipated over strength factor (1.66). It appears that introducing semi-rigid connections in frames Ff1 and Ff2 did not significantly reduce their ultimate strength as compared to that of the rigid frame Ffr, however, it significantly increase their ultimate strength as compared to that of the rigid frame Frr. The reason is that employing semi-rigid connections in frame Ff1 resulted in an increase in its total weight by about 15% as compared to frame Frr. This increase in section sizes and weight is associated with an increase in the frame's ultimate strength by about 25%. At failure, the maximum normal forces in the columns were about 15% of the elastic buckling loads. Load factors at the formation of the first plastic hinge in the beams, columns and at first connection yield are given in Table 6.9 for each frame. Comparing the load factors of frames Ffr, Ff1 and Ff2, it is observed that the load factors causing initial plastic hinging in the columns decreased, while the

load factors causing initiation of plastic hinges in the beams increased. This is because flexible connections attract less moment, which requires a higher load factor to cause the first plastic hinge in the beam. On the other hand, the more flexible the connections are, the larger are the moments developed at the column bases. In this case, lower load factors are needed to cause the first column plastic hinge. The maximum plastic rotation experienced by beams and columns as well as the maximum total connection rotation for each frame at failure are given in Table 6.10. Introducing semi-rigid connections in moment resisting frames has the effect of reducing the plastic rotation in the beams, while increasing the column plastic rotation in the columns.

## 6.6 Dynamic analysis of the 4-storey frames

Inclusion of semi-rigid connections in the dynamic analysis of a frame would be expected to affect its dynamic characteristics and its response. Frame Ff1 was designed for strength, drift and ductility with a connection strength equal to 1.3 times the plastic moment capacity of beams. This design was shown to be satisfactory under earthquake loading treated as an equivalent static load. Frame Ff1 will be studied under dynamic loading and compared with frame Ffr having rigid connections.

### 6.6.1 Dynamic characteristics of frames Ffr and Ff1

Incorporating connection flexibility in the frame analysis reduces the stiffness and lengthens the vibration periods of the frame. Computer program Drain-2DX was used to determine the periods of free vibrations of frames Ffr and Ff1. The first four

vibration periods for each frame are listed in Table 6.11. As noted, the fundamental period of frame Ff1 with flexible connections is about 1.15 times that of frame Ffr with infinitely rigid connections. However, this difference decreases in the higher modes. The analysis indicates that in both frames, about 85% of the effective total mass was associated with the first mode.

### 6.6.2 Proposed artificial ground excitations

The intensity, duration of strong shaking and frequency content of an earthquake record depends on a number of factors, such as the magnitude of the earthquake, the epicentral distance, the local geology and the site conditions. The differences among records can lead to significant differences in structural response. One important factor that has significant effect on structural response is the frequency content of the record. To account for the frequency content, the ratio of peak ground acceleration, "A" (expressed in units of gravitional acceleration "g") to peak ground velocity, "v" (expressed in units of m/s) has been used as an indicator. Records can be broadly divided into three categories, namely high A/v ratio (A/v $>$ 1.2), intermediate A/v ratios (1.2 $>$ A/v $>$ 0.8) and low A/v ratio (A/v $<$ 0.8). Statistically, records with high A/v ratios are normally associated with stiff and rock sites at short epicentral distances, while records with low A/v ratios are normally associated with soft sites and with strong earthquakes at long epicentral distances.

For the purpose of defining input motion in the present study, two artificial earthquake ground motions were generated to fit two specified target spectrums, one with

high A/v ratio and the other with a low A/v ratio.

a) **High A/v ratio earthquake record**

A time history was generated to represent an earthquake with a high A/v ratio in the Montreal region. According to the NBCC (1990), this area is expected to experience ground motions with high A/v ratios, peak ground accelerations ranging from 0.16g to 0.23g and a peak ground velocity ranging from 0.08 m/s to 0.11 m/s with a 10% probability of exceedence in 50 years. The first artifical record was generated such that it had a high A/v ratio with a peak ground acceleration equal to 0.22g.

b) **Low A/v ratio earthquake record**

Since the studied frames (Ffr and Ff1) have relatively long periods, as given in Table 6.11, (i.e, relatively low frequencies), they would be expected to have a strong response when subjected to an input ground motion record of low A/v ratio. In order to study the inelastic dynamic response of the frames, the generated record was scaled until a significant inelastic response was observed; a value of peak ground acceleration of 0.35g was found to be adequate in this respect.

### 6.6.3 Generation of artificial earthquake records

The computer program SYNTH (Naumoski, 1984) was used to generate artificial acceleration time histories whose spectrums were close to specified target spectra. The high A/v ratio record was generated to fit a target spectrum close to that specified by NBCC (1990) for the Montreal region. While the low A/v ratio record was generated to fit a specified target spectrum having low A/v ratio. The low A/v ratio spectrum was

taken as the average spectrum of fifteen actual records from earthquakes in the United States, Japan, Mexico, Yugoslavia and Canada having low A/v ratio, (Naumoski, 1988).

The specified target acceleration spectrum and the generated spectrum of the artificial high and low A/v records are shown in Fig 6.12 and Fig 6.13 respectively. The generated acceleration-time histories and the corresponding velocity-time histories for the two A/v input motions are shown in Fig 6.14 and Fig 6.15 respectively. The high A/v record had a value for A/V ratio equal to 1.7 (greater than 1.2), while the low record had a value of A/V equal to 0.74 (less than 0.8).

### 6.6.4 Dynamic response to the high A/v ratio record

The response of the flexible frame Ff1 was found to be elastic during this event, while plastic hinges were formed only in first floor beams of frame Ffr (rigid connections). The reason for this result is the fact that rigid connections attract higher moments. The elastic response of the frame was expected for two reasons. Firstly, the design base shear according to NBCC (1990) was evaluated based on a period of 0.48 s, with the computed periods of frames Ffr and Ff1 being 1.53 and 1.75 s respectively. This results in a significant reduction in the effective elastic base shear on the frames when subjected to the code acceleration spectrum given in Fig 6.12. The second reason was that the sizes of the frame members were governed by the code drift limitations rather that the strength reqirements for the specified earthquake loads. The predicted storey shear envelopes for both frames are shown in Fig 6.16. The insignificant difference in the two results is due to the flatness of the code response spectrum in the

range of the fundamental periods of both frames as indicated in Fig 6.12. Meanwhile, the maximum base shear experienced by Ffr and Ff1 were 2.73 and 2.80 times the design base shear, respectively. The calculated floors displacement envelopes are shown in Fig 6.17, while the roof displacement histories of both frames are shown in Fig 6.18. Frame Ff1 with semi-rigid connections exhibited a 17% increase in roof displacement as compared to frame Ffr with rigid connections.However, this increase is less than the 35% computed for the case of static loading.

### 6.6.5 Dynamic response to the low A/v ratio record

The floor displacement envelopes and the floor displacements at the instant of the peak roof displacement for Ffr and Ff1 are shown in Fig 6.19. Examining this figure, supports the previous conclusion regarding the effect of connection flexibility on increasing the frame lateral deflections. In addition, the response of both frames during the event was dominated by the first mode. At 11.4 seconds from the start of this event, the peak positive acceleration (0.27g) had caused plastic hinges in all column bases in Ff1. This resulted in severe inelastic action causing it to deform significantly in the positive direction. Subsequent vibrations were about the deformed position. On the other hand, plastic hinges were delayed in frame Ffr until a reversal in acceleration took place, i.e. at. 12.2 seconds (Fig 6.15). They formed at all column bases at the instant of peak negative acceleration (0.35g), causing the frame to deform significantly in the negative direction. This was the reason for Ff1 experiencing significantly higher positive displacements than Ffr and also about equal negative displacements (Fig 6.19). On the

other hand, the displacement envelope of frame Ffr was much more biased towards the negative displacement side. The same observation can be noted in Fig 6.20 which shows the roof displacement histories for both frames.

The calculated storey shear and interstorey drift envelopes for the frames are plotted in Fig 6.21. Due to the connection flexibilities of Ff1, it attracted less interstorey shear compared to Ffr with rigid connections. The maximum base shear during this event was found to be 3.98 and 3.83 times the design base shear according to NBCC (1990) for frames Ffr and Ff1, respectively. Meanwhile, the maximum interstorey drift of Ffr was 2.63% at the first floor level (Fig 6.21), while that for Ff1 was 2.14% at the second floor. These drift values are slightly higher than the code limit for inelastic action (2%).

Envelopes of bending moments and normal forces for exterior and interior columns of both frames are shown in Fig 6.22 and Fig 6.23, respectively. The bending moments envelopes for both exterior and interior columns in frame Ff1 tend to be inside those of Ffr, indicating that the columns in the flexible frame design attract less moment. However, a slight variation was observed in the normal force envelopes for the exterior and interior columns. This may be due to the variation of beam moments resulting from strain-hardening at plastic hinges due to connection flexibilities.

At the end of the 30 second event, plastic hinges in beams and base columns were determined to have formed in both Ffr and Ff1. The resulting plastic hinges with the corresponding maximum plastic rotation for frames Ffr and Ff1 are shown in Figs 6.24 and 6.25, respectively. Both frames tended to experience sway mechanisms as a result of the adopted strong column-weak beam design concept. Frame sway mechanisms allow

plastic hinges to form in a large number of beams. In seismic design, this process provides for higher ductility and energy dissipation capability of the frame. However, due to the connection flexibility, plastic hinges were formed up to the second floor beams in frame Ff1, while plastic hinges formed up to the third floor beams in the rigid frame Ffr. From comparing Fig 6.24 and Fig 6.25 it is noted that, due to connection flexibilities in Ff1, beam plastic hinge rotations were reduced which diminishes the demand on beam ductility, while column plastic hinge rotations were increased. All connections in frame Ff1 behaved mainly elastically during this event, except the ones on the first floor which experienced insignificant plastic rotations.

## 6.7 Summary

Extended end-plate connections employing HSBB between W-shape beams and HSS columns were used in a 4-storey moment resisting steel frame. The connections were modeled as semi-rigid connections. The frame response with extended end-plate connections was compared with the response of a rigid frame design when subjected to either static or dynamic loading. On the basis of the results obtained from the analysis, the following conclusions are summarized.

1- For moment resisting frames where drift limitations control the design, employing such a semi-rigid connection increases a frame's member weight slightly. However, this increase in member weights improves the performance of the frame in terms of its stiffness and strength at higher stages of loading when compared to rigid frame design. Frames where gravity loads control the design and drift is relatively unimportant,

member weights are expected to be iess than comparable rigid frame design.

2- The use of such semi-rigid connections in frames subjected to lateral loads tende to increase lateral deflections by about 35%, reduce the moments in the interior connections of the beams by about 30%, while increasing the base moment in columns by about 13%.

3- For frames where wind loads govern the design, connections can be designed so that their plastic moment is equal to the plastic moment of the attached beam. While for frames where earthquake loads govern the design it is preferable to design the connection so that its plastic moment equal to 1.3 times the beam's plastic moment. In such case, the connections will behave mainly elastically up to the beam plastic moment and with minimal plastic deformation during a severe earthquake event and without significant degradation in its stiffnesses.

4- Either designing the connection so that its plastic moment equal to Mp or 1.3Mp (Mp is the beam's plastic moment), the ultimate strength of the frame is not significantly reduced as compared to the strength of rigid frames with the same size of members.

5- Introducing extended end-plate semi-rigid connections in the frame analysis, will have the effect of lengthening the natural period of the frame by about 15%. This is associated with slight reduction in base shear as compared to rigid frames.

6- Non-linear dynamic analysis showed that although the connections behaved mainly elastic during the analysis, the flexibility of such connections affect the frame dynamic response. These effects were found to be increasing lateral deflection envelopes, decreasing the number of beam plastic hinges and their plastic rotations, thus decreasing the resulting damage, and increasing the plastic rotations experienced by the columns at the base.

7- The flexibility of semi-rigid connections should be included in both static and dynamic analyses to determine a frame's structural behaviour more realistically. The Canadian Standard CAN3-S16.1-M89 (1989) does not account for the effects of connection flexibility in assessing the frame structural behaviour.

Table 6.1 Member sizes for frame Frr

| | | 1st, 2nd & 3rd Floor | 4th Floor |
|---|---|---|---|
| Beam Sizes | | W 360 X 39 | W 250 X 33 |
| Column Sizes (mm) | Exterior | HSS 254X254X11.13 | HSS 203X203X11.13 |
| | Interior | HSS 304X304X11.13 | HSS 254X254X11.13 |

Table 6.2 Member sizes for frames Ff1,Ff2 and Ffr

| | | 1st, 2nd & 3rd Floor | 4th Floor |
|---|---|---|---|
| Beam Sizes | | W 410 X 46 | W 360 X 33 |
| Column Sizes (mm) | Exterior | HSS 254X254X12.7 | HSS 203X203X12.7 |
| | Interior | HSS 304X304X12.7 | HSS 254X254X12.7 |

Table 6.3 End-plate design for Frame Ff1

| Floor Level | Connection Location | End-plate Dimension (mm) | End-plate Thickness (mm) | Number and Size of HSBB (mm) | Doubler Plate Thickness (mm) |
|---|---|---|---|---|---|
| 1st, 2nd, | Exterior | 625X250 | 24 | 8 - 26 | 12 |
| and 3rd. | Interior | 625X300 | 22 | 8 - 26 | 12 |
| 4th floor | Exterior | 580X200 | 24 | 8 - 24 | 10 |
| | Interior | 580X250 | 22 | 8 - 24 | 10 |

Table 6.4 Connection model parameters* for Frame Ff1

| Floor level | Connection location | $K_i$+ | $K_t$+ | $K_p$+ | $M_{pc}/M_p$ | $M_1/M_p$ | $M_2/M_p$ |
|---|---|---|---|---|---|---|---|
| 1st, 2nd | Exterior | 79000 | 13430 | 3950 | 1.37 | 0.99 | 1.50 |
| and 3rd | Interior | 44510 | 8011 | 2225 | 1.37 | 1.00 | 1.48 |
| 4th floor | Exterior | 84000 | 13692 | 4200 | 1.36 | 0.98 | 1.51 |
| | Interior | 45359 | 8074 | 2268 | 1.36 | 1.00 | 1.48 |

* Bi-linear model uses $K_i$, $K_p$ and $M_{pc}$ parameters
* Tri-linear model uses $K_i$, $K_t$, $K_p$, $M_1$ and $M_2$ parameters
+ Stiffnesses are in kN.m/rad
$M_p$ : beam's nominal plastic moment
$M_{pc}$ : connection's plastic moment

Table 6.5 End-plate design for Frame Ff2

| Floor Level | Connection Location | End-plate Dimension (mm) | End-plate Thickness (mm) | Number and Size of HSBB (mm) | Doubler Plate Thickness (mm) |
|---|---|---|---|---|---|
| 1st, 2nd, | Exterior | 625X250 | 22 | 8 - 24 | 8 |
| and 3rd. | Interior | 625X300 | 19 | 8 - 24 | 6 |
| 4th floor | Exterior | 580X200 | 22 | 8 - 20 | 6 |
| | Interior | 580X250 | 19 | 8 - 20 | 6 |

Table 6.6 Connection model parameters* for Frame Ff2

| Floor level | Connection Location | $K_i$+ | $K_t$+ | $K_p$+ | $M_{pc}/M_p$ | $M_1/M_p$ | $M_2/M_p$ |
|---|---|---|---|---|---|---|---|
| 1st, 2nd | Exterior | 63000 | 10710 | 3150 | 1.05 | 0.76 | 1.15 |
| and 3rd | Interior | 31644 | 6012 | 1582 | 1.05 | 0.78 | 1.13 |
| 4th floor | Exterior | 71820 | 11850 | 3591 | 1.05 | 0.76 | 1.16 |
| | Interior | 36110 | 6247 | 1805 | 1.05 | 0.77 | 1.15 |

* Bi-linear model uses $K_i$, $K_p$ and $M_{pc}$ parameters
* Tri-linear model uses $K_i$, $K_t$, $K_p$, $M_1$ and $M_2$ parameters
+ Stiffnesses are in kN.m/rad
$M_p$ : beam's nominal plastic moment
$M_{pc}$: connection's plastic moment

Table 6.7 Fixity factors of the connections

| | 1st,2nd and 3rd floor | | 4th floor | |
|---|---|---|---|---|
| | Exterior Connections | Interior Connections | Exterior Connections | Interior Connections |
| Frame Ff1 | 0.84 | 0.74 | 0.91 | 0.85 |
| Frame Ff2 | 0.80 | 0.67 | 0.89 | 0.81 |

Table 6.8 Weight comparison between frames Frr and Ff1

| | Beams weight (kN) | Columns weight (kN) | Total weight (kN) |
|---|---|---|---|
| Frame Frr | 35.35 | 61.17 | 96.50 |
| Frame Ff1 | 40.32 | 69.07 | 109.40 |
| Percentage of weight increase in Ff1 | 14% | 13% | 13.4% |

Table 6.9 Comparison of frames load factors

| | Load factor at | | | | |
|---|---|---|---|---|---|
| | first beam plastic hinge | first column plastic hinge | first connection yielded | max. allowed roof deflection | failure |
| Frame Frr | 1.472 | 2.304 | N/A | 2.81 | 3.04 |
| Frame Ffr | 2.148 | 2.906 | N/A | 3.62 | 3.81 |
| Frame Ff1 | 2.494 | 2.776 | 2.456 | 3.42 | 3.78 |
| Frame Ff2 | 2.778 | 2.645 | 1.710 | 3.28 | 3.72 |

Table 6.10 Maximum rotations at failure

| | Max. plastic rotation in beams (rad) | Max. plastic rotation in columns (rad) | Max. total rotation in connections (rad) |
|---|---|---|---|
| Frame Frr | 0.052 | 0.046 | N/A |
| Frame Ffr | 0.049 | 0.048 | N/A |
| Frame Ff1 | 0.051 | 0.05 | 0.0104 |
| Frame Ff2 | 0.048 | 0.057 | 0.022 |

Table 6.11 Free vibration periods of frames Ffr and Ff1

| | Vibration periods (s) | | | |
|---|---|---|---|---|
| | 1st Mode | 2nd Mode | 3rd Mode | 4th Mode |
| Frame Ffr | 1.53 | 0.49 | 0.302 | 0.216 |
| Frane Ff1 | 1.75 | 0.54 | 0.317 | 0.220 |

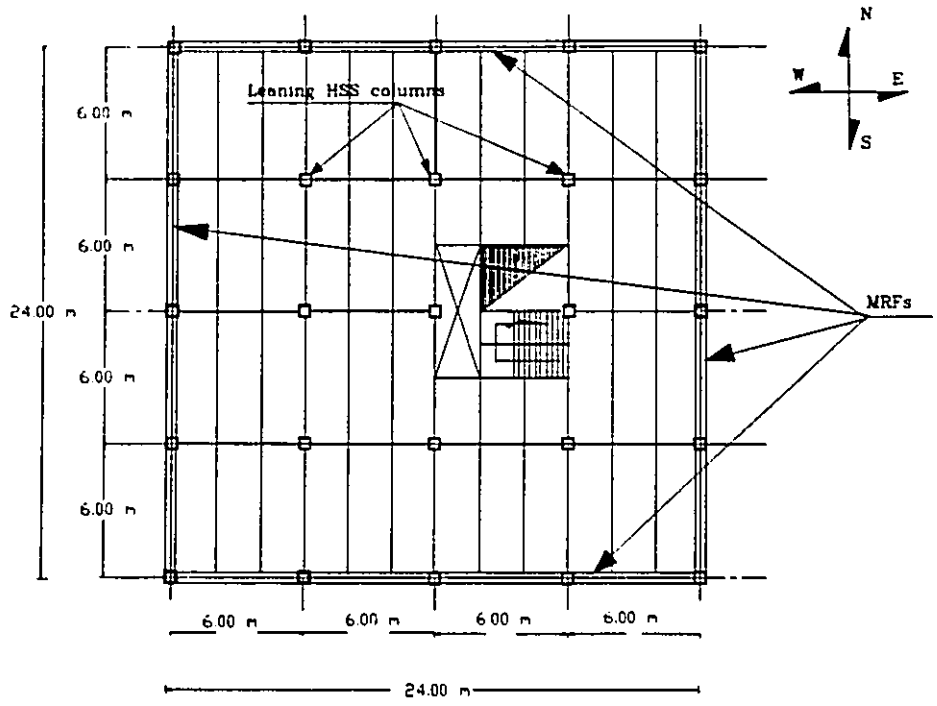


Fig 6.1 Plan of a 4-storey steel building

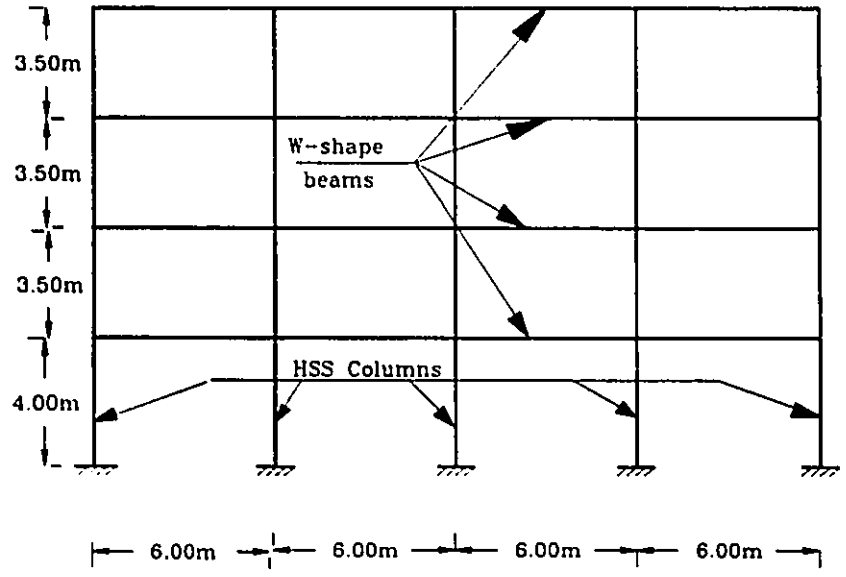


Fig 6.2 Elevation of the moment resisting frame in E-W or N-S direction

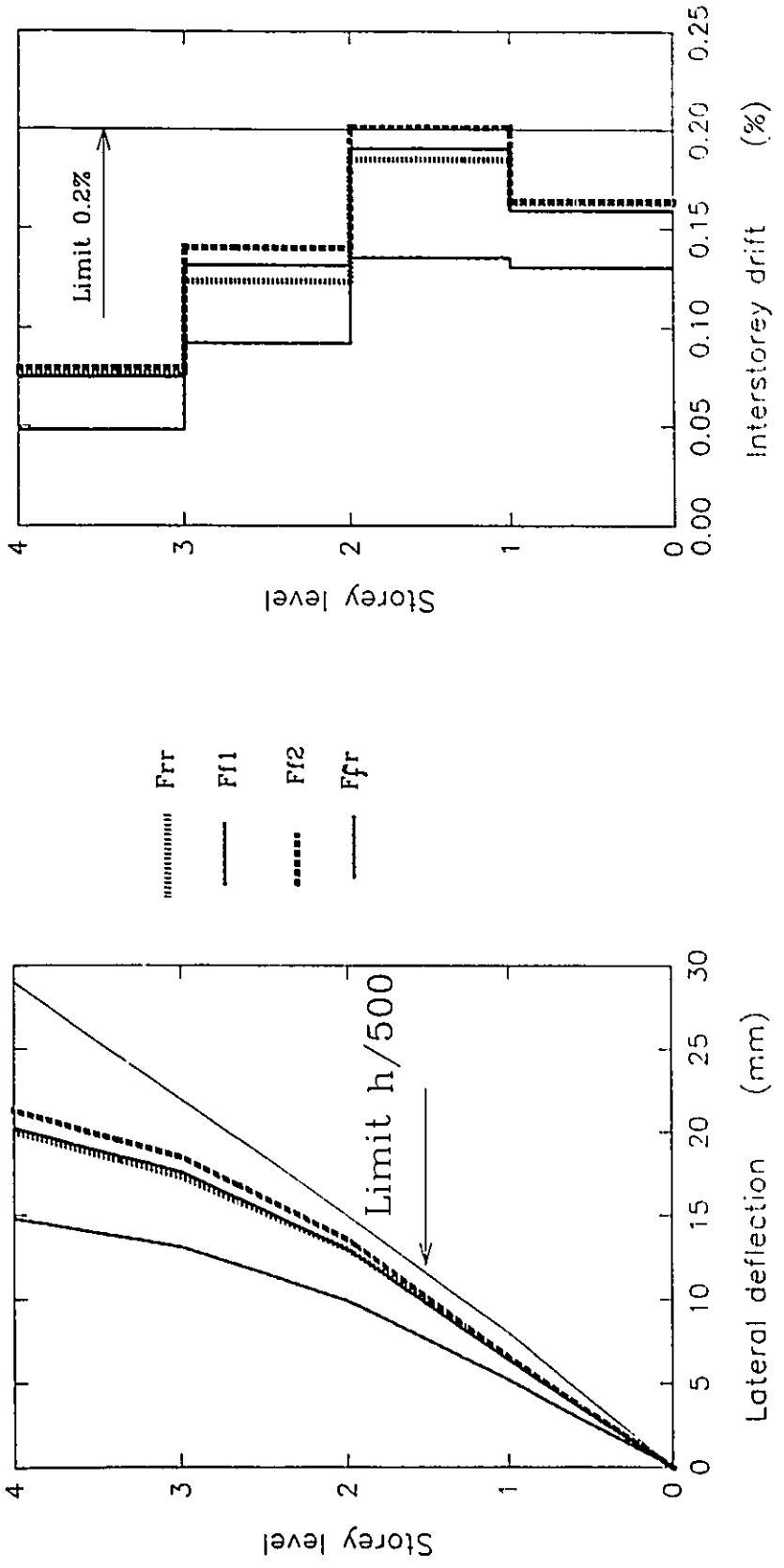


Fig 6.3 Frames' lateral deflection and interstory drift due to the specified wind loads

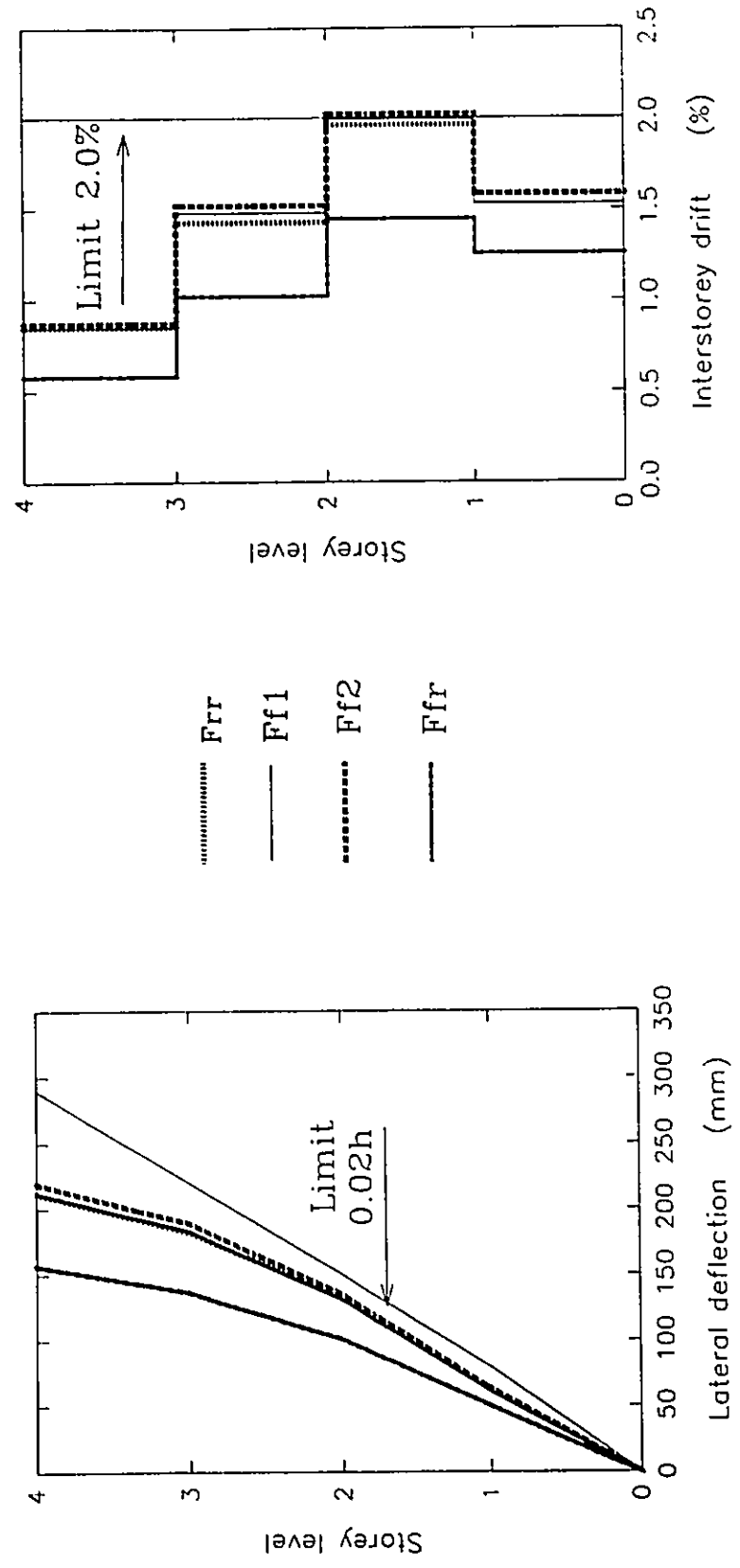


Fig 6.4 Frames' lateral deflection and interstorey drift due to the anticipated earthquake loads

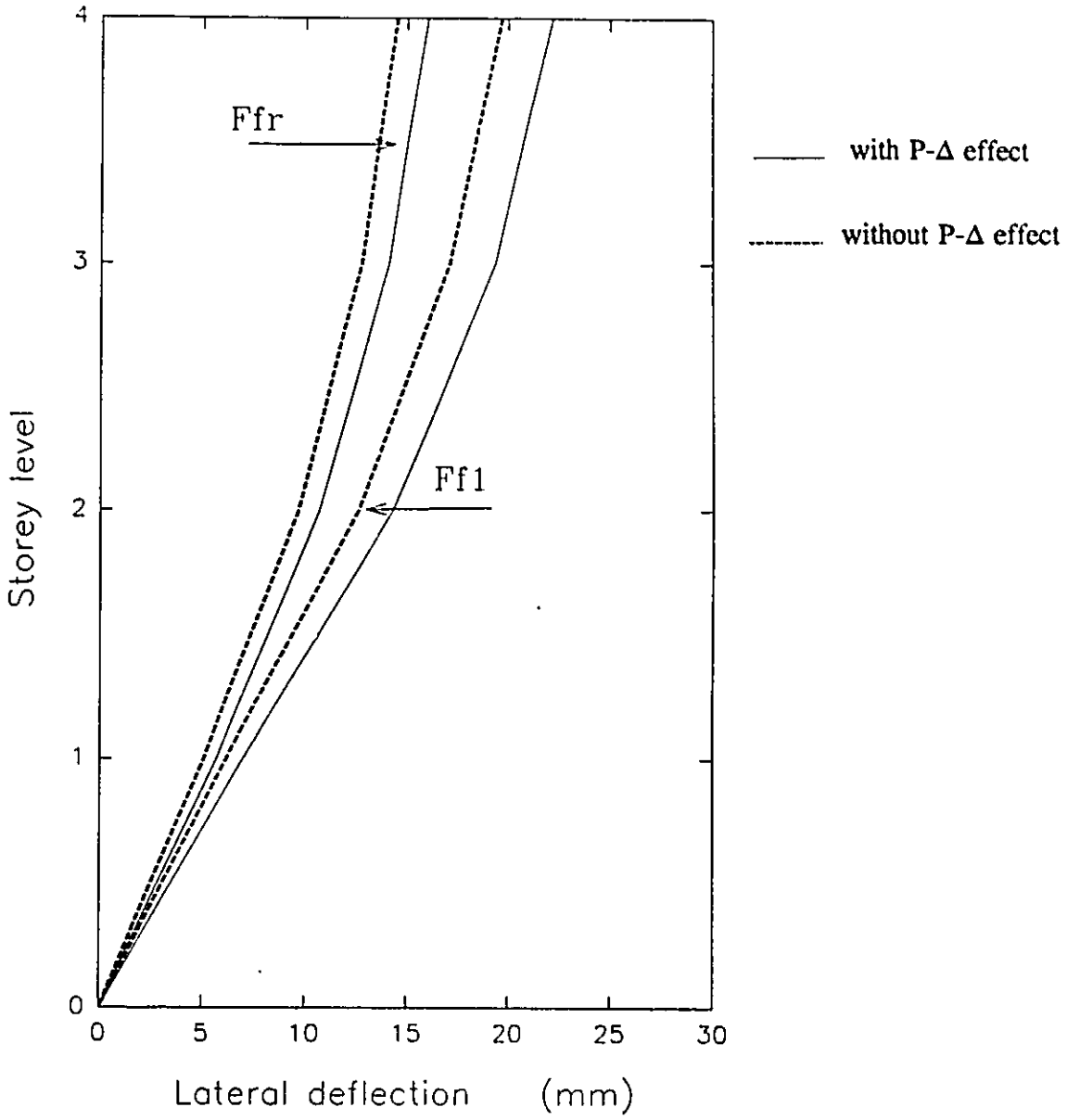


Fig 6.5 Effect of connection flexibility on lateral deflections of frames

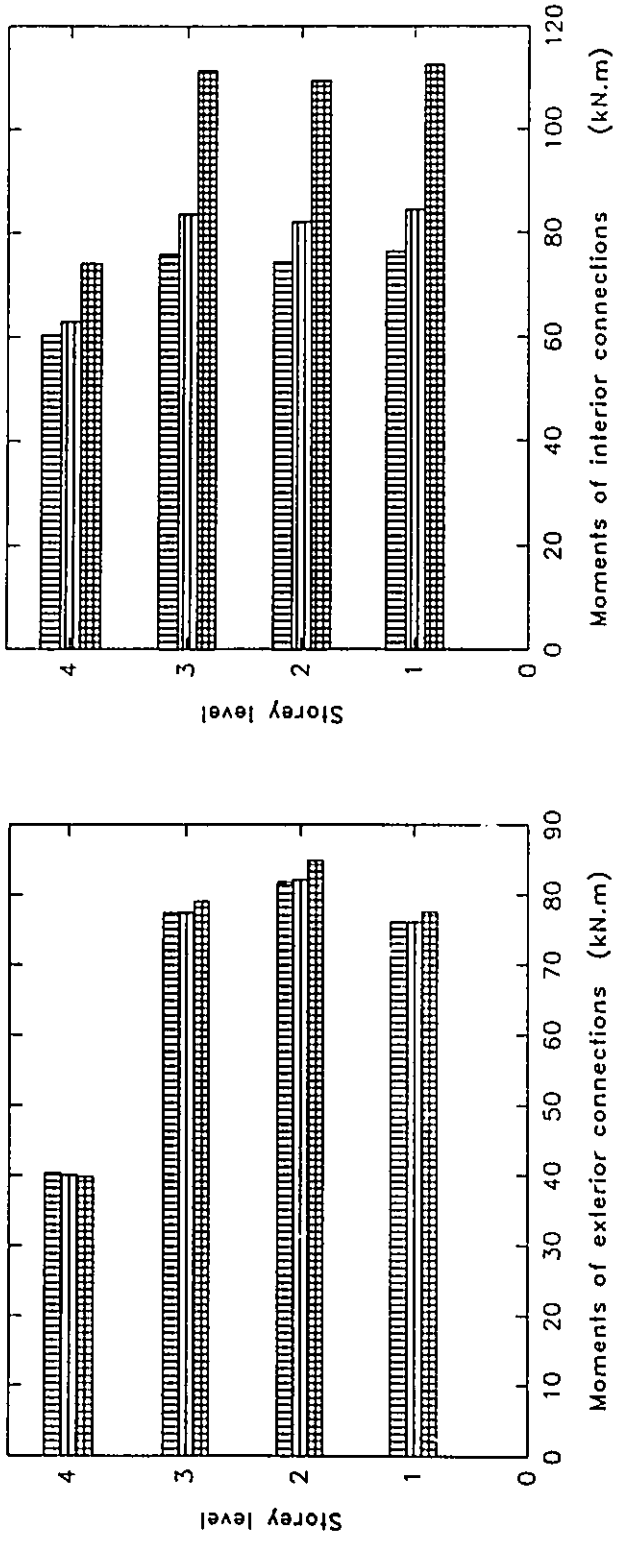


Fig 6.6 Effect of connection flexibility on its moments due to factored gravity loads

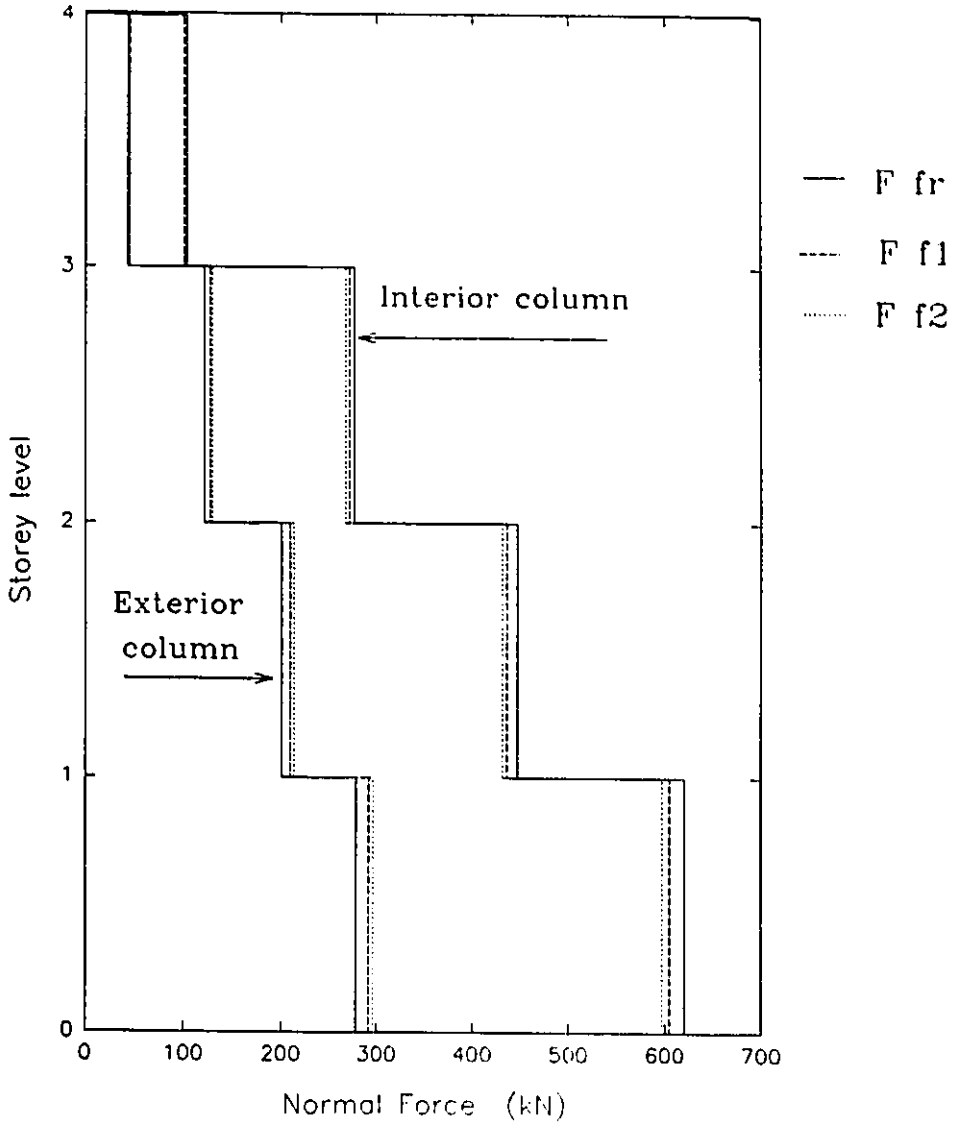


Fig 6.7 Effect of connection flexibility on columns' normal forces due to factored gravity loads

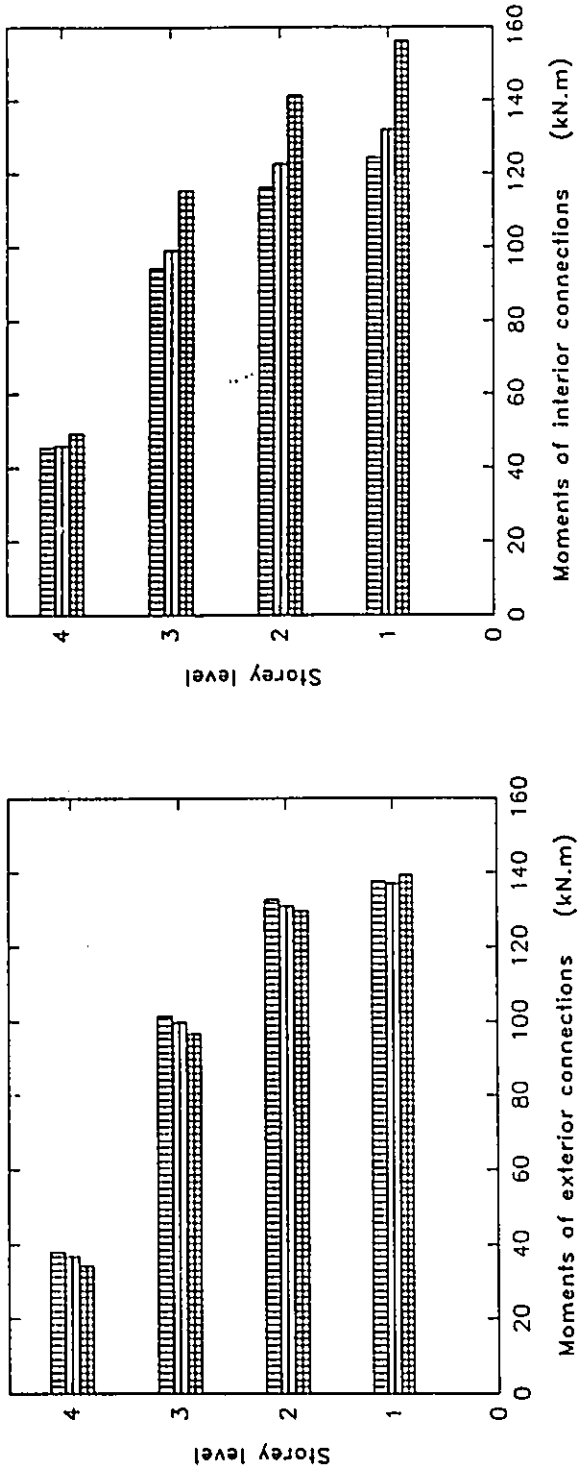


Fig 6.8 Effect of connection flexibility on its moments due to 1.25D + Q

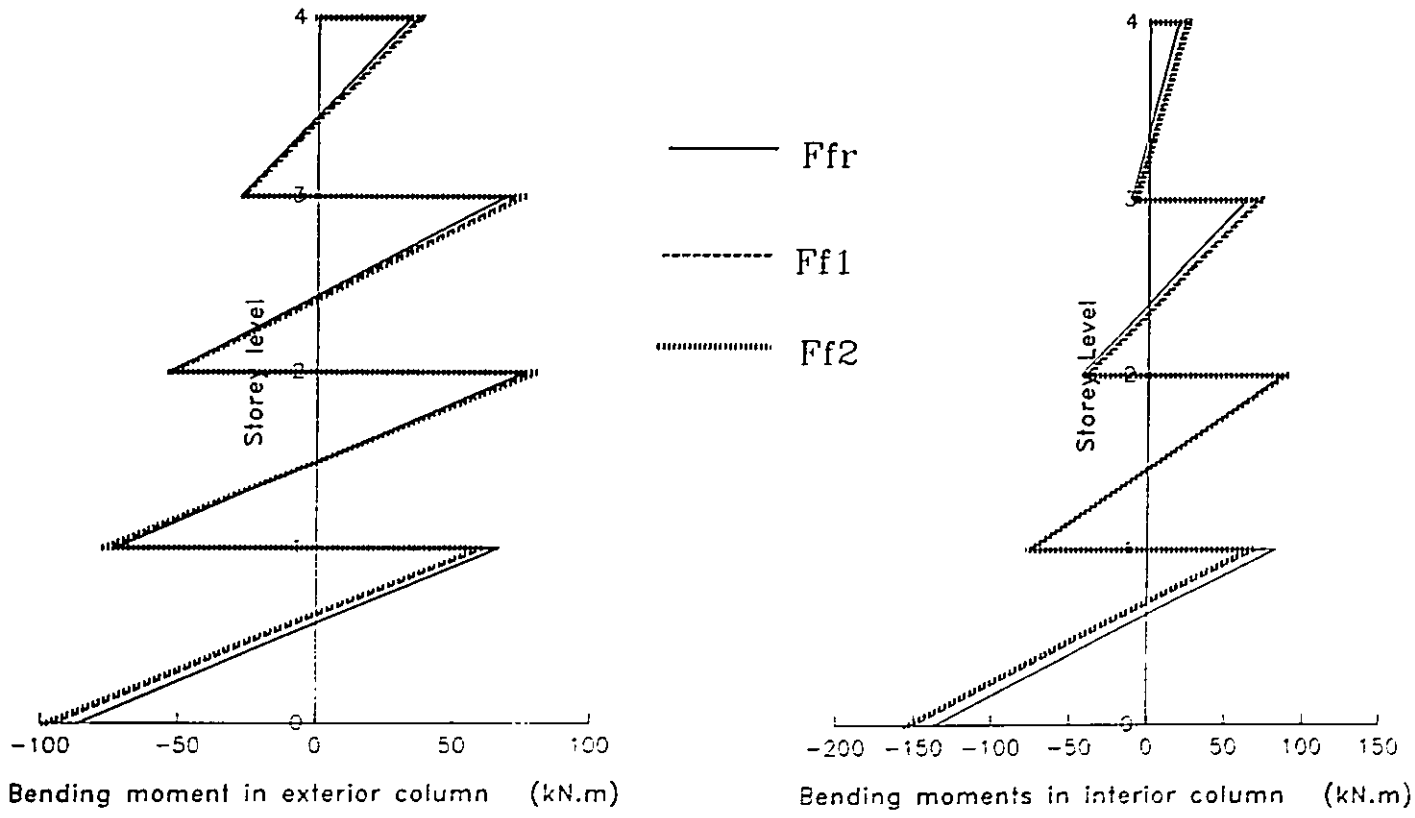


Fig 6.9 Effect of connection flexibility on columns' bending moments due to 1.25D + Q

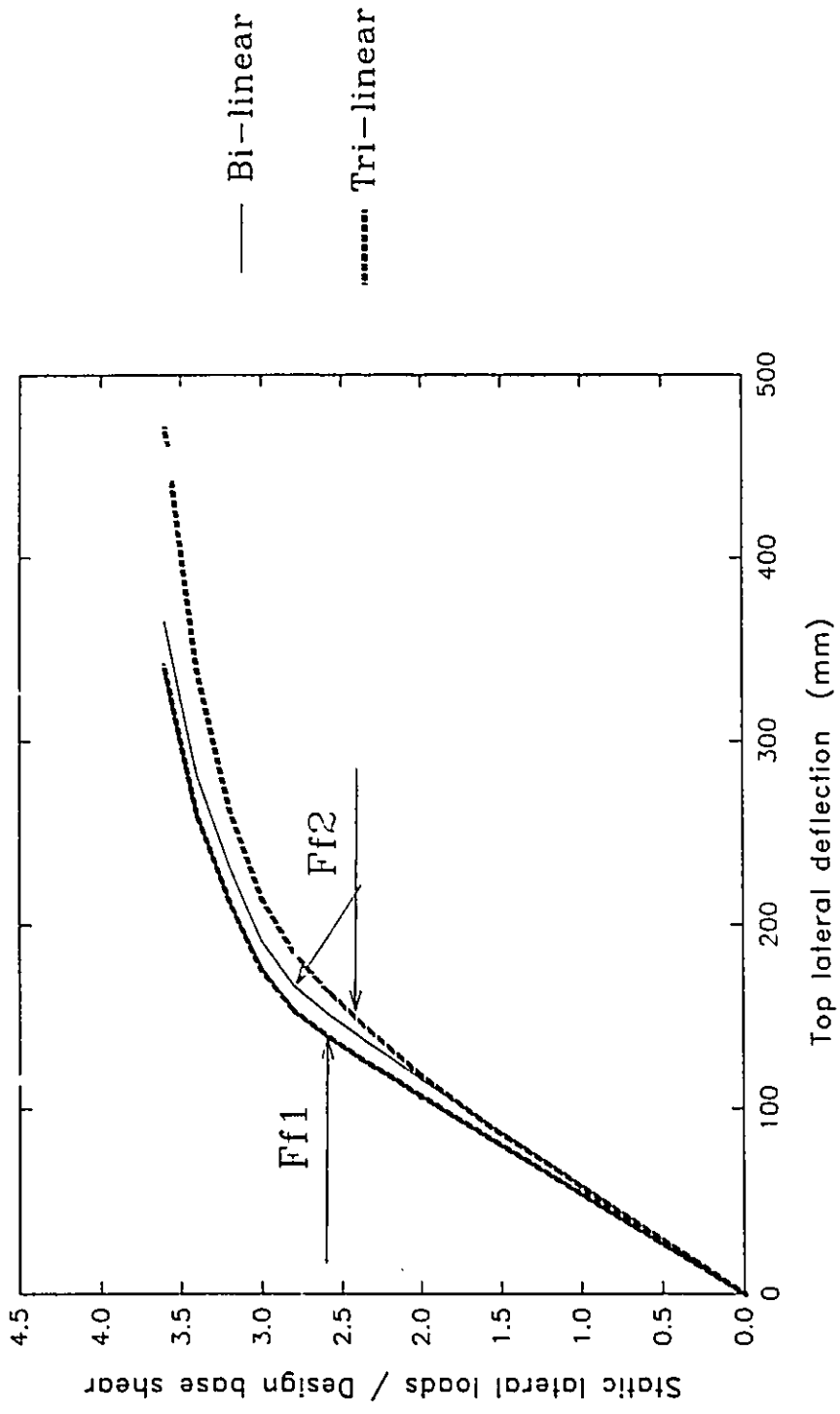


Fig 6.10 Effect of connection modelling on the static roof deflection

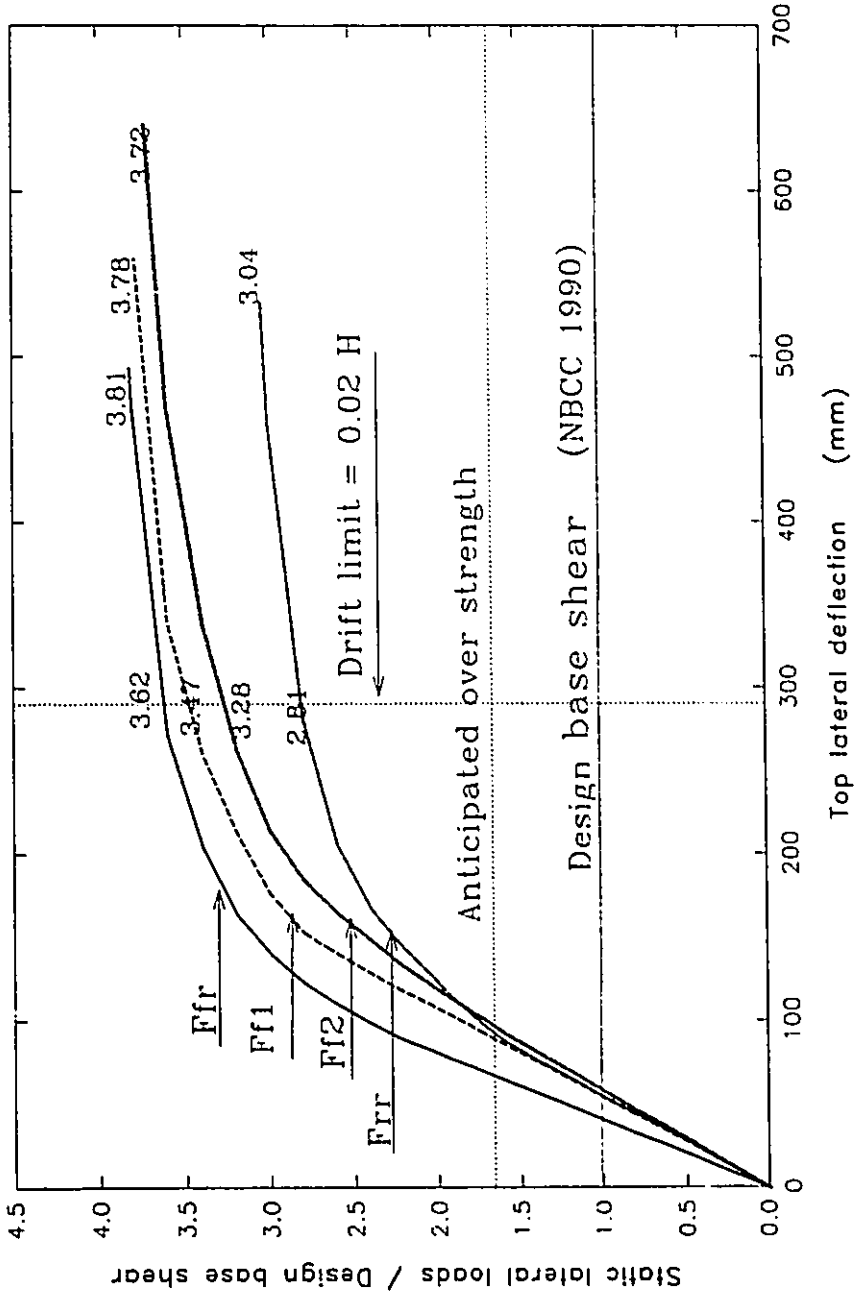


Fig 6.11 Effect of connection flexibility on the frames' roof static deflection

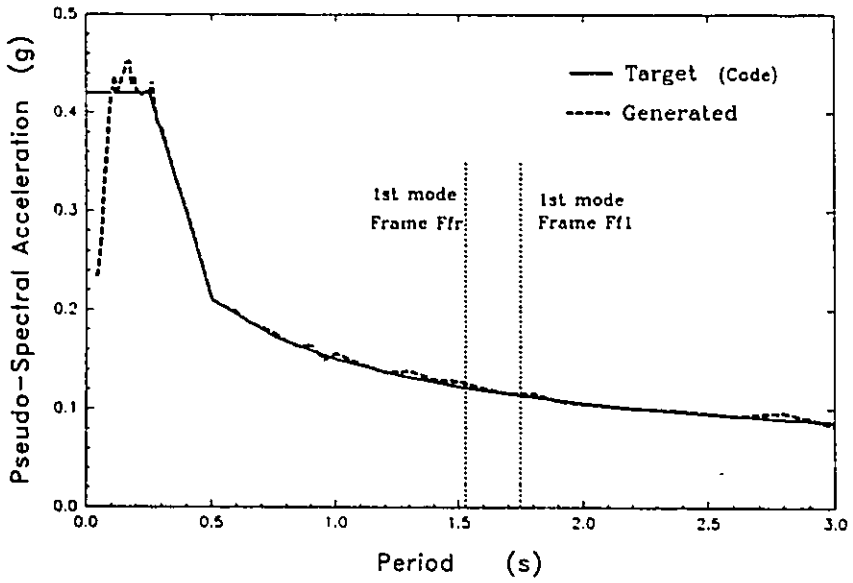


Fig 6.12 Target and generated spectral acceleration for high A/v ratio record

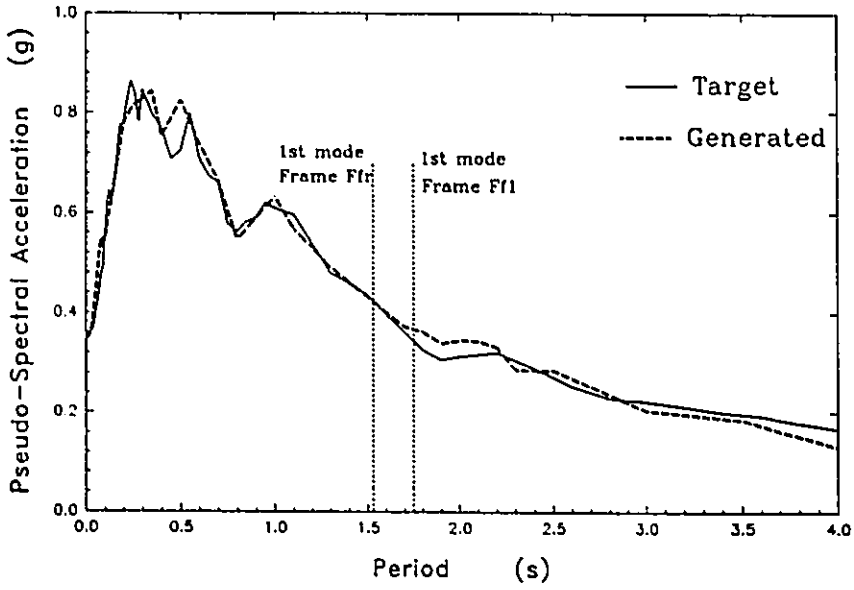


Fig 6.13 Target and generated spectral acceleration for low A/v ratio record

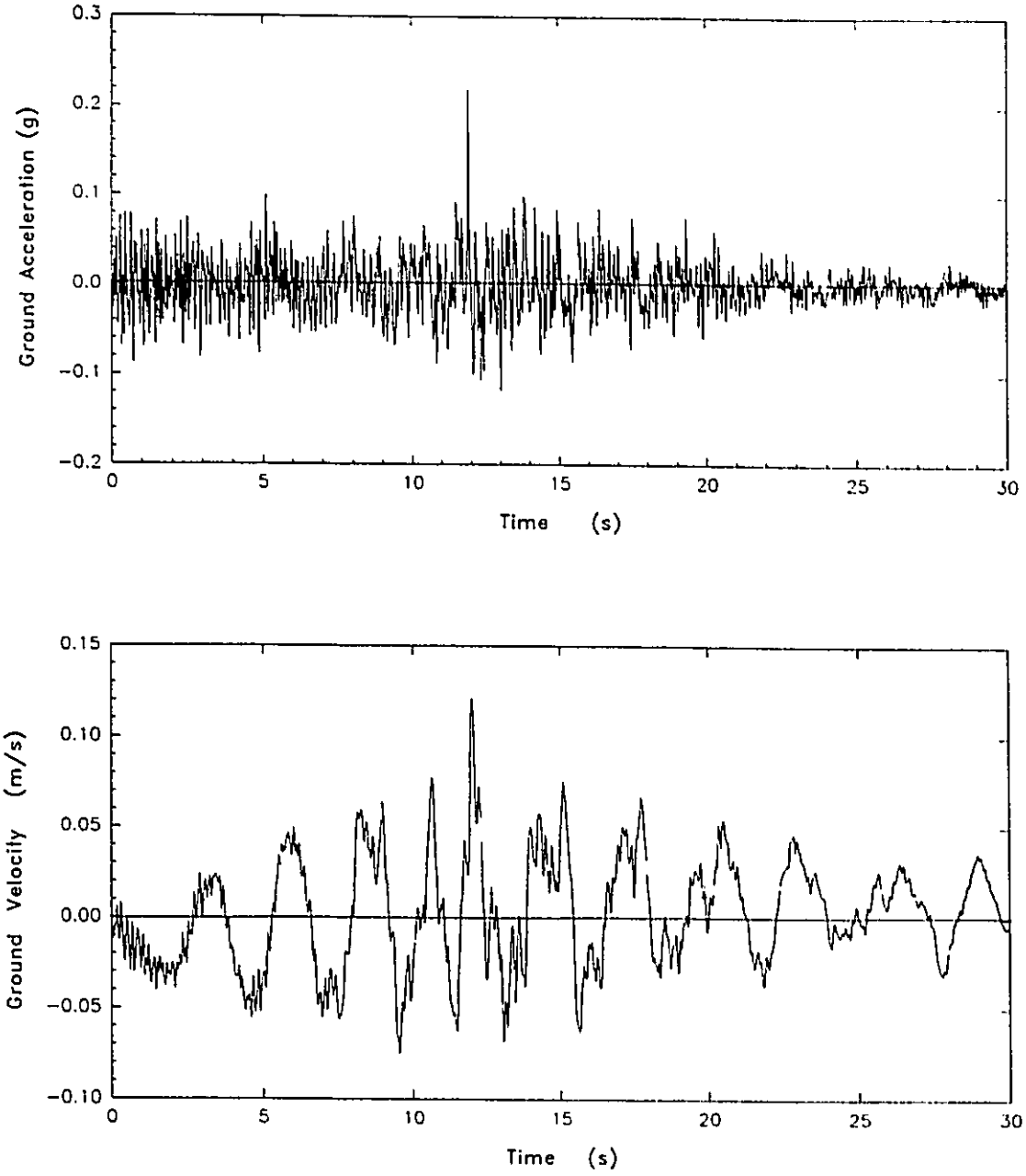


Fig 6.14 Ground acceleration and velocity time histories for high A/v ratio record

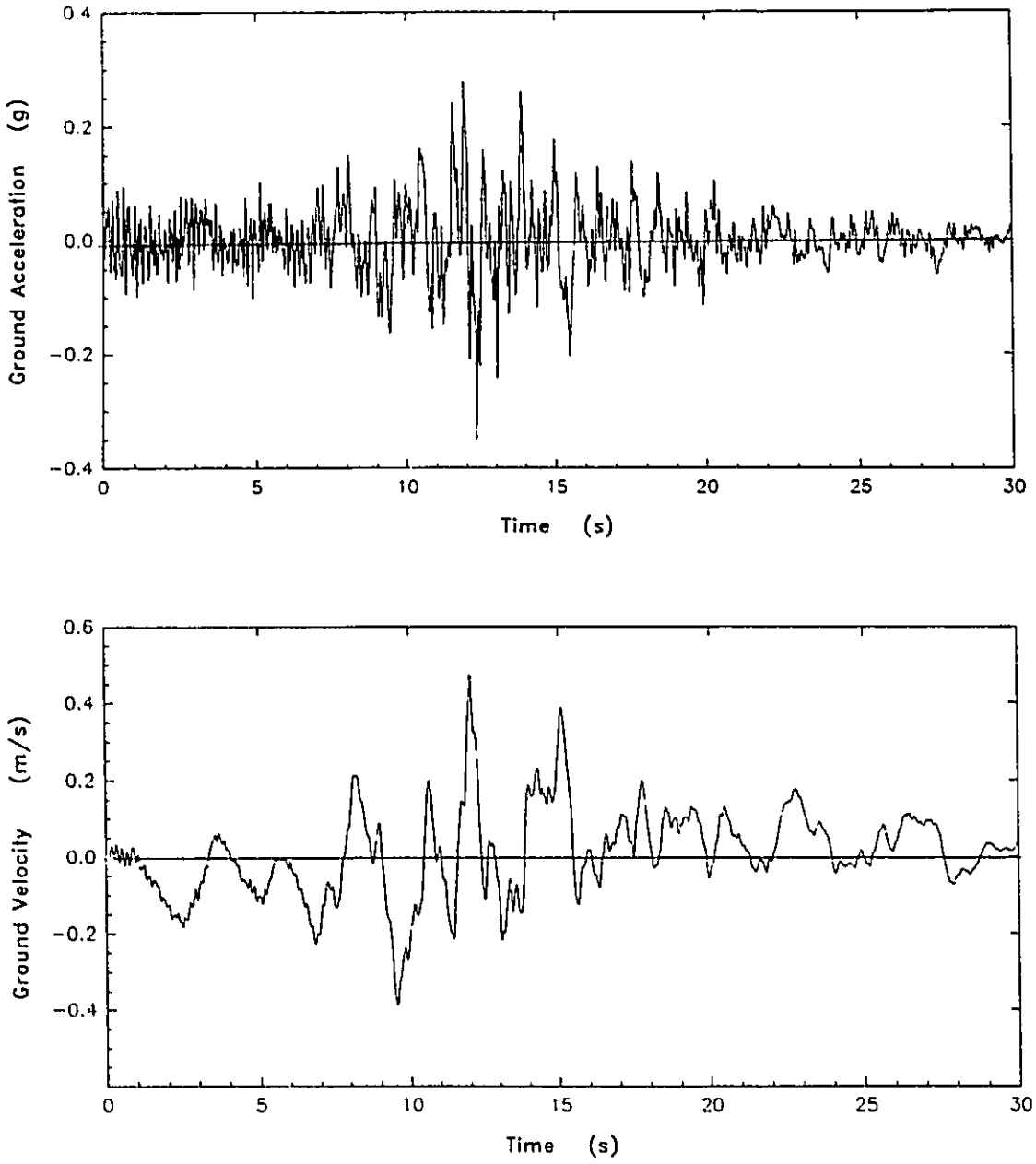


Fig 6.15 Ground acceleration and velocity time histories for low A/v ratio record

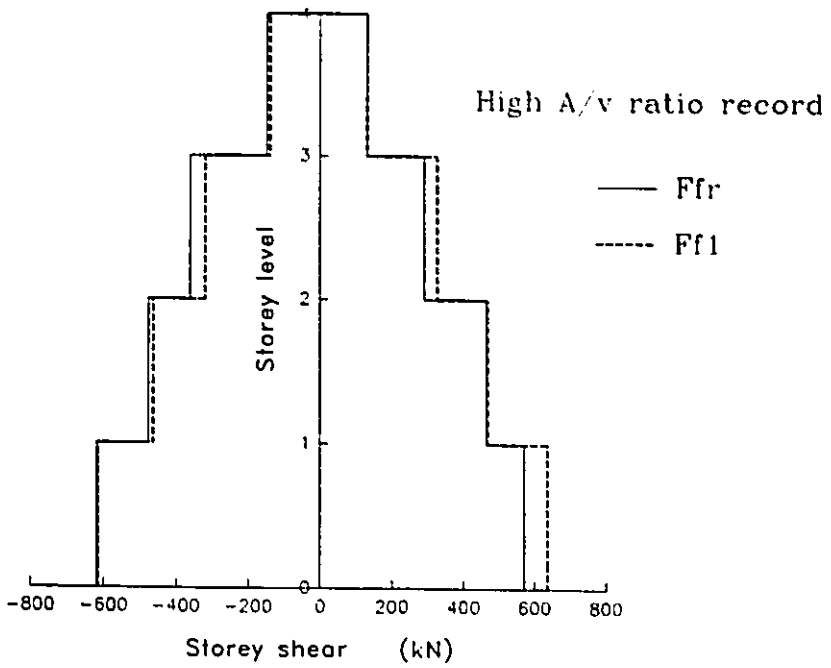


Fig 6.16 Effect of connection flexibility on storey shear envelopes

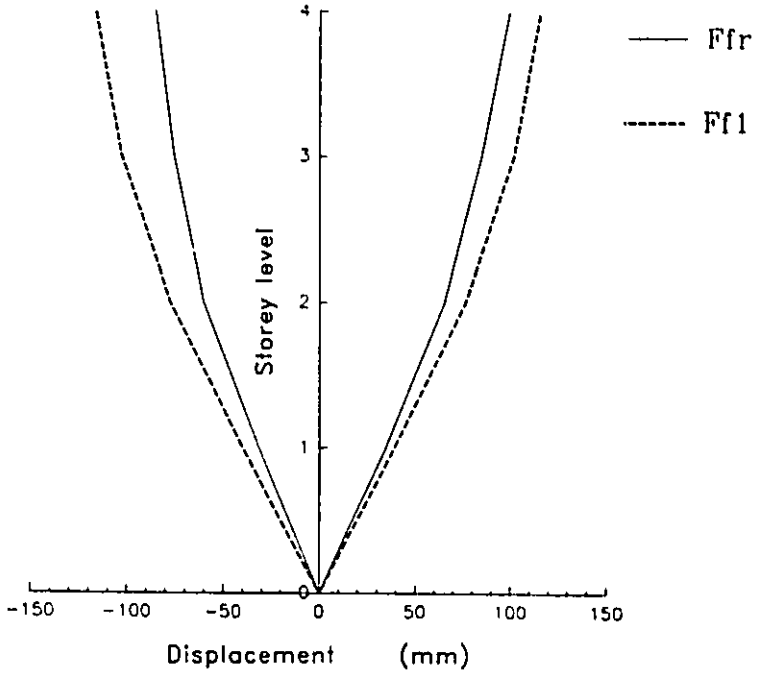


Fig 6.17 Effect of connection flexibility on floor displacement envelopes

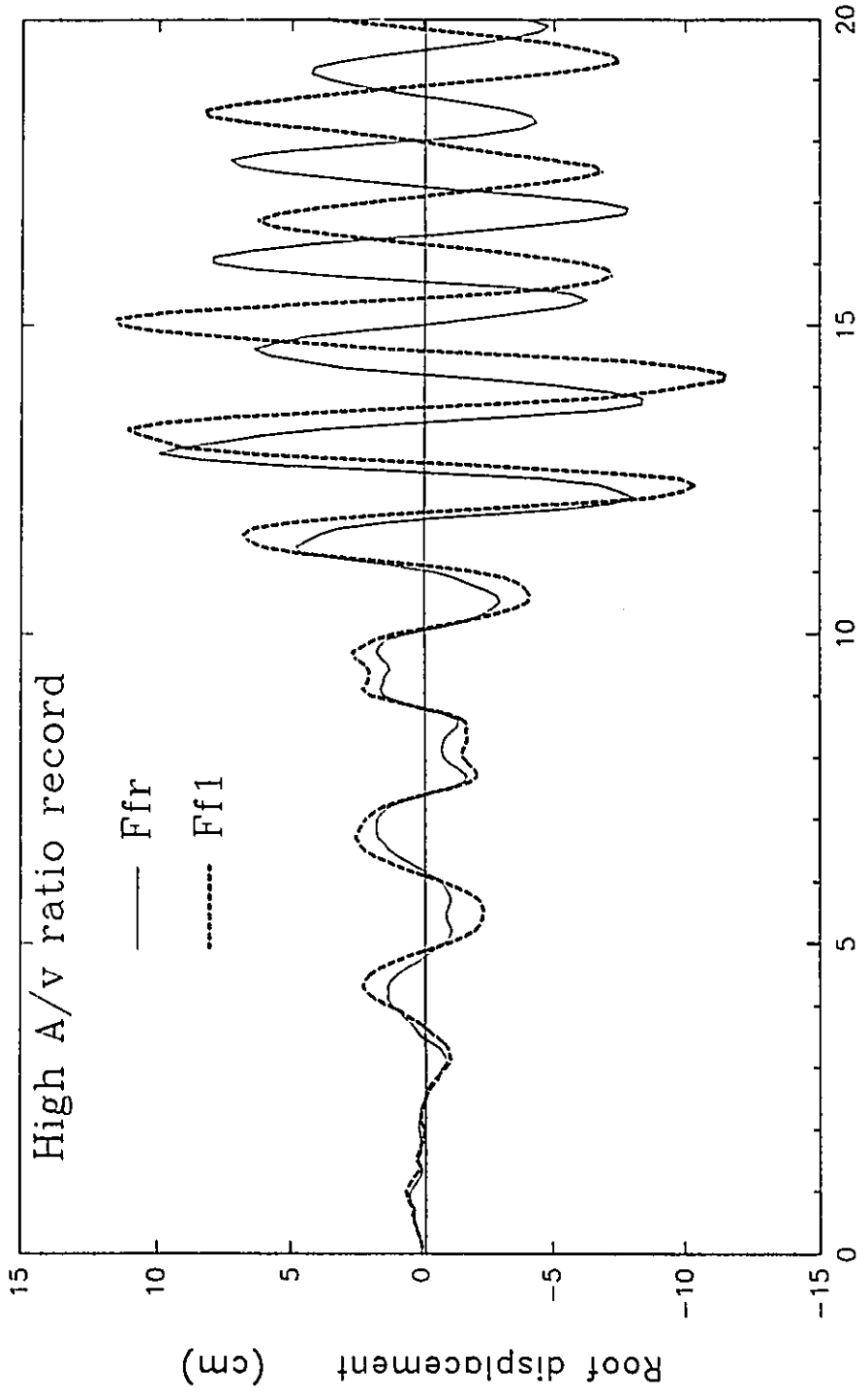


Fig 6.18 Effect of connection flexibility on roof displacement history

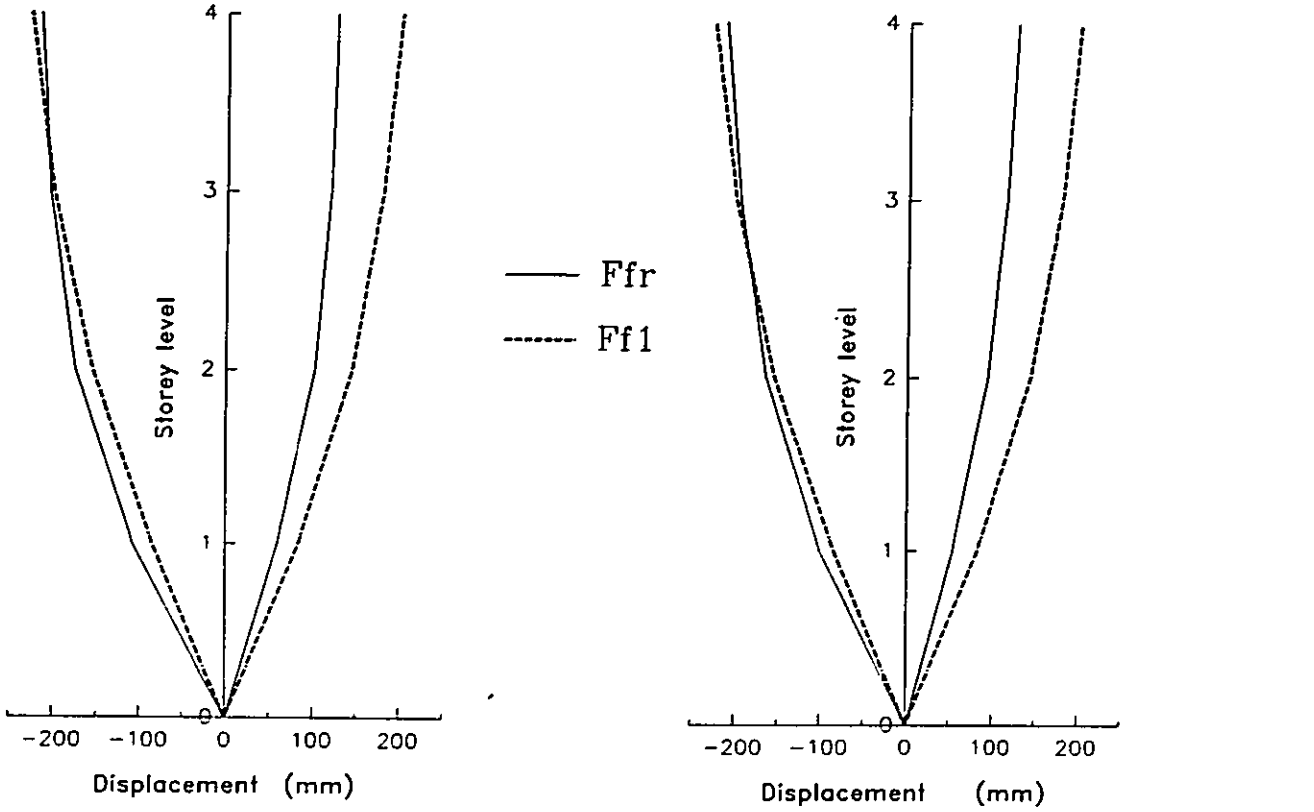


a) Floor displacement envelopes

b) Floor displacements at peak roof displacement

Fig 6.19 Effect of connection flexibility on the floor displacements

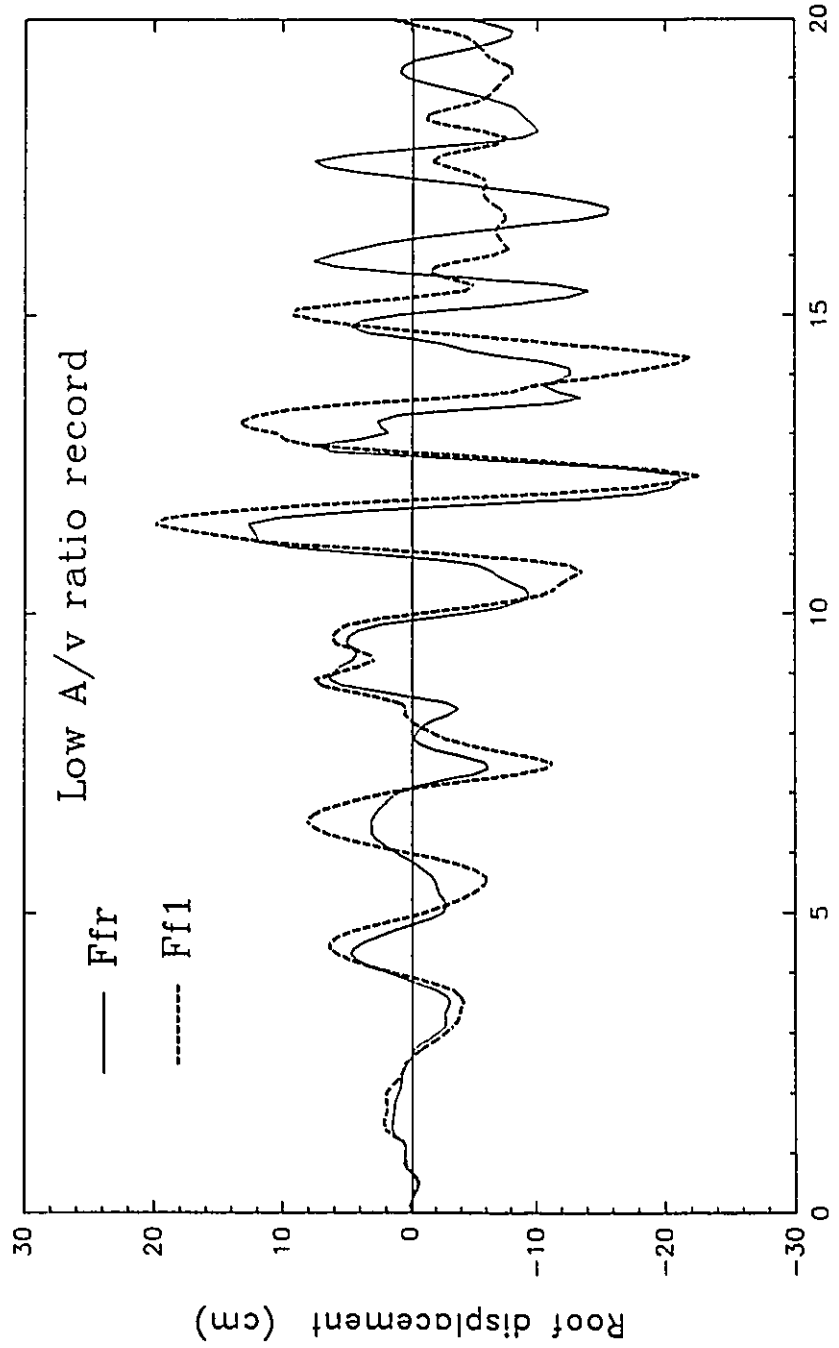


Fig 6.20 Effect of connection flexibility on roof displacement history

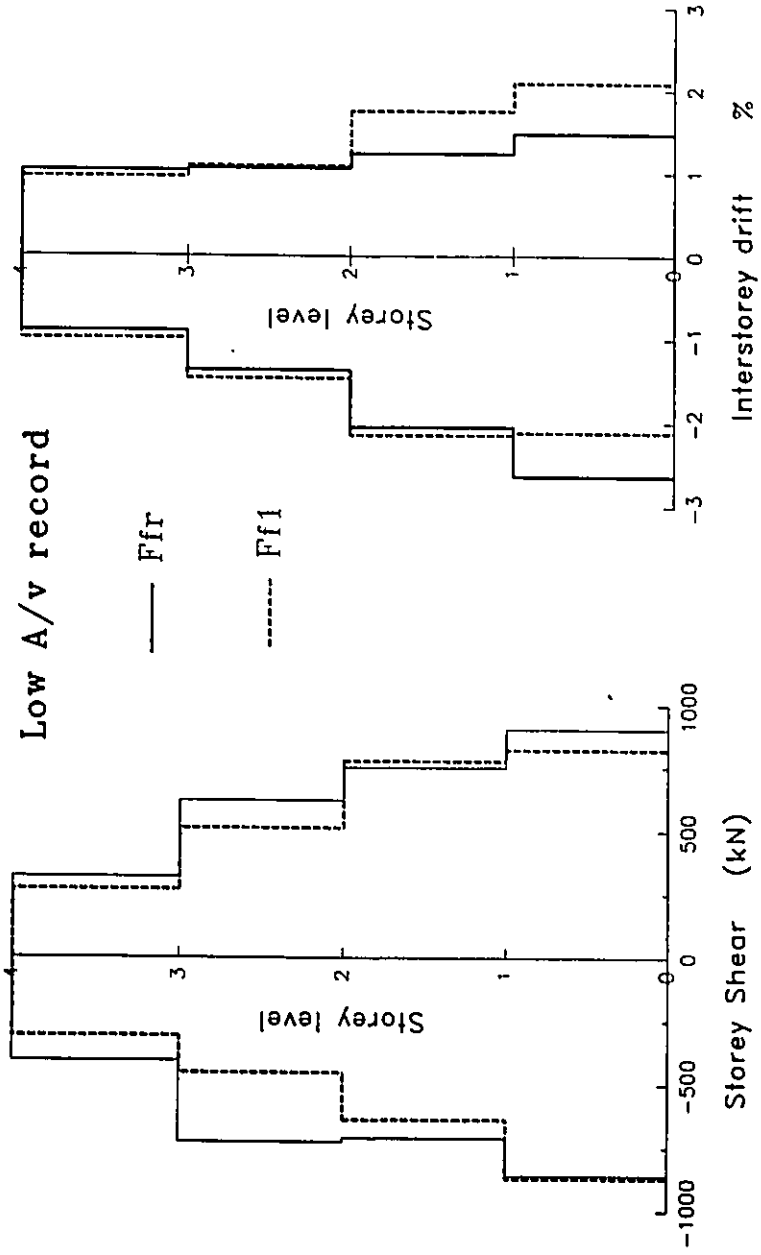


Fig 6.21 Storey shear and interstorey drift envelopes (Low A/v record)

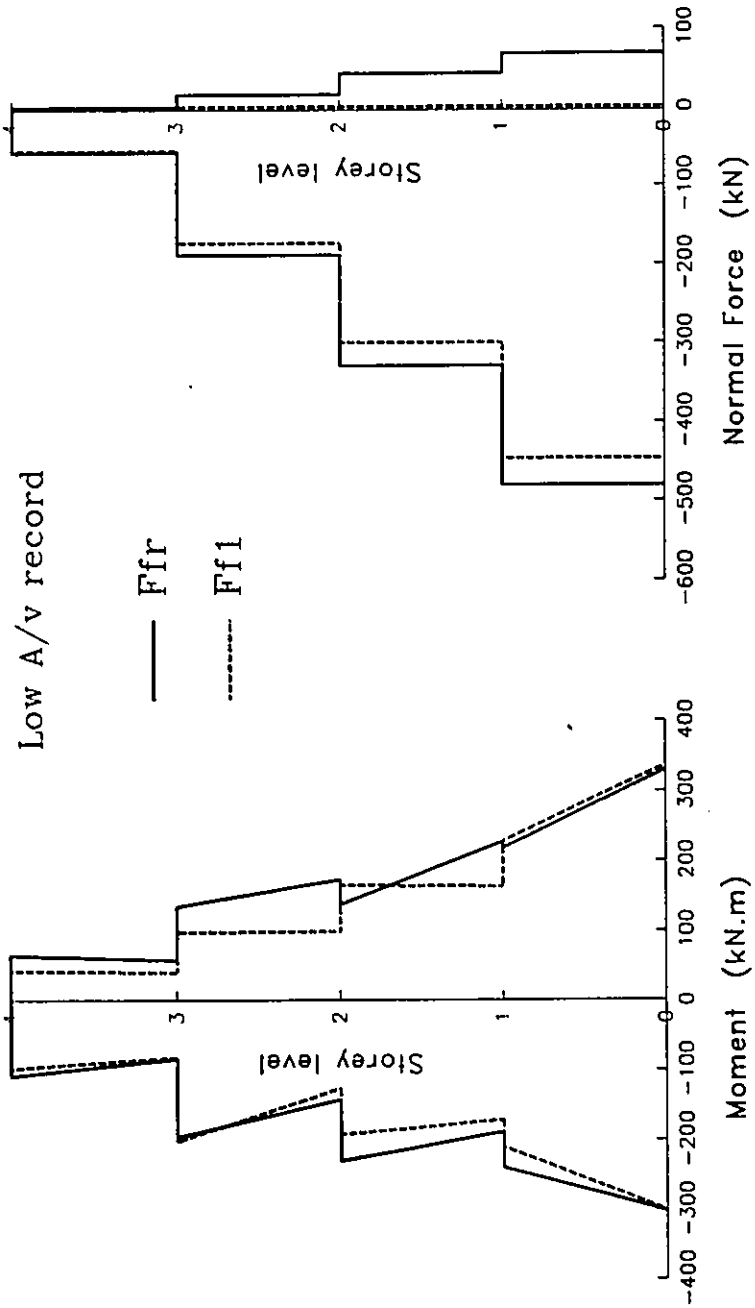


Fig 6.22 Effect of connection flexibility on bending moments and normal forces envelopes of exterior columns

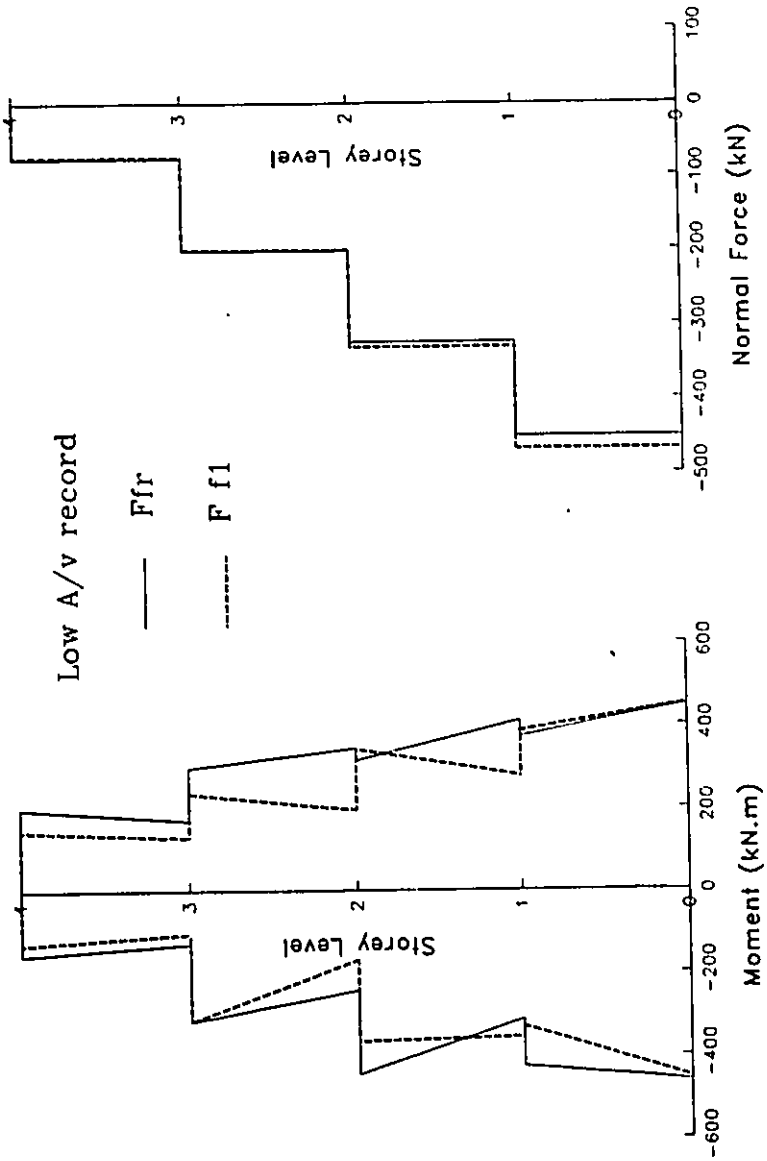


Fig 6.23 Effect of connection flexibility on bending moments and normal forces envelopes of interior columns

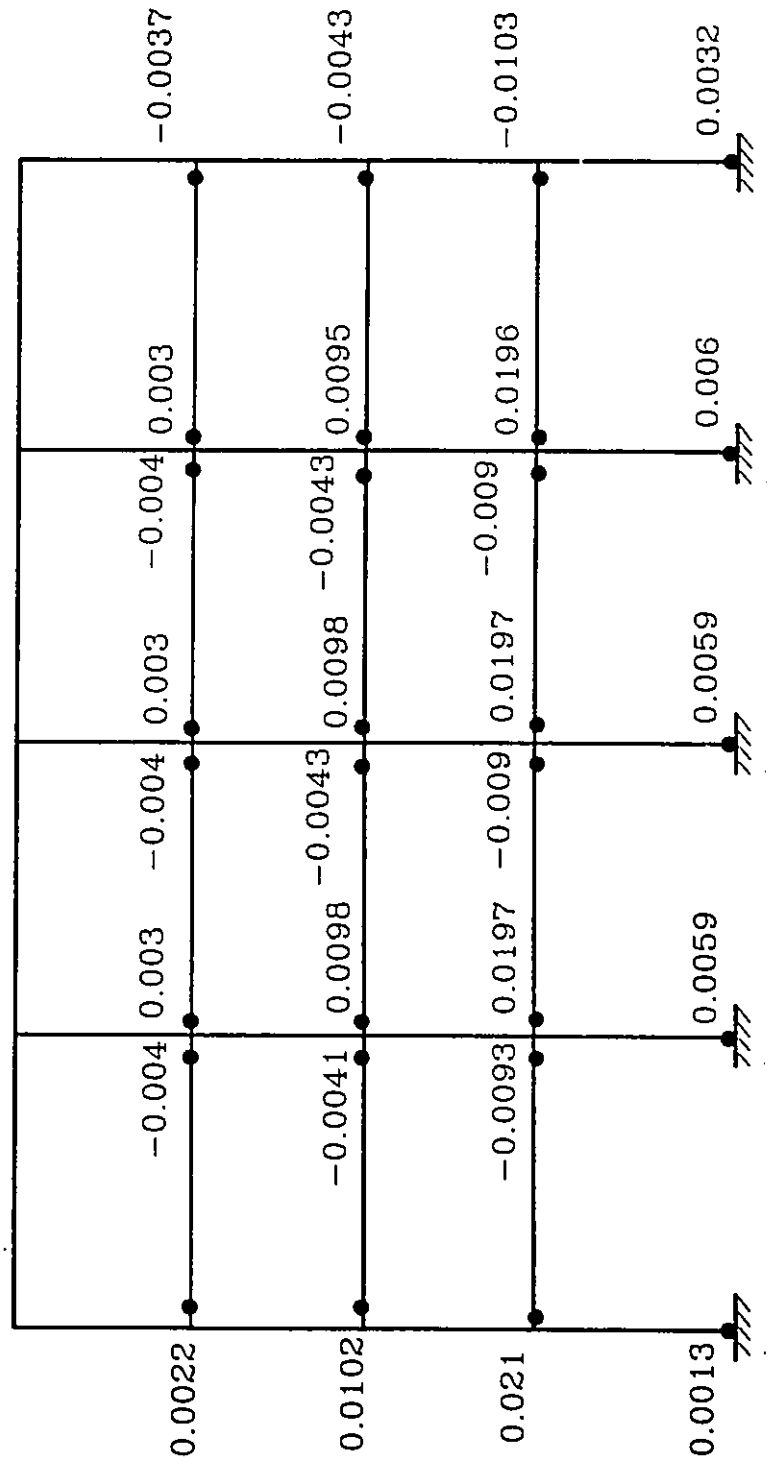


Fig 6.24 Maximum plastic hinge rotation in beams and columns of frame Ffr
(Rigid frame)

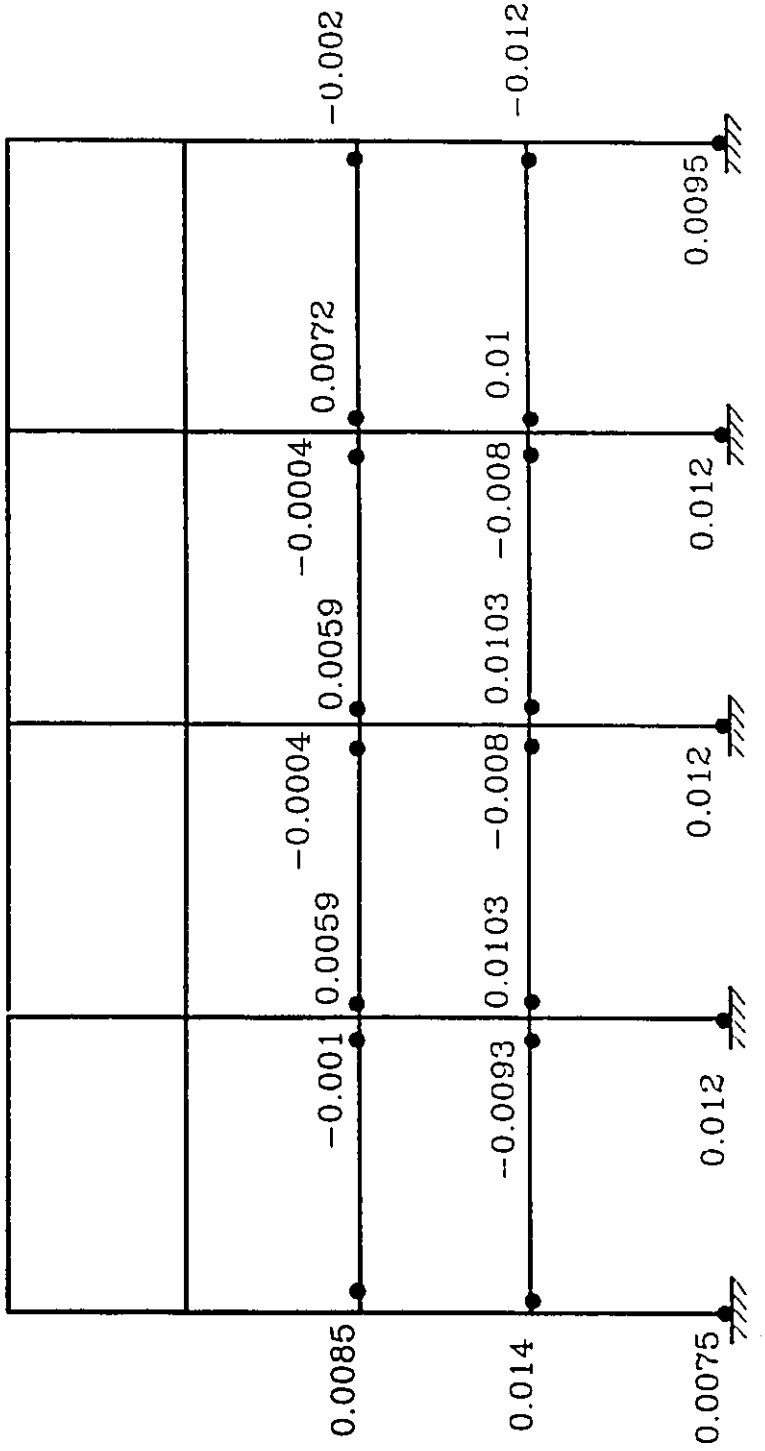


Fig 6.25 Maximum plastic hinge rotation in beams :.nd columns of frame Ff1
(Flexible frame)

# CHAPTER 7

# CONCLUSIONS

## 7.1 Summary

The main objectives of this research program were to develop a blind bolted moment connection between a W-shape beam and a square HSS column and to investigate experimentally its behaviour under monotonic and cyclic loading. In addition, it was deemed important to study analytically the effect of the proposed connection response on the behaviour of moment resisting frames.

A blind fastening system which included two types of fasteners, BOM and HSBB, has been the subject of study. Seven full-scale beam-to-column end-plate connections subassemblages were subjected to increasingly monotonic loading, while two connections underwent cyclic loading. Information about the connection behaviour and their individual components were compiled and have been discussed.

An analytical model was developed to predict the connection behaviour in terms of its moment-rotation relationship. The model predictions were compared with the experimental results obtained from the tests. A design procedure for the bolted end-plate connection has been proposed. The behaviour of the connection was incorporated into the Drain-2DX computer program in order to analyze the response of moment resisting steel frames taking into account the effect of connection flexibility.

A four-storey moment resisting steel frame was used to study the effects of connection flexibility on frame response. Non-linear static and dynamic analyses of the frame response were performed. The results of the analyses has provided several insights into the effect of the flexibility of the proposed connection on the frame response.

## 7.2 Conclusions

Based on experimental observation and a critical assessment of the experimental and theoretical analyses, the following conclusions can be drawn:

1- High strength blind bolts (HSBBs) have a comparable strength to the A325 high strength bolts, which indicates that they have a promising potential for use in structural moment connections.

2- The extended end-plate connection using HSBB is a viable and practical field connection for rectangular and square hollow section (HSS) columns. Its behaviour was judged to be favourable in comparison with the behaviour of a connection using A325 bolts.

3- A minimum HSS column flange thickness is recommended in order that the flange resists the maximum tensile strength of HSBB precluding shear failure underneath the HSBB primary sleeve. The minimum column flange thickness is therefore a function of the HSBB size. Should the required minimum thickness be less than the HSS column

flange thickness, a doubler plate welded onto the HSS column flange has been shown to be effective, since the use of washers on the blind side of the connection is not practical.

4- Welding a doubler plate onto the HSS column flange improves the performance of the extended end-plate connection utilizing HSBB fasteners. The doubler plate prevents the column flange shear failure and causes an increase in the column flange plastic capacity as well as a slight increase in the connection initial stiffness resulting in reduced column flange deformation.

5- The connection deformation on both the tension and compression sides were significantly reduced when filling the HSS column with concrete, and resulted in a major increase in the connection's initial stiffness. Infilling did not, however, affect the ultimate moment capacity of the connection, since the same column flange shear failure was achieved.

6- As would be expected from an extended end-plate connection, improved performance can be achieved by using thicker end-plates and installing the HSBB fasteners closer to the beam flange. Such arrangements reduce a bolt's bending and prying action.

7- In seismic design of moment frames, the connection should not be relied upon for energy dissipation. The connection has limited ductility and significant degradation in stiffness is experienced when subjected to cyclic loading.

8- To minimize connection stiffness degradation and to take advantage of the good ductility characteristics of the moment hinging in beams and their ability to dissipate energy, it is proposed that connections be designed so that their plastic moments equal to at least 1.3 times that of the attached beams.

9- The proposed analytical model is capable of accurately simulating the behaviour of the connection in terms of its moment-rotation relationship. Its principle virtue is that, it is based on determining four connection parameters. These parameters are the initial and post-elastic stiffnesses, and the plastic and ultimate moment capacities.

10- The inclusion of the connection flexibilities into the moment frame analyses affects its static and dynamic characteristics as well as the internal force distribution in the frame. This results in increasing the frame lateral deflections, lengthening the frame free vibration periods and increasing the frame member sizes if drift limitations provided by the National Building Code of Canada are to be satisfied.

11- Non-linear dynamic analysis of the frame response has shown that the flexibility of the proposed connections affects the dynamic response of the frame. These effects were found to involve increasing lateral deflection envelopes, a decrease in the number of beam plastic hinges and their plastic rotations, and therefore a decrease in the predicted damage; at the same time there was found to be an increase in the plastic rotations experienced by the columns at their bases.

12- The flexibility of semi-rigid connections should be included in both static and dynamic analyses to determine a frame's structural behaviour more realistically. The Canadian Standard CAN3-S16.1-M89 (1989) does not account for connection flexibility in assessing the frame structural behaviour.

## 7.3 Recommendations for future research

The following research programmes are suggested for future studies;

1- Special attention should be directed to measure the forces in HSBBs in an extended end-plate connection, in order to investigate possible degradation in their pre-tensioning forces as well as to estimate the prying action and to compare these with the available analytical models.

2- Further cyclic loading tests are proposed for beams and columns joined with extended end-plate connections designed according to the proposed procedure herein, in order to evaluate the behaviour of both the beam and the connection under cyclic loading.

3- Further research is needed to study the effect of the HSS column axial force and panel zone on connection behaviour.

4- Both experimental and sophisticated analytical studies are needed to evaluate the ultimate capacity of the HSS column flange and the end-plate in such a proposed moment connection.

5- Through both an experimental and analytical program, such proposed blind bolted extended end-plate connection, need to be studied when rectangular hollow section columns are employed.

# APPENDIX A

## DETERMINATION OF END-PLATE EFFECTIVE THICKNESS

An effective end-plate thickness $t_{ep}(eff)$ was obtained on the basis of allocating proportionate areas ($A_1$, $A_2$ and $A_3$) with the corresponding equivalent thicknesses ($t_1$, $t_2$ and $t_3$), as illustrated in Fig A.1. The area "$A_1$" is defined as the area on the end-plate around the bolts' washers and is considered in full contact with the column flange. Area "$A_2$" is defined as the area on the end-plate around the beam flange and is considered sliding on the column flange. Meanwhile area "$A_3$" is the rest area on the end-plate considered sliding on the column flange. Therefore, the effective thickness of the end-plate "$t_{ep}(eff)$" is given by:

$$t_{ep}(eff) = t^* - t_{cf} \tag{A.1}$$

where;

$$t^* = \frac{A_1 t_1 + A_2 t_2 + A_3 t_3}{A_1 + A_2 + A_3} \tag{A.2}$$

$A_1 = 4\pi (r_w + t_{ep} + t_{cf})^2$ , $t_1 = t_{cf} + t_{ep}$

$A_2 = (b_f + 2w_{bf} + 2t_{ep} + 2t_{cf})(t_{bf} + 2w_{bf} + 2t_{ep} + 2t_{cf})$ , $t_2 = \{(t_{cf})^3 + (t_{ep} + w_{bf})^3\}^{1/3}$

$A_3 = (H_o - 2t_o)L_{ep} - A_1 - A_2$ , $t_3 = \{(t_{cf})^3 + (t_{ep})^3\}^{1/3}$

where;

- $r_w$ : radius of bolt's washer
- $w_{bf}$ : size of beam flange fillet weld
- $b_f$ : beam flange width
- $t_{ep}$ : end-plate thickness
- $t_{cf}$ : equivalent column flange thickness as given by Eq. 4.2
- $t_{bf}$ : beam flange thickness
- $L_{ep}$ : length of the modeled end-plate, as shown in Fig A.1

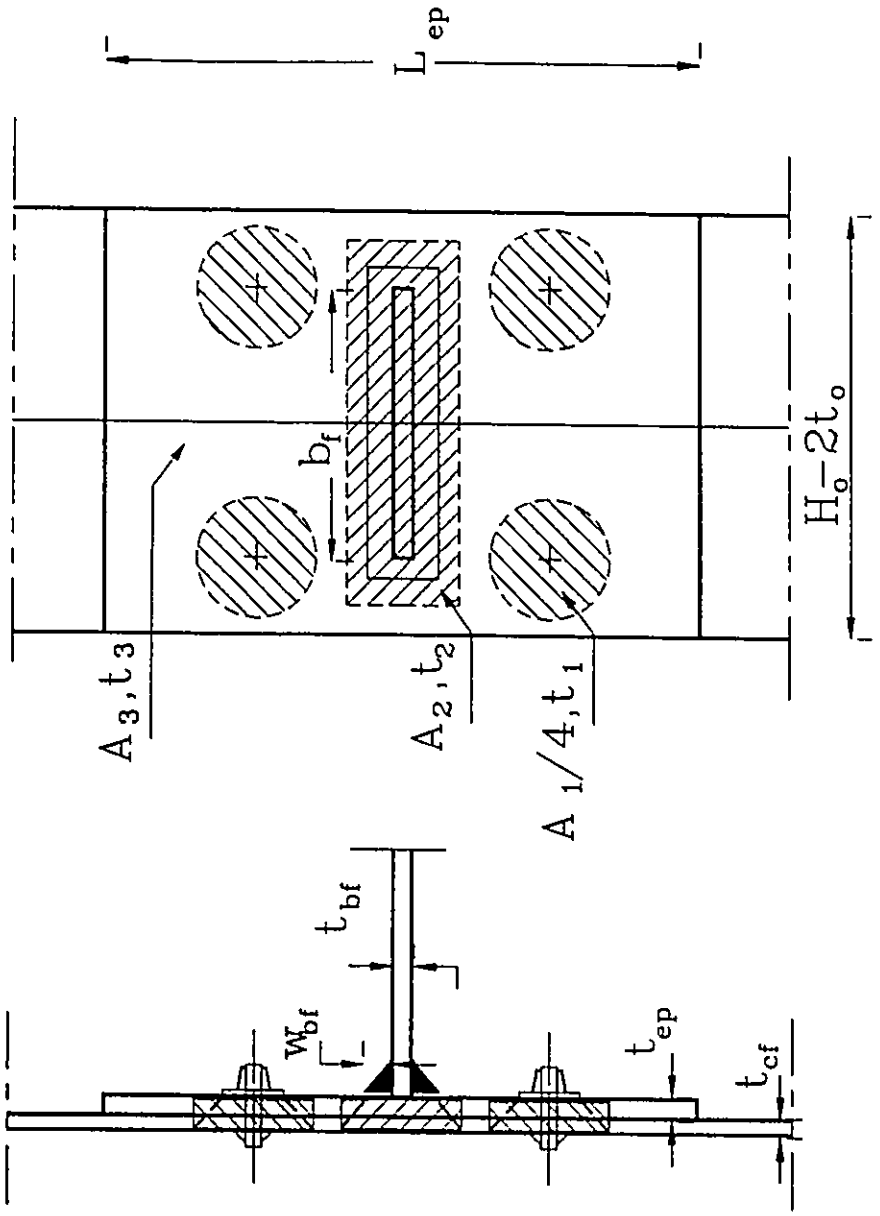


Fig A.1 Different portion areas of the end-plate on the compression side of the connection

# APPENDIX B

## MODIFIED SLOPE DEFLECTION SOLUTION FOR THE END-PLATE MODEL

The modified slope deflection equations (Azizinamini et al., 1987) to account for shear deformation effects for a beam segment MN, Fig B.1, are given as follows;

$$M_{MN} = \frac{EI}{L(1+r)} [(4+r)\theta_M + (2-r)\theta_N - \frac{6\Delta}{L}] \quad \text{(B.1)}$$

$$M_{NM} = \frac{EI}{L(1+r)} [(2-r)\theta_M + (4+r)\theta_N - \frac{6\Delta}{L}] \quad \text{(B.2)}$$

where,

r = $12EI/(L^2GA_s)$
E = Young's modulus of elasticity
G = shear modulus
L = length of the beam segment
I = moment of interia of the beam segment
$A_s$ = effective shear area of beam section

Applying the modified slope deflection equations on each segment of the end-plate model shown in Fig B.2, (linked to Fig 4.6 (b)), leads to the following equations;

$$M_{AB} = \frac{E\, I_{ep}}{a(1+r_a)} [\, (4+r_a)\theta_A + (2-r_a)\theta_B \,] \quad \text{(B.3)}$$

$$M_{BA} = \frac{E\, I_{ep}}{a(1+r_a)} [\, (2-r_a)\theta_A + (4+r_a)\theta_B \,] \quad \text{(B.4)}$$

$$M_{BC} = \frac{E\,I_{ep}}{b_1(1+r_{b_1})}\left[\,(4+r_{b_1})\theta_B + (2-r_{b_1})\theta_C + \frac{6\Delta}{b_1}\right] \qquad \text{(B.5)}$$

$$M_{CB} = \frac{E\,I_{ep}}{b_1(1+r_{b_1})}\left[\,(2-r_{b_1})\theta_B + (4+r_{b_1})\theta_C + \frac{6\Delta}{b_1}\right] \qquad \text{(B.6)}$$

$$M_{CD} = \frac{E\,I_{ep}}{b_2(1+r_{b_2})}\left[\,(4+r_{b_2})\theta_C + (2-r_{b_2})\theta_D - \frac{6\Delta}{b_2}\right] \qquad \text{(B.7)}$$

$$M_{DC} = \frac{E\,I_{ep}}{b_2(1+r_{b_2})}\left[\,(2-r_{b_2})\theta_C + (4+r_{b_2})\theta_D - \frac{6\Delta}{b_2}\right] \qquad \text{(B.8)}$$

$$M_{DE} = \frac{E\,I_{ep}}{a(1+r_a)}\left[\,(4+r_a)\theta_D + (2-r_a)\theta_E\,\right] \qquad \text{(B.9)}$$

$$M_{ED} = \frac{E\,I_{ep}}{a(1+r_a)}\left[\,(2-r_a)\theta_D + (4+r_a)\theta_E\,\right] \qquad \text{(B.10)}$$

In the above equations $\theta_C=0$, since the end-plate is not allowed to rotate at point C, because of the existence of the rigid beam flange. The other five unknowns ($\theta_A$, $\theta_B$, $\theta_D$, $\theta_E$ and $\Delta$) can be obtained in terms of the applied force "P" by using the following five relations:

$$M_{AB} = 0 \qquad \text{(B.11)}$$

$$M_{ED} = 0 \qquad \text{(B.12)}$$

$$M_{BA} + M_{BC} = 0 \qquad \text{(B.13)}$$

$$M_{DC} + M_{DE} = 0 \qquad \text{(B.14)}$$

and $Q_1 + Q_2 + F_1 + F_2 + P = 0$ (B.15)

Solving the above equations, leads to the end-plate deflection "$\Delta_{ep}$", which can be written in the following form:

$$\Delta_{ep} = \frac{P}{R_{ep}} \tag{B.16}$$

where,

$$R_{ep} = \frac{12E\,I_{ep}}{b_2^3(1+r_{b_2})}\left[1 - \frac{3}{b_2(1+r_{b_2})}\frac{1}{\frac{4+r_{b_2}}{b_2(1+r_{b_2})}+\frac{12}{a(4+r_a)}}\right]$$

$$+ \frac{12E\,I_{ep}}{b_1^3(1+r_{b_1})}\left[1 - \frac{3}{b_1(1+r_{b_1})}\frac{1}{\frac{4+r_{b_1}}{b_1(1+r_{b_1})}+\frac{12}{a(4+r_a)}}\right] \tag{B.17}$$

In the case of $b_1=b_2=$'', Eq B.17 can be reduced to

$$R_{ep} = \frac{12\,E\,I_{ep}}{b^3(1+r_b)}\left[2 - \frac{6}{b(1+r_b)}\frac{1}{\frac{4+r_b}{b(1+r_b)}+\frac{12}{a(4+r_a)}}\right] \tag{B.18}$$

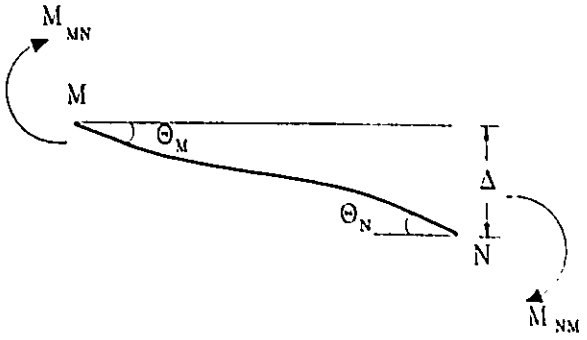


Fig B.1 Positive sign convention for beam segment MN

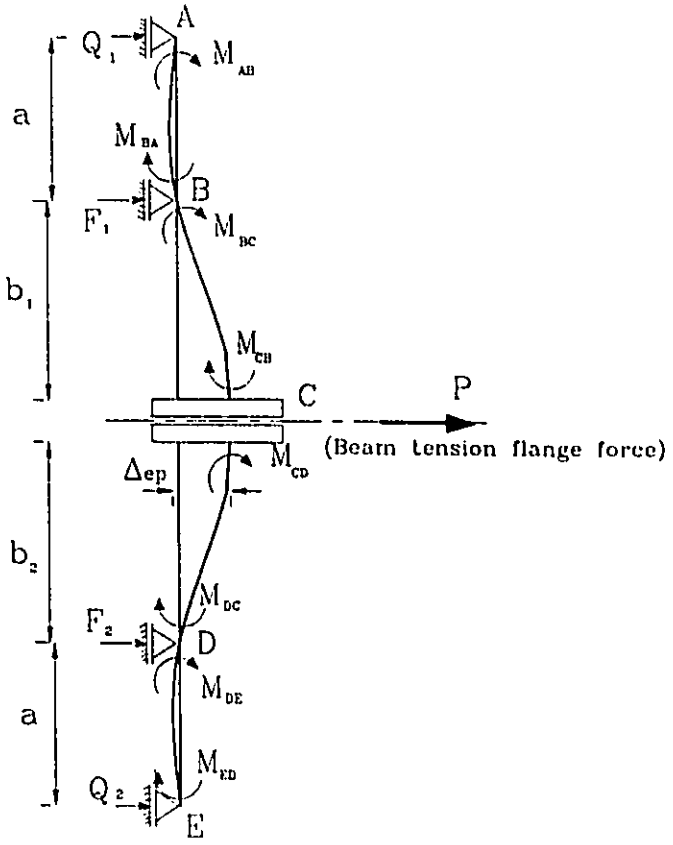


Fig B.2 End-plate model

# APPENDIX C

# DETERMINATION OF COLUMN FLANGE DEFLECTION AT BOLT LOCATIONS

## C.1 Hollow steel box column

A long simply supported column flange with span equal to ($B_f$) has been solved by the finite element program for different values of "$\beta_o$" and "$\eta_o$" to determine the deflection $\Delta_{cfts}$ at a bolt location, using the elastic plate bending theory. where;

$$\beta_o = \frac{X_B}{B_f} \qquad \eta_o = \frac{Y_B}{B_f} \tag{C.1}$$

$B_f$ : width of the simply supported plate, in this case = $H_o$-2$t_o$
$X_B$ : horizontal spacing between the bolts
$Y_B$ : vertical spacing between the bolts

Results are plotted in Fig C.1 in terms of coefficient $\gamma_s$. The deflection $\Delta_{cfts}$ is given by;

$$\Delta_{cfts} = \frac{\gamma_s P (H_o - 2t_o)^2}{D_{cf}} \tag{C.2}$$

where,

P : beam flange force
$D_{cf}$: plate bending rigidity of column flange = $E t_{cf}^3 / (12(1-\nu^2))$
$t_{cf}$: equivalent thickness of HSS column flange as given by Eq. 4.2

For a given bolt spacing, the reduction factor "R*" in deflection due to rotational restraints along the corner edges mainly depends on the ratio between the rotational spring stiffness of the HSS side walls "$K_{sw}$" and the column flange bending stiffness $D_{cf}/B_f$.

$$K_{sw} = \frac{4\ D_{sw}}{L_s} \qquad (C.3)$$

$L_s$ : side wall length, $H_o$-$t_o$, Fig 4.1
$D_{sw}$ : plate bending rigidity of HSS side walls = $E\ t^3_{sw}/(12(1-\nu^2))$
$t_{sw}$ : thickness of HSS side walls

Therefore,

$$\frac{K_{sw}}{D_{cf}/B_f} = \frac{4\ t^3_{sw}\ (H_o-2t_o)}{t^3_{cf}\ (H_o-t_o)} \qquad (C.4)$$

It was found that the reduction factor "R*" also depends on the horizontal spacing of the bolts $\beta_o$ and slightly on the vertical spacing of the bolts $\eta_o$. For a fixed value of $\beta_o$, and varying $\eta_o$ from 0.3 to 0.7, and for values of $K_{sw}\ B_f/D_{cf}$ ranging from 0 to 20, the maximum difference in the reduction factor is only 6%. Therefore, $\eta_o$ was chosen to have a fixed value equal to 0.5, in determining the reduction factors "R*" for different values of $\beta_o$ and $K_{sw}\ B_f/D_{cf}$. Results are plotted in Fig C.2. The deflection of the column flange at bolt location " $\Delta_{cfi}$" taking into account the rotational restraints at the corners of the HSS column can be obtained as follows;

$$\Delta_{cfi} = R^*\ \Delta_{cfts} \qquad (C.5)$$

## C.2 Concrete filled HSS column

For the case when the HSS column is filled with concrete, the assumption is made that only the longitudinal edges of the HSS flange plate are fixed. Therefore, a similar graph was obtained for the case of a long plate with fixed longitudinal edges to evaluate

the deflection of column flange at bolt location $\Delta_{cft(concrete)}$ in terms of coefficient $\gamma_f$ as shown in Fig C.3. The deflection $\Delta_{cft(concrete)}$ is given by;

$$\Delta_{cft(concrete)} = \frac{\gamma_f \; P \; (H_o - 2t_o)^2}{D_{cf}} \qquad (C.6)$$

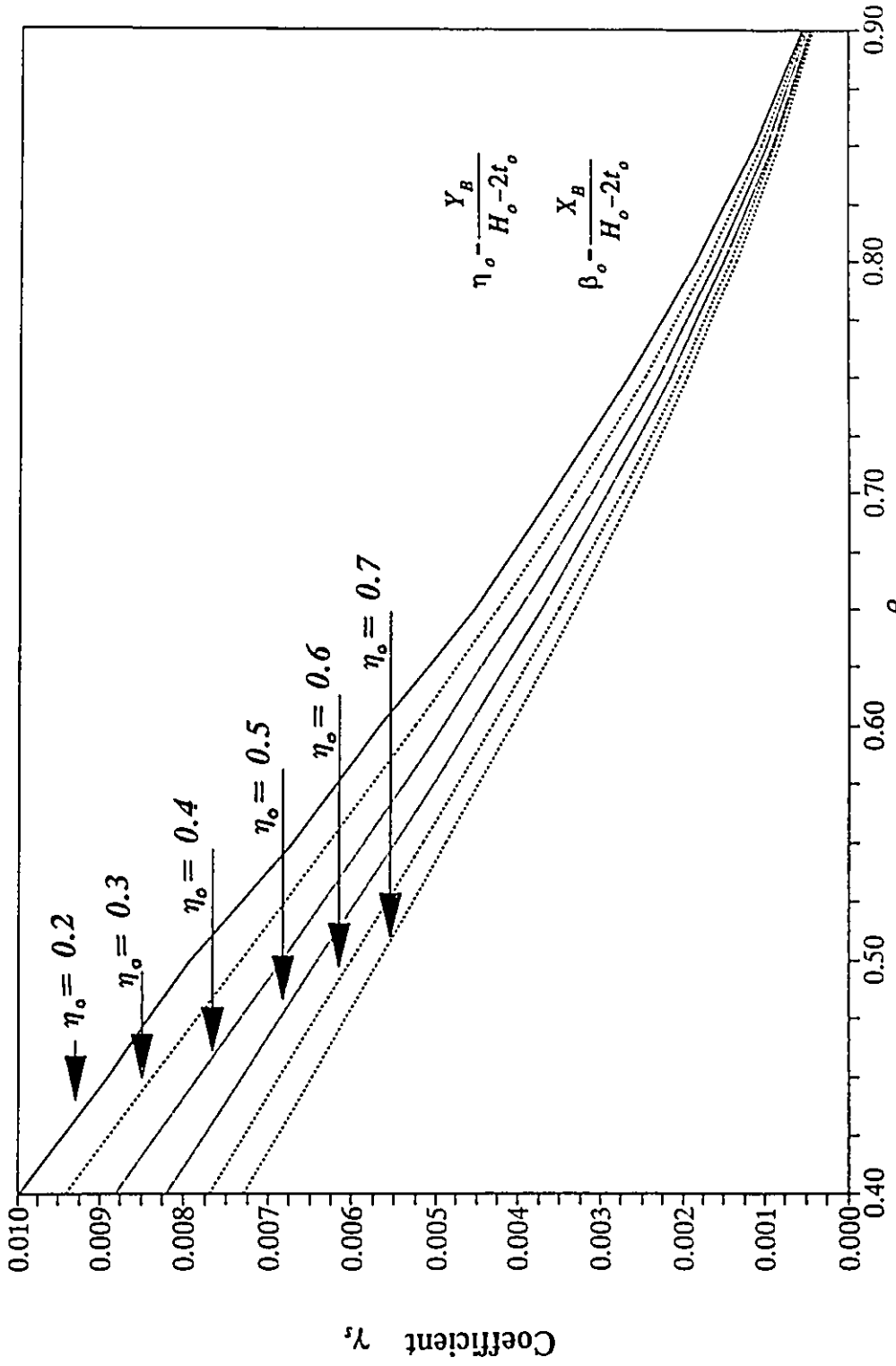


Fig C.1 Deflection coefficients for simply supported column flange loaded at bolt locations

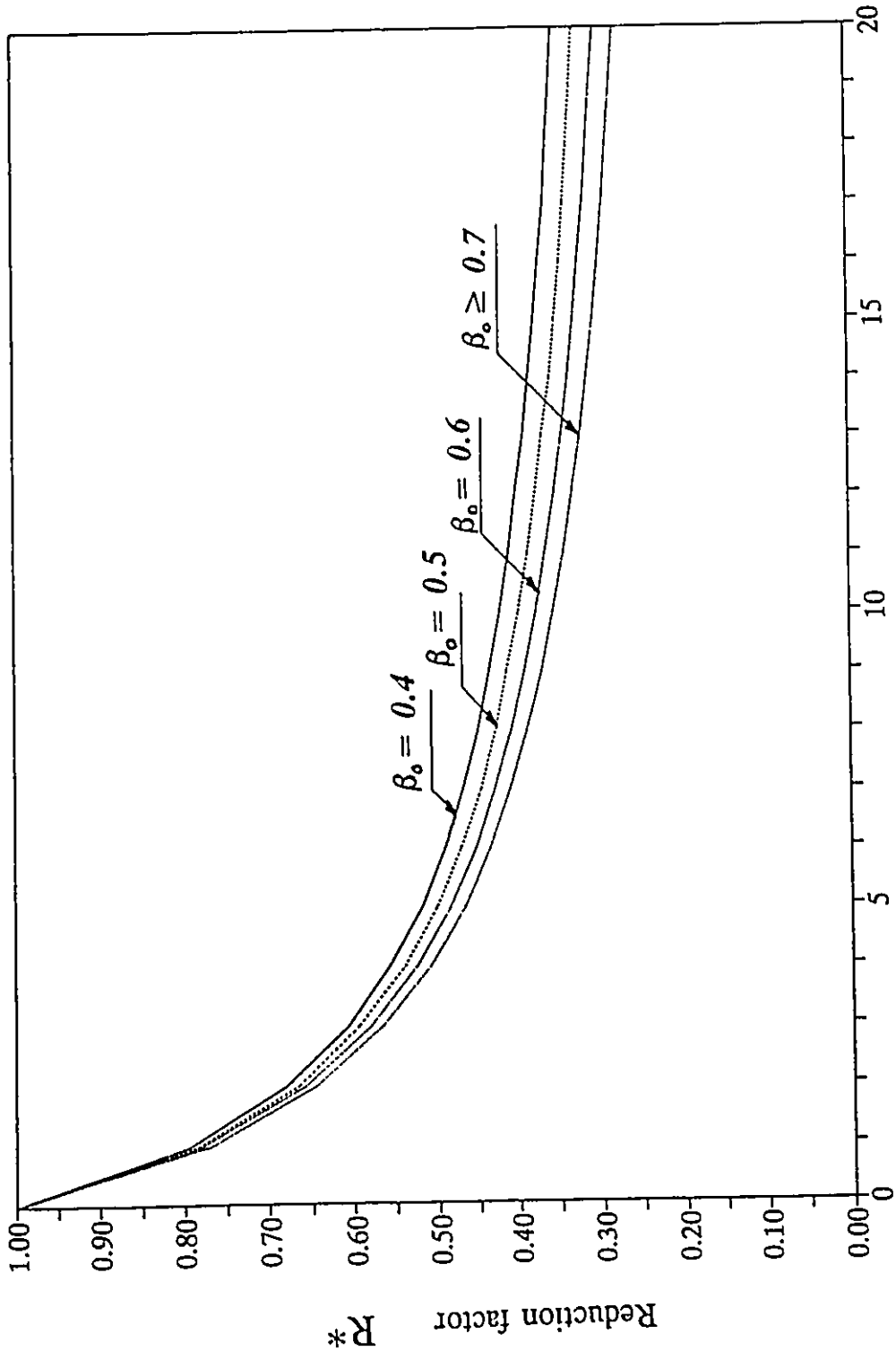


Fig C.2 Reduction factors for column flange deflections at the tension side of the connection

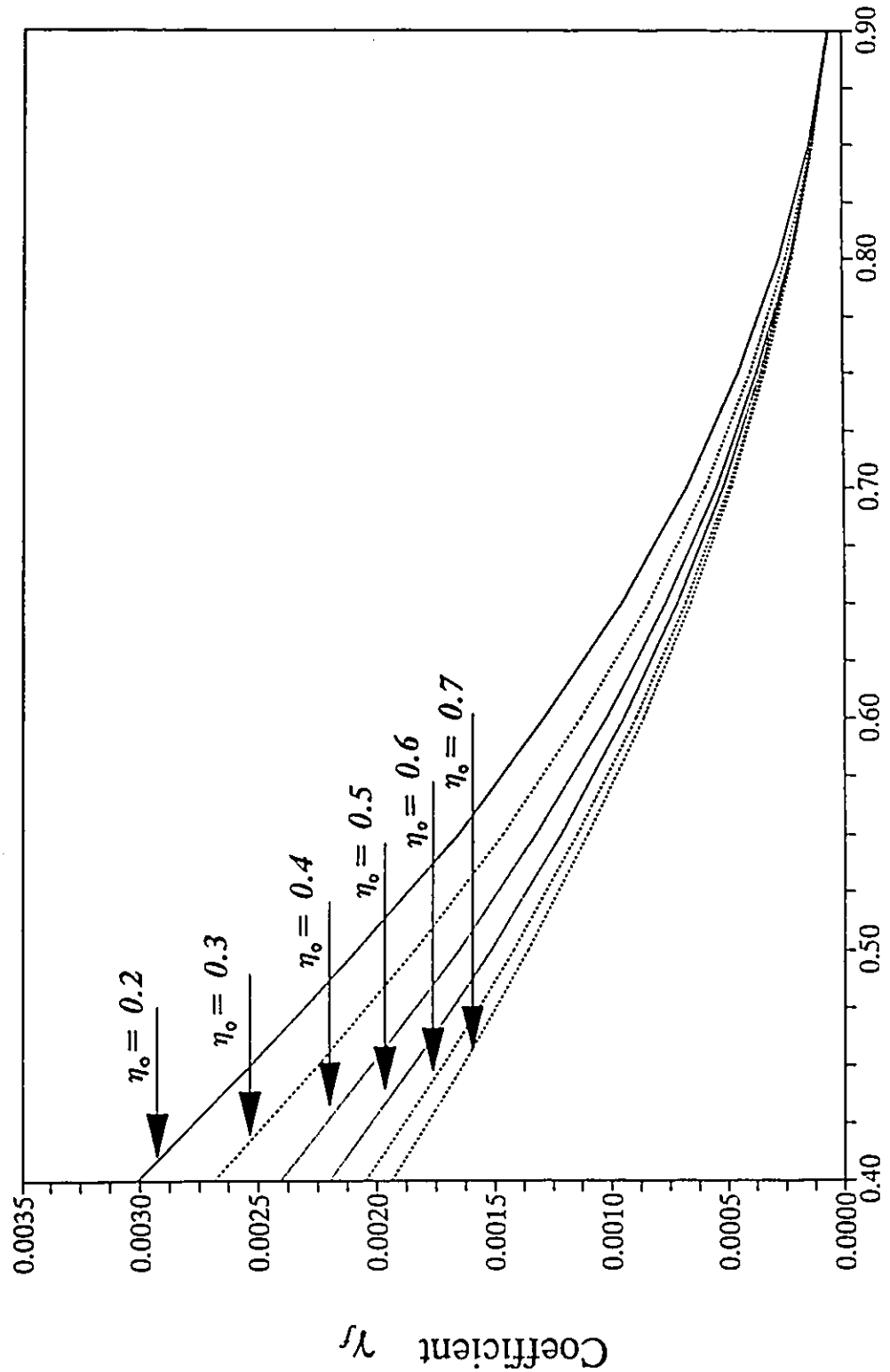


Fig C.3 Deflection coefficients for column flange with fixed longitudinal edges loaded at bolt locations

# APPENDIX D

## DETERMINATION OF THE AVERAGE COLUMN FLANGE DEFLECTION ON THE COMPRESSION SIDE

The average elastic deflection of the column flange across the compression beam flange $\Delta_{cfc}$ can be calculated from the formula ;

$$\Delta_{cfc} = \alpha_c \, 10^{-3} \, P \qquad (D.1)$$

where, "$\Delta_{cfc}$" is in (mm), "P" is the beam flange force in "kN", and "$\alpha_c$" is a coefficient determined analytically from the finite element program. For a direct determination of coefficient "$\alpha_c$" tables were prepared from the finite element analysis for different sizes of square HSS columns and end-plates (Table D.1 to Table D.4). From these tables, coefficient "$\alpha_c$" can be evaluated directly for different parameter values $L_x$, $L_y$ and $t_{cp}(eff)/t_{cf}$, where;

$L_x$ : $(b_f+2w_{bf}) / (H_o-2t_o)$
$L_y$ : $L_{cp}/(H_o-2t_o)$
$L_{cp}$ : length of the modeled end-plate = $2(a+b)+t_{bf}$, Fig 4.3
$t_{cp}(eff)/t_{cf}$ : ratio of effective end-plate thickness to column flange thickness

For parameter values which lie between the ones listed in the tables, linear interpolation is applicable without significant errors. In these tables, $t_{bf}+2w_{bf}$ was taken to have a fixed value equal to 35 mm which represents an average practical value, and the average column flange deflection was taken across $0.75(b_f+2w_{bf})$ which is assumed to be approximately equal to the beam flange width "$b_f$".

# Table D.1 $\alpha_c$ values for HSS 177.8 x 177.8 mm

| | | HSS 177.8 X 177.8 X7.95 | | | | | | HSS 177.8 X 177.8 X 9.53 | | | | | | HSS 177.8 X 177.8 X 11.13 | | | | | | HSS 177.8 X 177.8 X 12.70 | | | | | |
|---|---|---|---|---|---|---|---|---|---|---|---|---|---|---|---|---|---|---|---|---|---|---|---|---|---|
| tep(eff)/ tcf | | 0.5 | 1 | 1.5 | 2 | 2.5 | 3 | 0.5 | 1 | 1.5 | 2 | 2.5 | 3 | 0.5 | 1 | 1.5 | 2 | 2.5 | 3 | 0.5 | 1 | 1.5 | 2 | 2.5 | 3 |
| | Lx | | | | | | | | | | | | | | | | | | | | | | | | |
| | 0.5 | 10.5 | 6.06 | 3.72 | 2.39 | 1.61 | 1.12 | 5.90 | 3.40 | 2.08 | 1.34 | 0.90 | 0.63 | 3.56 | 2.04 | 1.25 | 0.81 | 0.54 | 0.38 | 2.30 | 1.32 | 0.81 | 0.52 | 0.35 | 0.24 |
| | 0.6 | 9.30 | 5.36 | 3.30 | 2.12 | 1.43 | 0.99 | 5.20 | 2.99 | 1.84 | 1.19 | 0.80 | 0.55 | 3.14 | 1.81 | 1.12 | 0.71 | 0.48 | 0.33 | 2.03 | 1.17 | 0.72 | 0.46 | 0.31 | 0.22 |
| Ly=0.6 | 0.7 | 8.02 | 4.63 | 2.85 | 1.84 | 1.23 | 0.86 | 4.48 | 2.59 | 1.59 | 1.03 | 0.69 | 0.48 | 2.71 | 1.56 | 0.96 | 0.62 | 0.42 | 0.29 | 1.75 | 1.01 | 0.62 | 0.40 | 0.27 | 0.19 |
| | 0.8 | 6.73 | 3.90 | 2.40 | 1.55 | 1.04 | 0.73 | 3.76 | 2.18 | 1.34 | 0.87 | 0.58 | 0.40 | 2.27 | 1.31 | 0.81 | 0.52 | 0.35 | 0.24 | 1.47 | 0.85 | 0.52 | 0.34 | 0.23 | 0.16 |
| | 0.9 | 5.47 | 3.18 | 1.96 | 1.26 | 0.85 | 0.59 | 3.06 | 1.77 | 1.09 | 0.71 | 0.47 | 0.33 | 1.85 | 1.07 | 0.66 | 0.43 | 0.29 | 0.20 | 1.19 | 0.69 | 0.43 | 0.27 | 0.18 | 0.13 |
| | 0.5 | 9.62 | 5.14 | 3.01 | 1.89 | 1.25 | 0.86 | 5.37 | 2.87 | 1.69 | 1.06 | 0.70 | 0.48 | 3.24 | 1.73 | 1.01 | 0.64 | 0.42 | 0.29 | 2.10 | 1.12 | 0.66 | 0.41 | 0.27 | 0.19 |
| | 0.6 | 8.48 | 4.55 | 2.68 | 1.68 | 1.11 | 0.76 | 4.74 | 2.54 | 1.50 | 0.93 | 0.62 | 0.43 | 2.86 | 1.54 | 0.90 | 0.56 | 0.37 | 0.26 | 1.85 | 0.99 | 0.58 | 0.36 | 0.24 | 0.17 |
| Ly=0.8 | 0.7 | 7.32 | 3.94 | 2.32 | 1.45 | 0.96 | 0.66 | 4.09 | 2.20 | 1.29 | 0.81 | 0.54 | 0.37 | 2.47 | 1.33 | 0.78 | 0.49 | 0.32 | 0.22 | 1.59 | 0.86 | 0.50 | 0.32 | 0.21 | 0.14 |
| | 0.8 | 6.14 | 3.32 | 1.95 | 1.23 | 0.81 | 0.56 | 3.43 | 1.85 | 1.09 | 0.68 | 0.45 | 0.31 | 2.07 | 1.12 | 0.66 | 0.41 | 0.27 | 0.19 | 1.34 | 0.72 | 0.42 | 0.27 | 0.18 | 0.12 |
| | 0.9 | 4.99 | 2.70 | 1.59 | 1.00 | 0.66 | 0.45 | 2.79 | 1.51 | 0.89 | 0.56 | 0.37 | 0.25 | 1.68 | 0.91 | 0.54 | 0.34 | 0.22 | 0.15 | 1.09 | 0.59 | 0.35 | 0.22 | 0.14 | 0.10 |
| | 0.5 | 9.05 | 4.62 | 2.63 | 1.61 | 1.05 | 0.72 | 5.06 | 2.58 | 1.47 | 0.90 | 0.59 | 0.40 | 3.05 | 1.56 | 0.88 | 0.54 | 0.35 | 0.24 | 1.97 | 1.01 | 0.57 | 0.35 | 0.23 | 0.16 |
| | 0.6 | 7.99 | 4.10 | 2.33 | 1.43 | 0.93 | 0.64 | 4.46 | 2.29 | 1.30 | 0.80 | 0.52 | 0.36 | 2.69 | 1.38 | 0.78 | 0.48 | 0.31 | 0.22 | 1.74 | 0.89 | 0.51 | 0.31 | 0.20 | 0.14 |
| Ly=1.0 | 0.7 | 6.89 | 3.54 | 2.02 | 1.24 | 0.81 | 0.55 | 3.85 | 1.98 | 1.13 | 0.69 | 0.45 | 0.31 | 2.32 | 1.19 | 0.68 | 0.42 | 0.27 | 0.19 | 1.50 | 0.77 | 0.44 | 0.27 | 0.18 | 0.12 |
| | 0.8 | 5.78 | 2.98 | 1.70 | 1.05 | 0.68 | 0.47 | 3.23 | 1.67 | 0.95 | 0.58 | 0.38 | 0.26 | 1.95 | 1.00 | 0.57 | 0.35 | 0.23 | 0.16 | 1.26 | 0.65 | 0.37 | 0.23 | 0.15 | 0.10 |
| | 0.9 | 4.71 | 2.43 | 1.39 | 0.85 | 0.56 | 0.38 | 2.63 | 1.36 | 0.77 | 0.48 | 0.31 | 0.21 | 1.59 | 0.82 | 0.47 | 0.29 | 0.19 | 0.13 | 1.03 | 0.53 | 0.30 | 0.19 | 0.12 | 0.08 |
| | 0.5 | 8.70 | 4.32 | 2.40 | 1.46 | 0.94 | 0.64 | 4.86 | 2.41 | 1.34 | 0.81 | 0.52 | 0.36 | 2.93 | 1.45 | 0.81 | 0.49 | 0.32 | 0.22 | 1.90 | 0.94 | 0.52 | 0.32 | 0.20 | 0.14 |
| | 0.6 | 7.68 | 3.82 | 2.13 | 1.29 | 0.84 | 0.57 | 4.29 | 2.14 | 1.19 | 0.72 | 0.47 | 0.32 | 2.59 | 1.29 | 0.72 | 0.43 | 0.28 | 0.19 | 1.67 | 0.83 | 0.46 | 0.28 | 0.18 | 0.12 |
| Ly=1.2 | 0.7 | 6.63 | 3.31 | 1.85 | 1.12 | 0.73 | 0.49 | 3.70 | 1.85 | 1.03 | 0.63 | 0.40 | 0.28 | 2.23 | 1.11 | 0.62 | 0.38 | 0.24 | 0.17 | 1.44 | 0.72 | 0.40 | 0.24 | 0.16 | 0.11 |
| | 0.8 | 5.57 | 2.79 | 1.56 | 0.95 | 0.61 | 0.42 | 3.11 | 1.56 | 0.87 | 0.53 | 0.34 | 0.23 | 1.87 | 0.94 | 0.52 | 0.32 | 0.21 | 0.14 | 1.21 | 0.61 | 0.34 | 0.21 | 0.13 | 0.09 |
| | 0.9 | 4.53 | 2.27 | 1.27 | 0.77 | 0.50 | 0.34 | 2.53 | 1.27 | 0.71 | 0.43 | 0.28 | 0.19 | 1.53 | 0.76 | 0.43 | 0.26 | 0.17 | 0.11 | 0.99 | 0.49 | 0.28 | 0.17 | 0.11 | 0.07 |
| | 0.5 | 8.49 | 4.13 | 2.27 | 1.37 | 0.88 | 0.60 | 4.74 | 2.31 | 1.27 | 0.76 | 0.49 | 0.33 | 2.86 | 1.39 | 0.76 | 0.46 | 0.29 | 0.20 | 1.85 | 0.90 | 0.49 | 0.30 | 0.19 | 0.13 |
| | 0.6 | 7.50 | 3.66 | 2.02 | 1.21 | 0.78 | 0.53 | 4.19 | 2.04 | 1.12 | 0.68 | 0.43 | 0.29 | 2.52 | 1.23 | 0.68 | 0.41 | 0.26 | 0.18 | 1.63 | 0.80 | 0.44 | 0.26 | 0.17 | 0.11 |
| Ly=1.4 | 0.7 | 6.47 | 3.17 | 1.75 | 1.05 | 0.68 | 0.46 | 3.61 | 1.77 | 0.97 | 0.59 | 0.38 | 0.26 | 2.18 | 1.07 | 0.59 | 0.35 | 0.23 | 0.15 | 1.41 | 0.69 | 0.38 | 0.23 | 0.15 | 0.10 |
| | 0.8 | 5.43 | 2.67 | 1.47 | 0.89 | 0.57 | 0.39 | 3.03 | 1.49 | 0.82 | 0.49 | 0.32 | 0.22 | 1.83 | 0.90 | 0.49 | 0.30 | 0.19 | 0.13 | 1.18 | 0.58 | 0.32 | 0.19 | 0.12 | 0.08 |
| | 0.9 | 4.43 | 2.18 | 1.20 | 0.72 | 0.47 | 0.32 | 2.47 | 1.21 | 0.67 | 0.40 | 0.26 | 0.18 | 1.49 | 0.73 | 0.40 | 0.24 | 0.16 | 0.11 | 0.96 | 0.47 | 0.26 | 0.16 | 0.10 | 0.07 |
| | 0.5 | 8.36 | 4.02 | 2.19 | 1.31 | 0.84 | 0.57 | 4.67 | 2.25 | 1.22 | 0.73 | 0.47 | 0.32 | 2.82 | 1.35 | 0.74 | 0.44 | 0.28 | 0.19 | 1.82 | 0.87 | 0.48 | 0.28 | 0.18 | 0.12 |
| | 0.6 | 7.38 | 3.56 | 1.94 | 1.16 | 0.75 | 0.50 | 4.12 | 1.99 | 1.08 | 0.65 | 0.42 | 0.28 | 2.48 | 1.20 | 0.65 | 0.39 | 0.25 | 0.17 | 1.61 | 0.77 | 0.42 | 0.25 | 0.16 | 0.11 |
| Ly=1.6 | 0.7 | 6.37 | 3.08 | 1.69 | 1.01 | 0.65 | 0.44 | 3.56 | 1.72 | 0.94 | 0.56 | 0.36 | 0.24 | 2.14 | 1.04 | 0.57 | 0.34 | 0.22 | 0.15 | 1.39 | 0.67 | 0.37 | 0.22 | 0.14 | 0.09 |
| | 0.8 | 5.35 | 2.60 | 1.42 | 0.85 | 0.55 | 0.37 | 2.99 | 1.45 | 0.79 | 0.47 | 0.30 | 0.21 | 1.80 | 0.87 | 0.48 | 0.29 | 0.18 | 0.12 | 1.16 | 0.56 | 0.31 | 0.18 | 0.12 | 0.08 |
| | 0.9 | 4.36 | 2.12 | 1.16 | 0.69 | 0.45 | 0.30 | 2.44 | 1.18 | 0.65 | 0.39 | 0.25 | 0.17 | 1.47 | 0.71 | 0.39 | 0.23 | 0.15 | 0.10 | 0.95 | 0.46 | 0.25 | 0.15 | 0.10 | 0.07 |

## Table D.2 $\alpha_c$ values for HSS 203 x 203 mm

| | tep(eff) | HSS 203 X 203 X 7.95 | | | | | | HSS 203 X 203 X 9.53 | | | | | | HSS 203 X 203 X 11.13 | | | | | | HSS 203 X 203 X 12.70 | | | | | |
|---|---|---|---|---|---|---|---|---|---|---|---|---|---|---|---|---|---|---|---|---|---|---|---|---|---|
| | tcf | 0.5 | 1.0 | 1.5 | 2.0 | 2.5 | 3.0 | 0.5 | 1.0 | 1.5 | 2.0 | 2.5 | 3.0 | 0.5 | 1.0 | 1.5 | 2.0 | 2.5 | 3.0 | 0.5 | 1.0 | 1.5 | 2.0 | 2.5 | 3.0 |
| | Lx | | | | | | | | | | | | | | | | | | | | | | | | |
| | 0.5 | 14.2 | 8.11 | 4.96 | 3.20 | 2.14 | 1.49 | 7.95 | 4.55 | 2.80 | 1.79 | 1.20 | 0.84 | 4.84 | 2.76 | 1.70 | 1.09 | 0.73 | 0.51 | 3.15 | 1.80 | 1.10 | 0.71 | 0.47 | 0.33 |
| | 0.6 | 12.5 | 7.18 | 4.41 | 2.84 | 1.91 | 1.33 | 7.04 | 4.03 | 2.48 | 1.60 | 1.07 | 0.74 | 4.26 | 2.45 | 1.50 | 0.97 | 0.65 | 0.45 | 2.77 | 1.59 | 0.98 | 0.63 | 0.42 | 0.29 |
| Ly=0.6 | 0.7 | 10.8 | 6.21 | 3.82 | 2.46 | 1.65 | 1.15 | 6.05 | 3.49 | 2.14 | 1.38 | 0.93 | 0.65 | 3.68 | 2.12 | 1.30 | 0.84 | 0.56 | 0.39 | 2.39 | 1.38 | 0.85 | 0.54 | 0.37 | 0.26 |
| | 0.8 | 9.04 | 5.22 | 3.21 | 2.07 | 1.39 | 0.97 | 5.08 | 2.93 | 1.80 | 1.16 | 0.78 | 0.54 | 3.09 | 1.78 | 1.10 | 0.71 | 0.47 | 0.33 | 2.01 | 1.16 | 0.71 | 0.46 | 0.31 | 0.21 |
| | 0.9 | 7.35 | 4.25 | 2.62 | 1.69 | 1.13 | 0.79 | 4.13 | 2.39 | 1.47 | 0.95 | 0.64 | 0.44 | 2.51 | 1.45 | 0.89 | 0.58 | 0.39 | 0.27 | 1.63 | 0.94 | 0.58 | 0.37 | 0.25 | 0.17 |
| | 0.5 | 12.9 | 6.90 | 4.04 | 2.53 | 1.67 | 1.15 | 7.27 | 3.87 | 2.27 | 1.42 | 0.94 | 0.65 | 4.41 | 2.35 | 1.38 | 0.86 | 0.57 | 0.39 | 2.87 | 1.53 | 0.90 | 0.56 | 0.37 | 0.25 |
| | 0.6 | 11.4 | 6.11 | 3.59 | 2.24 | 1.48 | 1.02 | 6.40 | 3.43 | 2.02 | 1.26 | 0.83 | 0.57 | 3.89 | 2.08 | 1.22 | 0.76 | 0.50 | 0.35 | 2.53 | 1.35 | 0.79 | 0.50 | 0.33 | 0.23 |
| Ly=0.8 | 0.7 | 9.84 | 5.28 | 3.11 | 1.94 | 1.28 | 0.88 | 5.52 | 2.97 | 1.74 | 1.09 | 0.72 | 0.50 | 3.35 | 1.80 | 1.06 | 0.66 | 0.44 | 0.30 | 2.18 | 1.17 | 0.69 | 0.43 | 0.28 | 0.20 |
| | 0.8 | 8.26 | 4.45 | 2.62 | 1.64 | 1.08 | 0.75 | 4.64 | 2.50 | 1.47 | 0.92 | 0.61 | 0.42 | 2.81 | 1.51 | 0.89 | 0.56 | 0.37 | 0.25 | 1.83 | 0.99 | 0.58 | 0.36 | 0.24 | 0.17 |
| | 0.9 | 6.72 | 3.62 | 2.13 | 1.34 | 0.88 | 0.61 | 3.77 | 2.04 | 1.20 | 0.75 | 0.49 | 0.34 | 2.29 | 1.24 | 0.73 | 0.45 | 0.30 | 0.21 | 1.49 | 0.80 | 0.47 | 0.30 | 0.20 | 0.13 |
| | 0.5 | 12.2 | 6.22 | 3.53 | 2.17 | 1.41 | 0.97 | 6.84 | 3.49 | 1.98 | 1.22 | 0.79 | 0.54 | 4.15 | 2.12 | 1.20 | 0.74 | 0.48 | 0.33 | 2.70 | 1.38 | 0.78 | 0.48 | 0.31 | 0.21 |
| | 0.6 | 10.8 | 5.51 | 3.13 | 1.92 | 1.26 | 0.86 | 6.04 | 3.09 | 1.76 | 1.08 | 0.70 | 0.48 | 3.66 | 1.87 | 1.07 | 0.65 | 0.43 | 0.29 | 2.38 | 1.22 | 0.69 | 0.43 | 0.28 | 0.19 |
| Ly=1.0 | 0.7 | 9.27 | 4.76 | 2.71 | 1.67 | 1.09 | 0.74 | 5.21 | 2.67 | 1.52 | 0.94 | 0.61 | 0.42 | 3.16 | 1.62 | 0.92 | 0.57 | 0.37 | 0.25 | 2.06 | 1.05 | 0.60 | 0.37 | 0.24 | 0.16 |
| | 0.8 | 7.79 | 4.01 | 2.29 | 1.41 | 0.92 | 0.63 | 4.37 | 2.25 | 1.28 | 0.79 | 0.51 | 0.35 | 2.65 | 1.36 | 0.78 | 0.48 | 0.31 | 0.21 | 1.73 | 0.89 | 0.51 | 0.31 | 0.20 | 0.14 |
| | 0.9 | 6.34 | 3.27 | 1.86 | 1.15 | 0.75 | 0.51 | 3.56 | 1.84 | 1.05 | 0.64 | 0.42 | 0.29 | 2.16 | 1.11 | 0.63 | 0.39 | 0.25 | 0.17 | 1.40 | 0.72 | 0.41 | 0.25 | 0.17 | 0.11 |
| | 0.5 | 11.7 | 5.81 | 3.24 | 1.96 | 1.27 | 0.86 | 6.59 | 3.27 | 1.82 | 1.10 | 0.71 | 0.48 | 3.99 | 1.98 | 1.10 | 0.67 | 0.43 | 0.29 | 2.60 | 1.29 | 0.71 | 0.43 | 0.28 | 0.19 |
| | 0.6 | 10.4 | 5.15 | 2.87 | 1.74 | 1.13 | 0.77 | 5.81 | 2.89 | 1.61 | 0.97 | 0.63 | 0.43 | 3.52 | 1.75 | 0.98 | 0.59 | 0.38 | 0.26 | 2.29 | 1.14 | 0.63 | 0.38 | 0.25 | 0.17 |
| Ly=1.2 | 0.7 | 8.93 | 4.45 | 2.49 | 1.51 | 0.98 | 0.66 | 5.01 | 2.50 | 1.39 | 0.85 | 0.55 | 0.37 | 3.04 | 1.52 | 0.85 | 0.51 | 0.33 | 0.23 | 1.98 | 0.98 | 0.55 | 0.33 | 0.22 | 0.15 |
| | 0.8 | 7.5 | 3.75 | 2.09 | 1.27 | 0.82 | 0.56 | 4.21 | 2.11 | 1.18 | 0.71 | 0.46 | 0.31 | 2.55 | 1.28 | 0.71 | 0.43 | 0.28 | 0.19 | 1.66 | 0.83 | 0.46 | 0.28 | 0.18 | 0.12 |
| | 0.9 | 6.11 | 3.06 | 1.71 | 1.04 | 0.67 | 0.46 | 3.43 | 1.72 | 0.96 | 0.58 | 0.38 | 0.26 | 2.08 | 1.04 | 0.58 | 0.35 | 0.23 | 0.16 | 1.35 | 0.68 | 0.38 | 0.23 | 0.15 | 0.10 |
| | 0.5 | 11.4 | 5.57 | 3.06 | 1.84 | 1.18 | 0.80 | 6.43 | 3.13 | 1.72 | 1.03 | 0.66 | 0.45 | 3.90 | 1.89 | 1.04 | 0.62 | 0.40 | 0.27 | 2.54 | 1.23 | 0.68 | 0.41 | 0.26 | 0.18 |
| | 0.6 | 10.1 | 4.93 | 2.71 | 1.63 | 1.05 | 0.71 | 5.67 | 2.77 | 1.52 | 0.91 | 0.59 | 0.40 | 3.44 | 1.68 | 0.92 | 0.55 | 0.36 | 0.24 | 2.24 | 1.09 | 0.60 | 0.36 | 0.23 | 0.16 |
| Ly=1.4 | 0.7 | 8.71 | 4.27 | 2.35 | 1.41 | 0.91 | 0.62 | 4.89 | 2.39 | 1.32 | 0.79 | 0.51 | 0.35 | 2.97 | 1.45 | 0.80 | 0.48 | 0.31 | 0.21 | 1.93 | 0.94 | 0.52 | 0.31 | 0.20 | 0.14 |
| | 0.8 | 7.33 | 3.59 | 1.98 | 1.19 | 0.77 | 0.52 | 4.11 | 2.02 | 1.11 | 0.67 | 0.43 | 0.29 | 2.49 | 1.22 | 0.67 | 0.41 | 0.26 | 0.18 | 1.62 | 0.79 | 0.44 | 0.26 | 0.17 | 0.11 |
| | 0.9 | 5.97 | 2.93 | 1.62 | 0.97 | 0.63 | 0.43 | 3.35 | 1.65 | 0.91 | 0.55 | 0.35 | 0.24 | 2.03 | 1.00 | 0.55 | 0.33 | 0.21 | 0.14 | 1.32 | 0.65 | 0.36 | 0.21 | 0.14 | 0.09 |
| | 0.5 | 11.3 | 5.42 | 2.95 | 1.77 | 1.13 | 0.77 | 6.33 | 3.04 | 1.66 | 0.99 | 0.63 | 0.43 | 3.84 | 1.84 | 1.00 | 0.60 | 0.38 | 0.26 | 2.50 | 1.20 | 0.65 | 0.39 | 0.25 | 0.17 |
| | 0.6 | 9.96 | 4.80 | 2.62 | 1.57 | 1.00 | 0.68 | 5.59 | 2.69 | 1.47 | 0.88 | 0.56 | 0.38 | 3.39 | 1.63 | 0.89 | 0.53 | 0.34 | 0.23 | 2.20 | 1.06 | 0.58 | 0.35 | 0.22 | 0.15 |
| Ly=1.6 | 0.7 | 8.59 | 4.16 | 2.27 | 1.36 | 0.87 | 0.59 | 4.82 | 2.33 | 1.27 | 0.76 | 0.49 | 0.33 | 2.92 | 1.41 | 0.77 | 0.46 | 0.30 | 0.20 | 1.90 | 0.92 | 0.50 | 0.30 | 0.19 | 0.13 |
| | 0.8 | 7.22 | 3.50 | 1.91 | 1.15 | 0.74 | 0.50 | 4.05 | 1.96 | 1.07 | 0.64 | 0.41 | 0.28 | 2.46 | 1.19 | 0.65 | 0.39 | 0.25 | 0.17 | 1.60 | 0.77 | 0.42 | 0.25 | 0.16 | 0.11 |
| | 0.9 | 5.89 | 2.86 | 1.56 | 0.94 | 0.60 | 0.41 | 3.31 | 1.60 | 0.88 | 0.52 | 0.34 | 0.23 | 2.01 | 0.97 | 0.53 | 0.32 | 0.20 | 0.14 | 1.30 | 0.63 | 0.34 | 0.21 | 0.13 | 0.09 |

# Table D.3 $\alpha_c$ values for HSS 254 x 254 mm

| | tep(eff)/ | HSS 254 X 254 X 7.95 | | | | | | 254 X 254 X 9.53 | | | | | | HSS 254 X 254 X 11.13 | | | | | | HSS 254 X 254 X 12.70 | | | | | |
|---|---|---|---|---|---|---|---|---|---|---|---|---|---|---|---|---|---|---|---|---|---|---|---|---|---|
| | tcf | 0.5 | 1.0 | 1.5 | 2.0 | 2.5 | 3.0 | 0.5 | 1.0 | 1.5 | 2.0 | 2.5 | 3.0 | 0.5 | 1.0 | 1.5 | 2.0 | 2.5 | 3.0 | 0.5 | 1.0 | 1.5 | 2.0 | 2.5 | 3.0 |
| | Lx | | | | | | | | | | | | | | | | | | | | | | | | |
| | 0.5 | 23.1 | 13.2 | 8.10 | 5.18 | 3.48 | 2.42 | 13.1 | 7.46 | 4.57 | 2.93 | 1.96 | 1.37 | 8.01 | 4.57 | 2.79 | 1.80 | 1.20 | 0.84 | 5.25 | 2.99 | 1.83 | 1.18 | 0.79 | 0.55 |
| | 0.6 | 20.4 | 11.7 | 7.16 | 4.59 | 3.09 | 2.15 | 11.5 | 6.61 | 4.05 | 2.60 | 1.75 | 1.22 | 7.05 | 4.04 | 2.46 | 1.59 | 1.07 | 0.74 | 4.63 | 2.65 | 1.62 | 1.04 | 0.70 | 0.49 |
| Ly=0.6 | 0.7 | 17.6 | 10.1 | 6.20 | 3.99 | 2.67 | 1.86 | 9.95 | 5.71 | 3.50 | 2.26 | 1.51 | 1.05 | 6.08 | 3.49 | 2.14 | 1.38 | 0.92 | 0.64 | 3.99 | 2.29 | 1.40 | 0.90 | 0.61 | 0.42 |
| | 0.8 | 14.8 | 8.49 | 5.22 | 3.36 | 2.25 | 1.57 | 8.35 | 4.80 | 2.95 | 1.90 | 1.27 | 0.89 | 5.11 | 2.94 | 1.80 | 1.16 | 0.78 | 0.54 | 3.35 | 1.93 | 1.18 | 0.76 | 0.51 | 0.36 |
| | 0.9 | 12.0 | 6.91 | 4.25 | 2.74 | 1.84 | 1.28 | 6.79 | 3.91 | 2.40 | 1.55 | 1.04 | 0.72 | 4.15 | 2.39 | 1.47 | 0.95 | 0.64 | 0.44 | 2.72 | 1.57 | 0.96 | 0.62 | 0.42 | 0.29 |
| | 0.5 | 21.1 | 11.3 | 6.58 | 4.11 | 2.71 | 1.87 | 12.0 | 6.36 | 3.73 | 2.33 | 1.53 | 1.06 | 7.32 | 3.89 | 2.27 | 1.42 | 0.94 | 0.64 | 4.80 | 2.55 | 1.49 | 0.93 | 0.61 | 0.42 |
| | 0.6 | 18.7 | 9.95 | 5.84 | 3.65 | 2.41 | 1.66 | 10.6 | 5.63 | 3.30 | 2.07 | 1.36 | 0.94 | 6.44 | 3.45 | 2.02 | 1.26 | 0.83 | 0.57 | 4.23 | 2.26 | 1.32 | 0.83 | 0.55 | 0.38 |
| Ly=0.8 | 0.7 | 16.1 | 8.61 | 5.05 | 3.16 | 2.09 | 1.44 | 9.09 | 4.87 | 2.86 | 1.79 | 1.18 | 0.81 | 5.56 | 2.98 | 1.75 | 1.09 | 0.72 | 0.50 | 3.65 | 1.95 | 1.14 | 0.72 | 0.47 | 0.33 |
| | 0.8 | 13.5 | 7.25 | 4.26 | 2.67 | 1.76 | 1.21 | 7.64 | 4.10 | 2.41 | 1.51 | 0.99 | 0.69 | 4.67 | 2.51 | 1.47 | 0.92 | 0.61 | 0.42 | 3.06 | 1.64 | 0.96 | 0.60 | 0.40 | 0.27 |
| | 0.9 | 11.0 | 5.91 | 3.47 | 2.17 | 1.44 | 0.99 | 6.21 | 3.34 | 1.96 | 1.23 | 0.81 | 0.56 | 3.80 | 2.04 | 1.20 | 0.75 | 0.50 | 0.34 | 2.49 | 1.34 | 0.79 | 0.49 | 0.32 | 0.22 |
| | 0.5 | 19.9 | 10.1 | 5.76 | 3.53 | 2.30 | 1.57 | 11.3 | 5.74 | 3.26 | 2.00 | 1.30 | 0.89 | 6.90 | 3.50 | 1.99 | 1.22 | 0.80 | 0.54 | 4.53 | 2.30 | 1.30 | 0.80 | 0.52 | 0.36 |
| | 0.6 | 17.6 | 8.98 | 5.11 | 3.13 | 2.04 | 1.40 | 9.95 | 5.09 | 2.88 | 1.77 | 1.15 | 0.79 | 6.08 | 3.11 | 1.76 | 1.08 | 0.70 | 0.48 | 3.99 | 2.03 | 1.16 | 0.71 | 0.46 | 0.32 |
| Ly=1.0 | 0.7 | 15.2 | 7.77 | 4.42 | 2.72 | 1.77 | 1.21 | 8.58 | 4.40 | 2.50 | 1.54 | 1.00 | 0.68 | 5.25 | 2.69 | 1.53 | 0.94 | 0.61 | 0.42 | 3.44 | 1.76 | 1.00 | 0.61 | 0.40 | 0.27 |
| | 0.8 | 12.7 | 6.55 | 3.73 | 2.29 | 1.49 | 1.02 | 7.21 | 3.70 | 2.11 | 1.29 | 0.84 | 0.58 | 4.41 | 2.26 | 1.29 | 0.79 | 0.52 | 0.35 | 2.89 | 1.48 | 0.84 | 0.52 | 0.34 | 0.23 |
| | 0.9 | 10.4 | 5.34 | 3.04 | 1.87 | 1.22 | 0.83 | 5.87 | 3.02 | 1.72 | 1.06 | 0.69 | 0.47 | 3.59 | 1.84 | 1.05 | 0.65 | 0.42 | 0.29 | 2.35 | 1.21 | 0.69 | 0.42 | 0.28 | 0.19 |
| | 0.5 | 19.2 | 9.51 | 5.28 | 3.20 | 2.07 | 1.41 | 10.9 | 5.37 | 2.99 | 1.81 | 1.17 | 0.80 | 6.64 | 3.28 | 1.82 | 1.10 | 0.71 | 0.49 | 4.35 | 2.16 | 1.19 | 0.72 | 0.47 | 0.32 |
| | 0.6 | 17.0 | 8.41 | 4.69 | 2.84 | 1.84 | 1.25 | 9.59 | 4.76 | 2.65 | 1.60 | 1.04 | 0.71 | 5.86 | 2.91 | 1.62 | 0.98 | 0.63 | 0.43 | 3.84 | 1.90 | 1.06 | 0.64 | 0.42 | 0.28 |
| Ly=1.2 | 0.7 | 14.6 | 7.28 | 4.06 | 2.46 | 1.59 | 1.08 | 8.27 | 4.12 | 2.29 | 1.39 | 0.90 | 0.61 | 5.06 | 2.52 | 1.40 | 0.85 | 0.55 | 0.37 | 3.31 | 1.65 | 0.92 | 0.56 | 0.36 | 0.25 |
| | 0.8 | 12.3 | 6.13 | 3.42 | 2.08 | 1.34 | 0.91 | 6.95 | 3.47 | 1.94 | 1.17 | 0.76 | 0.52 | 4.25 | 2.12 | 1.18 | 0.72 | 0.46 | 0.32 | 2.78 | 1.39 | 0.77 | 0.47 | 0.30 | 0.21 |
| | 0.9 | 10.0 | 5.00 | 2.79 | 1.69 | 1.10 | 0.75 | 5.66 | 2.83 | 1.58 | 0.96 | 0.62 | 0.42 | 3.46 | 1.73 | 0.96 | 0.58 | 0.38 | 0.26 | 2.27 | 1.13 | 0.63 | 0.38 | 0.25 | 0.17 |
| | 0.5 | 18.8 | 9.13 | 5.00 | 3.00 | 1.93 | 1.31 | 10.6 | 5.15 | 2.83 | 1.70 | 1.09 | 0.74 | 6.49 | 3.15 | 1.73 | 1.04 | 0.67 | 0.45 | 4.25 | 2.07 | 1.13 | 0.68 | 0.44 | 0.30 |
| | 0.6 | 16.6 | 8.07 | 4.44 | 2.67 | 1.72 | 1.16 | 9.37 | 4.56 | 2.51 | 1.51 | 0.97 | 0.66 | 5.72 | 2.79 | 1.53 | 0.92 | 0.59 | 0.40 | 3.75 | 1.83 | 1.00 | 0.60 | 0.39 | 0.26 |
| Ly=1.4 | 0.7 | 14.3 | 6.99 | 3.85 | 2.31 | 1.49 | 1.01 | 8.08 | 3.95 | 2.17 | 1.31 | 0.84 | 0.57 | 4.94 | 2.41 | 1.33 | 0.80 | 0.51 | 0.35 | 3.24 | 1.58 | 0.87 | 0.52 | 0.34 | 0.23 |
| | 0.8 | 12.0 | 5.89 | 3.24 | 1.95 | 1.26 | 0.85 | 6.79 | 3.33 | 1.83 | 1.10 | 0.71 | 0.48 | 4.15 | 2.03 | 1.12 | 0.67 | 0.43 | 0.29 | 2.72 | 1.33 | 0.73 | 0.44 | 0.28 | 0.19 |
| | 0.9 | 9.8 | 4.80 | 2.65 | 1.59 | 1.03 | 0.70 | 5.54 | 2.72 | 1.50 | 0.90 | 0.58 | 0.39 | 3.39 | 1.66 | 0.91 | 0.55 | 0.35 | 0.24 | 2.22 | 1.09 | 0.60 | 0.36 | 0.23 | 0.16 |
| | 0.5 | 18.5 | 8.88 | 4.84 | 2.89 | 1.85 | 1.25 | 10.5 | 5.02 | 2.74 | 1.63 | 1.05 | 0.71 | 6.40 | 3.07 | 1.67 | 1.00 | 0.64 | 0.43 | 4.19 | 2.01 | 1.09 | 0.65 | 0.42 | 0.28 |
| | 0.6 | 16.3 | 7.86 | 4.29 | 2.57 | 1.65 | 1.11 | 9.23 | 4.45 | 2.43 | 1.45 | 0.93 | 0.63 | 5.64 | 2.72 | 1.48 | 0.88 | 0.57 | 0.38 | 3.70 | 1.78 | 0.97 | 0.58 | 0.37 | 0.25 |
| Ly=1.6 | 0.7 | 14.1 | 6.81 | 3.72 | 2.22 | 1.43 | 0.97 | 7.97 | 3.85 | 2.10 | 1.26 | 0.81 | 0.55 | 4.87 | 2.35 | 1.28 | 0.77 | 0.49 | 0.33 | 3.19 | 1.54 | 0.84 | 0.50 | 0.32 | 0.22 |
| | 0.8 | 11.9 | 5.74 | 3.14 | 1.88 | 1.20 | 0.82 | 6.70 | 3.24 | 1.77 | 1.06 | 0.68 | 0.46 | 4.09 | 1.98 | 1.08 | 0.65 | 0.42 | 0.28 | 2.68 | 1.30 | 0.71 | 0.42 | 0.27 | 0.18 |
| | 0.9 | 9.7 | 4.68 | 2.56 | 1.53 | 0.98 | 0.67 | 5.47 | 2.65 | 1.45 | 0.87 | 0.56 | 0.38 | 3.34 | 1.62 | 0.88 | 0.53 | 0.34 | 0.23 | 2.19 | 1.06 | 0.58 | 0.35 | 0.22 | 0.15 |

# Table D.4 $\alpha_e$ values for HSS 304 x 304 mm

| | tep(eff)/ tcf | HSS 304 X 304 X 7.95 | | | | | | HSS 304 X 304 X 9.53 | | | | | | HSS 304 X 304 X 11.13 | | | | | | HSS 304 X 304 X 12.70 | | | | | |
|---|---|---|---|---|---|---|---|---|---|---|---|---|---|---|---|---|---|---|---|---|---|---|---|---|---|
| | Lx | 0.5 | 1.0 | 1.5 | 2.0 | 2.5 | 3.0 | 0.5 | 1.0 | 1.5 | 2.0 | 2.5 | 3.0 | 0.5 | 1.0 | 1.5 | 2.0 | 2.5 | 3.0 | 0.5 | 1.0 | 1.5 | 2.0 | 2.5 | 3.0 |
| | 0.5 | 34.2 | 19.4 | 11.9 | 7.67 | 5.11 | 3.56 | 19.4 | 11.1 | 6.76 | 4.34 | 2.90 | 2.03 | 11.9 | 6.78 | 4.14 | 2.66 | 1.79 | 1.24 | 7.87 | 4.48 | 2.74 | 1.76 | 1.17 | 0.82 |
| | 0.6 | 30.2 | 17.3 | 10.5 | 6.80 | 4.54 | 3.18 | 17.1 | 9.79 | 5.99 | 3.85 | 2.59 | 1.80 | 10.5 | 6.00 | 3.68 | 2.37 | 1.58 | 1.10 | 6.95 | 3.96 | 2.42 | 1.56 | 1.04 | 0.73 |
| Ly=0.6 | 0.7 | 26.0 | 14.9 | 9.13 | 5.88 | 3.95 | 2.74 | 14.9 | 8.46 | 5.19 | 3.34 | 2.24 | 1.56 | 9.08 | 5.20 | 3.19 | 2.05 | 1.37 | 0.96 | 5.98 | 3.43 | 2.10 | 1.35 | 0.91 | 0.63 |
| | 0.8 | 21.8 | 12.5 | 7.70 | 4.96 | 3.32 | 2.31 | 12.4 | 7.12 | 4.37 | 2.81 | 1.88 | 1.31 | 7.61 | 4.37 | 2.68 | 1.73 | 1.16 | 0.81 | 5.02 | 2.88 | 1.77 | 1.14 | 0.76 | 0.53 |
| | 0.9 | 17.8 | 10.2 | 6.27 | 4.04 | 2.71 | 1.89 | 10.1 | 5.80 | 3.56 | 2.29 | 1.54 | 1.07 | 6.20 | 3.56 | 2.19 | 1.41 | 0.94 | 0.66 | 4.08 | 2.35 | 1.44 | 0.93 | 0.62 | 0.43 |
| | 0.5 | 31.3 | 16.6 | 9.74 | 6.07 | 4.00 | 2.75 | 17.8 | 9.46 | 5.53 | 3.45 | 2.27 | 1.57 | 10.9 | 5.80 | 3.39 | 2.12 | 1.40 | 0.96 | 7.19 | 3.82 | 2.23 | 1.39 | 0.92 | 0.63 |
| | 0.6 | 27.6 | 14.7 | 8.62 | 5.39 | 3.55 | 2.45 | 15.7 | 8.37 | 4.89 | 3.07 | 2.02 | 1.39 | 9.64 | 5.14 | 3.01 | 1.88 | 1.24 | 0.85 | 6.35 | 3.38 | 1.98 | 1.24 | 0.82 | 0.56 |
| Ly=0.8 | 0.7 | 23.8 | 12.7 | 7.46 | 4.67 | 3.08 | 2.12 | 13.5 | 7.23 | 4.24 | 2.65 | 1.75 | 1.21 | 8.31 | 4.44 | 2.60 | 1.63 | 1.07 | 0.74 | 5.47 | 2.93 | 1.71 | 1.07 | 0.71 | 0.49 |
| | 0.8 | 20.0 | 10.7 | 6.29 | 3.94 | 2.60 | 1.79 | 11.4 | 6.09 | 3.57 | 2.24 | 1.47 | 1.02 | 6.97 | 3.74 | 2.19 | 1.37 | 0.91 | 0.62 | 4.59 | 2.46 | 1.44 | 0.90 | 0.60 | 0.41 |
| | 0.9 | 16.3 | 8.73 | 5.13 | 3.21 | 2.12 | 1.46 | 9.24 | 4.96 | 2.91 | 1.82 | 1.20 | 0.83 | 5.68 | 3.05 | 1.79 | 1.12 | 0.74 | 0.51 | 3.74 | 2.01 | 1.18 | 0.74 | 0.49 | 0.34 |
| | 0.5 | 29.5 | 15.0 | 8.53 | 5.22 | 3.40 | 2.32 | 16.8 | 8.54 | 4.84 | 2.96 | 1.93 | 1.32 | 10.30 | 5.24 | 2.97 | 1.82 | 1.19 | 0.81 | 6.80 | 3.45 | 1.96 | 1.20 | 0.78 | 0.53 |
| | 0.6 | 26.1 | 13.3 | 7.55 | 4.63 | 3.02 | 2.07 | 14.8 | 7.55 | 4.29 | 2.63 | 1.72 | 1.17 | 9.10 | 4.64 | 2.64 | 1.62 | 1.05 | 0.72 | 5.99 | 3.06 | 1.73 | 1.06 | 0.69 | 0.47 |
| Ly=1.0 | 0.7 | 22.5 | 11.5 | 6.54 | 4.01 | 2.62 | 1.79 | 12.8 | 6.54 | 3.72 | 2.28 | 1.49 | 1.02 | 7.85 | 4.01 | 2.28 | 1.40 | 0.91 | 0.62 | 5.17 | 2.64 | 1.50 | 0.92 | 0.60 | 0.41 |
| | 0.8 | 18.9 | 9.68 | 5.51 | 3.39 | 2.21 | 1.51 | 10.7 | 5.50 | 3.13 | 1.92 | 1.25 | 0.86 | 6.59 | 3.38 | 1.92 | 1.18 | 0.77 | 0.53 | 4.34 | 2.23 | 1.27 | 0.78 | 0.51 | 0.35 |
| | 0.9 | 15.4 | 7.90 | 4.50 | 2.76 | 1.80 | 1.23 | 8.74 | 4.49 | 2.55 | 1.57 | 1.02 | 0.70 | 5.37 | 2.76 | 1.57 | 0.96 | 0.63 | 0.43 | 3.54 | 1.82 | 1.03 | 0.63 | 0.41 | 0.28 |
| | 0.5 | 28.5 | 14.1 | 7.83 | 4.74 | 3.06 | 2.09 | 16.2 | 8.00 | 4.44 | 2.69 | 1.74 | 1.18 | 9.92 | 4.91 | 2.72 | 1.65 | 1.07 | 0.73 | 6.55 | 3.23 | 1.80 | 1.09 | 0.70 | 0.48 |
| | 0.6 | 25.1 | 12.5 | 6.93 | 4.20 | 2.71 | 1.85 | 14.3 | 7.08 | 3.94 | 2.39 | 1.54 | 1.05 | 8.77 | 4.35 | 2.42 | 1.47 | 0.95 | 0.64 | 5.78 | 2.86 | 1.59 | 0.96 | 0.62 | 0.42 |
| Ly=1.2 | 0.7 | 21.7 | 10.8 | 6.01 | 3.64 | 2.36 | 1.60 | 12.3 | 6.12 | 3.41 | 2.07 | 1.34 | 0.91 | 7.57 | 3.76 | 2.10 | 1.27 | 0.82 | 0.56 | 4.98 | 2.48 | 1.38 | 0.84 | 0.54 | 0.37 |
| | 0.8 | 18.2 | 9.08 | 5.07 | 3.07 | 1.99 | 1.35 | 10.4 | 5.16 | 2.88 | 1.75 | 1.13 | 0.77 | 6.35 | 3.17 | 1.77 | 1.07 | 0.69 | 0.47 | 4.19 | 2.09 | 1.16 | 0.71 | 0.46 | 0.31 |
| | 0.9 | 14.8 | 7.41 | 4.13 | 2.51 | 1.62 | 1.11 | 8.43 | 4.21 | 2.35 | 1.42 | 0.92 | 0.63 | 5.18 | 2.58 | 1.44 | 0.87 | 0.57 | 0.38 | 3.41 | 1.70 | 0.95 | 0.58 | 0.37 | 0.25 |
| | 0.5 | 27.8 | 13.5 | 7.41 | 4.45 | 2.86 | 1.94 | 15.8 | 7.69 | 4.21 | 2.53 | 1.62 | 1.10 | 9.71 | 4.72 | 2.59 | 1.55 | 1.00 | 0.68 | 6.40 | 3.10 | 1.70 | 1.02 | 0.66 | 0.45 |
| | 0.6 | 24.5 | 12.0 | 6.57 | 3.95 | 2.54 | 1.73 | 14.0 | 6.80 | 3.73 | 2.24 | 1.44 | 0.98 | 8.58 | 4.17 | 2.29 | 1.38 | 0.89 | 0.60 | 5.64 | 2.75 | 1.51 | 0.91 | 0.58 | 0.40 |
| Ly=1.4 | 0.7 | 21.2 | 10.4 | 5.70 | 3.43 | 2.20 | 1.50 | 12.0 | 5.88 | 3.24 | 1.94 | 1.25 | 0.85 | 7.40 | 3.61 | 1.99 | 1.19 | 0.77 | 0.52 | 4.87 | 2.38 | 1.31 | 0.79 | 0.51 | 0.34 |
| | 0.8 | 17.8 | 8.72 | 4.80 | 2.89 | 1.86 | 1.26 | 10.1 | 4.95 | 2.73 | 1.64 | 1.06 | 0.72 | 6.21 | 3.04 | 1.67 | 1.01 | 0.65 | 0.44 | 4.09 | 2.00 | 1.10 | 0.66 | 0.43 | 0.29 |
| | 0.9 | 14.5 | 7.12 | 3.92 | 2.36 | 1.52 | 1.03 | 8.26 | 4.04 | 2.23 | 1.34 | 0.86 | 0.58 | 5.07 | 2.48 | 1.37 | 0.82 | 0.53 | 0.36 | 3.34 | 1.64 | 0.90 | 0.54 | 0.35 | 0.24 |
| | 0.5 | 27.4 | 13.2 | 7.18 | 4.29 | 2.75 | 1.86 | 15.6 | 7.49 | 4.07 | 2.43 | 1.56 | 1.06 | 9.57 | 4.60 | 2.50 | 1.49 | 0.96 | 0.65 | 6.31 | 3.03 | 1.65 | 0.98 | 0.63 | 0.43 |
| | 0.6 | 24.2 | 11.7 | 6.36 | 3.80 | 2.43 | 1.65 | 13.8 | 6.63 | 3.61 | 2.16 | 1.38 | 0.94 | 8.46 | 4.07 | 2.22 | 1.33 | 0.85 | 0.58 | 5.57 | 2.68 | 1.46 | 0.87 | 0.56 | 0.38 |
| Ly=1.6 | 0.7 | 20.9 | 10.1 | 5.51 | 3.30 | 2.11 | 1.43 | 11.9 | 5.73 | 3.13 | 1.87 | 1.20 | 0.81 | 7.30 | 3.52 | 1.92 | 1.15 | 0.74 | 0.50 | 4.81 | 2.32 | 1.26 | 0.76 | 0.48 | 0.33 |
| | 0.8 | 17.6 | 8.51 | 4.65 | 2.78 | 1.78 | 1.21 | 9.99 | 4.83 | 2.64 | 1.58 | 1.01 | 0.69 | 6.13 | 2.97 | 1.62 | 0.97 | 0.62 | 0.42 | 4.04 | 1.95 | 1.07 | 0.64 | 0.41 | 0.28 |
| | 0.9 | 14.4 | 6.95 | 3.80 | 2.27 | 1.46 | 0.99 | 8.16 | 3.94 | 2.16 | 1.29 | 0.83 | 0.56 | 5.01 | 2.42 | 1.32 | 0.79 | 0.51 | 0.34 | 3.30 | 1.60 | 0.87 | 0.52 | 0.33 | 0.23 |

## APPENDIX E

## YIELD LINE SOLUTION OF A STIFFENED HSS COLUMN FLANGE

For a stiffened column flange with a welded doubler plate, it is assumed that the yield lines are compatible on both plates and there is no shear transfered between them. The assumed mechanism is shown in Fig E.1, with the only variable "u". The tension beam flange force "P" is assumed to be transmitted to the column flange by 4 equal forces each of P/4 at the bolt locations. The plastic moment capacities per unit length of the column flange and the doubler plate are $m_p$ and $m_p^*$ respectively.

where,

$m_p = \sigma_{yc}\, t_o^2/4$
$m_p^* = \sigma_{yd}\, t_{dp}^2/4$
$\sigma_{yc}$ = yield stress of the column flange
$\sigma_{yd}$ = yield stress of the doubler plate
$t_o$ = column flange thickness
$t_{dp}$ = doubler plate thickness

Applying the principle of the yield line theory ( external work = internal work), leads to the following:

$$4(\frac{P}{4})\delta - m_p \left[ 2\,(2b_c-2d)\frac{\delta}{u} + 2\,(2Y_B+4u-2d)\,\frac{2\delta}{(b_c-X_B)}\right]$$

$$+ m_p^* \left[ 2\,(2d_{dp}-2d)\,\frac{\delta}{u} + 2\,(Y_B+2u\,(\frac{b_{dp}-X_B}{b_c-X_B})-2d)\,\frac{2\delta}{(b_c-X_B)}\right] \qquad \text{(E.1)}$$

Therefore,

$$P = m_p \left[\frac{4(b_c-d)}{u}+8\frac{(Y_B+2u-d)}{(b_c-X_B)}\right] + m_p^{\bullet}\left[\frac{4(b_{dp}-d)}{u}+\frac{4}{(b_c-X_B)}\left\{Y_B+2u\left(\frac{b_{dp}-X_B}{b_c-X_B}\right)\right\}-2d\right.$$

(E.2)

For a minimum value of "P", set dP/du =0 which leads to;

$$u = \sqrt{\frac{(b_c-X_B)^2\ [(b_c-d)+g(b_{dp}-d)]}{4(b_c-X_B)+2g(b_{dp}-X_B)}} \qquad \text{(E.3)}$$

Note that,

P = $P_{p(cft)}$ in Eq E.2,
g = $m_p^{\bullet}/m_p$, and
d = bolt's hole diameter

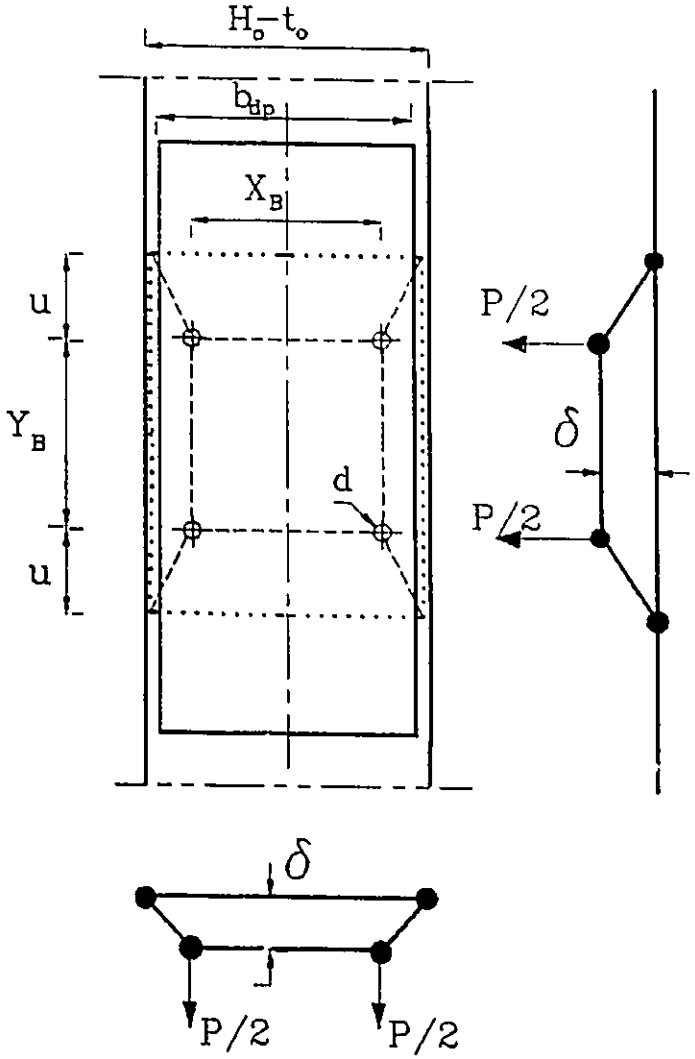


Fig E.1 Yield line mechanism of a stiffened column flange

## APPENDIX F

## DEFLECTION DUE TO MEMBRANE ACTION

The foregoing applies to both the cases of the end-plate and the column flange. Consider the horizontal equilibrium in Fig F.1 for the end-plate, or the vertical equilbrium in Fig F.2 for the HSS column flange:

$$\Delta P^{*} = 2\ T\ \sin\ (\theta_y + \Delta\theta) \tag{F.1}$$

where,

T : tension membrane force in the plate
$\Delta\theta$: rotation of the plate due to $\Delta P^{*}$
$\theta_y$: rotation of the plate at yield deflection = $(\Delta)_y/l$

where, "l" is the length of the plate subjected to the tensile membrane force;
l = b for the end-plate case
l = $(b_c - X_B)/2$ for the column flange case

The axial strain $\epsilon$ is given by;

$$\epsilon = \frac{\Delta l}{l} = \frac{\frac{l}{\cos\ \Delta\theta} - l}{l} = \sec\ \Delta\theta - 1 \tag{F.2}$$

Since the normal stresses developed in the yield lines due to bending and inplane stresses should not exceed the ultimate stress of the material at that level of loading, any axial stresses in the plate operating between yield lines are assumed to be in the elastic range. As such,

$$T = (\sec \Delta\theta - 1)\, E\, A^{*} \tag{F.3}$$

where, "$A^{*}$" is the cross section area of the plate and "E" is Young's modulus of elasticity

$A^{*} = B_{ep}\, t_{ep}$ for the end-plate,
$A^{*} = (Y_B+u)(t_o+t_{dp})$ for the case of column flange

It should be noted that, from equilibrium, the axial stresses in the rigid plate segments must be $\leq(\sigma_u-\sigma_y)$, where $\sigma_u$ and $\sigma_y$ are the ultimate and yield strength of the material, respectively. Eliminating the tension force between Eqs F.1 and F.3

$$\frac{\Delta P^{*}}{2\, E\, A^{*}} = (\sec\Delta\theta - 1)\ \ \sin(\theta_y+\Delta\theta) \tag{F.4}$$

The value of $\Delta\theta$ can be obtained by solving Eq F.4 by trial and error. Once the correct value of $\Delta\theta$ is obtained, then $(\Delta)_m$ is given by;

$$(\Delta)_m = \frac{l \sin(\Delta\theta)}{\cos(\theta_y+\Delta\theta)} \tag{F.5}$$

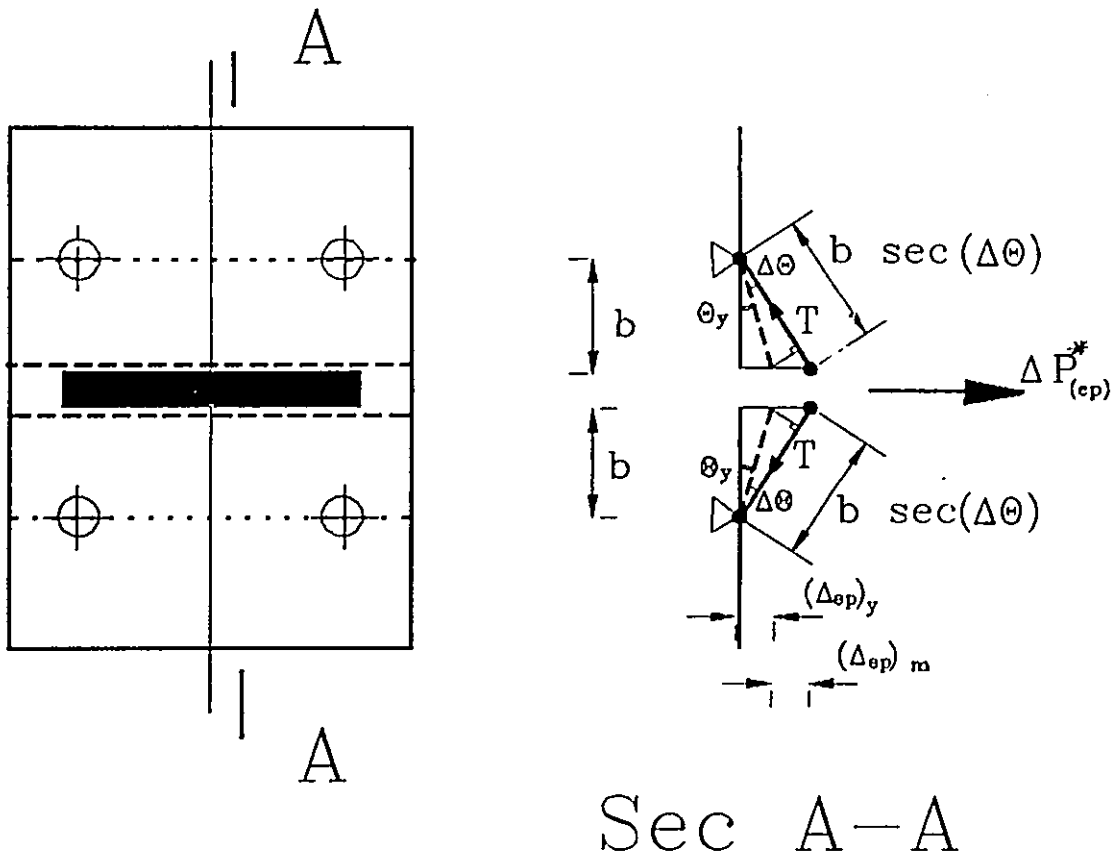


Fig F.1 Deflection due to membrane action in the end-plate

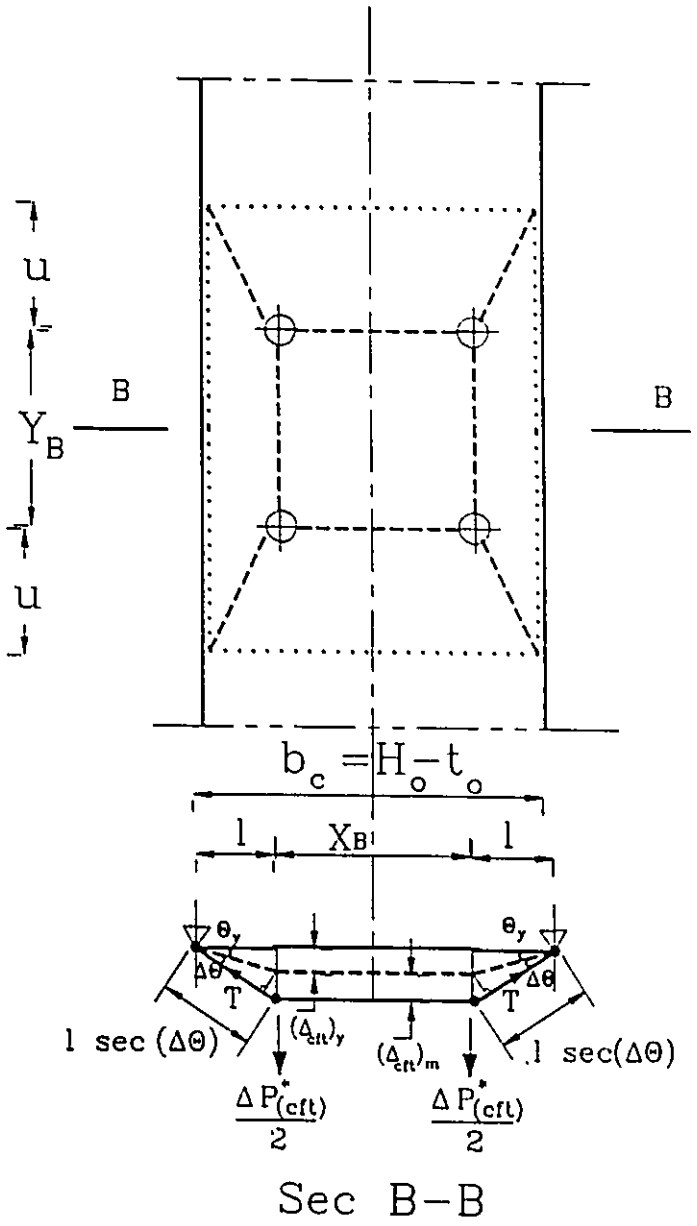


Fig F.2 Deflection due to membrane action in HSS column

# REFERENCES


Agerskov, H. (1977), "Analysis of bolted connections subjected to prying", Journal of Structural Engineering, ASCE, Vol.103, ST11, pp. 2195-2163.

Allahabadi, R. and Powell, G.H., (1988), "DRAIN-2DX user guide". Department of Civil Engineering, University of California, Berkely. EERC report No.88/06. U.S.A.

Almuti, A.M. and Hanson, R.D. (1973). "Static and dynamic cyclic yielding of steel beams", Journal of Structural Engineering, ASCE, Vol.99, ST6, pp.1273-1285.

American Institute of steel Construction (1986). "LRFD, Specification for structural steel buildings", Chicago, U.S.A.

American Institute of steel Construction (1980). "Manual of steel construction", AISC, 8th edn, Chicago, U.S.A.

Ang, K.M. and Morris, G.A. (1984). "Analysis of three dimensional frames with flexible beam-column connections". Canadian Journal of Civil Engineering, 11, pp. 245-254.

ASTM Standards "High-Strength Bolts for Structural Steel Joints". (1991) No. A325 M-91.

ASTM Standards "Standard Test Methods and Definitions for Mechanical Testing of Steel Products". (1992) No. A370-92.

Azizinamini, A., Bradburn, J.H. and Radziminski, J.B. (1987). "Initial stiffness of semi-rigid steel beam-to-column connections". Journal of Const. Steel Research, 8, pp. 71-80.

Ballio, G., Calado, L., DeMartino, A., Faella, C., and Mazzolani, F.M. (1986) "Steel beam-to-column joints under cyclic loads, experimental and analytical apprroach". Proc. 8th European Conf. on Earthquake Eng., Lisbon, pp. 7.2/9 - 7.2/16.

Canadian Institute of Steel Construction (CISC), (1989), "Handbook of Steel Construction", Canada

Chasten, C.P., Lu, L., and Driscoll, G., (1992), "Prying and shear in end-plate connection design", Journal of Structural Engineering, ASCE, Vol.118, ST5, pp. 1295-1311.

Clough, R.W., and Penzien, J., (1975), "Dynamics of structures", McGraw-Hill, U.S.A.

CSA-S16.1-M89. (1989) Canadian Steel Structures for Buildings. (Limit State Design) CSA-Standards, Ontario, Canada.

CSA-G40.21-92. (1992) Structural Quality Steel. Canadian Standards Association, Ontario, Canada.

CSA. (1989). "Welded Steel Construction", No. W59-1989, Canadian Standard Assosiation, Ontario, Canada.

Dawe, J. L. and Grondin, G. Y. (1990) W-shape beam to RHS column connections. Canadian Journal of Civil Engineering, 17, pp 788-797.

El-Hifnawy, L., (1980), " Elasto-plastic Finite element analysis of rectangular hollow section T-joints", M.Sc Thesis, McMaster University, Hamilton, Ontario,

Fisher, J., Galambos, T., Kulak, G. and Ravindra, M. (1978). "Load and resistance factor design criteria for connectors". Journal of the Structural Division, ASCE, Vol.104, ST9, pp. 1427-1441.

Fisher, J.W., and Struik, J. (1974), " Guide to design criteria for bolted and riveted joints", 1st. Ed., John Wiley and Sons Inc., New York., N.Y.

Frye, M.J. and Morris, G.A. (1976). "Analysis of flexibly connected steel frames". Canadian journal of Civil Engineering, 2, pp. 280-291.

Ghobarah, A., Korol, A., and Osman, A. (1992). "Cyclic behaviour of extended end-plate joints". Journal of Structural Engineering, ASCE, Vol.118, ST5, pp. 1333-1353.

Ghobarah, A., Osman, A., and Korol, R.M. (1990) " Behaviour of extended end-plate connections under cyclic loading". Engineering Structures, 12, pp. 15-27.

Ghobarah, A., Mourad, S. and Korol, R.M. (1993). "Behaviour of blind bolted moment connection for HSS columns". Tubular Structures V, Proceedings. of the Fifth International Symposium, Nottingham, United Kingdom, pp. 125-132.

Grundy, P., Thomas, I.R., and Bennetts, I.D., (1980), "Beam-to-column moment connections", Journal of Structural Engineering, ASCE, Vol.106, ST1, pp. 313-330.

Huck International Inc. (1990) "Industrial fastening systems". Irvine, California, U.S.A

Johnstone, N.D. and Walpole, W.R. (1982) "Behaviour of steel beam to column connections, made using bolted end-plates". Bull, New Zealand, Nat. Soc. for Earthquake Eng., 15, No.2, pp. 82-92.

Jones, S.W., Kirby, P.A. and Nethercot, D.A. (1982). "Columns with semi-rigid joints", Journal of Structural Engineering, ASCE, Vol.108, ST2, pp. 361-372.

Kanatani, H., Tabuchi, M., Kamba, T. and Ishikawa, M. (1987) A study on concrete filled RHS column to H-beam connections fabricated with HT-bolts in rigid frames. Proceedings of an Engineering Foundation Conference on Composite Construction in Steel and Concrete, Henniker, NH, pp 614-635.

Kato, B.(1989) Bolted beam-to-column moment connection. Proceedings of International Colloquium on Bolted and Special Structural Joints, Moscow, volume 2, pp 29-38.

Kato, B., Maeda, Y., and Sakae, K. (1981) Behaviour of rigid frame sub-assemblages subject to horizontal force. Joints in Structural Steelwork, John Wiley Sones, New York, U.S.A. pp. 1.54-1.73.

Kennedy, N.A., Vinnakota, S., and Sherbourne, A.N., (1981), "The split tee analogy in bolted splices and beam-column connections", Proc. of the Int. Conf. on Joints in Structural Steelwork, Teesside Polytechnic, U.K., pp. 2.138-2.157.

Korol, R.M., El Zanaty, M., and Brady, F.J. (1977), "Unequal width connections of square hollow sections in Vierendeel trusses", Canadian Journal of Civil Engineering, 4, pp. 190-201.

Korol, R.M., Ghobarah, A. and Osman, A. (1991) "Extended end-plate connections under cyclic loading: behaviour and design". Journal of Const. Steel Research., 16(4), pp. 253-280.

Korol, R.M., Ghobarah, A. and Mourad, S. (1993) "Blind bolting W-shape beams to HSS columns". Journal of Structural Division, ASCE. Vol.119 , ST12, pp 3463- 3481.

Korol, R.M., and Mansour, M.H. (1979), "Theoritical analysis of haunch-reniforced T-joints in square hollow sections", Canadian Journal of Civil Engineering, 6, pp. 601-609.

Korol, R.M., Mitri, H., and Mirza, F.A., (1982), "Plate reinforced square hollow section T-joints of unequal width", Canadian Journal of Civil Engineering,9, pp.143-148.

Krishnamurthy, N. (1978) " A Fresh look at bolted end-plate behavior and design". Engineering Journal, American Institute of Steel Construction, 15 (2), pp. 39-49.

Mann, A.P. and Morris, L.J. (1979) "Limit design of extended end-plate connections". Journal of Structural Engineering, ASCE. Vol.105, ST3, pp 511-527.

Maquoi, R., Navean, X. and Rondal, J. (1984) Beam-column welded stud connections. Journal of Const. Steel Research, 4, pp 3-26.

Monforton, G.R., and Wu, T.S., (1963), "Matrix analysis of semi-rigidly connected steel frames", Journal of Structural Engineering, ASCE, Vol.89, ST6, pp. 13-42.

Morris, L.J., (1964), "Tests on fillet welded rigid connections between universal beams and stanchions in high yield stress steel to BS.968:1962", Spring meeting, British Welding Institute, England.

Mourad, S., Korol, R. and Ghobarah, A. (1993) "A newly developed bolted moment connection for hollow structural columns". Proceedings of the Annual Conference of the Canadian Socity of Civil Engineering, Frederiction, New Brunswick, Canada, pp. 155-164.

Murray, T.M (1988) " Recent development for the design of moment end-plate connections". Journal of Const. Steel Research, 10, pp. 133-162.

Mzzalani, T.M. (1987). "Mathematical model for semi-rigid joints under cyclic loads". Proc. of State-of-the-art workshop on connections and the behaviour, strength and design of steel structures, Laboratorie de Mecanique et Technologie, Cachan, France.

Naumoski, N., (1984), SYNTH Computer Program, "Generation of artificial time history compatible with a target spectrum", McMaster Earthquake Engineering Research Group, McMaster University, Hamilton, Ontario, Canada.

Naumoski, N., Tso, W.K, and Heidebrecht, A.C., (1988) "A selection of representative strong motion earthquake records having different A/V ratios", McMaster Earthquake Engineering Research Group, (EERG report 88-01), McMaster University, Hamilton, Ontario, Canada.

NBCC. (1990), "National Building Code of Canada", Associate Committee on the National Building Research Code, National Research Council of Canada, Ottawa, Canada.

NBCC. (1990), "Supplement to the National Building Code of Canada 1990", National Research Council of Canada, Ottawa, Canada.

Nethercot, D.A. and Zandonini, R. (1989), "Methods of prediction of joint behaviour: beams-to-column connections", Structural connections: stability and strength, Edited by R. Narayanan, Elsevier Applied Science, London.

Osman, A., Ghobarah, A. and Korol, R.M., (1991) "Moment-rotation relationship for extended end-plate connections". Proceedings of the Annual Conference of the Canadian Socity of Civil Engineering, Hamilton, Ontario, Canada, pp. IV.517-IV.536.

Packer, J.A. and Henderson, J.E. (1992) "Design guide for hollow structural section

connections", Edited by the Canadian Institute of Steel Construction.

Packer, J.A. and Morris, L.J. (1977) "A limit state design for tension region of bolted beam to column connections". The Structural Engineer, Vol.55, pp 446-458.

Picard, A. and Giroux, Y. (1976) "Moment connections between wide flange beams and square tubular columns" Canadian Journal of Civil Engineering, 3(2), pp. 174-185.

Picard, A. and Giroux, Y. (1977) "Rigid connections for tubular columns", Canadian Journal of Civil Engineering, 3(2), pp 134-144.

Popov, E.P., and Bertero, V.V. (1973) "Cyclic loading of steel beams and connections", Journal of Structyral Engineering, ASCE, Vol.99, ST6, pp.1189-1204.

Prakash, V. and Powell, G.H. (1992) "DRAIN-2DX user guide" Department of Civil Engineering, University of California, Berkely, California, U.S.A.

Rodgers-Wilson, P. (1985) "Cost effective high strength fastening systems". Proceeding of the Third Conference on Steel Developments, Melbourne, Australia, pp. 28-36.

Shehata, A. (1983), "Elasto-plastic modelling of RHS T-joints", Ph.D Thesis, McMaster University, Hamilton, Ontario, Canada.

Sherman, D.R. and Ales, J.M. (1991) "The design of shear tabs with tubular columns". Procceedings, AISC National Steel Construction Conference, Washington, U.S.A, pp. 1.2-1.22.

Surtees, J.O., and Mann, A.P., (1970), "End-plate connections in plastically designed structures", Coference on joints in structures, Vol.1, Paper 5, University of Sheffield, England.

Tabuchi, M. Kanatani, H. and Kamba, T (1988) Behaviour of tubular column to H-beam connections under seismic loading. Proceedings of the Ninth world Conference on Earthquake Engineering, Tokyo, Japan (vol.IV), pp 181-186.

Timoshenko, S. and Woinowsky-K. Riegor, S. (1959) "Theory of Plates and Shells". 2nd. edtion. McGraw-Hill, U.S.A.

Ting, L.C., Shanmugam, N.E., and Lee, S.L. (1991) " Box-column to I-beam connections with external stiffners" Journal of Const. steel Research, 18, pp. 209-226.

Tsai, K. and Popov, E.P. (1990) "Cyclic behaviour of end-plate moment connections". Journal of Structural Engineering, ASCE, Vol.116, ST11, pp. 2917-2930.

Walpole, W.R. (1985) "Beam-column Joints", Bulletin of the New Zealand National Sociat for Earthquake Engineering, Vol.18, No.4, pp. 369-379.

White, R. and Fang, P. (1966) " Framing connections for square structural tubing". Journal of Structural Engineering, ASCE. Vol.92, ST2, pp. 175-193.

Whittaker, D., and Walpole, W.R., (1982), " Bolted end-plate connections for seismically designed steel frames", Research report 82-11 Dept. of Engineering, University of Canterbury, New Zealand.

Witteveen, J., Stark, J., Bijlaard, F. and Zoetemeijer, P. (1982) " Welded and bolted beam-to-column connections". Journal of Structural Engineering, ASCE. Vol, 108, ST2, pp. 433-455.

Xu, L., Sherbourne, A.N., and Grierson, D.E., (1993), "Design automation of steel frames with semi-rigid connections", Proceedings of the Annual Conference of the Canadian Socity of Civil Engineering, Fredericton, New Brunswick, Canada, pp. 225-234.

Yee, Y.L., and Melcher, R.E. (1986) "Moment-rotation curves for bolted connections". Journal of Structural Engineering, ASCE. Vol.112 , ST3, pp.615-630.

Zoetemeijer, P. (1974) "A design method for the tension side of statically loaded bolted beam-to-column connection", Heron 20, No.1, Delft University, Delft, Netherland.